PRODUCTION AND CHARACTERIZATION OF CELLULOSE NANOFIBRILS AND BIOPOLYMER COMPOSITES FOR PACKAGING APPLICATIONS

by

PRABAHARAN GRACERAJ PONNUSAMY

(Under the Direction of Sudhagar Mani)

ABSTRACT

The cellulose reinforced biopolymer composites are emerging as a potential packaging material due to their biodegradability, biocompatibility, and superior material properties. Cellulose Nanofibrils (CNF), a nanostructured cellulose can be reinforced with biopolymers such as chitosan, polylactic acid (PLA) to produce composites for flexible packaging applications. To produce highly dispersible and consistent quality CNF, cellulose pulp was subjected to a combination of mechanical (ball milling) and chemical (Carboxyl methylcellulose, CMC dispersion & NaOH swelling) pretreatments. The pretreated cellulose was fibrillated using a high-pressure homogenizer to produce CNF with up to 6% solid content and uniform fibril width from 20 to 40 nm. The CNF was reinforced with chitosan and crosslinked using citric acid to improve mechanical and hydrophobicity of flexible packaging films. The water uptake and water vapor permeability (WVP) of composite films were reduced by up to 86 and 50% respectively. The optimal amount of CNF and citric acid was determined as 20% and 25% respectively. Cellulose microfibers (CMF) produced from cotton noil was reinforced with PLA biopolymer. The tensile, WVP and UV barrier properties were improved by better dispersion stability and interfacial adhesion of CMF in PLA. The tensile stress and Young's modulus of 1% CMF reinforcement were

46 and 30% higher than the films without CMF reinforcement and the WVP of 20% CMF reinforcement was less than 29%. The UV light absorbance was improved between 41 and 90% for the CMF reinforcement of 1 to 20%. The environmental benefits of Chitosan-CNF composite films were investigated using a life cycle assessment method to use as a proof-of-concept for large scale production. It was found that about 79% of the environmental impacts were caused by the citric acid and heat energy used in the film manufacturing process. The carbon footprint of composite film manufacturing process was about 7 and 16% less than that of the fossil-based low-density polyethylene (LDPE) and PLA biopolymer films respectively. In overall, micro and nano fibrils of cellulose can be used as a reinforcing agent to improve the mechanical and barrier properties of biopolymer composites without compromising its carbon footprint for flexible packaging applications.

INDEX WORDS: Nano cellulose, Biopolymer composite, Crosslinking, Tensile properties, Barrier properties, Packaging films, Life cycle assessment

PRODUCTION AND CHARACTERIZATION OF CELLULOSE NANOFIBRILS AND BIOPOLYMER COMPOSITES FOR PACKAGING APPLICATIONS

by

PRABAHARAN GRACERAJ PONNUSAMY

B.E., Government College of Technology, India, 1998

M.S., VIT University, India, 2015

A Dissertation Submitted to the Graduate Faculty of The University of Georgia in Partial Fulfillment of the Requirements for the Degree

DOCTOR OF PHILOSOPHY

ATHENS, GEORGIA

2021

PRODUCTION AND CHARACTERIZATION OF CELLULOSE NANOFIBRILS AND BIOPOLYMER COMPOSITES FOR PACKAGING APPLICATIONS

by

PRABAHARAN GRACERAJ PONNUSAMY

Major Professor:	Sudhagar Mani
Committee:	K. C. Das
	Hitesh Handa
	Ke (Luke) Li
	Suraj Sharma

Electronic Version Approved:

Ron Walcott
Vice Provost for Graduate Education and Dean of the Graduate School
The University of Georgia
December 2021

DEDICATION

I dedicate this dissertation to my beloved wife Priscilla Sherene Latha, my dear son Ajay Samuel Prashinne, my parents and parents in-laws.

ACKNOWLEDGEMENTS

Expanding my boundaries academically and geographically, in pursuit of excellence, has been an intellectually rewarding and memorable experience of a lifetime. I am very grateful to all my professors, learned scholars, mentors and well-wishers who shared their knowledge and dedicated their time to help me achieve my academic goal.

First and foremost, I extend my heartfelt thanks to Dr. Sudhagar Mani, Supervisor, who was my pillar of support, monitoring my progress and guiding me to the finish. I thank him for his relentless faith and confidence in me. I also place on record my sincere thanks to Dr. Suraj Sharma, Advisory Committee member for his valuable advices during my experiments. I also would like to thank Dr. Keshav C Das, Dr. Hitesh Handa and Dr. Ke (Luke) Li, Advisory Committee members, for their suggestions and scholarly advice whenever needed.

I thank Dr. James Warnock and Dr. William Kisaalita, for giving me an opportunity to be a Teaching Assistant, and entrusting me with the responsibility of class evaluation. My sincere thanks to all the teaching faculties and teaching assistants who taught various courses of my program of study. I thank the staff members of Graduate Coordinator's office, college of engineering for their support and advices.

I am also grateful to my Church families; members of the Prayer Fellowship groups and friends for their prayers and support. I am very thankful to my family who stood by me through thick and thin throughout my academic quest, and above all I thank the Lord for His providence and for sustaining me to the very end.

TABLE OF CONTENTS

Page

ACKNOWLEDGEMENTS v

LIST OF TABLES x

LIST OF FIGURES xii

CHAPTER

1 INTRODUCTION AND RESEARCH OBJECTIVES 1

Introduction 1

Objectives 9

Dissertation organization 10

References 12

2 LITERATURE REVIEW 19

Cellulose biopolymer 19

Nanocellulose biopolymer 20

CNF/CNC reinforced biopolymer composites 25

Environmental performance of biopolymers 35

References 39

3 PRODUCTION AND CHARACTERIZATION OF HIGH SOLID CONTENT CELLULOSE NANOFIBRILS FROM PRETREATED FLUFF PULP 50

Abstract 51

Introduction 52

Materials and methods 55
Results and discussion 61
Conclusion 77
Acknowledgements 78
References 79
4 PREPARATION AND CHARACTERIZATION OF CITRIC ACID CROSSLINKED CHITOSAN-CELLULOSE NANOFIBRILS COMPOSITES FOR PACKAGING APPLICATIONS 87
Abstract 88
Introduction 89
Materials and methods 92
Results and discussion 97
Conclusion 114
Acknowledgements 116
References 117
5 COTTON NOIL BASED CELLULOSE MICROFIBERS REINFORCED POLYLACTIC ACID COMPOSITES FOR THE IMPROVEMENT OF WATER VAPOR AND UV BARRIER PROPERTIES IN PACKAGING FILMS 126
Abstract 127
Introduction 128
Experimental 130
Results and discussion 134
Conclusion 144

References 146

6 LIFE CYCLE ASSESSMENT OF MANUFACTURING CELLULOSE NANOFIBRILS REINFORCED CHITOSAN COMPOSITE FILMS FOR PACKAGING APPLICATIONS 155

Abstract 156

Introduction and background 158

LCA methodology 162

Results and discussion 174

Conclusion 183

Acknowledgements 184

References 185

7 CONCLUSION AND RECOMMENDATIONS 193

Conclusion 193

Recommendations 196

APPENDICES

A SUPPLEMENTARY INFORMATION – PRODUCTION AND CHARACTERIZATION OF HIGH SOLID CONTENT CELLULOSE NANOFIBRILS FROM PRETREATED FLUFF PULP 197

B SUPPLEMENTARY INFORMATION - COTTON NOIL BASED CELLULOSE MICROFIBERS REINFORCED POLYLACTIC ACID COMPOSITES FOR THE IMPROVEMENT OF WATER VAPOR AND UV BARRIER PROPERTIES IN PACKAGING FILMS……..... 205

C SUPPLEMENTARY INFORMATION – LIFE CYCLE ASSESSMENT OF MANUFACTURING CELLULOSE NANOFIBRILS REINFORCED CHITOSAN COMPOSITE FILMS FOR PACKAGING APPLICATIONS 206

LIST OF TABLES

Page

Table 1-1: Biodegradation abilities of bio-based polymers 5

Table 2-1: Energy demand and global warming potential of CNF manufacturing processes 22

Table 2-2: The properties and manufacturing methods of CNF/CNC extracted from different biomass resources 23

Table 2-3: Mechanical and barrier properties of natural polymer – CNF composites 26

Table 2-4: CNF/CNC surface modification processes performed for the improvement of biopolymer composite development 29

Table 2-5: Manufacturing methods and properties of PHB-CNF/CNC composites 31

Table 2-6: Manufacturing methods and properties of PLA-CNF/CNC composites.....34

Table 2-7: Cumulative energy demand (CED) and global warming potential (GWP) of bio-based polymers.....37

Table 3-1: Experimental plan for different pretreatment conditions 57

Table 3-2: Solid content and zeta potential of manufactured and Ref. CNF samples 67

Table 4-1: The composite composition for the manufacture of 0.72 g packaging films with and without citric acid crosslinking.....93

Table 4-2: Comparison of tensile and water vapor barrier properties of crosslinked composite films with synthetic and biopolymer films 114

Table 5-1: Present transmittance of PLA and composite films at 600, 400 and 233 nm wavelength 140

Table 6-1: Summary of LCI input data used for manufacturing one kg of the chitosan-CNF composite films.....168
Table 6-2: Summary of LCI output data for manufacturing one kg of the chitosan-CNF composite films.....170

LIST OF FIGURES

Page

Figure 1-1: Different types bioplastics 4

Figure 2-1: The structure of cellulose microfiber 20

Figure 3-1: CNF production from pretreated cellulose powder.....56

Figure 3-2: Fiber dimensions and optical microscope images of ball mill treated cellulose fibers. a) Comparison of cellulose fiber width with respect to different pretreatment conditions. b) Comparison of cellulose fiber length with respect to different pretreatment conditions. c) Optical microscope image of a cellulose fiber after CMC dispersion-75 min ball milling pretreatment. d) Optical microscope image of a cellulose fiber after NaOH swelling-75 min ball milling pretreatment.....63

Figure 3-3: FTIR spectra of CNF manufactured by different treatment methods 68

Figure 3-4: XRD curves of CNF manufactured by different treatment methods 69

Figure 3-5: SEM images of CNF manufactured by different treatment methods.....72

Figure 3-6: Thermograms of CNF a) TG curves b) DTG curves 74

Figure 3-7: Comparison of tensile properties of Ref. and manufactured CNF films. a) Tensile strength. b) Young's modulus.....75

Figure 4-1: FTIR spectra of crosslinked and non-crosslinked chitosan-CNF composite films showing ester bond formation at 1710 frequency for the composites with CNF reinforcement of 10, 15, 20 % and CA crosslinking of 20, 25, and 30 % 98

Figure 4-2: The schematic representation of chitosan-CNF composite microstructure which was formed by the citric acid crosslinking of chitosan and CNF and the hydrogen bonding between chitosan and CNF 99

Figure 4-3: SEM images of composite films for 10 and 20 % CNF reinforcement and 20 and 30 % CA crosslinking a) non-crosslinked films with 10 % CNF reinforcement b) 20 % CA crosslinked films with 10 % CNF reinforcement c) 30 % CA crosslinked films with 10 % CNF reinforcement d) non-crosslinked films with 20 % CNF reinforcement e) 20 % CA crosslinked films with 20 % CNF reinforcement c) 30 % CA crosslinked films with 20 % CNF reinforcement 100

Figure 4-4: Water uptake behavior of chitosan-CNF composite films a) comparison of crosslinked and non-crosslinked composite films. It shows that the water uptake of the crosslinked composite films was 70 to 85 % less than the non-crosslinked films b) main effect plots which shows the effect of changing CNF reinforcement from 10 to 20 % and CA crosslinking from 20 to 30 % c) interaction plots which shows the interaction of reinforcement and crosslinking for 10, 15 and 20 % CNF and 20, 25 and 30 % CA.....103

Figure 4-5: The water contact angle of chitosan-CNF composite films. a) comparison of crosslinked and non-crosslinked composite films. It shows that the contact angle was increased for 20 and 25 % CA crosslinking in 10 and 15 % CNF reinforced films and for 20 % CA crosslinking in 20 % CNF reinforced films b) main effect plots which shows the effect of changing CNF reinforcement from 10 to 20 % and CA crosslinking from 20 to 30 %. c) interaction plots which shows the interaction of reinforcement and crosslinking for 10, 15 and 20 % CNF and 20, 25 and 30 % CA 104

Figure 4-6: Water vapor barrier behavior chitosan-CNF composite films a) comparison of crosslinked and non-crosslinked composite films. It shows the 5 to 50% less water vapor permeability in crosslinked composite films and the decreasing trend with increase in CA for 10 and 15 % CNF reinforcement and increasing trend with increase in CA for 20 % CNF reinforcement. b) main effect plots which shows the effect of changing CNF reinforcement from 10 to 20 % and CA crosslinking from 20 to 30 %. c) interaction plots which shows the interaction of reinforcement and crosslinking for 10, 15 and 20 % CNF and 20, 25 and 30 % CA 106

Figure 4-7: UV-Visible transmittance spectra of chitosan films and chitosan-CNF composite films with and without crosslinking. a) comparison of chitosan and non-crosslinked composite films shows the decreased transmittance. b) comparison of non-crosslinked and crosslinked composite films with 10 % CNF and 20, 25 and 30 % CA. c) comparison of non-crosslinked and crosslinked composite films with 15 % CNF and 20, 25 and 30 % CA. d) comparison of non-crosslinked and crosslinked composite films with 20 % CNF and 20, 25 and 30 % CA 108

Figure 4-8: Tensile strength of composite films. a) comparison of crosslinked and non-crosslinked composite films shows the reduced tensile strength in crosslinked film. b) main effect plots which shows the effect of changing CNF reinforcement from 10 to 20 % and CA crosslinking from 20 to 30 %. c) interaction plots which shows the interaction of reinforcement and crosslinking for 10, 15 and 20 % CNF and 20, 25 and 30 % CA .110

Figure 4-9: Overlaid contour plot of the tensile strength (TS), water contact angle (WCA), water vapor permeability (WVP), and water uptake (WU). The shaded region is the optimal solution region which gives the amount of CNF and CA for the best performance. The

composite film studied with 20 % CNF and 25 % CA was in the optimal solution region… 112
Figure 5-1: FTIR spectra of cotton noil and CMF 134
Figure 5-2: XRD diffractograms of cotton noil and CMF 136
Figure 5-3: Fiber size characterization of cotton noil and CMF from SEM images 137
Figure 5-4: Effect of CMF reinforcement in PLA matrix composite film translucency. a) qualitative assessment by visual observation. b) UV-Vis spectrometry.....138
Figure 5-5: Tensile test results of PLA films with and without CMF reinforcement. a) Effect of reinforcement in ultimate tensile stress and Young's modulus. b) and c) Tensile fractured surface morphology of composite films with 3 and 10% CMF reinforcement 140
Figure 5-6: Effect of CMF reinforcement in water vapor permeability of PLA matrix composites.....143
Figure 6-1: The system boundary of CNF reinforced chitosan composite film manufacturing process for environmental impact assessment 166
Figure 6-2: Contribution analysis of all environmental impacts of manufacturing one kg of Chitosan-CNF composite film (base case). Note: OD-Ozone Depletion in kg CFC-11 eq., GWP-Global Warming Potential in kg CO_2 eq., SF-Smog Formation in kg O_3 eq., AD-Acidification in kg SO_2 eq., EP-Eutrophication in kg N eq., CG-Carcinogenic in CTUh, NCG-Non-Carcinogenic in CTUh, RE-Respiratory Effects in kg PM2.5 eq., ET-Ecotoxicity in CTUe and FFD-Fossil Fuel Depletion in MJ surplus 174
Figure 6-3: The percent contributions of environmental impacts from the CNF manufacturing process in one kg of the composite film production. Note: GWP–Global Warming

Potential in kg CO_2 eq., SF-Smog Formation in kg O_3 eq., RE-Respiratory Effects in kg PM2.5 eq. and FFD-Fossil Fuel Depletion in MJ surplus 176

Figure 6-4: The percent contributions of environmental impacts from the chitosan manufacturing process in one kg composite film production. Note: OD-Ozone Depletion in kg CFC-11 eq., GWP-Global Warming Potential in kg CO_2 eq., SF-Smog Formation in kg O_3 eq., AD-Acidification in kg SO_2 eq., EP-Eutrophication in kg N eq., CG-Carcinogenic in CTUh, NCG-Non-Carcinogenic in CTUh, RE-Respiratory Effects in kg PM2.5 eq., ET-Ecotoxicity in CTUe and FFD-Fossil Fuel Depletion in MJ surplus 178

Figure 6-5: The percent contributions of environmental impacts from the film-casting process in one kg composite film production. Note: OD-Ozone Depletion in kg CFC-11 eq., GWP-Global Warming Potential in kg CO_2 eq., SF-Smog Formation in kg O_3 eq., AD-Acidification in kg SO_2 eq., EP-Eutrophication in kg N eq., CG-Carcinogenic in CTUh, NCG-Non-Carcinogenic in CTUh, RE-Respiratory Effects in kg PM2.5 eq., ET-Ecotoxicity in CTUe and FFD-Fossil Fuel Depletion in MJ surplus 179

Figure 6-6: Carbon footprint of the chitosan-CNF composite film along with fossil and biopolymer-based films and the environmental impact contribution by the film casting process. Note: LDPE-Low Density Polyethylene, HDPE-High density polyethylene, PP-Polypropylene, PLA-Polylactic Acid.....181

Figure 6-7: Sensitivity analysis on the major environmental impact categories of the chitosan-CNF composite film. Note: GWP-Global Warming Potential, ET-Ecotoxicity, CG-Carcinogenic, OD-Ozone Depletion, RE-Respiratory Effects, and EP-Eutrophication..182

CHAPTER 1

INTRODUCTION AND RESEARCH OBJECTIVES

Introduction

Plastic materials are an integral part of global economy. The polypropylene (PP), low density polyethylene (LDPE), high density polyethylene (HDPE), polyethylene terephthalate (PET), polystyrene (PS), polyurethane (PUR) and polyvinyl chloride (PVC) are the primary plastic materials which are used to manufacture about 80% of plastic products in the market [1]. They are primarily manufactured from fossil derived feedstock such as naphtha, natural gas and shale gases. The fossil-based plastic materials possess excellent functional characteristics such as rigidity, toughness, fatigue strength, specific weight, viscoelastic behavior, resistance to chemical, heat and electrical conductance, barrier and optical properties and economic processing capabilities [2-5]. Hence, they are predominantly used in packaging, building and construction, automotive, electrical & electronic, household & sports, agriculture and medical instruments manufacturing sector. The worldwide production of plastic products reached about 350 million tons in the year 2017 [6].

Out of many product application sectors, the packaging product market is the largest application sector for plastic materials. About, 40% of the total plastic material production are used for the manufacturing of packaging products [7]. Majority of the general and food packaging products uses plastic materials as raw materials due to their functional and processing capabilities. The plastic packaging products protect the packaged products from damage and contamination, prevent spoilage and spilling and provide means for logistics. There is a steep surge in use of plastic packaging products due to their high rate of performance and cost effectiveness [8].

The increase in production and usage of plastic packaging product raises serious environmental concerns due to faster accumulation on ocean and land base after its use. One of the most critical challenges with continual use of plastics are its end of life. Over the years, we exploit natural resources and convert into innovative products for human comfort, but forget about its end-of-life after its use. Recycling and reuse of plastic products are less attractive due to the difficulties in sorting and cleaning, low degree of recyclability, high energy demand for incineration, low demand for recycled plastics and the release of hazardous material during recycling process [9]. In addition, the plastics manufacturing industries are facing tough challenges to deliver value added products that reduces energy use and emissions during feedstock processing, products manufacturing, use and disposal. The production of polymer feedstock consumed about 2.5 to 4% of total U.S. primary energy consumption in 2008 [10]. In addition, the catalyst residues, residual thermal stabilizers and reactive flame retardants used during plastic material processing have created alarming threat to environmental and human health impacts [11, 12].

The high energy consumption and the increased plastic materials used for packaging products not only pose substantial recycling challenges but also the mismanaged and uncontrolled disposal of plastic waste, in the past 50 years, to the environment as microplastics in our food chain cause a major global threat to mankind [13]. The present practices on the end of life management options such as recovery of energy from MSW, recycling and composting of plastic waste led to marginal shift in land fill. They did not show any accelerated shift to reduce plastic waste in environment [14]. Almost 10% of plastic land litters are discharged into ocean through storm water, rivers and wind blow [15-17]. The plastic litters in land and marine environments are fragmented into micro and nanosized debris by degradation action. Some of the living species in marine and land habitats are ingesting the leaked plastic debris and are loading harmful pollutants

to their ecosystems [18-20]. This will result in cell death, oxidative stress, innate immune system and other health hazards [21, 22].

It is expected that plastic material production would be doubled by the year 2050 due to the increasing demand in packaging product and other applications [23]. This would put a major burden on fossil resource availability, increase in crude oil price and increase in waste disposal. The U.S. Environmental protection agency (EPA) reported that about 24.31 MMT of plastic were landfilled in the year 2017 causing loss in material value and threat to environment. As the fossil resources are finite and their prices are likely to be increased and the plastic materials production, use and disposal pose serious threat to the environment, a new material system is envisioned from renewable resources as an alternate material for fossil derived plastic materials especially for packaging product manufacturing.

The increasing environmental awareness and the need for alternate materials for fossil derived polymer materials insisted the use of non-fossilized and biodegradable biomass as resource for the production of plastics material. According to the technical committee CEN/TC 249 of the European Committee for Standardization (CEN) and International Union of Pure and Applied Chemistry (IUPAC), these materials were designated as bio-based polymers or bio-based plastics [24]. The European Bioplastics Agency (EBA) designated the polymer materials which are produced from bio-based resources or having biodegradable characteristics or both as bioplastic materials. The bio-based PE, PET and polyamide (PA) are non-biodegradable bioplastics. The poly (lactic acid) (PLA), polyhydroxyalkanoates (PHA), starch and cellulose are some of the bio-based and biodegradable bioplastic materials. The polybutylene adipate terephthalate (PBAT) and polycaprolactone are not from bio-based resources but they are biodegradable bioplastics. The different types of bioplastics are presented in the Figure 1-1.

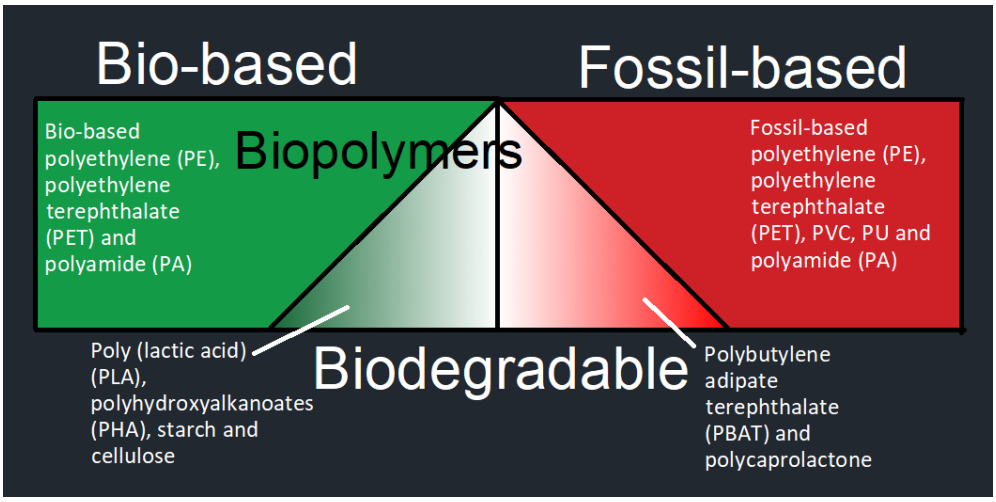

Figure1-1. Different types bioplastics

The interest on bio-based polymer materials are increasing among plastic product manufactures and use due to their attractive materials properties and plastic waste management options [25]. The demand for bioplastic materials are steadily increasing. It was predicted that global market for bioplastics would increase 15% in next five years. It was also projected that global bioplastics product production will reach to 2.4 MMT in 2022. There are many limitations that would prevail the growth of bioplastics market share. They are lack of industrial material standards, land use and environmental emission due to agriculture activities, production cost and consistent quality of bioproducts [26]. Even though, the manufacturing of bio-based plastic products has limitation to expand their application for various product applications, the end of life management options of bio-based plastic products is the key driving factor to consider them as a best alternate material for the fossil derived polymer materials. The biodegradation ability of bio-based polymer materials is summarized in Table 1-1.

Table 1-1. Biodegradation abilities of bio-based polymers

Bio-based polymers	Test standard and testing conditions	Percentage of Biodegradation	Ref.
PLA	ISO 20200, Temperature -58° C	90% disintegration after 14 days	[27]
Poly (hydroxybutyrate-co-hydroxy valerate) (PHBV)/PHA	ISO 14855-2 and 16929	81% after 35 days	[28]
Starch	ISO 14855	More than 70% after 45days	[29]
Cellulose	ISO 14855	86% after 45 days and 97% after 180 days	[30]
Chitosan	Aerobic composting environment at 58° C Temperature	More than 85% biodegradation after 180 days	[31]

The bio-based polymer materials are produced from biomass resources by two different ways such as direct extraction of biopolymer substance from biomass (natural biopolymers: proteins and polysaccharides) and synthesis of monomers extracted from micro-organisms and biomass by polymerization reactions (synthetic biopolymers). Some of the bio-based polymers which were synthesized from biomass had same physical and chemical properties as petroleum-based polymers (Eg. Bio Polyethylene derived from ethanol) and some exhibited unique properties as new class of materials (Eg. Polylactic Acid (PLA)) [32]. The functional properties of bio-based polymers, which were extracted as biopolymer substance (natural polymers) and which were synthesized from monomers of natural resources were investigated to use them as alternative materials for packaging applications. The hydrophilic and brittle nature of protein and polysaccharide-based natural polymers led to poor mechanical and barrier properties and limited their use as potential packaging materials.

In this context, attempts were made to develop natural polymer composite materials by combining two or more natural polymer materials extracted from natural resources to capture the

unique material characteristics which were attributed by their constituent materials. These two distinct constituent phases of composite materials are account for the anisotropy properties of materials in macro level [33, 34]. Considerable improvement in physical, thermal and mechanical properties was witnessed while reinforcing nonclay, carbon nanofiber and carbon nanotubes (CNT) in polymer matrix [35-37]. But, the recent environmental concerns of material development process and the demand for highly functional materials insisted the use of reinforcement material from natural resources and led to new class of biopolymer nanocomposites. Much attention was given cellulose based biopolymers such as cellulose nanofibrils (CNF) and cellulose nanocrystals (CNC) as they are available abundant in earth and possesses remarkable characteristics to use as reinforcement materials in biopolymer nanocomposite materials.

The CNF and CNC which were used as nanofiller or nano reinforcement materials are manufactured with wide spread width of 5 to 80 nm and length of 200 to 500 nm [38-41]. They are isolated from the biomass resources such as wood pulp, plant biomass, cotton linter, etc., by the series or combination of chemical and mechanical treatment process [42, 43]. The chemical methods of CNF manufacturing were demonstrated primarily in laboratory scale and have not developed yet to commercial scale due to the extensive use of chemicals. In the laboratory scale chemical manufacturing method, the CNC were extracted from their biomass resource by the combination of acid hydrolyzation and ultrasonic or high-pressure homogenization process. The extracted CNC had the width of 5~10 nm and length of 50~200 nm. Only 35 to 45 w % of CNC was able to be extracted from cellulose resource by acid hydrolysis process. The phase separation of CNC aqueous suspensions was occurred, if the CNF concentration reached beyond 3% [44, 45].

The mechanical disintegration processes are suggested for the commercial scale production of CNF due to the achievable higher production volume output and the restricted use of acids or

harmful chemicals in the production process. In the mechanical disintegration process, CNF are manufactured from the wood pulp slurry by passing it through a refiner and through a high-pressure homogenizer. The degree of fibrillization of cellulose in a high-pressure homogenizer is depended on number of passes and solid concentration of pulp in slurry. The CNF having width ranged from few microns to 100 nm were manufactured by passing the wood pulp with the slurry concentration of 3 wt.% in a refiner and a homogenizer by 30 and 14 times respectively. Increasing the number of passes in homogenizer did not improve neither the width of CNF to nanoscale nor to uniform distribution level [46, 47]. These CNF manufacturing methods associated concerns need to be addressed to accelerate the commercialization of CNF production and the use of CNF in various product applications.

The biodegradability, biocompatibility, abundant availability and tunable mechanical properties of biopolymer-CNF composites are the major technological breakthrough to consider these materials for packaging products [48, 49]. The composite films were manufactured by reinforcing CNF in chitosan, starch, PLA and other protein-based biopolymers. The mechanical properties of these composites were mainly affected by CNF loading percentage, dispersion and the degree at which it makes bonding with biopolymer matrix materials and the barrier properties were influenced by hydrophilic conditions and the loading percentage of CNF reinforcement [50, 51].

Chitosan is the second most abundant natural biopolymers with the advantages of bio degradation and bio compatibility, they were explored to consider as resource materials for various product application and matrix phase materials in nanocellulose composites [52]. The remarkable properties of chitosan increased their application in cosmetic, pharmaceutical and biomedical product sectors [53]. The chitosan molecule chains were synthesized and modified by functional

groups by chemical synthesis process to use in biomedical and pharmaceutical application fields. The chitosan molecules were synthesized by thiolation process and used in drug delivery applications. The phosphorylated chitosan and their derivatives were synthesized to improve water solubility and metal chelating tendency during tissue regeneration, drug delivery and fuel cell uses. The N-phthaloyl chitosan derivatives were developed to improve the solubility of chitosan in polar-organic solvents. The crosslinked, carboxylated and ionic chitosan were also synthesized to enhance drug delivery, antimicrobial and metal attachment characteristics of chitosan [54].

The composite packaging films and coating which were developed using chitosan and nanocellulose as constituent materials exhibited the increase in tensile strength while increasing the CNF mass fraction up to 20 % with various plasticizer [55]. But, the hydrophilic characteristics of chitosan increased the hydration degree of composite film and resulted the loss of barrier properties. In order to improve the barrier properties of biopolymer-CNF composites, the hydrophobic groups were substituted in hydrophilic groups of CNFs by physical and chemical processes. During this process, the acyl groups (R-C=O) of carboxylic acid derivatives were substituted in the amino group of glucosamine molecules and the improvement in hydrophobicity was achieved [56]. The manufacturing process of these composite films required twostep process namely esterification and film manufacturing processes. Furthermore, the acetic anhydride and pyridine which were used as surface modifier and catalyst were classified as extremely danger hazardous chemicals by global harmonized system (GHS). Hence, the development of hydrophobic chitosan-CNF composite material requires an environment friendly one step process for the packaging product development.

Similarly, PLA is the kind of synthetic biopolymers which were explored to use in packaging product manufacturing due to their attractive material properties and biodegradability

[57]. The PLA-CNF composites were developed for the improvements of toughness and gas bearing properties of PLA polymers. The CNF/CNC and PLA are incompatible phase materials due to the hydrophilic and hydrophobic nature of CNF/CNC and PLA respectively. The poor interfacial adhesion between CNF/CNC and PLA resulted the poor mechanical properties of these kind of nanocomposites [58]. In order to increase the interfacial adhesion of the constituent materials were blended with compatibilizers or PLA was reinforced with surface modified CNF/CNC. The environmentally friendly compatibilizer and the reduction of ductility are the critical issues during the PLA-CNF composite development process.

In addition to the functionality enhancement of materials, another important part in the value-added product development in packaging product applications is to adapt an environmental conscious manufacturing process [59]. The growing interest over the environmental performance assessment of biopolymer – CNF composites is to designate composite material system as promising environment friendly material in packaging product applications. The lifecycle analysis (LCA) is suggested as a holistic approach for the evaluation of environmental impact of bio-based materials and the products [60, 61]. It would highlight the concerns in energy consumption and ecological footprint of materials and manufacturing method used in the product manufacturing. It is important for the current packaging product market sector to elucidate the environmental impacts of biopolymer-CNF composite manufacturing process and to designate as prospective alternate materials for fossil-based polymer materials.

Objectives

The overall objective of the proposed study is to develop biopolymer-cellulose composites as potential packaging materials by addressing the research gap in nanocellulose and biopolymer-composite manufacturing processes. The specific objectives of the thesis are

1) To investigate the effect of pretreatment methods of cellulose pulp to produce high solid content cellulose nanofibrils (CNFs).
2) To investigate the in-situ cross linking of chitosan and cellulose nanofibrils to improve the water resistance and water vapor barrier properties of composite films for packaging applications.
3) To develop PLA-Cellulose Micro fibers (CMF) composites for tensile and UV and water vapor barrier properties improvement.
4) To conduct the Life Cycle Assessment (LCA) of manufacturing chitosan-CNF composite films by solvent casting process as a proof-of-concept for the production of large-scale production volume.

Dissertation organization

The experimental investigations of CNF manufacturing, cellulose reinforced composites development and the LCA of natural polymer composite manufacturing for packaging product applications are mainly focused in this dissertation. The outline of the thesis is as follows

The chapter 2 presents the review of literatures related to CNF manufacturing methods by mechanical fibrilization, combination of chemical and mechanical pre and main treatments and the properties of CNF extracted from different biomass resources. The development of natural biopolymer-CNF composites and synthetic biopolymer-CNF composites for packaging applications and the environmental impact assessment of biopolymers were also discussed in this chapter.

The chapter 3 to 6 are manuscripts submitted to the peer-reviewed journals. The chapter 3 is the experimental investigation of CNF production by CMC dispersion-ball milling and NaOH swelling-ball milling pretreatments and high-pressure homogenization main treatment method.

The chapter 4 and 5 is about the development of chitosan-CNF composite and PLA-cellulose micro fibers (CMF) composite for packaging film manufacturing. The experimental studies on in-situ crosslinking of chitosan-CNF composites for the improvement of hydrophobicity and water vapor barrier properties and reinforcing cotton noil CMF in PLA biopolymer matrix for the improvement of tensile and water vapor barrier properties were discussed in chapter 4 and 5 respectively. The chapter 6 contains the environmental impact assessment of chitosan-CNF composites manufacturing process by LCA method.

The chapter 7 discusses about the conclusions and the recommendations for future works that could be carried out in biopolymer composite development processes for the packaging product applications. The supplementary information submitted to the journals were attached in the Appendix section.

References

1. Crippa, M., et al., A circular economy for plastics: Insights from research and innovation to inform policy and funding decisions. 2019.
2. Shah, V., Handbook of plastics testing and failure analysis. Vol. 21. 2007: John Wiley & Sons.
3. Dodiuk, H. and S.H. Goodman, Handbook of thermoset plastics / edited by Hanna Dodiuk, Sidney H. Goodman. 3rd ed.. ed. 2014: San Diego : William Andrew.
4. Grellmann, W. and B. Langer, Deformation and Fracture Behaviour of Polymer Materials edited by Wolfgang Grellmann, Beate Langer. 1st ed. 2017.. ed. 2017: Cham : Springer International Publishing : Imprint: Springer.
5. Bercea, M., Polymer materials with smart properties / Maria Bercea, editor. 2013: New York : Nova Science Publishers.
6. Europe, P., Plastics—The Facts 2016. An analysis of European plastics production, demand and waste data, 2016: p. 1-38.
7. UNEP, Marine Plastic Debris and Microplastics: Global Lessons and Research to Inspire Action and Guide Policy Change. 2016: UN.
8. EPA, U., Advancing sustainable materials management: 2017fact sheet. 2019.
9. Leal Filho, W., et al., An overview of the problems posed by plastic products and the role of extended producer responsibility in Europe. Journal of Cleaner Production, 2019. 214: p. 550-558.
10. Hamman, C.W., Energy for Plastic. 2010, Submitted as coursework for Physics.

11. Kutz, M., Applied plastics engineering handbook processing and materials / edited by Myer Kutz. 1st ed.. ed. 2011, Waltham, Mass.: Waltham, Mass. : William Andrew, an imprint of Elsevier.
12. Liepins, R. and E.M. Pearce, Chemistry and toxicity of flame retardants for plastics. Environmental Health Perspectives, 1976. 17: p. 55-63.
13. Barnes, S.J., Understanding plastics pollution: The role of economic development and technological research. Environmental Pollution, 2019. 249: p. 812-821.
14. EPA, Advancing Sustainable Materials Management: 2015 Fact Sheet 2018. p. 1-23.
15. Napper, I.E. and R.C. Thompson, Chapter 22 - Marine Plastic Pollution: Other Than Microplastic, in Waste (Second Edition), T.M. Letcher and D.A. Vallero, Editors. 2019, Academic Press. p. 425-442.
16. Avio, C.G., S. Gorbi, and F. Regoli, Plastics and microplastics in the oceans: From emerging pollutants to emerged threat. Marine Environmental Research, 2017. 128: p. 2-11.
17. Jambeck, J.R., et al., Plastic waste inputs from land into the ocean. Science, 2015. 347(6223): p. 768-771.
18. Ng, E.-L., et al., An overview of microplastic and nanoplastic pollution in agroecosystems. Science of The Total Environment, 2018. 627: p. 1377-1388.
19. Barnes, D.K.A., et al., Accumulation and fragmentation of plastic debris in global environments. Philosophical Transactions of the Royal Society B: Biological Sciences, 2009. 364(1526): p. 1985-1998.
20. Derraik, J.G.B., The pollution of the marine environment by plastic debris: a review. Marine Pollution Bulletin, 2002. 44(9): p. 842-852.

21. Lehner, R., et al., Emergence of nanoplastic in the environment and possible impact on human health. Environmental Science & Technology, 2019. 53(4): p. 1748-1765.

22. Wright, S.L. and F.J. Kelly, Plastic and human health: A micro issue?. Environmental Science & Technology, 2017. 51(12): p. 6634-6647.

23. Allwood, J.M., J.M. Cullen, and R.L. Milford, Options for achieving a 50% cut in industrial carbon emissions by 2050. Environmental Science & Technology, 2010. 44(6): p. 1888-1894.

24. Carroad, P.A. and R.A. Tom, Bioconversion of shellfish chitin wastes: process conception and selection of microorganisms. Journal of Food Science, 1978. 43(4): p. 1158-1161.

25. Foschi, E. and A. Bonoli, The commitment of packaging industry in the framework of the European strategy for plastics in a circular economy. Administrative Sciences, 2019. 9(1): p. 18.

26. Mozaffari, N. and A. Kholdebarin, A review: investigation of plastics effect on the environment, bioplastic global market share and its future perspectives. 2019.

27. Luzi, F., et al., Study of dis-integrability in compost and enzymatic degradation of PLA and PLA nanocomposites reinforced with cellulose nanocrystals extracted from Posidonia Oceanica. Polymer Degradation and Stability, 2015. 121: p. 105-115.

28. Weng, Y.-X., et al., Biodegradation behavior of PHBV films in a pilot-scale composting condition. Polymer Testing, 2010. 29(5): p. 579-587.

29. Du, Y.-L., et al., Biodegradation behaviors of thermoplastic starch (TPS) and thermoplastic dialdehyde starch (TPDAS) under controlled composting conditions. Polymer Testing, 2008. 27(8): p. 924-930.

30. Saha Dr, N.C., G. Madhu Dr, and D.B. Kadu Ms, Evaluation of biodegradability characteristics of cellulose-based film as per IS/ISO 14855-1. Journal of Applied Packaging Research, 2019. 11(3): p. 2.

31. Dean, K., et al., Glycerol plasticised chitosan: A study of biodegradation via carbon dioxide evolution and nuclear magnetic resonance. Polymer Degradation and Stability, 2013. 98(6): p. 1236-1246.

32. Rudin, A. and P. Choi, Chapter 13 - Biopolymers, in The Elements of Polymer Science & Engineering (Third Edition), A. Rudin and P. Choi, Editors. 2013, Academic Press: Boston. p. 521-535.

33. Vinson, J.R. and R.L. Sierakowski, Strength and failure theories, in The Behavior of Structures Composed of Composite Materials, J.R. Vinson and R.L. Sierakowski, Editors. 2008, Springer Netherlands: Dordrecht. p. 303-332.

34. Wagner, H.D., Reinforcement, in Encyclopedia of Polymer Science and Technology. 2002.

35. Goettler, L.A., K.Y. Lee, and H. Thakkar, Layered silicate reinforced polymer nanocomposites: Development and applications. Polymer Reviews, 2007. 47(2): p. 291-317.

36. Ci, L. and J. Bai, Novel micro/nanoscale hybrid reinforcement: Multiwalled carbon nanotubes on SiC particles. Advanced Materials, 2004. 16(22): p. 2021-2024.

37. Sandler, J., et al., Carbon-nanofibre-reinforced poly(ether ether ketone) composites. Composites Part A: Applied Science and Manufacturing, 2002. 33(8): p. 1033-1039.

38. Siró, I. and D. Plackett, Microfibrillated cellulose and new nanocomposite materials: a review. Cellulose, 2010. 17(3): p. 459-494.

39. Stelte, W. and A.R. Sanadi, Preparation and characterization of cellulose nanofibers from two commercial hardwood and softwood pulps. Industrial & Engineering Chemistry Research, 2009. 48(24): p. 11211-11219.

40. Barbash, V.A., O.V. Yaschenko, and O.M. Shniruk, Preparation and properties of nanocellulose from organosolv straw pulp. Nanoscale Research Letters, 2017. 12(1).

41. Chirayil, C., L. Mathew, and S. Thomas, Review of recent research in nano cellulose preparation from different lignocellulosic fibers. Reviews on Advanced Materials Science, 2014. 37: p. 20-28.

42. Phanthong, P., et al., Nanocellulose: Extraction and application. Carbon Resources Conversion, 2018. 1(1): p. 32-43.

43. Lee, H.V., S.B.A. Hamid, and S.K. Zain, Conversion of lignocellulosic biomass to nanocellulose: Structure and chemical process. The Scientific World Journal, 2014. 2014: p. 1-20.

44. Shafiei-Sabet, S., W.Y. Hamad, and S.G. Hatzikiriakos, Rheology of nanocrystalline cellulose aqueous suspensions. Langmuir, 2012. 28(49): p. 17124-17133.

45. Dong, X.M., J.-F. Revol, and D.G. Gray, Cellulose, 1998. 5(1): p. 19-32.

46. Iwamoto, S., et al., Optically transparent composites reinforced with plant fiber-based nanofibers. Applied Physics A, 2005. 81(6): p. 1109-1112.

47. Iwamoto, S., A.N. Nakagaito, and H. Yano, Nano-fibrillation of pulp fibers for the processing of transparent nanocomposites. Applied Physics A, 2007. 89(2): p. 461-466.

48. Abdul Khalil, H.P.S., et al., A review on nanocellulosic fibres as new material for sustainable packaging: Process and applications. Renewable and Sustainable Energy Reviews, 2016. 64: p. 823-836.

49. Sangroniz, A., et al., Packaging materials with desired mechanical and barrier properties and full chemical recyclability. Nature Communications, 2019. 10(1).

50. Azeredo, H.M.C., et al., Nanocellulose reinforced chitosan composite films as affected by nanofiller loading and plasticizer content. Journal of Food Science, 2010. 75(1): p. N1-N7.

51. Lee, K.-Y., et al., On the use of nanocellulose as reinforcement in polymer matrix composites. Composites Science and Technology, 2014. 105: p. 15-27.

52. Fernandes, S.C., et al., Novel materials based on chitosan and cellulose. 2011. 60(6): p. 875-882.

53. Zargar, V., M. Asghari, and A. Dashti, A review on chitin and chitosan polymers: Structure, chemistry, solubility, derivatives, and applications. ChemBioEng Reviews, 2015. 2(3): p. 204-226.

54. Negm, N.A., et al., Advancement on modification of chitosan biopolymer and its potential applications. International Journal of Biological Macromolecules, 2020.

55. Li, Q., J. Zhou, and L. Zhang, Structure and properties of the nanocomposite films of chitosan reinforced with cellulose whiskers. 2009. 47(11): p. 1069-1077.

56. Tangpasuthadol, V., N. Pongchaisirikul, and V.P. Hoven, Surface modification of chitosan films. 2003. 338(9): p. 937-942.

57. Jung, B.N., et al., The fabrication of flexible and oxygen barrier cellulose nanofiber/polylactic acid nanocomposites using cosolvent system. Journal of Applied Polymer Science, 2020. 137(47): p. 49536.

58. Abdulkhani, A., et al., Preparation and characterization of modified cellulose nanofibers reinforced polylactic acid nanocomposite. Polymer Testing, 2014. 35: p. 73-79.

59. Thoresen, J., Environmental performance evaluation — a tool for industrial improvement. Journal of Cleaner Production, 1999. 7(5): p. 365-370.

60. Curran, M.A., Life-Cycle Assessment, in Encyclopedia of Ecology (Second Edition), B. Fath, Editor. 2016, Elsevier: Oxford. p. 359-366.

61. Brusseau, M.L., Chapter 32 - Sustainable development and other solutions to pollution and global change, in Environmental and Pollution Science (Third Edition), M.L. Brusseau, I.L. Pepper, and C.P. Gerba, Editors. 2019, Academic Press. p. 585-603.

CHAPTER 2

LITERATURE REVIEW

Cellulose biopolymer

The cellulose is the most abundant biopolymer available in nature. The worldwide annual production of cellulose is about 1.3 x 10^{10} metric tons [1]. The nanostructured cellulose has potential to use as new material development platform for packaging, hygiene and absorbent products, automotive products, textile and clothing products and cement materials. The demand for nanocellulose materials is increasing every year and around 6 million metric tons of annual demand was estimated for the U.S. market. Out of which the major market demand of 2 million metric tons would be for packaging product applications [2].

The cellulose is available as carbohydrate chain in renewable resources such as plants, forest wood, agriculture residue, forest residue and food waste. The percentage of available cellulose varies from biomass to biomass resources. The forestry biomass resource has 40~50% of cellulose and agriculture biomass has 25 ~ 40 % of cellulose [3]. The cellulose in biomass are present as microfibril networks. The microfibrils contain cellulose chain structure which is formed from anhydroglucose rings linked by β 1-4 glucosidic bond [4]. The elementary microstructure of cellulose is represented as heterogeneous composite constituted with amorphous and crystalline cellulose, hemi cellulose and lignin as depicted in Figure 2-1.

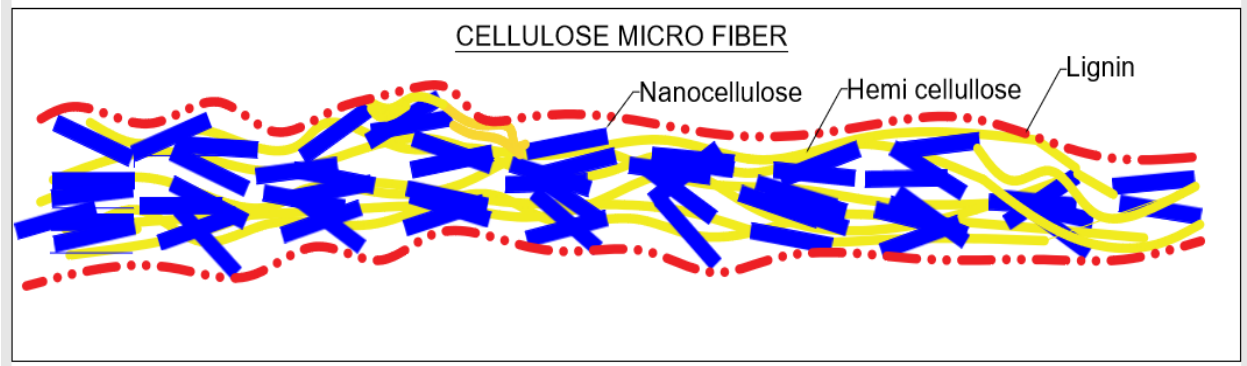

Figure 2-1. The structure of cellulose microfiber

Nanocellulose biopolymer

The nanostructured cellulose materials having fibril dimensions ranging from 1 to 100 nm is defined as nanocellulose materials. They exist as microfibril bundles in the cell walls of plants and wood biomass. The microfibril bundles are formed by many strong interfibrillar hydrogen bond network of nanocellulose. The nanocellulose are isolated from cellulose microfibrils as cellulose fibril networks (CNF) or rod like cellulose nanocrystals (CNC) structures. They show remarkable mechanical and surface properties. The high axial stiffness due to hydrogen bonding network in CNF and CNC provides the capability to reinforce them in polymer matrix materials [7]. The elastic modulus and tensile strength of wood based cellulose fibers are 12-27 GPa and 0.3-1.4 GPa respectively [8]. The CNF/CNCs also have reactive surface with many hydroxyl groups. It provides the opportunities to modify the surfaces by physical or chemical reactions to enhance the functional characteristics [9]. The attractive mechanical and surface properties of CNF/CNC increased its uses as material for pharmaceutical, packaging, cosmetics and electronics products [10].

CNF/CNC biopolymer

The increasing demand of nanocellulose materials in different product applications, requires efficient manufacturing process to produce durable and acceptable quality of

nanomaterials. Different types of nanocelluloses, namely cellulose nanofibrils (CNF), cellulose nanocrystal (CNC), tunicate cellulose nanocrystals (t-CNC), algae cellulose particles (AC), and bacterial cellulose (BC), are isolated from biomass resources such as microorganism, industrial waste, agriculture biomass, forest wood and plants [5, 6]. The cellulose microfibrils embedded in a protein matrix of tunicate sea animals are called as t-CNC. The cellulose microfibrils in algae cell walls were isolated as AC particles by biosynthesis process. The bacterial cellulose which were secreted in some bacteria under special culturing conditions were extracted as BC [6].

The CNF/CNC were isolated from wide range of wood and plant biomass resources [11]. They are extracted from biomass resources by chemical, mechanical and enzymatic processes. The acid hydrolysis chemical process is most widely followed for the extraction of crystalline CNCs from delignified cellulose pulp and cotton fibers. The CNFs were initially manufactured through mechanical disintegration processes. The energy requirement of CNF extraction processes by mechanical treatment processes varied from 12,000 to 70,000 kWh t^{-1}. However, the combination of mechanical and chemical manufacturing methods reduced the energy demand significantly. The introduction of pretreatment processes, reduced the energy consumption to 500 to 1500 kWh t^{-1} [5].

The chemical pretreatment processes used in CNF manufacturing were chloroacetic acid etherification, carboxy methylation, tempo oxidation and enzymatic treatment. The main treatment processes used for the CNF fibrilization were ultrasonication, high-pressure homogenization, disc refiner and microfluidizer processes [29, 30]. The limitation of chemical pretreatment processes are consumptions of chemicals and the harmful emissions. The lifecycle energy use and carbon footprint details of CNF pretreatment and main treatment processes are given in Table 2-1.

Table 2-1. Energy demand and global warming potential of CNF manufacturing processes

Chemical / Mechanical CNF manufacturing processes	GWP[a] (kg CO_2 eq./kg CNF)	CED[b] (MJ/kg CNF)	Reference
Chloroacetic acid Etherification	286	5186	[31]
Tempo Oxidation	112	2175	[31]
Carboxy Methylation	100	1900	[31, 32]
Sonication	869	11918~12166	[31]
Homogenizer	74.8	1047	[31]
Microfluidizer	0.095	22	[31, 32]

[a] Global warming potential and [b] Cumulative energy demand

The mechanical treatment processes are scalable and could achieve higher production output volume [33]. They also restrict the use of acids or harmful chemicals. The degree of fibrillization of nano-scale cellulose by mechanical disintegrations processes is depended on number of passes and solid concentration in pulp slurry. The CNF manufactured by high pressure homogenizer had the width distribution range from few microns to 100 nm while passing 30 and 14 times through a refiner and a homogenizer. The maximum wood pulp slurry concentration processed for the production of CNF was 3% wt./v. Increasing the number of passes in homogenizer did not improve neither the width of CNF to nanoscale nor to uniform distribution level [34, 35].

The isolated CNC/ CNF were predominantly explored as reinforcement materials in biopolymer composites manufacturing. The biopolymer composite materials are emerging out as the most fascinating renewable materials for packaging products as they are abundantly available in nature and has comparable physical, mechanical, surface characteristics to fossil-based polymer materials in addition to the biodegradability [36]. The quality of CNF extracted are greatly dependent on the manufacturing methods adapted and the type of biomass resource used. The CNF manufactured from different biomass resources and by different manufacturing methods resulted

widespread distribution in width (3 to 90 nm) and length (200 to 500 nm). The variation fiber dimensional quality attributed inconsistent mechanical and physical properties of products produced from them [12]. The characteristics of CNF/CNC extracted from different biomass resources and by different manufacturing methods are listed in Table 2-2.

Table 2-2. The properties and manufacturing methods of CNF/CNC extracted from different biomass resources

Feed stock	**Feedstock cellulose (%)**	**Pre-treatment process**	**Main treatment process**	**Crystallinity (%)**	**TD[@] (°C)**	**YM[#] (GPa)**	**TS[$] (MPa)**	**CA[&] (°C)**	**W* (nm)**	**Ref**
Banana	96.8	2% caustic soda, Steam explosion	Oxalic acid hydrolysis & Sonication	83.8.	326	--	--	--	5~40	
Jute Fiber	97.3			89.3	338	--	--	--	--	[13]
Pine apple leaf fiber	97.3			88.6	338	--	--	--	--	
Pine apple peel	--	Sodium chloride & sodium hydroxide	Sulfuric acid hydrolysis.	61.19	351	--	2.24	--	15	[14]
Pine cone	44	Grinding. Alkaline treatment	HCl Hydrolysis. Mass collider	70	400	--	--	--	6~35	[15]
Wheat straw micro crystalline cellulose	--	--	Enzymatic hydrolysis & Ultrasonic treatment	60.37~87.46	310~360	--	--	--	5 ~ 8, 40~50	[16]
Wheat straw pulp	44.2	Isobutyl alcohol-H2o-KOH-hydrazine & acetic acid and hydrogen peroxide	Sulfuric acid hydrolysis & Ultrasound	76.3	240	11.45	42.3	--	10~40	[17]

		with sulfuric acid								
Kenaf core	95	Grinding, autoclaving with alkali and bleaching	Electron beam irradiation and acid hydrolysis	71	300	--	--	--	--	[18]
Sisal fibers		Boiling in toluene/ethanol. Agitation with NaOH and ethanol. Hydrogen peroxide bleaching	Sulfuric acid hydrolysis	75	255	--	--	--	9~22	[19]
Bamboo Pulp	--	Mechanical disintegrator	FeCl3 + glycerol Hydrolysis. Ultrasonic treatment	79.4	350	--	--	--	5	[20]
Acacia fiber	47	Sodium hydroxide and sodium sulfide. Bleaching Chlorine di oxide	Sulfuric Acid hydrolysis and sonication	79	--	--	--	--	5~10	[21]
Ground bagasse	--	Sodium hydroxyl solution	Microwave treatment with BmimCL solution and homogenization	60	280	--	--	--	10~20	[22]
Filter paper	--	--	Acid hydrolysis	80	--	--	--	--	--	[23]
Cotton Linter	76.91	--	Grinding. Sulfuric acid hydrolysis	90.45	350	--	--	23.2	12	[24]
Soft wood	77.6	Chlorite treatment	Enzymatic, TEMPO and	76.71	305	10.6	--	10.8	1~5	[25]

			Homogenizer							
Hard wood	79.3			77.13	320	4.6		17.7	1~15	
Tunicate	99.1	Alkali treatment		89.94	314	12.7		35.8	1~13	
Hard- and soft wood cellulose pulp	97	--	Disk refiner and homogenizer	--	--	2.8	80	--	10 ~25	[26]
Micro cellulose powder (MCC)	--	--	Sulfuric acid and ultrasonication	73	240	--	--	--	368	[27]
Soft wood pulp	--	--	Ball milling	70	--	--	--	--	--	[28]

[@] TD- Thermal degradation temperature, [#] YM-Young's modulus, [$]TS- Tensile strength, [&]CA- Contact angle, *W - Width

CNF/CNC reinforced biopolymer composites

The CNF/CNC reinforced biopolymer composites are the subject of focus among material researchers due to their excellent material properties such as stiffness, tensile strength, optical transparency, biocompatibility, nontoxic and the use of renewable resources [37]. The attractive mechanical properties of biopolymer-CNF composites are major technological breakthrough to consider them for packaging products [11, 38]. The biopolymers used in CNF composites are either directly extracted as polymeric chain from biomass or being synthesized from the monomers extracted from biomass. The natural polymer chain is present in animals and plants as proteins (macro molecules of amino acids bonded by peptide bonds) or as polysaccharides (macromolecules of monosaccharides bonded by glycosidic bonds) or as lipids (long chain hydrocarbon molecules containing a carboxylic acid moiety). The casein, gelatin, gluten, zein, soy protein isolate, chitosan and starch are some of the natural polymers used in the production of

packaging films. The biopolymers which are chemically synthesized from natural monomers behave as fossil based polymers called as synthetic biopolymers [39]. Some of the synthetic biopolymers used in packaging products are poly lactic acid (PLA), Polyhydroxyalkanoates (PHA) and Polyhydroxybutyrate (PHB).

CNF reinforced natural biopolymer composites

The CNF were reinforced in protein and polysaccharides natural polymers to manufacture bio-nanocomposites. The packaging films made of bio-nanocomposites showed improved mechanical and barrier properties. Initially, the native biopolymer packaging film manufacturing processes required plasticizer for the improvement of brittleness and percentage of elongation. The reinforcement of CNF with different percentages in biopolymer matrix increased the tensile and barrier properties of composite materials. The composite having suitable composition reinforcement materials were suggested for the packaging product productions. The mechanical and barriers properties of CNF reinforced natural polymer composites with different loading percentages are given in Table 2-3.

Table 2-3. Mechanical and barrier properties of natural polymer – CNF composites

Biopolymer Composite	**CNF Loading (%)**	**WVP** (g m /Pa h m^2)**	**TS$^{\$}$ (MPa)**	**YM$^{\#}$ (MPa)**	**Elongation (%)**	**Ref.**
Whey-CNF	5	3.5 x10^{-8}	4	100	10~27	[40]
Gelatin-CNF	5		100	5000	5	[41]
Sericin - CNF	10		28.2	805960	5	[42]
Gluten -CNF	8	8x 10^{-11}	5.4		285	[43]
SPI-CNF	20		31.19	1023	17	[44, 45]
SPI - CNC	6	1.6 x 10^{-10}	11		60	

Chitosan-CNF	10	1.12×10^{-8}	55.53	1424	8	[46]
Chitosan-CNC	20		120		6	[47]
Starch-CNF	20	$3.32 \pm 0.11 \times 10^{-7}$	57.35	19.88	80	[48]

**WVP- Water vapor permeability, # YM-Young's modulus, $TS- Tensile strength

The mechanical strength of CNF reinforced natural polymer composite films were very much comparable to fossil-based polypropylene (PP) and low-density polyethylene (LDPE) materials. Among many natural-CNF composites, chitosan was extensively studied due to their abundant availability and other advantages such as antimicrobial, bio degradation and bio compatibility characteristics [49, 50]. The films developed from chitosan-CNF composites, were found suitable for food and other general packaging application [51, 52]. However, the hydrophilic nature of CNF affected the dispersion ability of CNF in biopolymer matrix and reduced the barrier properties of films for CNF loading of 20% and more [53]. The hydration degree of chitosan composite films was affected by the hydrophilic nature chitosan and CNF and reduced the barrier properties [54]. The hydrophilic hydroxyl groups of chitosan and CNF were replaced with hydrophobic groups by physical and chemical reactions to improve the hydrophobicity of composites. In physical cellulose surface modification processes, the cations of the polyelectrolytes were adsorbed into a CNF surfaces [55]. In the chemical surface modification processes, the acyl groups (R-C=O) were primarily attached to the C6 hydroxyl group of glucose unit [56].

The hydrophobic nature of CNF films was enhanced using surface modified. Božič, Vivod et al. (2015), prepared films using CNF which hydroxyl groups which were modified by acetic

anhydride and reported the improvement in hydrophobicity of native CNF film [57]. Willberg-Keyriläinen et al. (2017), domonstrated the improvement in barrier and mechanical properties of CNF films, coated with celllulose esters which were manufacutred by fatty acid chloride [58]. Huang et al. (2017), synthesised the CNC esters from the mixture of trifluoroacetic anhydride and fatty acids such as capric acid, lauric acid and stearic acid and found that hydrophobicity and oxygen barrier properties were increased in comparison to untreated CNC films [59].

The composite films reinforced with surface modified CNF or cellulose nanocrystals (CNC) showed improved barrier properties. Abraham et al. (2016), developed epoxy nanocomposite films reinforced with surface modified CNC using acetic anhydride as surface modifier [60]. They observed the improvement in hydrophobicity and thermal stability of composite films. Similarly, Trinh and Mekonnen (2018) modified CNC surfaces using lauroyl chloride and reinforced in epoxy matrix phase material. An impressive improvement in tensile and hydrophobic characteristics of composite structure was reported [61].

The hydrophobicity of chitosan films was increased by modifying film surface with acid chloride and acid anhydrides. In this process, the acyl groups (R-C=O) of carboxylic acid derivatives were substituted in the amino group of glucosamine molecules to obtain hydrophobicity [62]. The manufacturing of composite films with surface modified CNC required two-step reaction process. In the first step, CNF / CNC surfaces will be modified by physical or chemical processes. Then the surface modified CNF/CNC will be reinforced with biopolymer to manufacture biopolymer composites. The acetic anhydride and pyridine were used as surface modifier and catalyst in CNF esterification process. They were classified as extremely danger hazardous chemicals by global harmonized system (GHS). The brief summary of hydrophobic composite development is outlined in Table 2-4.

Table 2-4. CNF/CNC surface modification processes performed for the improvement of biopolymer composite development

Nano cellulose resource	Reagents used	Catalyst used	Degree of substitution	Properties improved	Ref
Wood pulp	Acetic anhydride	iodine	2.18	Hydrophobicity, thermal stability, tensile strength of epoxy composite	[60]
Wood pulp	Acetic, butyric and hexanoic anhydrides	--	0.1~0.3	Antibacterial improvement of composite Material	[63]
Softwood bleached kraft pulp	Alkenyl succinic anhydride, N-Methyl-2-pyrrolidone	K_2CO_3	0.44	Mechanical properties	[64]
Wood pulp	Acyl chloride	pyridine	0.4~1.1	Thermal stability	[65]
Softwood pulp	Fatty acid chloride	Anhydrous pyridine	0.8~1.3	Water vapor / moisture barrier properties	[58]
Wood pulp	Canola oil fatty acid methyl ester	Potassium carbonate + MeOH	--	Hydrophobicity, Thermal stability	[66]
Pine	Palmitoyl chloride	--	0.01~0.14	Hydrophobicity	[67]
Cellulose sludge	Acetic anhydride	Amano lipase A	0.07~0.18	Hydrophobicity improvement in native CNF Film	[57]
Microcrystalline cellulose	Acetic anhydride	--	0.62-1.15	Compatibility of CNF with PLA	[68]
Microcrystal cellulose	Succinic anhydride	--	--	Thermal stability improvement of composite Material	[69]
Microcrystal cellulose	Trifluoroacetic anhydride, capric acid,	--	2.15	Thermal stability, hydrophobicity, TS of composite Material	[59]

	lauric acid & stearic acid				
Wood derived CNC	Acetyl chloride	Triethylamine	0.15	Hydrophobicity and dispersibility of CNC	[70]
	Acetic anhydride	Pyridine	0.35		
	Acetic acid	1’1-Carbonyldiimidazole	0.5		
	Acetic acid	Hydrochloric acid	0.01		
BiNFi-S cellulose	N,N-Dimethylacetamide (DMAc) & Maleic anhydride	--	0.155	Dispersibility and polymerizability	[71]
Spray dried cellulose nanocrystals	Lauroyl chloride	Pyridine	0.2,0.8,2.4	Hydrophobicity	[61]
Banana peel and bract	Acetic anhydride /Lauroyl chloride	H2SO4	2.18 and 2.43	Thermal stability	[72]
		DMAP	2.12 and 2.34		
Cotton linters	Acetic/ butyric / hexanoic/ valeric	Pyridine/ 4-dimethylaminopyridine / pyrrolidinopyridine	2.4	Compatibility of LDPE matrix	[73]
Cotton linters	3-mercaptopropionic acid & hexane	lipase	--	Thermal stability	[74]

CNF reinforced synthetic biopolymer composites

The bio-based polymers are synthesized from the monomers extracted from renewable resources. The renewable resources such as lactic acid and microorganisms or bacteria were used

for the extraction of monomers. Polyhydroxyalkanoates (PHA), Polyhydroxybutyrate (PHB) and Poly lactic acid (PLA) were the biopolymers synthesized from natural monomers and were used with CNF /CNC for the development of composite materials.

The PHA/PHB are natural thermoplastics synthesized from the monomers extracted from microorganism. They are manufactured in commercial scale for developing bio-based packaging films. Different types of nanomaterials such as CNF/CNC were used as reinforcement materials to develop them as potential materials for different product applications. These materials were found suitable for conventional plastic material processing methods [75]. The brief overview of mechanical properties of CNF reinforced bio-based polymer composite films developed are given in Table 2-5.

Table 2-5. Manufacturing methods and properties of PHB-CNF/CNC composites

Composite Composition	**Composite Production Method**	**TS[$] (MPa)**	**YM[#] (GPa)**	**WVP** ($gs^{-1}m^{-1}Pa^{-1}$)**	**Ref.**
PHB+ 2% CNC	Dissolved in PHB in N, N-Dimethylformamide (DMF) and sonicated with CNC. Cast and dried @ 80°C for 12h.	24	1.9	7.5×10^{-13}	[76]
PHB+ 4% CNC		25	2	1.1×10^{-12}	
PHB+ 6% CNC		28	2.4	7.7×10^{-13}	
PHBH[a]+ 0.5% CNF	Cast CNF film freeze at -30°C. Ground and mixed with PHBH granules. Extrusion of filament and 3D printing	18.0 ± 0.6	0.807 ± 0.074	--	[77]
PHBH+1% CNF		14.9 ± 0.7	0. 770 ±0.044		
PHBH+3% CNF		11.7 ± 1.5	0.681 ± 0.112		
PHBV [b]+ 1% CNF		37.81±0.28	0.586± 0.022	--	[78]

PHBV+ 2% CNF	Melt compounding with twin screw extruder	36.46±0.41	0.604± 0.023
PHBV+ 3% CNF		35.42±0.53	0.612± 0.025
PHBV+4% CNF		33.67±0.32	0.622± 0.017
PHBV+5% CNF		32.25±0.45	0.646± 0.022
PHBV+6% CNF		31.08±0.32	0.724± 0.0189
PHBV+7% CNF		29.11±0.39	0.793± 0.024
PHBV+ 1% CNC		37.36±0.65	0.586± 0.027
PHBV+ 2% CNC		36.34±0.5	0.604± 0.023
PHBV+ 3% CNC		35.85±0.64	0.612± 0.025
PHBV+4% CNC		34.64±0.6	0.622± 0.0168
PHBV+5% CNC		33.28±0.57	0.646± 0.022
PHBV+6% CNC		32.78±0.54	0.724± 0.019
PHBV+7% CNC		32.01±0.5	0.793± 0.024

[$]TS- Tensile strength, [#] YM-Young's modulus, **WVP- Water vapor permeability, [a]3-hydroxybutyrate-co-3hydroxyhexanoate and [b]3-hydroxybutyrate-co-3hydroxyvalerate

The PLA is a kind of bio-based polymers which possesses interesting mechanical properties, transparency and crystallinity and capability to process in conventional processing methods [79, 80]. In order to extend the application of PLA material to the wide range of product categories by increasing its toughness and barrier properties, it was reinforced with cellulose

nanofibrils (CNF) or cellulose nanocrystals (CNC) and manufactured as PLA-nanocellulose bio composites.

The CNF/CNC and PLA of PLA-nanocellulose bio composites are incompatible due to the hydrophilic and hydrophobic nature of CNF/CNC and PLA. The poor interfacial adhesion between CNF/CNC and PLA exhibited poor mechanical properties of their nanocomposites. One of the methods adopted to increase the interfacial adhesion of two constituent materials is blending CNF/CNC and PLA with the compatibilizers. Arjmandi et al. (2015) developed a hybrid composite material from PLA, CNC and montmorillonite (MMT). The highest tensile strength was observed for the composite with MMT of 4 parts per hundred of PLA and CNC of 1 part per hundred of PLA. The thermal stability of composite material was also improved due to the better dispersion of CNC and MMT in PLA matrix material [81].

Dhar et al. (2017), synthesized dicumyl peroxide coated PLA – CNC composites by reactive processing technique with different compatibilizers such as MMT, nanosilica, alumina, carbon nanofiber, coconut oil and olive oil. The thermomechanical properties of the composite films were improved with different compatibilizers whereas the oxygen and water vapor barrier properties were reduced to the extent of 20 – 65 % and 27 – 50 % respectively [82]. Meng et al. (2018), investigated the mechanical strength of PLA-CNF composites with epoxidized soybean oil. They found that the mechanical properties were increased 5 to 10-fold for the lower CNF loading percentage (10 w%) [83].

The CNF/CNC surfaces were also modified by different surface treatment processes such as monomer grafting, silylation, acetylation and esterification before reinforcing into PLA matrix phase. Raquez et al (2012), used CNC modified with trialkoxysilanes in their PLA-CNC composites and recorded the improvement in thermomechanical properties [84]. In Song et al.

(2014), research studies, the hydrophobic butyl acrylate was grafted into CNF by radical polymerization reaction and mixed with PLA to prepare composite by solvent casting method. The lowest water vapor transmission rate (WVTR) was observed for 1% CNF composite [85]. Robles et al. (2015) modified the CNF with 3-aminopropyltriethoxysilane by silylation process and CNC with dodecanoyl chloride by esterification process. The composite was prepared in twin screw extruder for reinforcement loading of 0.5, 1 and 2 %. The ductility of composite was decreased while reinforcing more crystalline material [86]. Chi et al. (2017) modified the CNC surface with environment friendly lauric arginate and fabricated the PLA-CNC composite film by solvent casting method. The surface modified CNC with loading percentage up to 5 increased the interfacial adhesion between CNC and PLA and also facilitated the better dispersion of CNC in PLA matrix phase [87]. The investigations on PLA-CNF composites are briefed in Table 2-6.

Table 2-6. Manufacturing methods and properties of PLA-CNF/CNC composites

Composite Composition	**Composite Production Method**	**TS[$] (MPa)**	**YM[#] (GPa)**	**EOB* (%)**	**WVP** × 10−11 (g/m S Pa)**	**Remarks**	**Ref.**
PLA	Acetylated CNF with acetic anhydride & acetic acid. Solvent cast film	15.24	1.17	40.3	1.87	5% CNF had rough surface due to reduced compatibility with bio polymer	[88]
PLA+1% CNF		16.7	1.13	64.8	2.01		
PLA+3% CNF		33.1	1.2	188.9	2.04		
PLA+5% CNF		30.5	2.12	14.6	2.5		
PLA	Acetylated CNC with anhydride acetic & pyridine. Solvent cast film	52.7	2.7	--	--	--	[89]
PLA+1% CNC		57.9	2.8				
PLA+2% CNC		60.1	2.9				
PLA+3% CNC		66.2	3.2				

PLA @25° C	CNF in N-methylmorpholine - N oxide solvent. Compression molding	48.2	--	21	--	Presence of CNF did not affect the crystallization	[90]
PLA+2% CNF @25° C		50.7		12			
PLA @45° C		25.5		480			
PLA+2% CNF @45° C		34.2		10			
PLA @55° C		8.2		640			
PLA+2% CNF @55° C		11.4		400			
PLA+2% CNF @25° C	Electro spun CNF in N-methyl morpholine - N oxide solvent and compression molding	46.3	--	17	--	--	[90]
PLA+20% CNF @25° C		54.1		6			
PLA	PLA -CNF casting and crushing. Extrusion and injection molding.	58.9	2.9	3.4	--	Comparable results with composite theoretical material model	[91]
PLA+1% CNF		63.1	3.3	2.8			
PLA+3% CNF		65.1	3.4	2.7			
PLA+5% CNF		71.2	3.6	2.7			

[$]TS- Tensile strength, [#] YM-Young's modulus, *Elongation at break& **WVP- Water vapor permeability

Environmental performance of biopolymers

The current concern on fossil resource depletion and environmental protection increased the attraction on biopolymers for packaging film production. The packaging films developed from polysaccharide-based biopolymers and their nanocellulose reinforced composites showed comparable material characteristics with fossil-based polymer materials such as low-density poly ethylene (LDPE) and polypropylene (PP) [93]. The environmental performance biopolymers are important while considering biopolymers as substitute materials for fossil-based polymer resin.

The evaluation of environmental impacts of biopolymer packaging films is the crucial pressure and growing interest among material researchers.

Many LCA studies were performed to assess environmental burdens created by polysaccharide-based biopolymers used for the manufacturing of packaging films. They were conducted to elaborate environmental impact of natural biopolymers such as cellulose nanofibrils (CNF), cellulose nanocrystals (CNC), chitosan and starch. Li et al. (2013) investigated the LCA of four different CNF manufacturing methods. They evaluated CNF manufacturing processes comprising tempo-oxidation & sonication, tempo oxidation & homogenization, chloroacetic acid etherification & sonication and chloroacetic etherification & homogenization. It was concluded that the CNF manufacturing method by tempo oxidation and homogenization treatment had the lowest environment impacts in terms of energy use and global warming potential. The chloroacetic etherification and tempo oxidation pretreatment processes contributed higher environmental impacts [31].

Arvidsson et al. (2015) investigated three manufacturing methods of CNF from wood pulp. The combination pretreatment and main treatment used for this study were enzymatic with micro fluidizer, carboxy methylation with microfluidizer and only main treatment by homogenizer. It was found from the study that the enzymatic manufacturing process had lower environmental impact and carboxy methylation had higher environmental impact due to the consumption of more solvent made from fossil resources [32].

Muñoz et al. (2018) investigated the LCA of chitosan and chitin manufactured from snow crab and shrimp shells in Europe and India. Their study revealed that the global warming potential (GWP) and water depletion were high in the Europe manufacturing plant where as the acidification and the eutrophication were high in Indian manufacturing plant [94]. Dinkel et al. (1996)

performed LCA of thermoplastic starch (TPS) polymers with a goal to compare the results with low-density polyethylene (LDPE) polymer. It was inferred from LCA study that TPS had better advantage while compared to LDPE in energy demand, GHG emissions, human toxicity and salinization except for eutrophication. The CED and GWP results of LCA studies on natural and bio-based polymers are briefed in Table 2-7.

Table 2-7. Cumulative energy demand (CED) and global warming potential (GWP) of bio-based polymers

Biopolymer	**CED (MJ/Kg of polymer)**	**GWP (kg CO_2 eq. /kg of polymer)**	**Remarks**	**Ref.**
CNF	14589	984	Bleached kraft pulp processed by Tempo Oxidation & Sonication processes	[31]
	3470	190	Bleached kraft pulp processed by Tempo Oxidation & Homogenizer processes	
	17352	1155	Bleached kraft pulp processed by Chloroacetic acid Etherification & Sonication processes	
	6481	364	Bleached kraft pulp processed by Chloroacetic acid Etherification & Homogenizer processes	
	107	0.905	Bleached kraft pulp processed by Enzymatic pretreatment & Microfluidizer treatment	[32]
	1992	101	Bleached kraft pulp processed by Carboxy Methylation & Microfluidizer	
	350	1.71	Bleached kraft pulp processed by No pretreatment & Homogenizer treatment	
	86	0.78	Unbleached kraft pulp processed by Enzymatic pretreatment & Microfluidizer treatment	
	1771	97.481	Unbleached kraft pulp processed by Carboxy Methylation & Microfluidizer	
	240	1.21	Unbleached kraft pulp processed by No pretreatment & Homogenizer treatment	

Chitosan-Resin	--	12.2	--	[94]
TPS - Film	29.3665	1.131	Waste Management: 80% incinerated and 20% landfilled	[95]
PHA - Resin by Fermentation	81	--	--	[96]
PHA - Resin Other processes	66~573	--	--	
PHA - Carrier bags	81	34	Environmental impact due to film production was ignored	[97]
PLA - Resin	54.1	2	PLA from Nature work was used by Cargill Dow LLC for study	[98]
PLA -Resin	54	3.45	Waste Management: Incineration	[96]

References

1. Lee, H.V., S.B.A. Hamid, and S.K. Zain, Conversion of Lignocellulosic Biomass to Nanocellulose: Structure and Chemical Process. The Scientific World Journal, 2014. 2014: p. 1-20.
2. Cowie, J., et al., Market projections of cellulose nanomaterial-enabled products--Part 2: Volume estimates. TAPPI JOURNAL, Volume 13 Number 6, 2014; pp. 57-69., 2014. 13(6): p. 57-69.
3. Wang, S., et al., Lignocellulosic biomass pyrolysis mechanism: a state-of-the-art review. Progress in Energy and Combustion Science, 2017. 62: p. 33-86.
4. Gardner, K.H. and J. Blackwell, The structure of native cellulose. Biopolymers, 1974. 13(10): p. 1975-2001.
5. Klemm, D., et al., Nanocelluloses: a new family of nature-based materials. Angewandte Chemie International Edition, 2011. 50(24): p. 5438-5466.
6. Moon, R.J., et al., Cellulose nanomaterials review: structure, properties and nanocomposites. Chemical Society Reviews, 2011. 40(7): p. 3941-3994.
7. Moon, R.J., G.T. Schueneman, and J. Simonsen, Overview of cellulose nanomaterials, their capabilities and applications. Jom, 2016. 68(9): p. 2383-2394.
8. Mott, L., L. Groom, and S. Shaler, Mechanical properties of individual southern pine fibers. Part II. Comparison of earlywood and latewood fibers with respect to tree height and juvenility. Wood and Fiber Science, 2007. 34(2): p. 221-237.
9. Islam, M.T., M.M. Alam, and M. Zoccola, Review on modification of nanocellulose for application in composites. Int J Innov Res Sci Eng Technol, 2013. 2(10): p. 5444-5451.

10. Abitbol, T., et al., Nanocellulose, a tiny fiber with huge applications. Current opinion in biotechnology, 2016. 39: p. 76-88.
11. Abdul Khalil, H.P.S., et al., A review on nanocellulosic fibres as new material for sustainable packaging: Process and applications. Renewable and Sustainable Energy Reviews, 2016. 64: p. 823-836.
12. Li, F., E. Mascheroni, and L. Piergiovanni, The potential of nanocellulose in the packaging field: a review. Packaging Technology and Science, 2015. 28(6): p. 475-508.
13. Abraham, E., et al., Extraction of nanocellulose fibrils from lignocellulosic fibres: A novel approach. Carbohydrate Polymers, 2011. 86(4): p. 1468-1475.
14. Dai, H., et al., Utilization of pineapple peel for production of nanocellulose and film application. Cellulose, 2018. 25(3): p. 1743-1756.
15. Rambabu, N., et al., Production of nanocellulose fibers from pinecone biomass: Evaluation and optimization of chemical and mechanical treatment conditions on mechanical properties of nanocellulose films. Industrial Crops and Products, 2016. 83: p. 746-754.
16. Cui, S., et al., Green preparation and characterization of size-controlled nanocrystalline cellulose via ultrasonic-assisted enzymatic hydrolysis. Industrial Crops and Products, 2016. 83: p. 346-352.
17. Barbash, V., O. Yaschenko, and O. Shniruk, Preparation and properties of nanocellulose from organosolv straw pulp. Nanoscale Research Letters, 2017. 12(1): p. 241.
18. Kim, D.-Y., et al., Preparation of nanocellulose from a kenaf core using E-beam irradiation and acid hydrolysis. Cellulose, 2016. 23(5): p. 3039-3049.

19. Morán, J.I., et al., Extraction of cellulose and preparation of nanocellulose from sisal fibers. Cellulose, 2008. 15(1): p. 149-159.

20. Lu, Q., et al., Preparation and characterization of cellulose nanocrystals via ultrasonication-assisted FeCl 3-catalyzed hydrolysis. Cellulose, 2014. 21(5): p. 3497-3506.

21. Jasmani, L. and S. Adnan, Preparation and characterization of nanocrystalline cellulose from Acacia mangium and its reinforcement potential. Carbohydrate Polymers, 2017. 161: p. 166-171.

22. Li, J., et al., Homogeneous isolation of nanocellulose from sugarcane bagasse by high pressure homogenization. Carbohydrate Polymers, 2012. 90(4): p. 1609-1613.

23. Lu, Z., et al., Preparation, characterization and optimization of nanocellulose whiskers by simultaneously ultrasonic wave and microwave assisted. Bioresource Technology, 2013. 146: p. 82-88.

24. Morais, J.P.S., et al., Extraction and characterization of nanocellulose structures from raw cotton linter. Carbohydrate Polymers, 2013. 91(1): p. 229-235.

25. Zhao, Y., et al., Cellulose Nanofibers from Softwood, Hardwood, and Tunicate: Preparation–Structure–Film Performance Interrelation. ACS Applied Materials & Interfaces, 2017. 9(15): p. 13508-13519.

26. Stelte, W. and A.R. Sanadi, Preparation and Characterization of Cellulose Nanofibers from Two Commercial Hardwood and Softwood Pulps. Industrial & Engineering Chemistry Research, 2009. 48(24): p. 11211-11219.

27. Tang, Y., et al., Preparation and characterization of nanocrystalline cellulose via low-intensity ultrasonic-assisted sulfuric acid hydrolysis. Cellulose, 2014. 21(1): p. 335-346.

28. Zhang, L., T. Tsuzuki, and X. Wang, Preparation of cellulose nanofiber from softwood pulp by ball milling. Cellulose, 2015. 22(3): p. 1729-1741.

29. Kerley MS, Allee GL (2003) Modifications in soybean seed composition to enhance animal feed use and value: Moving from a dietary ingredient to a functional dietary component. Ag Bio Forum 6(1,2):14–17.

30. Alle, M., et al., Recent trends in isolation of cellulose nanocrystals and nanofibrils from various forest wood and nonwood products and their application, in Nanomaterials for Agriculture and Forestry Applications. 2020, Elsevier. p. 41-80.

31. Li, Q., et al., Nanocellulose Life Cycle Assessment. ACS Sustainable Chemistry & Engineering, 2013. 1(8): p. 919-928.

32. Arvidsson, R., D. Nguyen, and M. Svanström, Life Cycle Assessment of Cellulose Nanofibrils Production by Mechanical Treatment and Two Different Pretreatment Processes. Environmental Science & Technology, 2015. 49(11): p. 6881-6890.

33. Nechyporchuk, O., M.N. Belgacem, and J. Bras, Production of cellulose nanofibrils: A review of recent advances. Industrial Crops and Products, 2016. 93: p. 2-25.

34. Iwamoto, S., et al., Optically transparent composites reinforced with plant fiber-based nanofibers. Applied Physics A, 2005. 81(6): p. 1109-1112.

35. Iwamoto, S., A.N. Nakagaito, and H. Yano, Nano-fibrillation of pulp fibers for the processing of transparent nanocomposites. Applied Physics A, 2007. 89(2): p. 461-466.

36. Ferrer, A., L. Pal, and M. Hubbe, Nanocellulose in packaging: Advances in barrier layer technologies. Industrial Crops and Products, 2017. 95: p. 574-582.

37. Hubbe, M.A., et al., Cellulosic nanocomposites: a review. BioResources, 2008. 3(3): p. 929-980.

38. Sangroniz, A., et al., Packaging materials with desired mechanical and barrier properties and full chemical recyclability. Nature Communications, 2019. 10(1).

39. Meraldo, A., 4 - Introduction to Bio-Based Polymers, in Multilayer Flexible Packaging (Second Edition), J.R. Wagner, Editor. 2016, William Andrew Publishing. p. 47-52.

40. Qazanfarzadeh, Z. and M. Kadivar, Properties of whey protein isolate nanocomposite films reinforced with nanocellulose isolated from oat husk. 2016. 91: p. 1134-1140.

41. Mondragon, G., et al., Bionanocomposites based on gelatin matrix and nanocellulose. 2015. 62: p. 1-9.

42. Kwak, H.W., et al., Facile and green fabrication of silk sericin films reinforced with bamboo-derived cellulose nanofibrils. Journal of Cleaner Production, 2018. 200: p. 1034-1042.

43. Rafieian, F., et al., Mechanical, thermal and barrier properties of nano-biocomposite based on gluten and carboxylated cellulose nanocrystals. 2014. 53: p. 282-288.

44. Han, Y., M. Yu, and L. Wang, Soy protein isolate nanocomposites reinforced with nanocellulose isolated from licorice residue: Water sensitivity and mechanical strength. Industrial Crops and Products, 2018. 117: p. 252-259.

45. Wang, Y., X. Cao, and L. Zhang, Effects of Cellulose Whiskers on Properties of Soy Protein Thermoplastics. 2006. 6(7): p. 524-531.

46. Azeredo, H.M.C., et al., Nanocellulose Reinforced Chitosan Composite Films as Affected by Nanofiller Loading and Plasticizer Content. 2010. 75(1): p. N1-N7.

47. Li, Q., J. Zhou, and L. Zhang, Structure and properties of the nanocomposite films of chitosan reinforced with cellulose whiskers. 2009. 47(11): p. 1069-1077.

48. Savadekar, N.R. and S.T. Mhaske, Synthesis of nano cellulose fibers and effect on thermoplastics starch based films. Carbohydrate Polymers, 2012. 89(1): p. 146-151.

49. Szymańska, E. and K. Winnicka, Stability of chitosan—a challenge for pharmaceutical and biomedical applications. Marine drugs, 2015. 13(4): p. 1819-1846.

50. Fernandes, S.C., et al., Novel materials based on chitosan and cellulose. 2011. 60(6): p. 875-882.

51. Dehnad, D., et al., Thermal and antimicrobial properties of chitosan–nanocellulose films for extending shelf life of ground meat. Carbohydrate Polymers, 2014. 109: p. 148-154.

52. Marín-Silva, D.A., S. Rivero, and A. Pinotti, Chitosan-based nanocomposite matrices: Development and characterization. International Journal of Biological Macromolecules, 2019. 123: p. 189-200.

53. Azeredo, H.M.C., et al., Nanocellulose Reinforced Chitosan Composite Films as Affected by Nanofiller Loading and Plasticizer Content. Journal of Food Science, 2010. 75(1): p. N1-N7.

54. Toivonen, M.S., et al., Water-Resistant, Transparent Hybrid Nanopaper by Physical Cross-Linking with Chitosan. Biomacromolecules, 2015. 16(3): p. 1062-1071.

55. Alila, S., et al., Adsorption of a Cationic Surfactant onto Cellulosic Fibers I. Surface Charge Effects. 2005. 21(18): p. 8106-8113.

56. Eyley, S. and W. Thielemans, Surface modification of cellulose nanocrystals. Nanoscale, 2014. 6(14): p. 7764-7779.

57. Božič, M., et al., New findings about the lipase acetylation of nanofibrillated cellulose using acetic anhydride as acyl donor. Carbohydrate Polymers, 2015. 125: p. 340-351.

58. Willberg-Keyriläinen, P., et al., Hydrophobization and smoothing of cellulose nanofibril films by cellulose ester coatings. Carbohydrate Polymers, 2017. 170: p. 160-165.

59. Huang, F., et al., Acylation of cellulose nanocrystals with acids/trifluoroacetic anhydride and properties of films from esters of CNCs. Carbohydrate Polymers, 2017. 155: p. 525-534.

60. Abraham, E., et al., Highly Modified Cellulose Nanocrystals and Formation of Epoxy-Nanocrystalline Cellulose (CNC) Nanocomposites. ACS Applied Materials & Interfaces, 2016. 8(41): p. 28086-28095.

61. Trinh, B.M. and T. Mekonnen, Hydrophobic esterification of cellulose nanocrystals for epoxy reinforcement. Polymer, 2018. 155: p. 64-74.

62. Tangpasuthadol, V., N. Pongchaisirikul, and V.P. Hoven, Surface modification of chitosan films. 2003. 338(9): p. 937-942.

63. Missoum, K., et al., Antibacterial activity and biodegradability assessment of chemically grafted nanofibrillated cellulose. Materials Science and Engineering: C, 2014. 45: p. 477-483.

64. Igarashi, Y., et al., Manufacturing process centered on dry-pulp direct kneading method opens a door for commercialization of cellulose nanofiber reinforced composites. Chemical Engineering Journal, 2018. 354: p. 563-568.

65. Agustin, M.B., F. Nakatsubo, and H. Yano, Improving the thermal stability of wood-based cellulose by esterification. Carbohydrate Polymers, 2018. 192: p. 28-36.

66. Wei, L., et al., Chemical modification of nanocellulose with canola oil fatty acid methyl ester. Carbohydrate polymers, 2017. 169: p. 108-116.

67. David, G., et al., Exploring the potential of gas-phase esterification to hydrophobize the surface of micrometric cellulose particles. European Polymer Journal, 2019. 115: p. 138-146.

68. Jamaluddin, N., et al., Surface modification of cellulose nanofiber using acid anhydride for poly (lactic acid) reinforcement. Materials Today Communications, 2019. 21: p. 100587.

69. Leszczyńska, A., et al., Thermal stability of cellulose nanocrystals prepared by succinic anhydride assisted hydrolysis. Thermochimica Acta, 2018. 663: p. 145-156.

70. Peng, S.X., et al., A comparative guide to controlled hydrophobization of cellulose nanocrystals via surface esterification. Cellulose, 2016. 23(3): p. 1825-1846.

71. Kobe, R., et al., Stretchable composite hydrogels incorporating modified cellulose nanofiber with dispersibility and polymerizability: Mechanical property control and nanofiber orientation. Polymer, 2016. 97: p. 480-486.

72. Harini, K., K. Ramya, and M. Sukumar, Extraction of nano cellulose fibers from the banana peel and bract for production of acetyl and lauroyl cellulose. Carbohydrate polymers, 2018. 201: p. 329-339.

73. Anžlovar, A., et al., Nanocomposites of LLDPE and surface-modified cellulose nanocrystals prepared by melt processing. Molecules, 2018. 23(7): p. 1782.

74. Ram, B. and G.S. Chauhan, New spherical nanocellulose and thiol-based adsorbent for rapid and selective removal of mercuric ions. Chemical Engineering Journal, 2018. 331: p. 587-596.

75. Bhardwaj, U., et al., Polyhydroxyalkanoates (PHA)-cellulose based nanobiocomposites for food packaging applications, in Food additives and packaging. 2014, ACS Publications. p. 275-314.

76. Seoane, I.T., et al., Development and characterization of bionanocomposites based on poly (3-hydroxybutyrate) and cellulose nanocrystals. 2016.

77. Valentini, F., et al., Polyhydroxyalkanoates/fibrillated nanocellulose composites for additive manufacturing. Journal of Polymers and the Environment, 2019. 27(6): p. 1333-1341.

78. Jun, D., et al., Crystallization and mechanical properties of reinforced PHBV composites using melt compounding: Effect of CNCs and CNFs. Carbohydrate polymers, 2017. 168: p. 255-262.

79. Castro-Aguirre, E., et al., Poly(lactic acid)—Mass production, processing, industrial applications, and end of life. Advanced Drug Delivery Reviews, 2016. 107: p. 333-366.

80. Lim, L.T., R. Auras, and M. Rubino, Processing technologies for poly(lactic acid). Progress in Polymer Science, 2008. 33(8): p. 820-852.

81. Arjmandi, R., et al., Partial replacement effect of montmorillonite with cellulose nanowhiskers on polylactic acid nanocomposites. 2015. 81: p. 91-99.

82. Dhar, P., et al., Reactive Extrusion of Polylactic Acid/Cellulose Nanocrystal Films for Food Packaging Applications: Influence of Filler Type on Thermomechanical, Rheological, and Barrier Properties. Industrial & Engineering Chemistry Research, 2017. 56(16): p. 4718-4735.

83. Meng, X., et al., Toughening of nanocelluose/PLA composites via bio-epoxy interaction: Mechanistic study. Materials & Design, 2018. 139: p. 188-197.

84. Raquez, J.M., et al., Surface-modification of cellulose nanowhiskers and their use as nanoreinforcers into polylactide: A sustainably-integrated approach. Composites Science and Technology, 2012. 72(5): p. 544-549.

85. Song, Z., H. Xiao, and Y. Zhao, Hydrophobic-modified nano-cellulose fiber/PLA biodegradable composites for lowering water vapor transmission rate (WVTR) of paper. Carbohydrate polymers, 2014. 111: p. 442-448.

86. Robles, E., et al., Surface-modified nano-cellulose as reinforcement in poly(lactic acid) to conform new composites. Industrial Crops and Products, 2015. 71: p. 44-53.

87. Chi, K. and J.M. Catchmark, Enhanced dispersion and interface compatibilization of crystalline nanocellulose in polylactide by surfactant adsorption. Cellulose, 2017. 24(11): p. 4845-4860.

88. Abdulkhani, A., et al., Preparation and characterization of modified cellulose nanofibers reinforced polylactic acid nanocomposite. Polymer Testing, 2014. 35: p. 73-79.

89. Lee, J.H., S.H. Park, and S.H. Kim, Surface modification of cellulose nanowhiskers and their reinforcing effect in polylactide. Macromolecular Research, 2014. 22(4): p. 424-430.

90. Kowalczyk, M., et al., Mechanical and thermal properties of PLA composites with cellulose nanofibers and standard size fibers. Composites Part A: Applied Science and Manufacturing, 2011. 42(10): p. 1509-1514.

91. Jonoobi, M., et al., Mechanical properties of cellulose nanofiber (CNF) reinforced polylactic acid (PLA) prepared by twin screw extrusion. Composites Science and Technology, 2010. 70(12): p. 1742-1747.

92. Bassas-Galià, M., Rediscovering Biopolymers, in Consequences of Microbial Interactions with Hydrocarbons, Oils, and Lipids: Production of Fuels and Chemicals, S.Y. Lee, Editor. 2017, Springer International Publishing: Cham. p. 529-550.

93. Luzi, F., et al., Bio- and Fossil-Based Polymeric Blends and Nanocomposites for Packaging: Structure–Property Relationship. Materials (Basel, Switzerland), 2019. 12(3): p. 471.

94. Muñoz, I., et al., Life cycle assessment of chitosan production in India and Europe. The International Journal of Life Cycle Assessment, 2018. 23(5): p. 1151-1160.

95. Dinkel, F., et al., Ökobilanz stärkehaltiger Kunststoffe (Nr. 271), B. Study prepared by CARBOTECH, for the Bundesamt für Umwelt und Landschaft (BUWAL), Bern, Switzerland, Editor. 1996.

96. Patel, M., et al., Environmental assessment of bio-based polymers and natural fibers. 2002, Utrecht University, Netherlands.

97. Yates, M.R. and C.Y. Barlow, Life cycle assessments of biodegradable, commercial biopolymers—A critical review. 2013. 78: p. 54-66.

98. Vink, E.T.H., et al., Applications of life cycle assessment to NatureWorks™ polylactide (PLA) production. Polymer Degradation and Stability, 2003. 80(3): p. 403-419.

CHAPTER 3

PRODUCTION AND CHARACTERIZATION OF HIGH SOLID CONTENT CELLULOSE NANOFIBRILS FROM PRETREATED FLUFF PULP[1]

[1] Prabaharan Graceraj Ponnusamy, Suraj Sharma and Sudhagar Mani. To be submitted to Cellulose.

Abstract

The increasing demand for cellulose nanofibrils to produce various bio-based products requires an efficient manufacturing process to produce consistent and acceptable quality. In this study, the methods to produce high solid content cellulose nanofibrils (CNF) from mechanical and mild alkaline treatments of fluff pulp by a high-pressure homogenizer were investigated. A combination of carboxymethylcellulose (CMC) dispersion-ball milling and NaOH swelling-ball milling processes were developed as pretreatment methods to effectively reduce the fiber dimensions before high-pressure homogenization. The cellulose slurry with three-fold higher concentration was processed in a homogenizer to produce up to 6% solid content CNF. The CNF had an average fibril width of 30 nm. A combination of NaOH swelling and 75 min ball milling treatment increased the CNF crystallinity by 12% with a slight increase in thermal stability. In conclusion, a mild NaOH treatment of short fibers increased the solid content with consistent quality CNF.

Keywords: Cellulose nanofibrils. Ball milling. Homogenization. Solid content. Crystallinity. Thermal stability

Introduction

Nanocellulose is the nanosized polysaccharides having both amorphous and crystalline cellulose comprised of D-glucose units linked by β-1, 4 glycosidic bonds. It is one of the promising nanomaterials for the development of bio-based and environment-friendly products due to its abundant availability, biocompatibility, biodegradability, and high material properties such as high aspect ratio, specific area, crystallinity, and tensile strength, and ability to form hydrogen bonding with other materials [1-5]. The surface modification and functionalization of nanocellulose have expanded its widespread application in various sectors of biomedical, pharmaceutical, food, packaging, electronics, and cosmetics [6-8]. Therefore, the market demand for nanocellulose has been increasing every year and is projected to be about 6 million metric tons [9]. Nanocellulose is produced in various forms and is often related to the source of biomass. Forest wood and plant biomass produce two types of nanocellulose: cellulose nanofibrils (CNF) and cellulose nanocrystals (CNC). In addition, the nanocellulose produced from the synthesis of bacterial microorganisms is bacterial cellulose (BC) often studied in the biomedical fields. The other forms of nanocellulose include tunicate cellulose nanocrystals (t-CNC) and algae cellulose particles (AC) which are isolated from tunicates and algal biomass [10, 11]

The most common types of nanocellulose are CNF and CNC and are predominantly produced from forest wood and plant biomass. CNF/CNCs exist as microfibril bundles in the cell walls of plants and wood. The microfibrils are connected by many strong interfibrillar hydrogen bonds to form cellulose macrofibres. Nanocellulose with 5 to 30 nm width and an aspect ratio greater than 50 are defined as CNF, and with rod-like structure, a width of 3 to 10 nm and aspect ratio less than 50 are defined as CNC according to the standard definition of nanomaterials by Technical Association of the Pulp and Paper Industry (TAPPI) [12]. A single micron-sized

cellulose fiber consists of numerous CNC and CNF. They are extracted from biomass resources by chemical, mechanical and enzymatic processes. The acid hydrolysis is most widely followed for the extraction of crystalline CNCs from delignified cellulose pulp and cotton fibers. However, the consumption of acids (64%) and low yield (~50%) poses a great challenge in the commercialization of CNC manufacturing process [13, 14].

The CNFs are manufactured from wood-based cellulose pulps through mechanical disintegration devices such as disc refiner, homogenizer, ball mill, microfluidizer, and ultrafine grinders [15-18]. The diluted cellulose pulp slurries were subjected to shear, impact, and cavitation pressure in mechanical processing units to break interfibrillar hydrogen bonds and to isolate nanostructured fibrils. The energy requirement of such processes varied from 12,000 to 70,000 kWh t^{-1}. In addition to high energy consumption, clogging and poor dispersibility of long fibers reduced the fibrilization efficiency mechanical process [19-23]. Moreover, the extracted CNFs showed widespread distribution in width (3 to 90 nm) and length (200 to 500 nm) [24]. To reduce the high energy consumption and to ease the fibrilization process, different chemical and mechanical pretreatment methods were investigated to produce CNF [25, 26]. The energy consumption of such manufacturing methods was reduced to the range of 1500 to 500 kWh t^{-1} [10]. However, the quality of isolated CNFs was inconsistent due to the poor dispersibility and agglomeration of cellulose in the input slurries.

The cellulose fibers from wood and plant-based resources are more prone to agglomeration and formation of network structure due to more unordered cellulose and cellulose Iα on fibril surface to make them stickier [27]. The agglomerated and network-structured cellulose fibers caused the clogging in the homogenizer valve and reduced fibrillation efficiency for increased cellulose concentration in the input slurry. The chemical pretreatment processes such as

chloroacetic acid etherification, carboxymethylation enzymatic hydrolysis, and TEMPO oxidation were studied to modify the surface and structure of cellulose for the improvement of fiber dispersibility during CNF isolation processes [28-30]. These processes consumed a considerable amount of hazardous chemicals and even led to low yield, and increased greenhouse gas emissions [31, 32].

The mechanical processes such as valley beater and PFI mill were also used to refine and improve dispersibility [23, 33]. The cellulose slurry with the concentration of 10 and 1.5 % was able to disperse in the PFI mill and Valley beater respectively. But, these pretreatment processes were not efficient in reducing fiber width and length [34]. The CNF fibrilization from lower concentration cellulose slurry and larger fiber width and length, increased the number of passes and clogging in a homogenizer and reduced the solid content percentage in CNF hydrogel. The CNF having fibril width of less than100 nm and 1% solid content was manufactured by passing cellulose slurry, 10 times through a grinder after processing 30 and 14 times in a refiner and homogenizer, respectively [35]. The CNF hydrogel with lower solid content increases bulk volume and causes transportation and handling issues. Moreover, the widespread distribution of fibril width attribute to inconsistent mechanical and physical properties of products produced from them [24]. Therefore, it is important to develop methods to produce highly dispersible, high solid content, and consistent quality CNFs for industrial applications.

The production of CNF was focused on mechanical fibrillation of long-fiber cellulose fibers into CNF [17, 23]. An earlier study by Lee and Mani (2016) found that the size reduction of fluff pulp by knife milling process not only reduced the fiber dimensions but also improved the fibrillation process to produce CNF. It was hypothesized that the use of short fibers will ease the mechanical fibrillation process and produce consistent quality CNF. A further reduction in fiber

dimension can be possible by the ball milling process and limited studies in the literature were investigated on the effect of ball milling of cellulose fibers on the production of CNF. In addition, the use of carboxymethylcellulose (CMC) as a dispersing agent to minimize fibril agglomeration was investigated and reported that the $-CH_2COO^-$ groups of anionic CMCs were adsorbed into cellulose fiber surface in the CMC dispersion process. More specifically, when CMC was added, the electrostatic repulsive force was induced between cellulose fibers to move them apart and exert uniformly distributed mechanical disintegration force on cellulose fibers [36, 37]. An alkaline treatment by low concentration (2%) sodium hydroxide (NaOH) was used to swell cellulose fibers before the fibrillation process and the resultant CNF exhibited improved thermal stability and dispersibility. The low cell-wall cohesion of swollen cellulose fibers improved the delamination and enabled ease isolation of fibril from bundles [10, 38, 39]. Therefore, the objectives of this study were to investigate the effects of ball milling in combination with CMC as a dispersing agent and NaOH as a swelling agent on high-pressure homogenization of fluff pulp and to determine the physical and mechanical properties of high-solid content CNFs.

Materials and methods

Materials

The cellulose powder for our study was manufactured from fluff pulp manufactured from forest biomass and was procured from a commercial paper mill in Georgia, U.S.A. The dried pulp size was reduced using the laboratory heavy-duty knife mill (Retsch SM 2000, Germany) with a 0.25 mm screen and three grinding passes. The three-pass shear cut cellulose powder was dried in an oven for 24 hours and was used as a feedstock for this study. Sodium carboxymethyl cellulose (CMC) (molecular weight (M.W) ~250,000 and degree of substitution 0.9) supplied by Sigma Aldrich was used as a dispersing agent and reagent grade sodium hydroxide (NaOH) in the form

of beads, purchased from Amresco was used as a swelling agent. A standard CNF produced by the University of Maine was purchased and used as a reference sample (Ref.).

CNF Production

The CNFs were fibrillated from three-pass knife milled fluff pulp by the combination of pretreatment methods and high-pressure homogenization process as shown in the Figure 3-1.

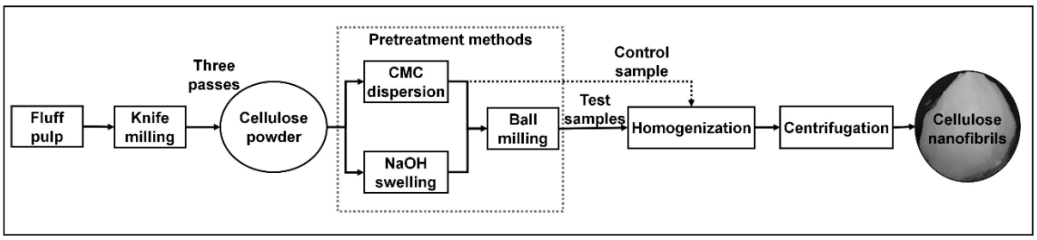

Figure 3-1. CNF production from pretreated cellulose powder

Pretreatment of knife milled cellulose

The fluff pulp was knife milled to produce cellulose powder and was treated by two different pretreatment methods namely CMC dispersion and NaOH swelling treatment followed by ball milling at various milling time to produce high-solid CNF in a high-pressure homogenizer. For CMC dispersion treatment, the 10% (w/v) of cellulose slurry in deionized water (DI) was prepared from knife-milled cellulose powder by mixing with 2% (w/w) CMC and heated at 80°C for 2h in a hot plate magnetic stirrer plate. The CMC dispersed cellulose slurry was treated in a vibratory ball mill (Retsch GmbH, Germany) with a 50 ml mill-jar and a 25 mm diameter stainless-steel ball. The high impact and shear forces by the vibratory motion of mill-jar and ball broke the hydrogen bonds between the cellulose fibers reduced their dimensions. About 10 g of CMC treated cellulose slurry was taken in the mill-jar along with ball and processed at 20 Hz vibration frequency and at various ball milling time as shown in the Table 3-1. After each treatment, the slurry samples were collected and stored at 4° C in a container for homogenization process. The CMC treated

sample without ball milling was chosen as a control sample. For NaOH treatment, the 10% (w/v) cellulose slurry was prepared from the cellulose powder and was soaked with 2% (w/v) NaOH aqueous solutions at 4°C for 24h. The swollen cellulose was neutralized with acetic acid and washed in DI water to remove excess NaOH as similar to the procedure described by Lee et al., (2016). The neutralized cellulose slurry was ball milled at various ball milling time as listed in the Table 3-1.

Table 3-1. Experimental plan for different pretreatment conditions

Sample ID	Dispersion / swelling agents	Ball mill treatment time (min)	Remarks
0MC	2% CMC (w/w of knife milled cellulose powder)	0	Control sample
15MC		15	Type 1-test samples
45MC		45	
75MC		75	
15MN	2% NaOH in aqueous solution	15	Type 2-test samples
45MN		45	
75MN		75	

CNF fibrilization process

The CNFs were primarily fibrillated from cellulose slurries at high-pressure homogenizer (APV-1000, SPXFLOW, U.S.A). The cellulose slurries were homogenized at 700 bar pressure. A positive displacement pump in the homogenizer circulated the cellulose slurry through a ceramic homogenizer valve at high pressure. The strong turbulence and cavity pressure generated at the homogenizer valve disrupted the intra and inter molecular hydrogen bonds of micro cellulose fiber bundles and fibrillated CNF. The 1% (w/v) CMC dispersed cellulose slurry was processed in a

high-pressure homogenizer to complete the manufacturing of CNF control samples. While increasing the cellulose concentration beyond 1% in control CNF sample production, the entangled fiber networks caused the clogging in homogenizer valve and prevented the CNF fibrilization. The cellulose slurry with 3% (w/v) concentration was able to process in the homogenizer for the test CNF sample production after CMC dispersion-ball milling and NaOH swelling-ball milling pretreatments. The pretreatment processes reduced the fiber dimensions and improved the dispersibility of cellulose fibers to increase the cellulose concentration to 3% (w/v) in the production of test CNF samples. The control and test sample input slurries were passed seven times to obtain stable CNF hydrogel. The initial temperature of cellulose slurry was 25° C and reached 80° C during the completion of homogenization processes. Three CNF replications were prepared from control and test type samples by homogenization treatments. Finally, all homogenized samples were centrifuged (5430 R Centrifuge, Eppendorf, Germany) at 6000 rpm at room temperature for 20 min to remove excess water from CNF hydrogel. The CNF samples were stored in a refrigerator at 4° C before using it for the characterization studies.

Optical microscope imaging

The dimensions of control and ball mill pretreated cellulose slurries were measured on DMLS2 optical microscope (Leica Microsystems, Germany). The samples were suspended in distilled water with 0.2% concentration and a drop was placed between the glass slide and coverslip. The images were captured for the magnification-20x, gain-1.0, and exposure time-100 ms. The length and width of fibers were measured using ImageJ software for analysis (Nechyporchuk et al. 2015; Vanderghem et al. 2012).

Total Solid content

The total solid content of the CNF was determined by drying the CNF samples in a convection oven. The oven temperature was set at 100 ± 5 °C. A known amount of CNF sample was weighed (W_i) and dried in the oven for about 12 hrs or until no change in the dried sample weight. The dried CNF sample was taken out and weighed (W_f) to determine the total solid content using the following equation. Each test was repeated three times.

$$Total\ solid\ content\ percentage = \frac{W_f}{W_i} \times 100$$

$Where$

$W_f = Weight\ of\ CNF\ sample\ after\ drying$

$W_i = Weight\ of\ CNF\ sample\ before\ dryiing$

Zeta potential

The Zeta potential values of CNF samples were determined by the electrophoretic light scattering (ELS) technique employed in the NanoBrook 90Plus zeta instrument (Brookhaven Instruments Corporation, U.S.A). A solid-state laser with 35 mW and 660 nm wavelength was used as a light source. The CNF sample suspension with 0.1 wt.% concentration was used for the measurement of 5 sequential readings with four replications.

Fourier-transformed infrared spectra (FTIR)

The chemical structure of CNF samples was characterized by FTIR spectra. The CNF films were manufactured by the film casting method and dried in a desiccator for 24 h before FTIR spectra measurements. The FTIR spectra for each sample were collected in absorbance mode using a Nicolet 6700 VariGATRTM spectrometer (Thermo Electron Corporation, U.S.A.). The CNF films were scanned with a resolution of 4 cm^{-1} in the range of wavenumbers from 4000 to 600 cm^{-1} and each test was triplicated.

X-ray diffraction (XRD)

The crystalline structure of CNF samples was studied by the D8 Advance model XRD system (Bruker, U.S.A) having X-ray source-Co tube and wavelength-1.79037 Å. The system was operated at 35kV voltage and 40mA amperage. Three replications from each sample were analyzed for diffraction angle (2θ) in the range of 10 to 40° and with the rate of 6°/min. The crystallinity index (CI) was calculated from crystalline peaks corresponding to the crystalline and amorphous regions as defined by International Center for Diffraction Data (ICDD) and using the following relationship for three replications.

$$CI = \frac{I_{0\,0\,2} - I_{am}}{I_{0\,0\,2}} \times 100 \ldots\ldots\ldots\ldots (1)$$

$I_{0\,0\,2} = Peak\ intensity\ corresponding\ to\ crystalline\ region\ for\ 2\theta\ between\ 26°\ and\ 27°$

$I_{am} = Peak\ intensity\ corresponding\ to\ amorphos\ region\ for\ 2\theta\ between\ 21°\ and\ 22°$

Scanning electron microscope (SEM) imaging

The SEM images of CNF films were used to determine the width distribution of CNF samples manufactured. The CNF films were coated with gold-palladium in Leica Mikrosysteme GmbH sputtering unit (coating thickness: 15 nm). The images were obtained from Thermo Fisher Scientific (FEI) Teneo (Thermo Fisher Scientific, Hillsboro, OR, USA), a field emission scanning electron microscope with an accelerating voltage of 5kV and spot size of 8 nm for three replications.

Thermal degradation analysis

The thermogravimetric analysis (TGA) was performed to study the thermal degradation behavior of CNF samples. The SDTA851e thermogravimetric analyzer (Mettler Toledo, U.S.A.) and STARe data analysis software were used to determine the thermal degradation temperature of

each sample. The CNF samples were heated in the range of 25 to 600 °C with a rate of 10 °C/min under an inert atmosphere of nitrogen and with a gas flow of 50 mL/min. The sample mass between 5 to 9 g was used.

Tensile test

The tensile properties of CNF films were determined by the film cast method. The dried CNF films were conditioned at 23° C and 50% RH for 24 h in a desiccator before tensile testing. The tensile tests were performed according to the ASTM D882 (Standard Test Method for Tensile Properties of Thin Plastic Sheeting). Five replications from each CNF sample were tested. A AGS-X tensile tester (Shimadzu, Japan) with a 1 kN load cell was used at 50 mm/min crosshead speed. The tests were performed at ambient temperature. The ultimate tensile strength and Young's modulus were recorded for the analysis.

Statistical analysis

The effect of ball milling time on fiber dimension reduction, solid content percentage, and fibril width was studied by the one-way ANOVA method. The multiple comparison method was also performed to determine which sample mean was different from others. The MATLAB software was used for statistical analysis and tests were conducted for the significance level of 5%.

Results and discussion

Effects of pretreatment on cellulose fiber dimensions

The untreated and pretreated knife-milled cellulose powder sample images were captured using the optical microscope to measure the fiber dimensions. The untreated knife-milled cellulose powder had an average fiber width of 32.60 ± 5.80 µm and length of 308.52 ± 200.91 µm. The increase in ball milling time reduced the fiber dimensions with CMC and NaOH treatment as

shown in Figure 3-2a and 3-2b. When CMC was used as a dispersing agent to prevent fiber agglomeration, the increase in ball milling time gradually reduced the fiber dimensions. An extensive reduction in fiber dimension was achieved at the ball milling time of 75 min when treated with CMC. On the other hand, when the cellulose fibers were treated with 2% NaOH as a swelling agent, there was a drastic change in the fiber dimension at the initial ball milling time of 15 min. A further increase in ball milling time did not substantially change the fiber dimensions. During ball milling, the collision of ball media on the treated cellulose fibers exerted repeated impact and shear load on them [40]. The continuous impact on cellulose fibers by the ball and mill-jar wall transferred kinetic energy to weak and break off hydrogen bonding and caused the reduction in fiber dimensions [18]. In overall, a combination of NaOH treatment with 15 min ball milling was effective in reducing the fiber dimensions before homogenization. The treatments of cellulose fiber by CMC dispersion/NaOH swelling along with ball milling reduced the fiber dimensions (width and length) up to 80% from the original dimensions.

The one-way ANOVA test showed that there was a significant reduction in cellulose fiber dimensions by the combination of dispersing/swelling agent (CMC/NaOH) and ball milling pretreatment methods (See supplementary document - Table 3-S1 and 3-S2). The multiple comparison test on the cellulose fiber dimensions of control and ball-milled samples was significantly different from the control sample (see the supplementary document – Figure 3-S1 and 3-S2). The mean fiber length of pretreated samples was significantly different among all combinations of pretreatment except for the 15MC sample (CMC dispersed and 15min ball milled). The CMC dispersion in the pretreatment process did not significantly change the mean width for 15- and 45-min ball milling times. Whereas, there was a significant reduction in the mean length of CMC dispersed slurries at all milling time. The hydrogen bonds of cellulose networks

were mainly affected by ball mill treatment in the CMC dispersion–ball milling pretreatment process. The swelling of cellulose fiber with NaOH followed by 15 min ball milling significantly reduced the fiber length. The cell wall reduction by NaOH swelling made the cellulose fibers more susceptible to weaken the intramolecular hydrogen bonds and to reduce width and length even for lower ball milling time. Most cellulose fiber bundles were cleaved by ball milling impacts as shown in Figure 3-2c. and 3-2d to enable efficient dimensional reduction.

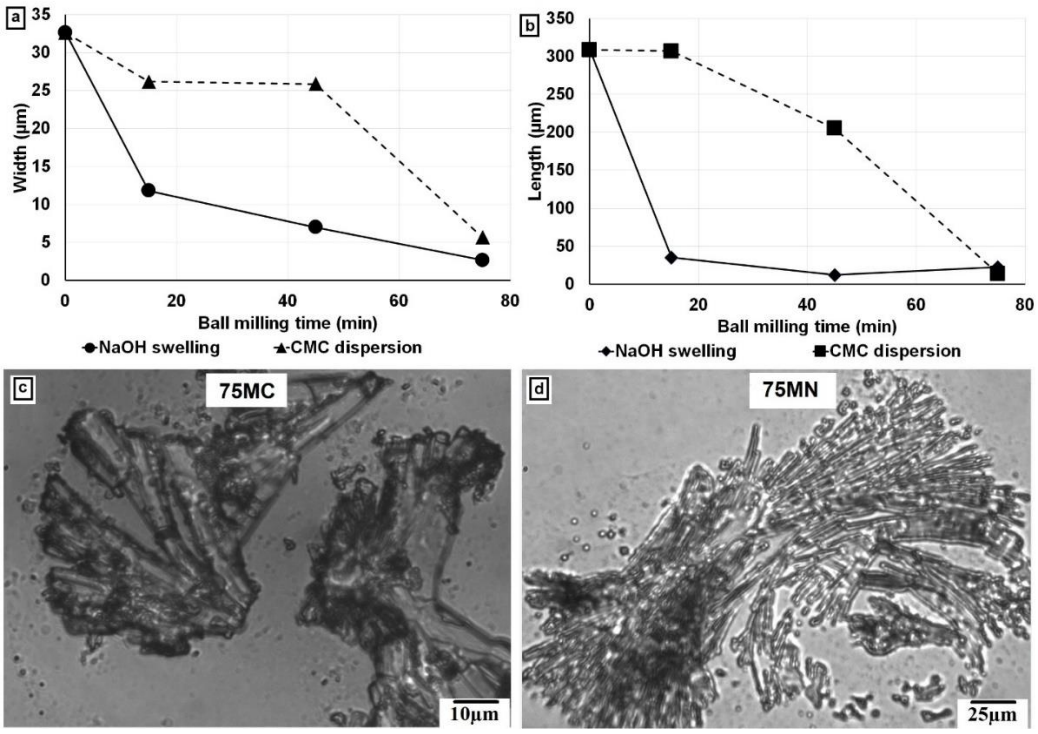

Figure 3-2. Fiber dimensions and optical microscope images of ball mill treated cellulose fibers. a) Comparison of cellulose fiber width with respect to different pretreatment conditions. b) Comparison of cellulose fiber length with respect to different pretreatment conditions. c) Optical microscope image of a cellulose fiber after CMC dispersion-75 min ball milling pretreatment. d) Optical microscope image of a cellulose fiber after NaOH swelling-75 min ball milling pretreatment.

Effects of pretreatment methods on the homogenization of cellulose fibers.

The refined CNFs were mainly fibrillated in a high-pressure homogenizer from pretreated cellulose slurries. The pretreatment processes determined the concentration of knife-milled cellulose slurries input to the homogenizer. The 1% knife-milled cellulose slurries with NaOH

treatment and without ball milling was not able to be processed in homogenizer. The swollen cellulose fibers which had poor dispersion abilities in slurry, clogged the homogenizer valve assembly. However, the CMC dispersed cellulose slurry without ball mill pretreatment (control sample), was able to process with a maximum concentration of 1%. Increasing the concentration of cellulose input slurry more than 1% resulted in pressure fluctuation and clogging of fibers in the homogenizer valve. The CMC dispersion-ball milling and NaOH swelling-ball milling pretreatment processes reduced fiber dimensions and thereby increased the dispersibility to enable the processing of 3% concentration cellulose slurries in a homogenizer for the production of test CNF samples. The turbulence, shear, and cavitation pressure exerted on cellulose fibers effectively fibrillated CNF in the homogenizer. While increasing slurry concentration beyond 3% concentration, the pumping ability of homogenizer decreased and CNF fibrilization reduced after few passes for the all test samples. It was observed that the increases in ball mill time from 15 min to 75 min did not play a significant influence in increasing the input slurry concentration beyond 3%.

The homogenized CNF samples were centrifuged to remove unattached free water in the CNF hydrogel and tested for solid content percentage (Table 3-2). The control sample (0MC) resulted with 4% solid content. The low cellulose concentration (1%) input slurry improved the dispersibility and avoided clogging during homogenization and resulted 4% solid content in control sample. The reduced fiber dimensions by the pretreatment methods played key role in increasing the solid content percentage in the CNF test samples. The CNF samples manufactured from CMC dispersion-15 min ball milling (15MC) and CMC dispersion-45 min ball milling (45MC) pretreatment methods resulted in 4% hydrogel after centrifuge as similar to control sample due to the minimal reduction (~20%) in fiber dimensions by pretreatment processes. The solid

content percentage of the CNF sample which was manufactured by CMC dispersion-75 min ball milling pretreatment (75MC) was increased to 6%, because of the substantial reduction (~80%) in fibers dimensions by the pretreatment method. The NaOH swelling-ball milling pretreated sample also showed a distinct solid content percentage than the control sample. The CNFs which were manufactured by NaOH swelling-15 min ball milling (15MN) and NaOH swelling-45 min ball milling (45MN) pretreatment method had 5% solid content as the pretreatment processes reduced the fibers dimensions more than 60% while compared to the control samples. The maximum solid content of 6% was found in CNF manufactured from NaOH swelling-75 min ball mill treated slurries (75MN) with fibers of ~ 80% reduced dimensions than the control sample.

The one-way ANOVA test also confirmed the significant difference in solid content percentage due to the different pretreatment methods (Table 3-S3). Further, the multiple comparison test showed that the mean solid content percentage of samples manufactured by control sample (0MC), CMC dispersion-15min ball milling (15MC), and CMC dispersion-45min ball milling (45MC) pretreatment methods were significantly different from the rest of the samples (75MC, 15MN, 45MN and 75MN) (Figure 3-S3). The reduced fiber length in 75MC, 15MN, 45MN, and 75MN samples decreased the entangled structure of CNF and reduced the water holding capacity of hydrogel [41-43].

Dispersion stability

The dispersion stability of CNF depends on the surface charge density of CNF emulsion. The strong repulsive forces would be generated by electric charges of CNF emulsion in water to prevent agglomeration [44, 45]. The surface charges of CNF samples were reported by zeta potential measurements. The nanocellulose suspension is stable while the absolute zeta potential value is greater than 15mV [46, 47]. The observed mean zeta potentials of Ref. and manufactured

CNF samples are presented in Table 3-2. The mean zeta potential values of CNF manufactured were close to -30 mV and were 60% higher than the Ref. sample. The higher electric charges of the cellulose chains indicated the higher Coulomb force between cellulose molecules. The higher repulsive forces between cellulose molecules prevented the agglomeration and improved the dispersion stability. When the zeta potential values are higher than the absolute value of 15 mV, the CNF suspensions in an aqueous solution were considered stable. The dispersion of cellulose in water is due to the interaction of cellulose chains and water molecules through electrostatic forces. The electrostatic forces appear between hydrogen atoms with δ+ charge and a cellulose chain carrying δ- charge [44, 48]. The one-way ANOVA statistical test was conducted on zeta potential data of manufactured CNF samples and Ref. sample. The test showed a significant difference between the mean value of CNF samples (Table 3-S4). Further, it was found from the pairwise multiple comparison test that sample means of CNFs which were manufactured by CMC dispersion-ball milling and NaOH swelling-ball milling were significantly different from the mean value of control and Ref. sample (Figure 3-S4). The CNF isolation processes with the pretreatment processes reduced fiber dimensions and increased the surface area. The increased surface area of pretreated CNF samples resulted higher surface charges than the control and Ref. samples. The CMC dispersion-ball milling and NaOH swelling-ball milling pretreatments along with high-pressure homogenization effectively controlled the CNF fibrilization with minimal variations in fibril dimensions to exhibit higher zeta potential.

Table 3-2. Solid content and zeta potential of manufactured and Ref. CNF samples

Sample ID	0MC	15MC	45MC	75MC	15MN	45MN	75MN	Ref
Solid content (%)	4±0.5	4±0.1	4±0.3	6±0.2	5±0.6	5±0.5	6±0.7	3±1.0
Zeta potential (mV)	29±1.5	29±1.8	30±3.7	30±2.6	31±2.8	32±2.0	29±3.0	18±1.5

FTIR analysis

The chemical structure of CNF was verified by Fourier-transformed infrared (FTIR) spectroscopy. The spectra of CNF samples manufactured by different treatment plans and Ref. samples are shown in Figure 3-3. There was no significant change between FTIR spectra of CNF samples manufactured. Further, the absorbance intensity peaks of all manufactured CNF were the same as peaks of cellulose reported in the literature and the Ref. sample [49-51]. The combination of CMC/NaOH and ball milling pretreatment and main homogenization treatment did not produce any new chemical bonds or cellulose derivatives. It helped to liberate fibrils with reduced dimension by breaking the inter and intramolecular hydrogen bonds as reported by Nuruddin et al. 2016 [52].

The characteristics peak with a broad region between 3,500 – 3,200 cm^{-1} corresponded to O-H groups' stretching vibrations. The stretching frequency at 2899 cm^{-1} was due to -CH groups. The mild peak around 1646 cm^{-1} frequency was attributed to the bending of -OH groups in absorbed water. The spectra peak of -CH_2- and -C-H groups were indicated by 1430 and 1320 cm^{-1} vibration frequencies [49-51]. The vibration frequencies of C-O stretching and C-OH have appeared in spectra at 1151 and 1112 cm^{-1}. The peak at 1043 and 896 cm^{-1} were attributed to C-

O-C skeletal vibration of pyranose rings and the deformation of β-glycosidic linkages respectively [53].

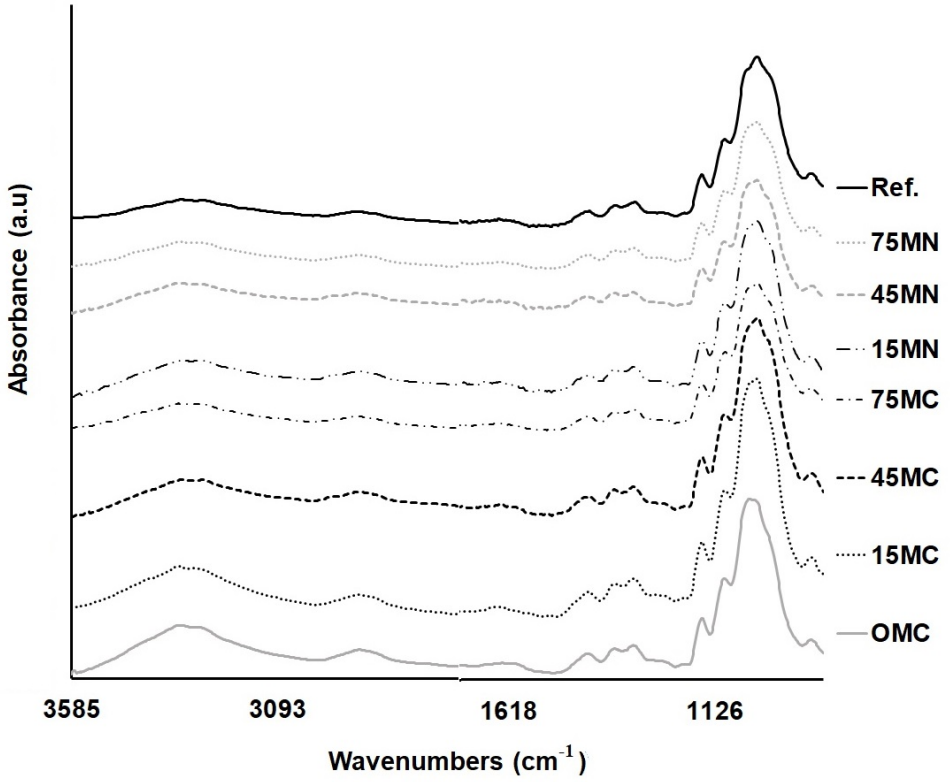

Figure 3-3. FTIR spectra of CNF manufactured by different treatment methods

Crystalline structure

The crystallinity of CNF samples was studied from X-ray diffractograms and crystallinity index. The X-ray diffractograms of CNF samples are shown in Figure 3-4. It shows the peaks at 2θ = 17 to 18° and 26 to 27° corresponding to cellulose crystallographic planes 1 0 1 and 0 0 2 defined by International Center for Diffraction Data – ICDD [54]. It also implies that the cellulose type I was not changed into type II allomorph by any of the treatment processes.

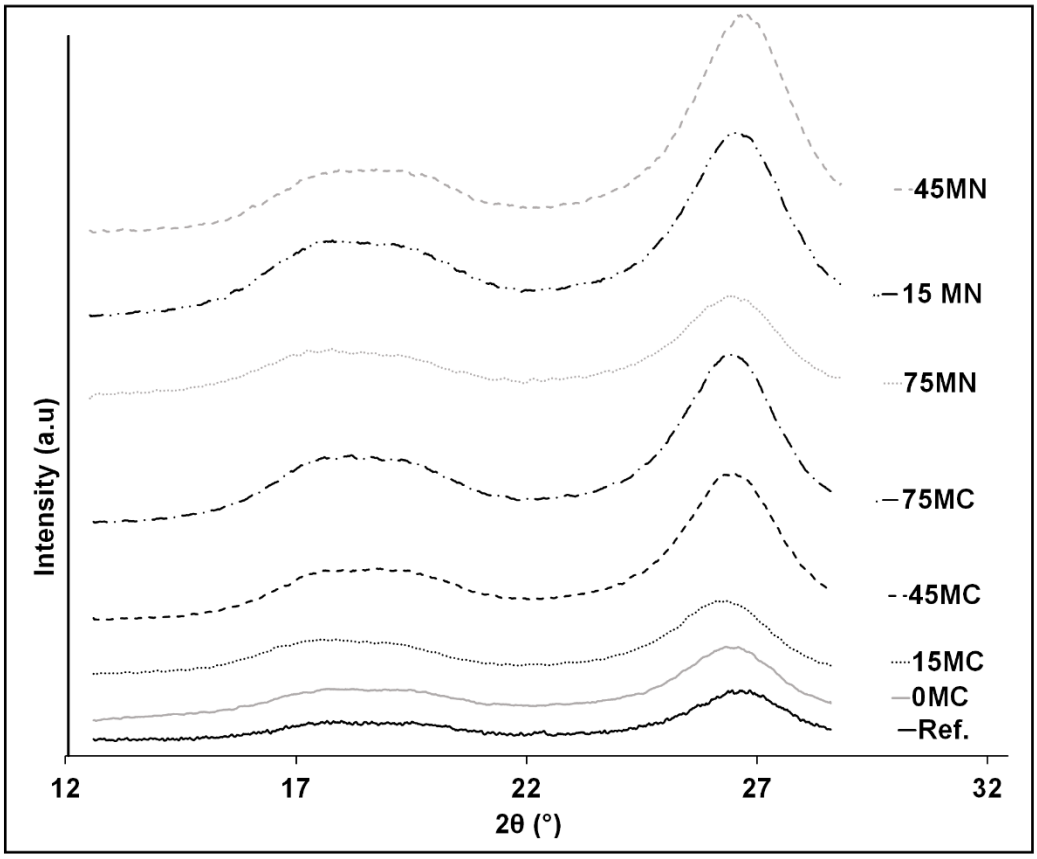

Figure 3-4. XRD curves of CNF manufactured by different treatment methods

The one-way ANOVA and multiple comparison tests inferred no difference in the mean crystallinity index of manufactured and Ref. CNF samples (Table and Figure 3-S5). The crystallinity of ~ 72 % was observed in control (0MC), Ref. and CMC dispersion-15, and 45 min ball mill pretreated CNF samples (15MC and 45MC). It further increased by 4% for 75 min ball milled sample (75MC). The impact and shear load applied over cellulose fibers were utilized during 75 min ball treatment to isolate fibers from the bundle and reduce amorphous regions without affecting the crystalline region as reported in the literature [18, 52, 55]. The NaOH treated samples showed slightly higher crystallinity than the CMC dispersed samples. The crystallinity was about 2 and 11% more for 15- and 45-min ball mill pretreated samples (15MN and 45MN) compared to the control sample. The NaOH swelling and ball milling processes decreased the surface amorphous regions of cellulose during the cell wall rupturing of the CNF fibrilization and

marginally increased the CI. The CI of NaOH swelling-75 min ball milling pretreated (75MN) sample was marginally less (2%) than the control sample. The NaOH and ball milling treatments disrupted only inter-fibrillar amorphous regions. However, the crystallinity was decreased by 2% while subjected to NaOH swelling-75 min ball milling pretreatment (75MN). The high ball mill time disrupted the crystalline plane and increased the amorphous regions of NaOH swollen cellulose fibers for the ball milling time of 75 min [39, 56]. The crystalline regions of the cellulose were affected by high shear and frictional forces of increased ball milling time and reduced crystallinity [57, 58].

Morphological Structure

The SEM images of CNF film samples were used to estimate the average width of cellulose fibrils as shown in Figure 3-5. A strong cellulose microstructure network with entangled fibrils was observed in the SEM images. The surface morphology of the fibrils was smooth in all the samples. The CMC dispersion, NaOH swelling and ball milling treatments affected the CNF fibril width. The control CNF sample (0MC) had an average fibrils width of about 43±19 nm. The average width of fibrils in 15MC and 45MC was between 20 to 30 nm and in 75MC, 15MN, 45MN and 75MN less than 20 nm fibril width. The reduction of cellulose fiber width and length to less than ~5 and 50 μm by pretreatment processes resulted smaller fibril width in 75MC, 15MN, 45MN and 75MN CNF samples.

A one-way ANOVA analysis of fibril width on various pretreatment methods indicated that there was significant difference between the treated and the control CNF samples (see appendix -Table S6). It was also found from multiple comparison tests that the group mean of fibril width isolated with pretreatment processes was significantly different from the control and Ref. sample. The group mean of fibril width in CNF samples-15MC and 45 MC were also

significantly different from rest of the samples (see appendix -Fig. 3-S6). The multi-comparison analysis confirmed that the reduction in fibril dimension by pretreatment processes such as CMC dispersion, NaOH swelling, and ball milling could significantly influence CNF fibril width. The impact and shear forces on cellulose fibers by the collision of balls broke the inter and intra molecular hydrogen bonds and reduced their dimensions in pretreatment processes. The consecutive pressurized flow of pretreated cellulose through nozzle ruptured the cell wall of the micro fibril bundles and liberated nanostructured fibrils of less than 30 nm in CNF isolation process at high-pressure homogenizer [59-61].

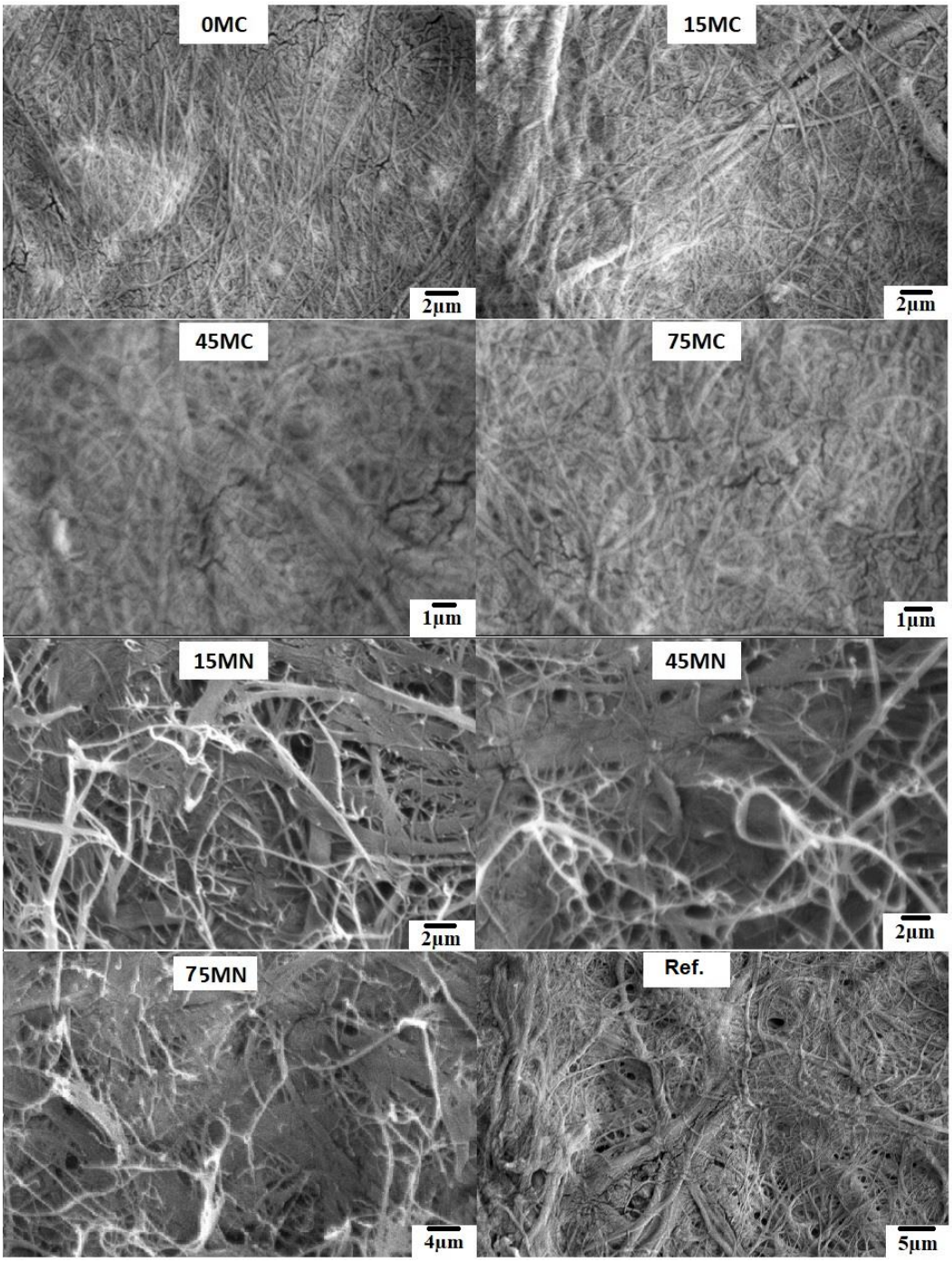

Figure 3-5. SEM images of CNF manufactured by different treatment methods

Thermal degradation analysis

The thermal degradation behavior of CNF was studied from thermogravimetric (TG) and derivative thermogravimetric (DTG) curves presented in Figure 3-6. In all samples, an initial

weight loss of 5% was observed between 40 to 100 °C due to absorbed moisture. The second stage of weight was due to the thermal degradation of cellulose. The pretreatment methods comprising CMC dispersion-ball milling and NaOH swelling-ball milling affected the thermal degradation of CNF. The weight loss varied between 45 to 60% for different pretreatment methods. It occurred between 313 to 370 °C for all samples. The third stage of degradation continued beyond 370 °C and left residual masses after degradation at 650 °C. The residual masses were slightly higher for CNF manufacturing methods that adapted combinations of CMC dispersion and ball milling as pretreatment methods. The pretreatment process comprising NaOH swelling and 15- and 45-min ball milling produced loosely packed nanofibrils to leave reduced residual masses [62].

The DTG curves showed the peak degradation temperature at 340°C for un-milled CNF (control sample-0MC) and 350 °C for all CNF manufactured by the combination of pretreatment methods and homogenization processes. This resembled the nanocellulose degradation behavior reported in the literatures [49, 63, 64]. Further, the improved thermal stability revealed the improvement in CNF fibrillation by the introduction of pretreatment processes [65]. The CNF, which was manufactured by NaOH-ball milling pretreatment process, showed improved thermal stability than CMC-ball milling pretreatment method. The NaOH ruptured the amorphous region and liberated smaller-sized particles to increase thermal stability [39].

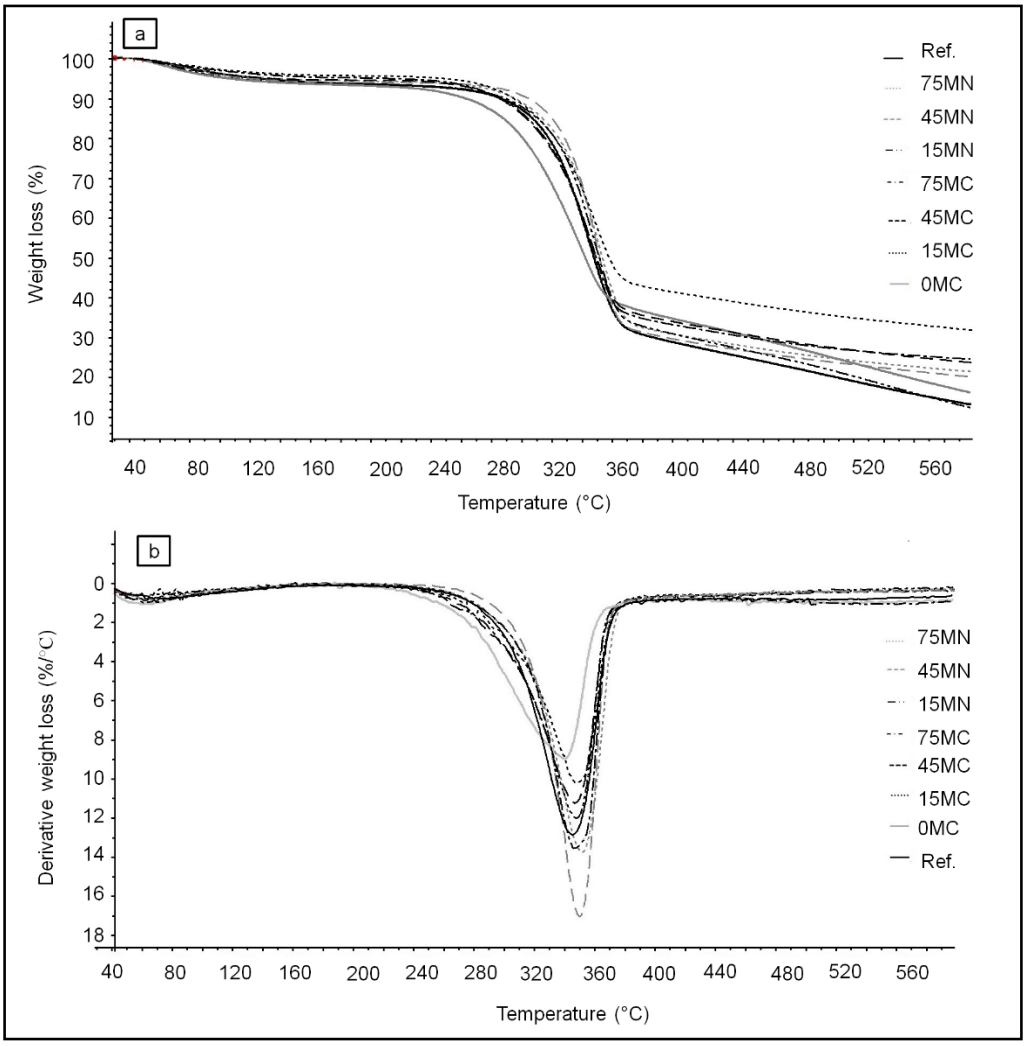

Figure 3-6. Thermograms of CNF a) TG curves b) DTG curves

Tensile strength

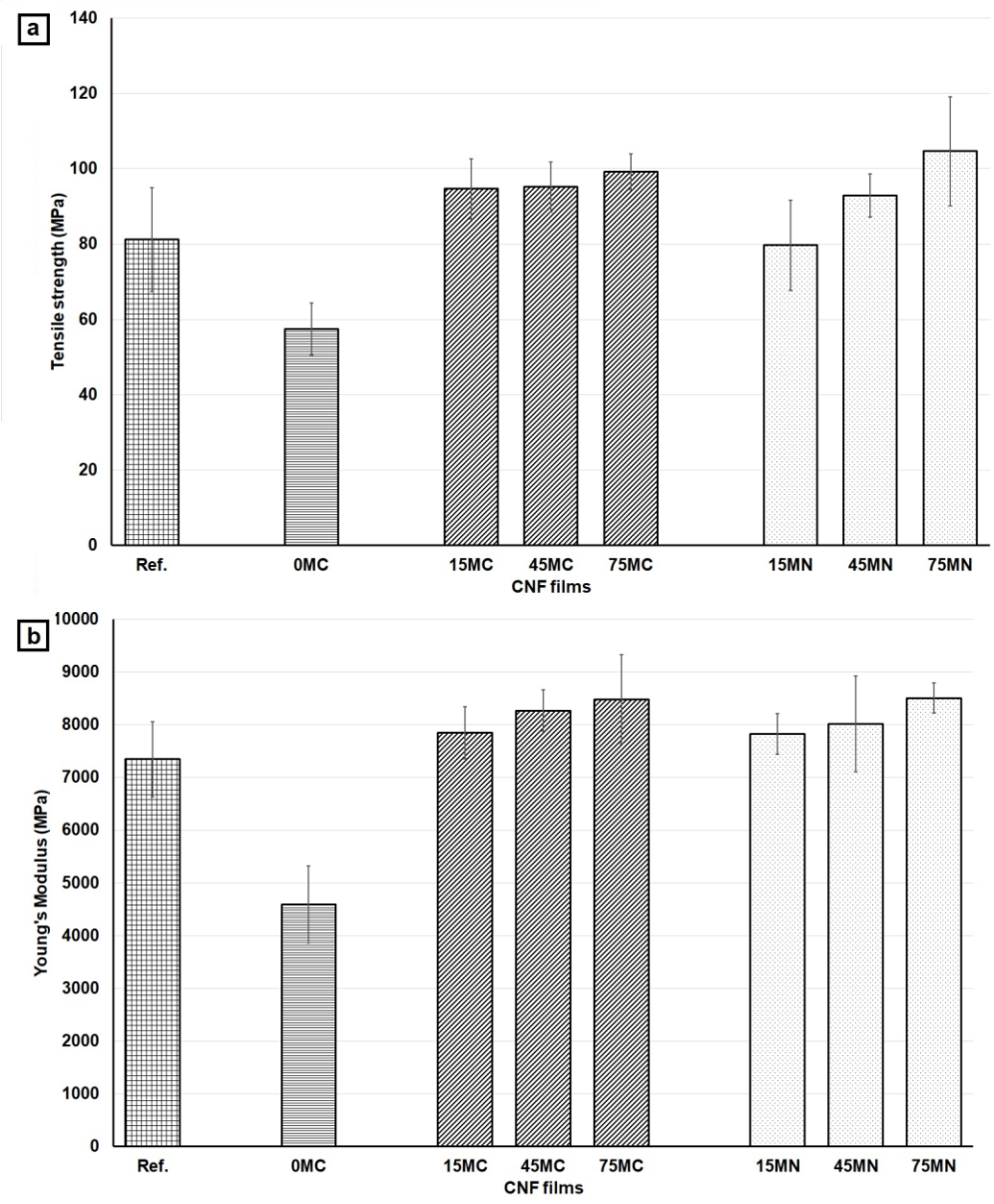

Figure 3-7. Comparison of tensile properties of Ref. and manufactured CNF films. a) Tensile strength. b) Young's modulus

The comparison of maximum tensile stress and Young's modulus of manufactured and Ref. CNF films are shown in Fig. 7. The deformation behavior of all CNF films was linear at a low strain rate of 1 to 2% and the maximum tensile stress was observed before the breaking point as reported in the literatures (Chun et al. 2011; Xu et al. 2018). The CMC and NaOH treatments

and ball milling time of the pretreatment processes affected the tensile properties of films. The maximum tensile stress and Young's modulus of the control CNF sample were 57.5±6 MPa and 4.6±0.7 GPa, respectively. The maximum tensile stress of CMC dispersion-ball mill treated CNF films were 65 to 73 % more than the control films. The 75MC CNF samples showed the maximum tensile stress of 99±5 MPa. The maximum tensile stress of NaOH-ball mill pretreated CNF samples were 39 to 72% more than control films. The 75MN CNF samples exhibited the highest tensile stress of 105±14 MPa. The maximum tensile stress of CNF manufactured with pretreatment processes was within the range (80~104MPa) reported in different studies [66-69].

The CMC/NaOH treatments and ball milling time also affected the Young's modulus of the CNF films. It was 71 to 85% more than the control films for CMC/NaOH treatment with different ball-milling times. The CNF manufactured from CMC/NaOH treatment, and 75min ball milling pretreatment (75MC and 75MN) had the maximum Young's modulus of 8 GPa. Moreover, the CNF samples manufactured with pretreatment processes showed about 30 and 15% higher tensile strength and Young's modulus than the Ref. sample.

The increased tensile properties of pretreated CNF samples indicated the presence of rigid nanofibril network structure in CNF films. The CNF fibrilization processes increased surface area of fibers for hydrogen bonding. The hydrogen bonded fibril network with reduced porosities increased the tensile strength of films prepared from pretreated CNF. It was evident from SEM images that a combination of CMC dispersion/NaOH swelling and ball milling effectively liberated nanostructured fibrils having a width up to 30 nm. The fibrils with reduced width exposed more hydroxyl groups for hydrogen bonding and enhanced entanglement of the network to resist deformation by higher tensile loading. The loosely packed network due to larger width fibrils resulted in lower tensile strength in control samples.

Conclusion

CNF manufacturing approaches with the pretreatments comprised of CMC dispersion, NaOH swelling and ball milling and a homogenization main treatment was developed to investigate the effects of pretreatments on CNF produced from fluff pulp. The CNF was successfully fibrillated from the pretreated cellulose slurries with 3% concentration in a high-pressure homogenizer at 700 bar operating pressure and seven passes. The fiber width and length reduction by the pretreatment processes enhanced the dispersion abilities and prevented the clogging of cellulose micro bundles during homogenization process. The cellulose slurries with triple-fold higher concentration was able to process after subjecting to pretreatment processes. The CMC dispersion-75 min ball mill and NaOH-15, 45- and 75-min ball mill treatments achieved more than 80% fiber dimension reduction. The NaOH-15 min ball mill treatment was the most effective pretreatment that used least ball milling treatment time for the greater fiber size reductions. The CNF with maximum of 6% solid content was manufactured by CMC dispersion and NaOH swelling-75 min ball mill pretreatment methods. It was found from the SEM images that the fibrils having less than 30 nm width could be isolated with the combination of CMC/NaOH-ball milling pretreatment and homogenization processes. The pretreatment method did not influence the chemical structure and dispersion abilities. The crystallinity was increased by 6 and 10% for CMC-45 min ball milling and NaOH-45 min ball milling pretreatments. Thermal degradation study revealed marginal improvement in thermal stability by pretreatment methods. The tensile strength of CNF films manufactured from pretreated CNF samples was between 80 to 105 MPa. Hence, CNF manufacturing methods with pretreatments such as CMC-ball milling or NaOH-ball milling and homogenization main treatment could be adapted to improve productivity and to obtain the consistent quality of CNF hydrogel. In the future, this manufacturing method will

be used to study the manufacturing of CNF from other cellulose resources such as cotton and agricultural waste.

Acknowledgments

This project was partly financially supported by National Science Foundation's (NSF) Center for Bioplastics and Bio composites (CB2) – A Industry-University Cooperative Research Centers (IUCRC) program. The authors acknowledge Dr. Jason Locklin, Dr. Eric Freeman, Dr. Gajanan Bhat, Dr. Rakesh K. Singh, Dr. Paul A Schroeder, Dr. Eric Formo, Dr. Raha Saremi, Ms. Michelle Massoud Makhoul-Mansour, Mr. Matthew Dean Seivert, Ms. Shruti Sharma, Ms. Smriti Dilliwar, Ms. Anh Hoang Truc Dang and Mr. Arjun Kumar Kotapalli of University of Georgia (UGA) for extending their support in the experimental study.

References

1. Bai, F.-W., S. Yang, and N.W.Y. Ho, 3.05 - Fuel Ethanol Production From Lignocellulosic Biomass, in Comprehensive Biotechnology (Third Edition), M. Moo-Young, Editor. 2019, Pergamon: Oxford. p. 49-65.
2. Brigham, C., Chapter 3.22 - Biopolymers: Biodegradable Alternatives to Traditional Plastics, in Green Chemistry, B. Török and T. Dransfield, Editors. 2018, Elsevier. p. 753-770.
3. Havstad, M.R., Chapter 5 - Biodegradable plastics, in Plastic Waste and Recycling, T.M. Letcher, Editor. 2020, Academic Press. p. 97-129.
4. Lokanathan, A.R., et al., 9.19 - Nanocellulose-Based Materials in Supramolecular Chemistry, in Comprehensive Supramolecular Chemistry II, J.L. Atwood, Editor. 2017, Elsevier: Oxford. p. 351-364.
5. Zhang, Y., et al., Cellulose Nanofibrils. Journal of Renewable Materials, 2013. 1(3): p. 195-211.
6. Abitbol, T., et al., Nanocellulose, a tiny fiber with huge applications. Current opinion in biotechnology, 2016. 39: p. 76-88.
7. Liu, L. and F. Kong, Influence of nanocellulose on in vitro digestion of whey protein isolate. Carbohydrate Polymers, 2019. 210: p. 399-411.
8. Selvaraj, T., V. Perumal, and S.F. Khor, 13 - Non-metallic nanomaterial productions from natural resources, in Nanoparticles in Analytical and Medical Devices, S.C.B. Gopinath and F. Gang, Editors. 2021, Elsevier. p. 247-276.

9. Cowie, J., et al., Market projections of cellulose nanomaterial-enabled products--Part 2: Volume estimates. TAPPI JOURNAL, Volume 13 Number 6, 2014; pp. 57-69., 2014. 13(6): p. 57-69.
10. Klemm, D., et al., Nanocelluloses: a new family of nature-based materials. Angewandte Chemie International Edition, 2011. 50(24): p. 5438-5466.
11. Moon, R.J., et al., Cellulose nanomaterials review: structure, properties and nanocomposites. Chemical Society Reviews, 2011. 40(7): p. 3941-3994.
12. TAPPI, TAPPI in WI 3021. 2017, Standard terms and their definition for cellulose nanomaterial. WI 3021: WI 3021.
13. Gu, H., et al. LCA study for pilot scale production of cellulose nano crystals (CNC) from wood pulp. in Proceedings from the LCA XV Conference. 2015.
14. Peng, B.L., et al., Chemistry and applications of nanocrystalline cellulose and its derivatives: A nanotechnology perspective. The Canadian Journal of Chemical Engineering, 2011. 89(5): p. 1191-1206.
15. Cheng, L., et al., Preparation of acetylated nanofibrillated cellulose from corn stalk microcrystalline cellulose and its reinforcing effect on starch films. International Journal of Biological Macromolecules, 2018. 111: p. 959-966.
16. Chirayil, C.J., L. Mathew, and S. Thomas, REVIEW OF RECENT RESEARCH IN NANO CELLULOSE PREPARATION FROM DIFFERENT LIGNOCELLULOSIC FIBERS. Reviews on advanced materials science, 2014. 37: p. 20-28.
17. Stelte, W. and A.R. Sanadi, Preparation and characterization of cellulose nanofibers from two commercial hardwood and softwood pulps. Industrial & engineering chemistry research, 2009. 48(24): p. 11211-11219.

18. Zhang, L., T. Tsuzuki, and X. Wang, Preparation of cellulose nanofiber from softwood pulp by ball milling. Cellulose, 2015. 22(3): p. 1729-1741.

19. Abdul Khalil, H.P.S., et al., A review on nanocellulosic fibres as new material for sustainable packaging: Process and applications. Renewable and Sustainable Energy Reviews, 2016. 64: p. 823-836.

20. Alle, M., et al., Recent trends in isolation of cellulose nanocrystals and nanofibrils from various forest wood and nonwood products and their application, in Nanomaterials for Agriculture and Forestry Applications. 2020, Elsevier. p. 41-80.

21. Arantes, V., et al., The current status of the enzyme-mediated isolation and functionalization of nanocelluloses: production, properties, techno-economics, and opportunities. Cellulose, 2020. 27(18): p. 10571-10630.

22. Kępa, K., et al., Evaluation of properties and specific energy consumption of spinifex-derived lignocellulose fibers produced using different mechanical processes. Cellulose, 2019. 26(11): p. 6555-6569.

23. Turbak, A., F. Snyder, and K. Sandberg, Microfibrillated Cellulose, in Washington, DC: US Patent and Trademark Office. 1983, International Telephone and Telegraph Corporation, New York, N.Y. .

24. Li, F., E. Mascheroni, and L. Piergiovanni, The Potential of NanoCellulose in the Packaging Field: A Review. Packaging Technology and Science, 2015. 28(6): p. 475-508.

25. Albornoz-Palma, G., et al., Effect of lignin and hemicellulose on the properties of lignocellulose nanofibril suspensions. Cellulose, 2020. 27(18): p. 10631-10647.

26. Pirich, C.L., et al., Disruptive enzyme-based strategies to isolate nanocelluloses: a review. Cellulose, 2020. 27(10): p. 5457-5475.

27. Lawoko, M., G. Henriksson, and G. Gellerstedt, Characterisation of lignin-carbohydrate complexes (LCCs) of spruce wood (Picea abies L.) isolated with two methods. Wood Research and Technology, 2006. 60(2): p. 156-161.

28. Adsul, M.G., et al., Enzymatic hydrolysis of delignified bagasse polysaccharides. Carbohydrate Polymers, 2005. 62(1): p. 6-10.

29. Ioelovich, M. and E. Morag, Effect of cellulose structure on enzymatic hydrolysis. BioResources, 2011. 6(3): p. 2818-2835.

30. Saito, T., et al., TEMPO-mediated oxidation of native cellulose: Microscopic analysis of fibrous fractions in the oxidized products. Carbohydrate Polymers, 2006. 65(4): p. 435-440.

31. Arvidsson, R., D. Nguyen, and M. Svanström, Life Cycle Assessment of Cellulose Nanofibrils Production by Mechanical Treatment and Two Different Pretreatment Processes. Environmental Science & Technology, 2015. 49(11): p. 6881-6890.

32. Li, Q., et al., Nanocellulose Life Cycle Assessment. ACS Sustainable Chemistry & Engineering, 2013. 1(8): p. 919-928.

33. Bilodeau, M.A. and M.A. Paradis, High efficiency production of nanofibrillated cellulose. 2018, University of Maine System.

34. Hai, L.V., H.J. Park, and Y.B. Seo, Effect of PFI mill and Valley beater refining on cellulose degree of polymerization, alpha cellulose contents, and crystallinity of wood and cotton fibers. Journal of Korea Technical Association of The Pulp and Paper Industry, 2013. 45(4): p. 27-33.

35. Iwamoto, S., et al., Optically transparent composites reinforced with plant fiber-based nanofibers. Applied Physics A, 2005. 81(6): p. 1109-1112.

36. Fras-Zemljič, L., et al., The effect of adsorbed carboxymethyl cellulose on the cotton fibre adsorption capacity for surfactant. Cellulose, 2006. 13(6): p. 655-663.

37. Laine, Studies on topochemical modification of cellulosic fibres. Part 1. Chemical conditions for the attachment of carboxymethyl cellulose onto fibres. 2000. 15(05): p. 520-526.

38. Cai, J. and L. Zhang, Rapid Dissolution of Cellulose in LiOH/Urea and NaOH/Urea Aqueous Solutions. Macromolecular Bioscience, 2005. 5(6): p. 539-548.

39. Lee, H., et al., Improved thermal stability of cellulose nanofibrils using low-concentration alkaline pretreatment. Carbohydrate Polymers, 2018. 181: p. 506-513.

40. Avolio, R., et al., A multitechnique approach to assess the effect of ball milling on cellulose. Carbohydrate Polymers, 2012. 87(1): p. 265-273.

41. Lasseuguette, E., D. Roux, and Y. Nishiyama, Rheological properties of microfibrillar suspension of TEMPO-oxidized pulp. Cellulose, 2008. 15(3): p. 425-433.

42. Pääkkö, M., et al., Enzymatic hydrolysis combined with mechanical shearing and high-pressure homogenization for nanoscale cellulose fibrils and strong gels. Biomacromolecules, 2007. 8(6): p. 1934-1941.

43. Salas, C., et al., Nanocellulose properties and applications in colloids and interfaces. Current Opinion in Colloid & Interface Science, 2014. 19(5): p. 383-396.

44. Chami Khazraji, A. and S. Robert, Self-Assembly and Intermolecular Forces When Cellulose and Water Interact Using Molecular Modeling. Journal of Nanomaterials, 2013. 2013: p. 745979.

45. Nishiyama, Y., Molecular interactions in nanocellulose assembly. Philosophical Transactions of the Royal Society A: Mathematical, Physical and Engineering Sciences, 2018. 376(2112): p. 20170047.

46. Khouri, S., Experimental characterization and theoretical calculations of responsive polymeric systems. 2010, University of Waterloo.

47. Mohaiyiddin, M.S., et al., Characterization of nanocellulose recovery from Elaeis guineensis frond for sustainable development. Clean Technologies and Environmental Policy, 2016. 18(8): p. 2503-2512.

48. Rizzato, S., et al., Dispersion-Driven Hydrogen Bonding: Predicted Hydrogen Bond between Water and Platinum(II) Identified by Neutron Diffraction. Angewandte Chemie International Edition, 2010. 49(41): p. 7440-7443.

49. Abraham, E., et al., Extraction of nanocellulose fibrils from lignocellulosic fibres: A novel approach. Carbohydrate Polymers, 2011. 86(4): p. 1468-1475.

50. Kasa, S.N., et al., Effect of Unmodified and Modified Nanocrystalline Cellulose Reinforced Polylactic Acid (PLA) Polymer Prepared by Solvent Casting Method Morphology, mechanical and thermal properties. Mater. Plast, 2017. 54: p. 91-97.

51. Lani, N., et al., Isolation, characterization, and application of nanocellulose from oil palm empty fruit bunch fiber as nanocomposites. Journal of Nanomaterials, 2014. 2014.

52. Nuruddin, M., et al., A novel approach for extracting cellulose nanofibers from lignocellulosic biomass by ball milling combined with chemical treatment. Journal of Applied Polymer Science, 2016. 133(9).

53. Zhao, Y., et al., Cellulose Nanofibers from Softwood, Hardwood, and Tunicate: Preparation–Structure–Film Performance Interrelation. ACS Applied Materials & Interfaces, 2017. 9(15): p. 13508-13519.

54. Morais, J.P.S., et al., Extraction and characterization of nanocellulose structures from raw cotton linter. Carbohydrate polymers, 2013. 91(1): p. 229-235.

55. Yu, Y. and H. Wu, Effect of ball milling on the hydrolysis of microcrystalline cellulose in hot-compressed water. AIChE Journal, 2011. 57(3): p. 793-800.

56. Lee, H., Preparation and characterization of cellulose nanofibrils using various pretreatment techniques. 2016, University of Georgia.

57. Amidon, G.E. and M.E. Houghton, The Effect of Moisture on the Mechanical and Powder Flow Properties of Microcrystalline Cellulose. Pharmaceutical Research, 1995. 12(6): p. 923-929.

58. Zhao, H., et al., Effects of Crystallinity on Dilute Acid Hydrolysis of Cellulose by Cellulose Ball-Milling Study. Energy & Fuels, 2006. 20(2): p. 807-811.

59. Hernández-Varela, J.D., et al., Effect of ball milling on cellulose nanoparticles structure obtained from garlic and agave waste. Carbohydrate Polymers, 2021. 255: p. 117347.

60. Mattonai, M., et al., Effect of ball-milling on crystallinity index, degree of polymerization and thermal stability of cellulose. Bioresource Technology, 2018. 270: p. 270-277.

61. Tarrés, Q., et al., Evaluation of the fibrillation method on lignocellulosic nanofibers production from eucalyptus sawdust: A comparative study between high-pressure homogenization and grinding. International Journal of Biological Macromolecules, 2020. 145: p. 1199-1207.

62. Peng, Y., et al., Influence of drying method on the material properties of nanocellulose I: thermostability and crystallinity. Cellulose, 2013. 20(5): p. 2379-2392.

63. Alvarez, V.A. and A. Vázquez, Influence of fiber chemical modification procedure on the mechanical properties and water absorption of MaterBi-Y/sisal fiber composites. Composites Part A: Applied Science and Manufacturing, 2006. 37(10): p. 1672-1680.

64. Yang, H., et al., Characteristics of hemicellulose, cellulose and lignin pyrolysis. Fuel, 2007. 86(12): p. 1781-1788.

65. Luo, X. and X. Wang, Preparation and characterization of nanocellulose fibers from NaOH/urea pretreatment of oil palm fibers. BioResources, 2017. 12(3): p. 5826-5837.

66. Bruce, D.M., et al., High-performance composites from low-cost plant primary cell walls. Composites Part A: Applied Science and Manufacturing, 2005. 36(11): p. 1486-1493.

67. Das, O., N.K. Kim, and D. Bhattacharyya, 16 - The mechanics of biocomposites, in Biomedical Composites (Second Edition), L. Ambrosio, Editor. 2017, Woodhead Publishing. p. 375-411.

68. Leitner, J., et al., Sugar beet cellulose nanofibril-reinforced composites. Cellulose, 2007. 14(5): p. 419-425.

69. Zimmermann, T., N. Bordeanu, and E. Strub, Properties of nanofibrillated cellulose from different raw materials and its reinforcement potential. Carbohydrate Polymers, 2010. 79(4): p. 1086-1093.

CHAPTER 4

PREPARATION AND CHARACTERIZATION OF CITRIC ACID CROSSLINKED CHITOSAN-CELLULOSE NANOFIBRILS COMPOSITE FILMS FOR PACKAGING APPLICATIONS[2]

[2] Prabaharan Graceraj, Jaya Sundaram and Sudhagar Mani. Submitted to Journal of Applied Polymer Science.

Abstract

The inferior water vapor permeability and water resistance properties are the major challenges that hindered the development of chitosan-CNF composites for packaging applications. In this study, the chitosan-CNF composite films were prepared with in situ crosslinking of Citric Acid (CA) to reduce the percent water uptake (WU) and water vapor permeability (WVP). The composite films were produced by the solvent casting method with 10, 15, and 20% CNF as a reinforcement, 20, 25, and 30% CA as a crosslinker, and 20% glycerol as a plasticizer. The crosslinking by CA is confirmed from the Fourier Transform Infra-Red (FTIR) spectra peak at 1710 cm^{-1}. The lowest WU of 39 and WVP of 9.99 $x10^{-7}$ $g/Pa.s.m^2$ is obtained. The crosslinked composite films exhibited the lowest WU of 39% and WVP of 9.99 $x10^{-7}$ $g/Pa.s.m^2$ with reduced light transmittance due to CNF reinforcement. The scanning electron microscopy (SEM) study showed the smooth surface morphology of composite films. The CA crosslinking slightly decreased the tensile strength of composite films. However, the composite film with optimal CNF and CA concentration (25 and 20 % respectively) exhibited comparable tensile strength with other synthetic and biopolymer composites and can be used as a potential biopolymer composite for packaging applications.

Keywords: Biopolymer composites, Chitosan, Cellulose nanofibrils, Crosslinking, Water uptake, Water vapor permeability, Tensile strength.

Introduction

Chitosan is the second most abundant biopolymer, next to cellulose on earth, and is a polysaccharide containing glycosidic bonded glucosamine monomers. It has excellent material properties such as optical transparency, biocompatibility, biodegradability, and nontoxicity [1, 2]. There is a growing interest to use chitosan-based polymers for packaging film production because of its attractive film forming and antimicrobial properties [3, 4]. However, the literature data showed that, despite these unique properties, the denser packing of chitosan molecular chains increased the brittleness during film formation and resulted in poor mechanical properties [5]. The cationic and hydrophilic characteristics of chitosan played a vital role in reducing water vapor barrier properties of chitosan films [6].

The emergence of nanocellulose as potential reinforcement materials, increased the attraction on the development of nanocellulose based composites for the improvement of material properties. The most widely used nanocellulose reinforcement materials in biopolymer composite development are the cellulose nanofibrils (CNF) and cellulose nanocrystal (CNC). The nanostructured cellulose with both amorphous and crystalline regions are CNF [7, 8]. They are extracted from wood, plant and forest residue resources as an aqueous gel, have a width ranging from 5 to 30 nm and an aspect ratio greater than 50 [9]. The CNC are the crystalline form of nanocellulose often produced from CNF after the high concentration acid hydrolysis process. They have a width of 3 to 10 nm and less than 50 aspect ratios [10]. The high tensile strength, low thermal expansion, and reactive hydroxyl surfaces of CNF and CNC increased its functionality as reinforcement materials in composite materials production [11].

The composite films of chitosan and CNF were found suitable for food and other general purpose packaging applications [1, 7, 12, 13]. The reinforcement of CNF having a high aspect ratio and specific surface area enabled numerous hydrogen bonds between chitosan and CNF and

increased the tensile strength [14-16]. However, the hydrophilic characteristics due to the polar groups of chitosan and CNF increased the hydration degree of composite film and increased the moisture absorbance and water uptake properties [17]. The chitosan-CNC composites were also developed for the improvement of chitosan material properties. The CNC reinforcement in chitosan improved the tensile and water uptake properties except water vapor permeability. The water vapor barrier properties chitosan composites were improved by reinforcing the surface modified CNC [18, 19]. Moreover, the production of CNC posed challenges such as high consumption of acids (64 %) and low yield (~50 %) to limit their use as nano reinforcement material and the commercialization in market [20, 21].

The hydrophobicity of chitosan and CNF was improved by replacing hydrophilic polar groups with hydrophobic groups through physical and chemical reactions. The cations of polyelectrolytes were adsorbed into the CNF surfaces in physical CNF surface modification processes [22]. Whereas in chemical surface modification processes, the acyl groups (R-C=O) were primarily attached to the C6 hydroxyl group of cellulose molecules [23]. The CNF films reinforced with surface-modified nanocellulose exhibited improved hydrophobic behavior [24-26].

Božič, Vivod et al. (2015) modified the hydroxyl groups of CNFs using acetic anhydride and Amano Lipase A enzyme and reported improvement in hydrophobicity with a contact angle of 84 ± 9 ° [24]. Willberg-Keyriläinen et al. (2017) studied barrier properties of CNF films, coated with cellulose esters. The CNF surfaces were modified by an esterification reaction using fatty acid chloride with anhydrous pyridine as a catalyst. The cellulose ester reduced water vapor transmission by 50 % [27]. Huang et al. (2017) synthesized cellulose nanocrystal (CNC) esters from the mixture of trifluoroacetic anhydride and fatty acids such as capric acid, lauric acid, and

stearic acid and reported an improved hydrophobicity (water contact angle ~ 88 to 112 °) of CNC films [25]. Similarly, the hydrophobicity of chitosan films was increased by modifying reactive groups of chitosan with acid chloride and acid anhydrides. The acyl groups (R-C=O) of carboxylic acid derivatives were substituted in amino group of glucosamine molecules to increase hydrophobicity to the significance level [28]. Trinh and Mekonnen (2018) modified CNC surfaces using lauroyl chloride and reinforced them in epoxy matrix phase material. The surface modified CNCs increased the tensile strength and contact angle of composite by 77 and 289 % respectively [29].

The surface-modified CNF exhibited poor dispersibility in matrix phase polymer and required a two-step reaction process. Due to agglomeration and micro-voids formation at higher concentrations (1 & 3 %), the lowest concentration (0.5 %) of surface-modified CNF was able to reinforce in matrix phase polymer [30]. Further, the surface modifier and catalyst (acetic anhydride and pyridine) used in the esterification process were classified as extremely dangerous hazardous chemicals by a globally harmonized system (GHS) [31]. Limited studies in the literature have focused on crosslinking of chitosan-CNF composite with non-toxic and environmentally-friendly chemicals for the improvement of water vapor barrier properties and hydrophobicity [32, 33]. In this study, the chitosan-CNF composite was crosslinked using environment-friendly CA by an in situ approach to improve water vapor barrier property and hydrophobicity. The CA is an organic tricarboxylic acid having three carboxyl and one hydroxyl reactive groups for crosslinking [34]. It formed strong ester bonds with many biopolymers and improved their functionality to use in various product applications [35-38]. The water resistance, water vapor permeability and mechanical properties of biopolymer such as protein, polyvinyl alcohols (PVA) starch, chitosan and cellulose were improved by CA crosslinking [39-41]. Moreover, the CA is non-toxic and safe

to use in food and drug administration [42]. Hence, in this study the CA was used as a crosslinking agent for the production of composite films. The composite films were manufactured by the film casting method and characterized by FTIR, SEM, water uptake, water contact angle, water vapor permeability, and tensile test. Furthermore, the effects of percent CNF and CA on the hydrophobic, water vapor permeability, and tensile properties of composite films were studied by statistical method, and optimal CNF and CA mass fraction of best barrier and tensile performance was determined.

Materials and methods

Materials

The 85 % deacetylated chitosan powder and anhydrous, American Chemical Society (ACS) grade, 99.5+ % crystalline citric acid were purchased from Alfa Aesar, Ward Hill, MA, U.S.A. The 3 % CNF was supplied by the University of Maine, Orono, Maine, U.S.A. Reagent Plus, ≥99 % Acetic acid, and ACS reagent, anhydrous ≥99.5 % glycerol were supplied by Sigma-Aldrich, St. Louis, MO, USA.

Citric acid in situ esterification process and film preparation

The 2 % chitosan solution was prepared in a 2 % acetic acid aqueous solution [43]. The CNF aqueous gel was added in chitosan solution and dispersed well by mixing in a magnetic stirrer for 1h at room temperature (20±2 ^{o}C). The CA was added slowly to the chitosan-CNF solution and was heated at 80 °C for 15 min in a hotplate magnetic stirrer plate under continuous stirring to complete the crosslinking reaction. After the crosslinking reaction, glycerol (GLY) was added to the solution and was mixed for 30 min at room temperature. The mixed solution was cast in a glass petri dish and was dried for 24 h in the fume hood. The films were washed in deionized water to

remove unreacted CA and dried again in the fume hood. The dried films were stored in a desiccator at 23 °C and 50 % relative humidity (RH) before testing.

A two-factor central composite design of the experimental method was used by varying the amount of CNF, and CA in the production of composite films. Based on the preliminary experiments, the mass fractions of CNF were 10, 15 and 20 % and the mass fractions of CA were 20, 25 and 30 % considered for composite film production. A 20 % glycerol amount was kept constant for all variants of composite films, which change the amount of chitosan in the composite film as shown in Table 4-1. The chitosan films (CS) without CNF and CA were also produced with 20 % glycerol to compare the results. For each composite and chitosan film, an estimated film weight of about 0.72 g was maintained. For each experimental condition, at least five specimen films were produced for properties analysis.

Table 4-1. The composite composition for the manufacture of 0.72 g packaging films with and without citric acid crosslinking.

Film variants	**[@]CNF (%)**	**[#]CA (%)**	**[$]GLY (%)**	**Chitosan (%)**
CS	0	0	20	80
1CN	10	0	20	70
2CN	15	0	20	65
3CN	20	0	20	60
1ACA	10	20	20	50
1BCA	10	25	20	45
1CCA	10	30	20	40
2ACA	15	20	20	45
2BCA	15	25	20	40

2CCA	15	30	20	35
3ACA	20	20	20	40
3BCA	20	25	20	35
3CCA	20	30	20	30

[@]CNF- Cellulose nanofibrils, [#]CA- Citric acid, [$]GLY- Glycerol

FTIR spectroscopy

The chemical structure modification of chitosan-CNF composite by the in situ crosslinking reaction was characterized using an FTIR instrument. The composite films were dried in a desiccator for 24 h and the FTIR spectra were collected using Thermo Scientific Nicolet 6700 VariGATRTM spectrometer in absorbance mode. The spectra were recorded by scanning the sample in the range of wavenumbers from 4000 to 600 cm^{-1} with a resolution of 4 cm^{-1}.

Scanning electron microscope (SEM)

The morphology of composite films was analyzed using a scanning electron microscopy (SEM) technique. The composite films were coated with gold-palladium for 15 nm thickness using Leica Mikrosysteme GmbH sputtering unit. The images were obtained from Thermo Fisher Scientific (FEI) Teneo (Thermo Fisher Scientific, Hillsboro, OR, USA), a field emission scanning electron microscope with an accelerating voltage of 5 kV and spot size of 8 nm.

Water uptake test (WU)

The water uptake test was conducted according to the ASTM D570-2005 (Standard Test Method for Water Absorption of Plastics) [44]. In this study, the five specimens from each variant were conditioned in a desiccator at 50 % RH and 23 °C for >24 h and weighed (W_i). The conditioned specimens were immersed in distilled water for 24 h at room temperature. After 24 h of immersion, the specimens were taken out from the water, all the surface water in the film was

wiped off and weights (W_e) were measured. The water uptake (WU) was calculated using following equation

$$WU = \left[{(W_e - W_i)}/{W_i}\right] \times 100\ \%$$

Where:

W_e = Equilibrium weight in g

W_i = Initial weight in g

Water contact angle (WCA)

The film sample was placed on a flat horizontal plate and 1 µl of a deionized water droplet was dropped on the film surface at room temperature [45]. The droplet image was recorded with a camera. The image analysis was performed using the contact angle plugin of ImageJ software. The WCA was determined from a sphere or ellipse fit on the image by selecting two points on the film surface and three points on the water droplet. The test was performed on four samples by placing the water droplet at least in three places.

Water vapor permeability (WVP)

The desiccant method of ASTM E96 (Standard Test Methods for Water Vapor Transmission of Materials) standard was used to determine the WVP of composite films [46]. Five specimens from each variant were conditioned at 50 % RH and 23 °C for >24 h before testing. The dried (at 200 °C) desiccants were filled in open mouth test cups with a mouth area of 140 mm^2 up to the level of 6 mm from the mouth. The composite films were attached to the open mouth and were sealed with vinyl chloride plastic, pressure-sensitive insulating tape. All the test cup assemblies were placed in a test chamber maintained at 50 % RH and 23 °C. The weights of test cup assemblies were recorded every 24 h with an accuracy of 0.0001 g. The changes in the weight

of a test cup assembly over time were calculated by fitting a linear regression line on recorded weight data. The WVP was calculated from the following equation

$$WVP = {}^{G}/_{[t \times A \times S \times (R_1 - R_2)]} \text{ g/Pa. s. m}^2$$

$Where$:

G = Weight change in test cup assembly in g

T = Time during which G occurred in s

A = Test cup mouth area in m^2

S = Saturation vapor pressure at 23 °C in Pa

R_1 = Relative humidity of chamber in fraction

R_2 = Relative humidity at the vapor sink in fraction

Ultraviolet-visible spectrometry

The translucence of chitosan and composite films was studied by ultraviolet-visible (UV-Vis) spectrometry technique. The UV-Vis spectra of crosslinked and non-crosslinked films were obtained from Varian Cary® 50 spectrometer (Agilent Technologies, U.S.A.). The spectrometer was operated at 600 nm/min scan rate, 1 nm data interval and 0.1 s average time. The scan software version 3.0 (Agilent Technologies, U.S.A.) was used to acquire the UV-Vis data in the wave length range of 200 to 800 nm. The thickness of the films studied was 0.1 ± 0.01 mm. Three replications of each film were tested at ambient conditions.

Tensile test

The composite films were conditioned at 23 °C and 50 % RH for 24 h and the tensile tests were performed according to the ASTM D882 (Standard Test Method for Tensile Properties of Thin Plastic Sheeting) [47]. A Shimadzu (AGS-X) tensile tester with a 1 kN load cell was used at

50 mm/min crosshead speed for testing. The samples that failed at grips were ignored. The maximum tensile strength (TS) was recorded for the analysis.

Statistical analysis

The Minitab® software was used for the statistical analysis. The test results were analyzed using the response surface method (RSM) in the software. The goodness of fit was evaluated from the estimated R^2 and F-values. The main effects and interaction plots were created to analyze the influence of CNF and CA on WU, WCA, WVP, and TS. The optimal values of the factors (CNF and CA) were determined by using – overlaid contour plot function. The lower and upper limits of all the responses were defined to the following criteria: $35 \leq TS \leq 45$ MPa, $70 \leq WCA \leq 78$ °, $1.2 \times 10^{-6} \leq WVP \leq 1.6 \times 10^{-6}$ g/Pa.s.m^{2}and $50 \leq WU \leq 54$ % to determine optimum characteristics of the developed composite films.

Results and discussion

Film thickness

The thickness of the film was measured by micrometer (PK-0505CPX, Mitutoyo Corporation, Japan) in five places of each replications and was 0.10 ± 0.01 mm. The change in CNF and CA did not change the thickness of the film. Further, all the film thickness was less than ASTM D4635-16 (Standard Specification for Plastic Films Made from Low-Density Polyethylene for General Use and Packaging Applications) specified thickness of 0.106 mm [48]. The weight of the solid content in biopolymer solutions which was prepared for the solvent casting was controlled without any variation to obtain the uniform film thickness [49].

FTIR spectra analysis

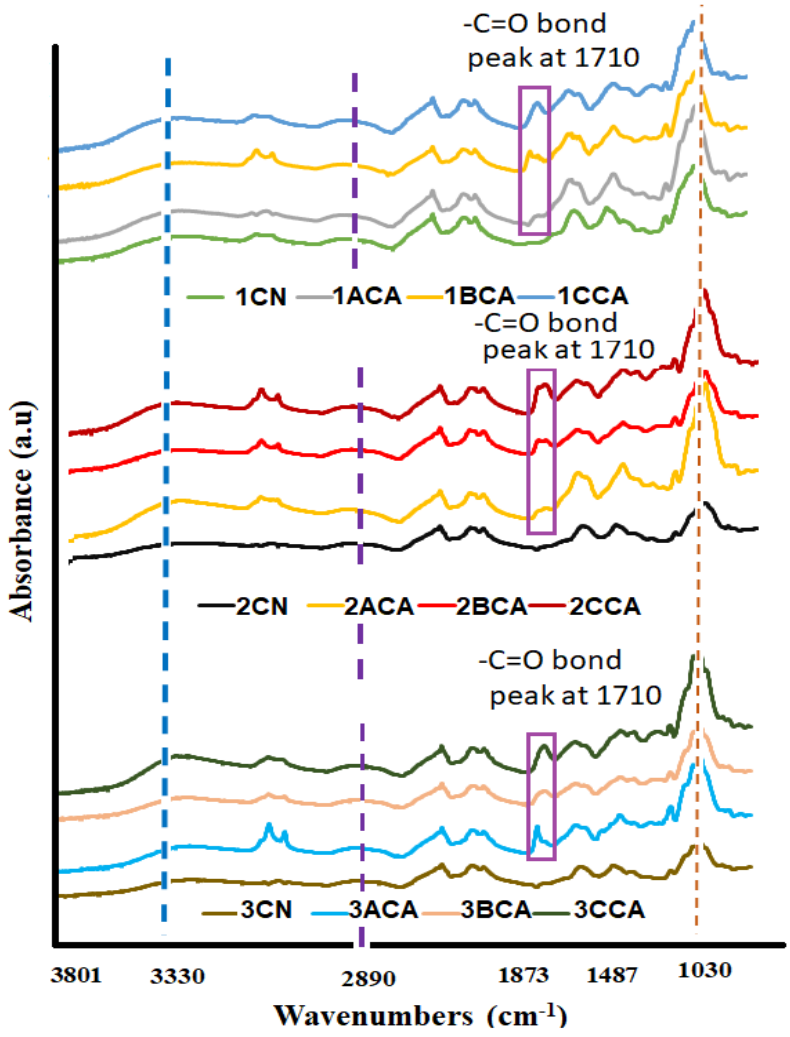

Figure 4-1. FTIR spectra of crosslinked and non-crosslinked chitosan-CNF composite films showing ester bond formation at 1710 frequency for the composites with CNF reinforcement of 10, 15, 20 % and CA crosslinking of 20, 25, and 30 %

The FTIR spectra of all variants of crosslinked and non-crosslinked composite films are shown in Figure 4-1. The attachment of ester groups on CNF and chitosan was evidenced by the new peak at 1710 cm^{-1} due to the stretching of the aldehyde group (-C=O) in CA-treated films [33]. The concentration of CNF and CA influenced the esterification process. The ester bond peaks were short for the composite films with 10 and 15 % CNF and 20 % CA. They were sharper and larger for higher CA concentration treatment in all other CNF mass fractions. The CA has

tricarboxylic functional groups in its molecular structure. The carboxylic groups of CA and hydroxyl/ amino groups of CNF/ chitosan interacted with each other and crosslinking is developed through -C=O ester bonds. The esterification reaction was observed in composite films for more than 20 % of CA concentration and at 80 °C reaction temperature. Increasing the reaction time (more than 15 min) and temperature (more than 80 °C), reduced the absorbance peak (1030 cm^{-1}) corresponding to -C-O-C bonds, indicating possible hydrolysis of chitosan and CNF.

The other characteristic peaks that appeared at 3330, 2890, and 1030 cm^{-1} were consistent as discussed by the other authors [5, 50-52]. The peak region referred by the vibration frequency 3330 cm^{-1} was wider and was attributed to the stretching of O-H and NH_2 groups. This indicated the intermolecular hydrogen bonding of chitosan and CNF molecules and also the crosslinking of chitosan by CA [33]. The absorption peak frequency at 2890 and 1030 cm^{-1} have represented the bending of C-H and stretching of C-O-C groups of chitosan and CNF [52]. It appeared that the structure of crosslinked composite film comprised of chitosan-CNF molecular structure with hydrogen bond, chitosan-chitosan molecular structure with ester bond, and CNF-CNF molecular structure with ester bond as shown in Figure 4-2 [33, 40, 53].

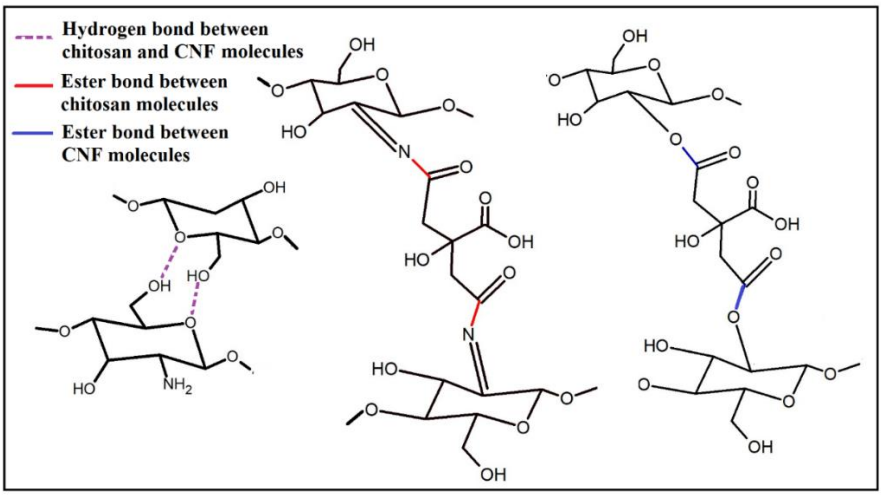

Figure 4-2. The schematic representation of chitosan-CNF composite microstructure which was formed by the citric acid crosslinking of chitosan and CNF and the hydrogen bonding between chitosan and CNF

SEM

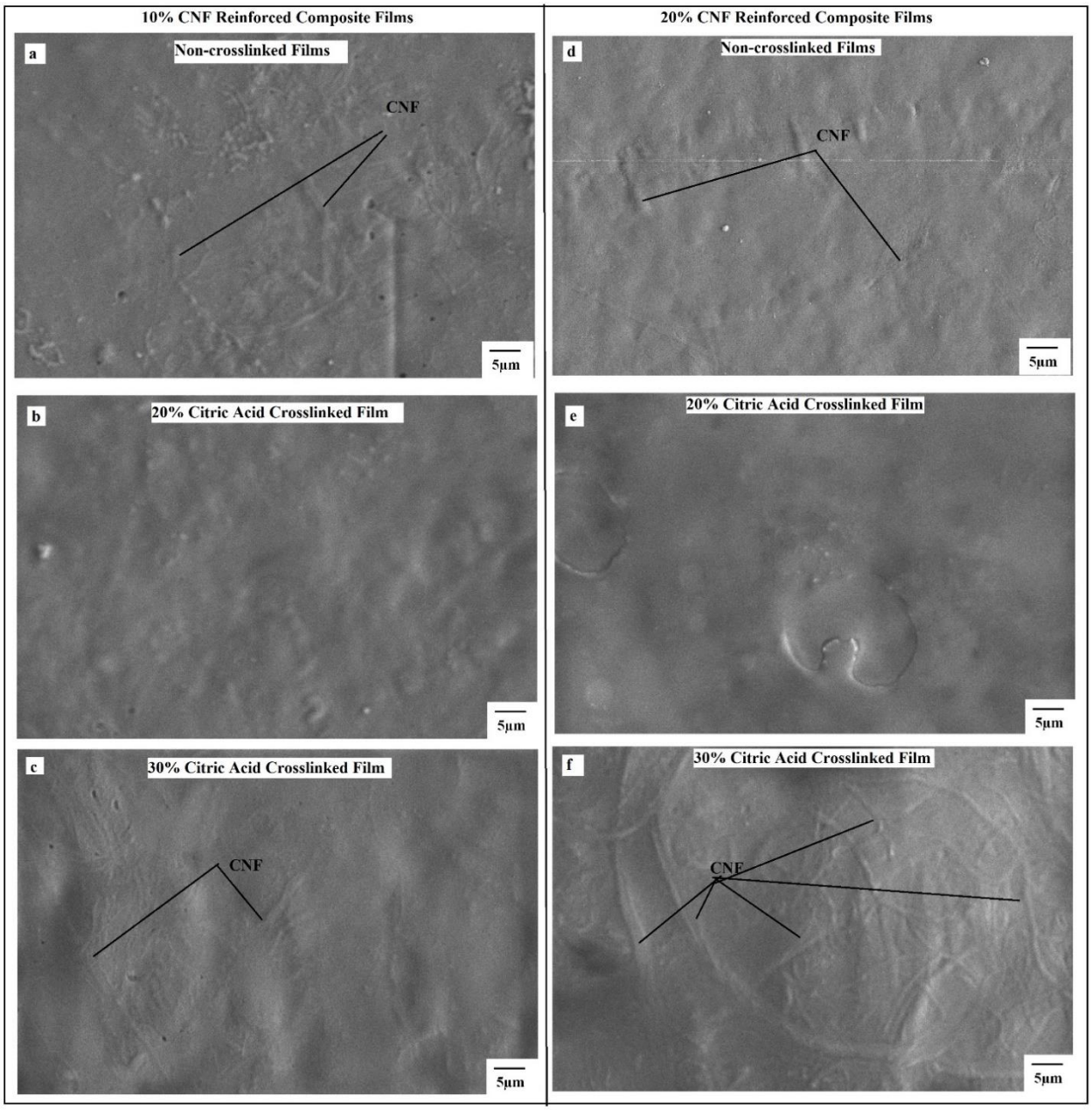

Figure 4-3. SEM images of composite films for 10 and 20 % CNF reinforcement and 20 and 30 % CA crosslinking a) non-crosslinked films with 10 % CNF reinforcement b) 20 % CA crosslinked films with 10 % CNF reinforcement c) 30 % CA crosslinked films with 10 % CNF reinforcement d) non-crosslinked films with 20 % CNF reinforcement e) 20 % CA crosslinked films with 20 % CNF reinforcement c) 30 % CA crosslinked films with 20 % CNF reinforcement

The surface morphologies of the non-crosslinked and crosslinked composite films were obtained from SEM images and are shown in Figure 4-3. There was no debonding of fibrils from

chitosan matrix in all film surfaces. The increase in CNF and CA slightly changed the surface smoothness and waviness of the non-crosslinked and crosslinked composite films. While increasing CNF from 10 to 20% in non-crosslinked films, the interfacial adhesion of CNF with chitosan was also increased to improve the surface smoothness (Figure 4-3a and 4-3d). The dispersion of CNF network was high for the composite films with 10 % CNF reinforcement. It was decreased and dense fibril networked composite structure was appeared while increasing the reinforcement from 10 to 20 %. The increased hydrogen bonding between chitosan and CNF on the film surfaces resulted closely packed chitosan-CNF composite microstructure and increased the surface smoothness of the composite films in 20 % CNF reinforced composites [54]. The structural stiffness of the composite film was increased by the reinforcement and improved the strength of the composite for the increased CNF reinforcement [55]. This indicated that the chitosan and CNF were compatible to manufacture the composites for packaging products.

The interconnected CNF network reinforced composite microstructure were prominently appeared on the surfaces of crosslinked composite films and attributed the waviness in film surfaces. The improved interfacial adhesion between chitosan and CNF and the dense molecular structure by crosslinking reactions may resulted this waviness and prominent appearance of CNF network in film surfaces [56]. It was increased while the CA was increased from 20 to 30 % as shown Figure 4-3b, 4-3c, 4-3e and 4-3f. The closely packed polymer chain network by the increased crosslinking exhibited smooth layered surfaces in composite films with the improved visibility of CNF networks (Figure 4-3c and 4-3f) [57].

Water uptake (WU)

The chitosan films (CS) showed extremely poor resistance to water. The films were dissolved in water in few minutes after immersion in DI water. The non-crosslinked films were

swollen and cleaved at some places whereas the crosslinked films were completely integrated without any damage. Figure 4-4a shows the percent water uptake of non-crosslinked and crosslinked composite films. The increase in CNF amount from 10 to 20 % decreased the present water uptake of non-crosslinked composite films from 306 to 164 with 46 % reduction. The reinforcement of CNF in the chitosan matrix has created the interlinking by the hydrogen bonds and thus reduced the reactive hydroxyl groups to weaken the adhesion of water molecules in the composite structure [58]. The increase in CNF substantially increased the hydrogen bonding between chitosan and CNF and reduced the hydroxyl groups to decrease the water uptake of non-crosslinked films. However, the hygroscopic nature of unreacted chitosan and CNF surfaces attracted the water molecules and had swollen the non-crosslinked composite films.

The present water uptake was drastically reduced in the CA crosslinked chitosan-CNF composite films while compared to the non-crosslinked composite films. In 10 % CNF reinforced composite films, the present water uptake was reduced from 306 to 40 with the 85 % reduction by the in situ crosslinking reactions with 20, 25, 30 % CA. Similarly, the present water uptake of 15 and 20 % CNF reinforced films were between 39~50 and 46~55 respectively after in situ crosslinking reactions. It was about 80 and 71 % less than the non-crosslinked composite films. CA crosslinking has created a chemical network structure with an ester bond between chitosan-CNF-CA molecules by esterification reaction [59]. The esterification reaction reduced the reactive hydroxyl groups in chitosan and CNF molecules and resisted the absorption of water molecules. The porosity of the composite structure was also reduced by the denser molecular structure created by crosslinking reactions. The CNF and CA have played a significant role to reduce the water uptake of chitosan-CNF composites. Figure 4-4b and 4-4c. depicts the main effects and interaction plots of CNF and CA on water uptake. It was evident from these plots that about 35 to 45 % of

WU could be achieved with less than 10 and 30 % of CNF and CA respectively or with less than 20 and 25 % of CNF and CA respectively. The increase in the amount of CA for crosslinking from 20 to 30 % slightly increased the percent water uptake due to excess availability of non-crosslinked hydroxyl and carboxyl groups, which attracts and retains water in the composite structure [41]. Overall, the CA crosslinking was effective in reducing the water update by up to 86 % on the composite films.

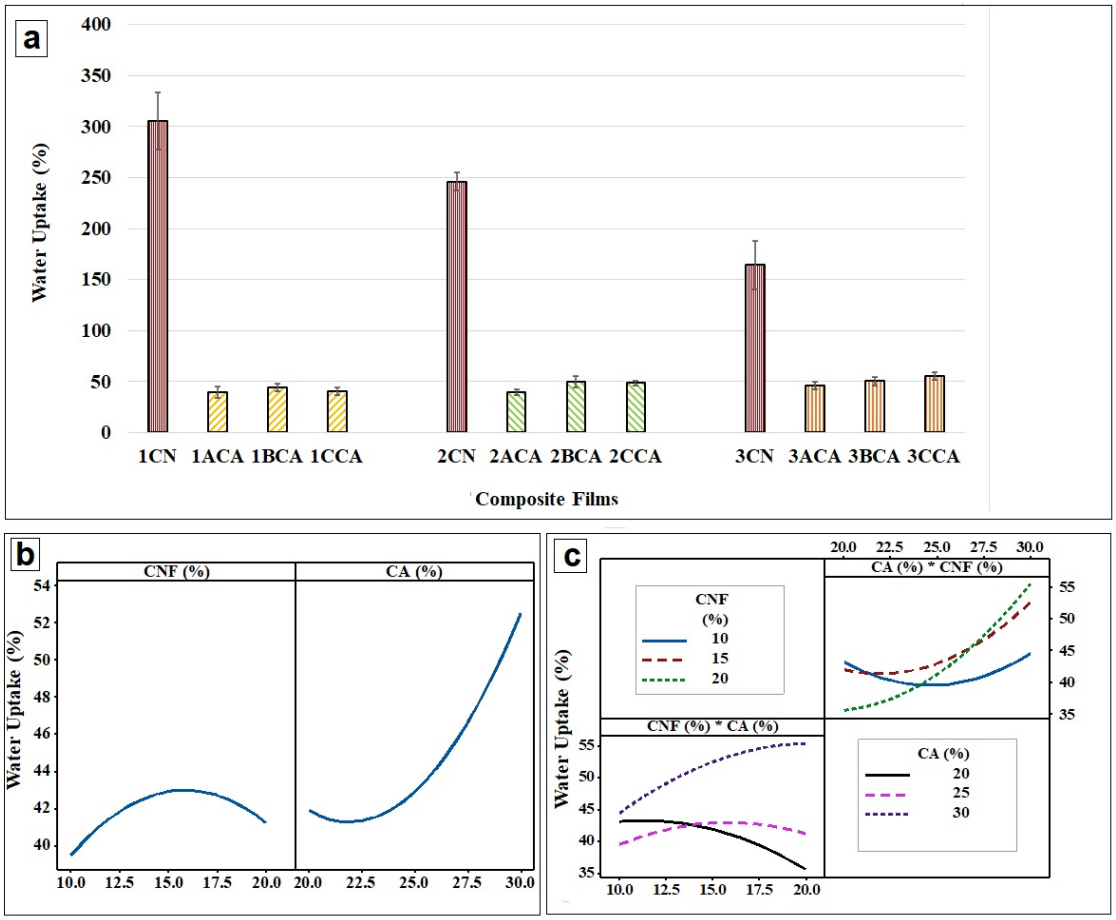

Figure 4-4. Water uptake behavior of chitosan-CNF composite films a) comparison of crosslinked and non-crosslinked composite films. It shows that the water uptake of the crosslinked composite films was 70 to 85 % less than the non-crosslinked films b) main effect plots which shows the effect of changing CNF reinforcement from 10 to 20 % and CA crosslinking from 20 to 30 % c) interaction plots which shows the interaction of reinforcement and crosslinking for 10, 15 and 20 % CNF and 20, 25 and 30 % CA

Water contact angle (WCA)

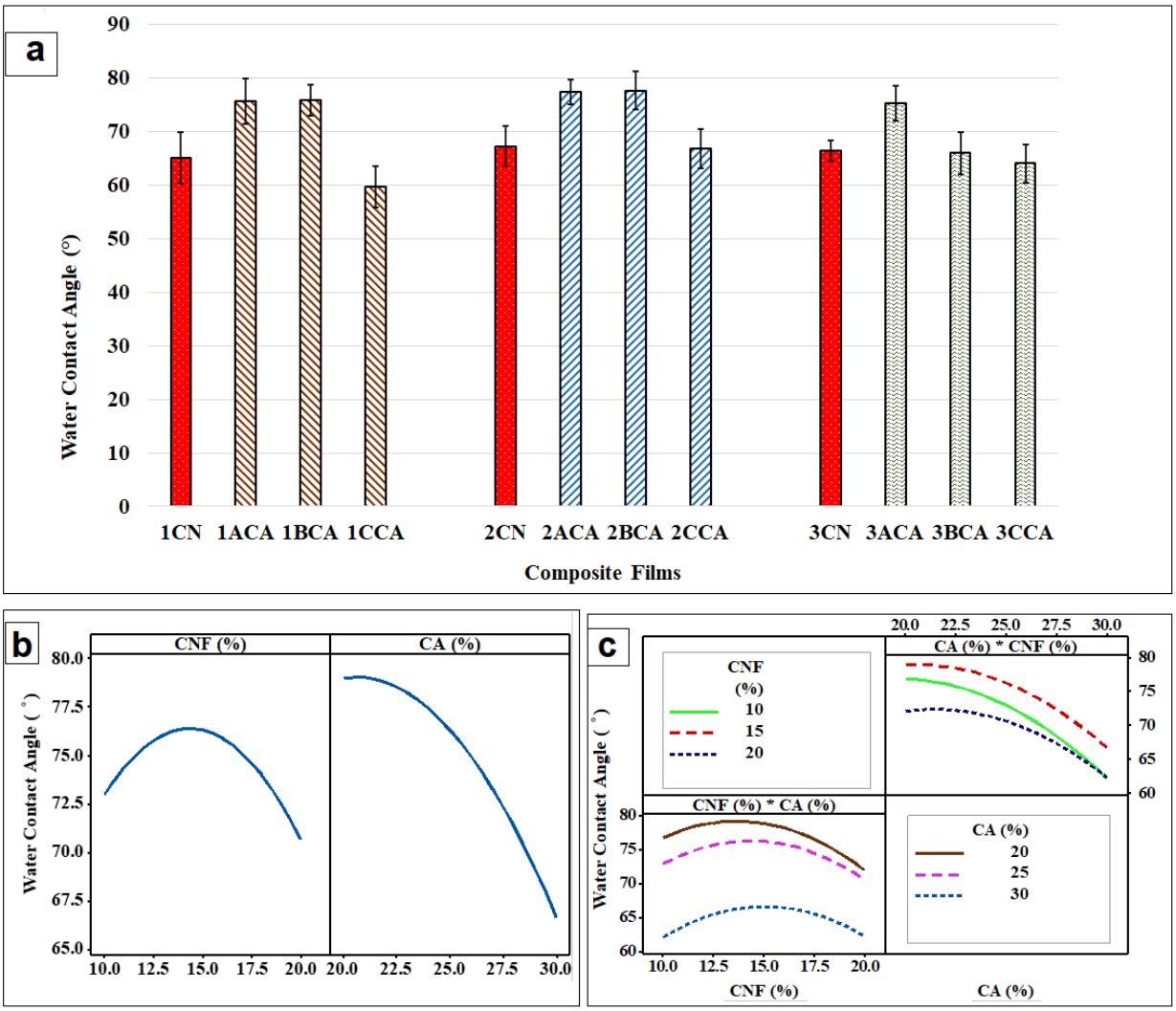

Figure 4-5. The water contact angle of chitosan-CNF composite films a) comparison of crosslinked and non-crosslinked composite films. It shows that the contact angle was increased for 20 and 25 % CA crosslinking in 10 and 15 % CNF reinforced films and for 20 % CA crosslinking in 20 % CNF reinforced films b) main effect plots which shows the effect of changing CNF reinforcement from 10 to 20 % and CA crosslinking from 20 to 30 % c) interaction plots which shows the interaction of reinforcement and crosslinking for 10, 15 and 20 % CNF and 20, 25 and 30 % CA

The water contact angle measurement on the composite film indicated the wettability and the degree of hydrophobicity. Figure 4-5a shows the water contact angle for both crosslinked and non-crosslinked composite films. The contact angle of non-crosslinked chitosan-CNF composite

films was about 68 ° and a similar observation was reported in the literature [60]. It was about 20 % lower than contact angle of the chitosan films (85 ± 2 °). The addition of CNF decreased the contact angle of composite films due to the hydrophilic nature of CNF. However, the CA crosslinked composite film increased the contact angle up to 78 ° due to the formation of hydrophobic ester groups between chitosan-CNF-CA. An increase in a CA amount from 20 to 30 % decreased the contact angle up to 8 % (60 to 67 °) due to excessive availability of free carboxyl and hydroxyl groups [61-63]. The statistical inference on the effect of CNF and CA on WCA is presented as main effect and interaction plots as shown in Figure 4-5b. and 4-5c. The increases in CNF to 20 % and CA to 30 % decreased the water contact angle due to the exposure of excessive hydroxyl groups on the film surfaces. Surface functionalization or pre-esterification of CNF could potentially improve the contact angle and the hydrophobicity of the composite films if more than 15 % of CNF is used for reinforcement.

Water vapor permeability (WVP)

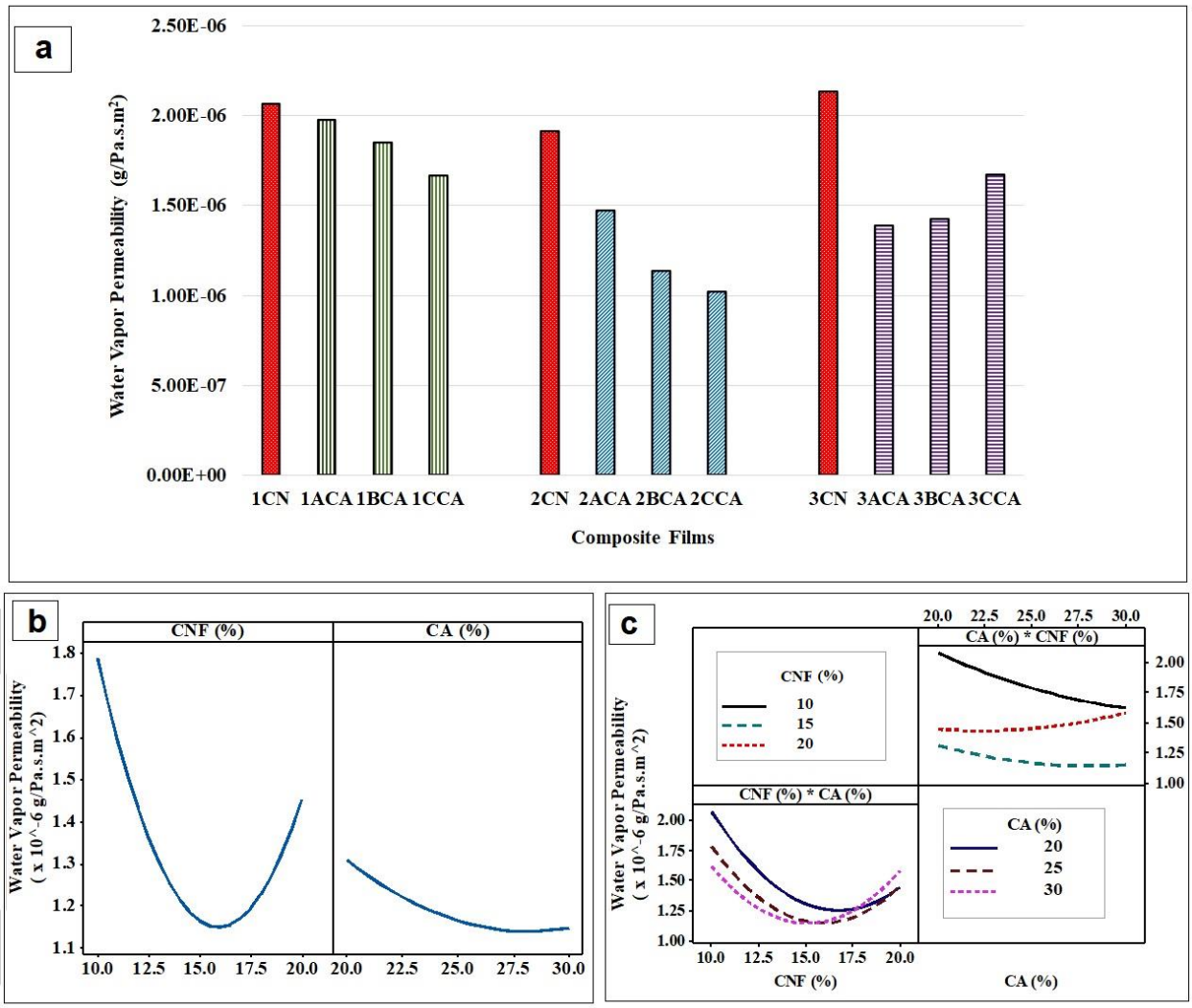

Figure 4-6. Water vapor barrier behavior chitosan-CNF composite films a) comparison of crosslinked and non-crosslinked composite films. It shows the 5 to 50% less water vapor permeability in crosslinked composite films and the decreasing trend with increase in CA for 10 and 15 % CNF reinforcement and increasing trend with increase in CA for 20 % CNF reinforcement. b) main effect plots which shows the effect of changing CNF reinforcement from 10 to 20 % and CA crosslinking from 20 to 30 %. c) interaction plots which shows the interaction of reinforcement and crosslinking for 10, 15 and 20 % CNF and 20, 25 and 30 % CA

Figure 4-6a compares the water vapor permeability of crosslinked and non-crosslinked composite films. The WVP of non-crosslinked composite film with 10, 15 and 20 % of CNF reinforcement was $2.02x10^{-6}$, $1.87x10^{-6}$ and $2.09x10^{-6}$ g/Pa.s.m^{2,} respectively which was

comparable to the data reported by Azeredo et al. (2010). It was slightly higher than the WVP of chitosan films ($1.84x10^{-6}$ g/Pa.s.m^2) without CNF and crosslinking. The hydrophilic nature of CNF marginally increased the WVP in non-crosslinked composite films. The WVP of crosslinked composite films was about 5 to 50 % less than that of non-crosslinked films with different CNF and CA mass fractions. It was between 1.93 to $1.63x10^{-6}$ g/Pa.s.m^2 for the crosslinked composite films with 10 % CNF reinforcement, $1.44x10^{-6}$ to $9.98x10^{-7}$ g/Pa.s.m^2 for the crosslinked composite films with 15 % CNF reinforcement and 1.63 to $1.36x10^{-6}$ g/Pa.s.m^2 for the crosslinked composite films with 20 % CNF reinforcement.

The significant reduction in WVP was attributed to the effective substitution of hydrophilic hydroxyl groups of chitosan and CNF by hydrophobic ester groups. This esterification reaction enabled the crosslinking between chitosan and CNF and made the composite structure denser to increase the water vapor barrier properties. However, the WVP of composite with 20 % CNF was increased while increasing CA amount from 25 to 30 % due to the plasticizing effect created by the excessive CA. The mobility and the interchain space of chitosan and CNF were increased by the free availability of CA molecules and increased the water vapor transfer abilities [64]. The main effect and interaction plot showed the effects of CNF and CA on WVP. They indicated that the composites constituted with 15 and 20 % of CNF and with 20 and 25 % of CA could achieve low WVP.

Transmittance of the composite films

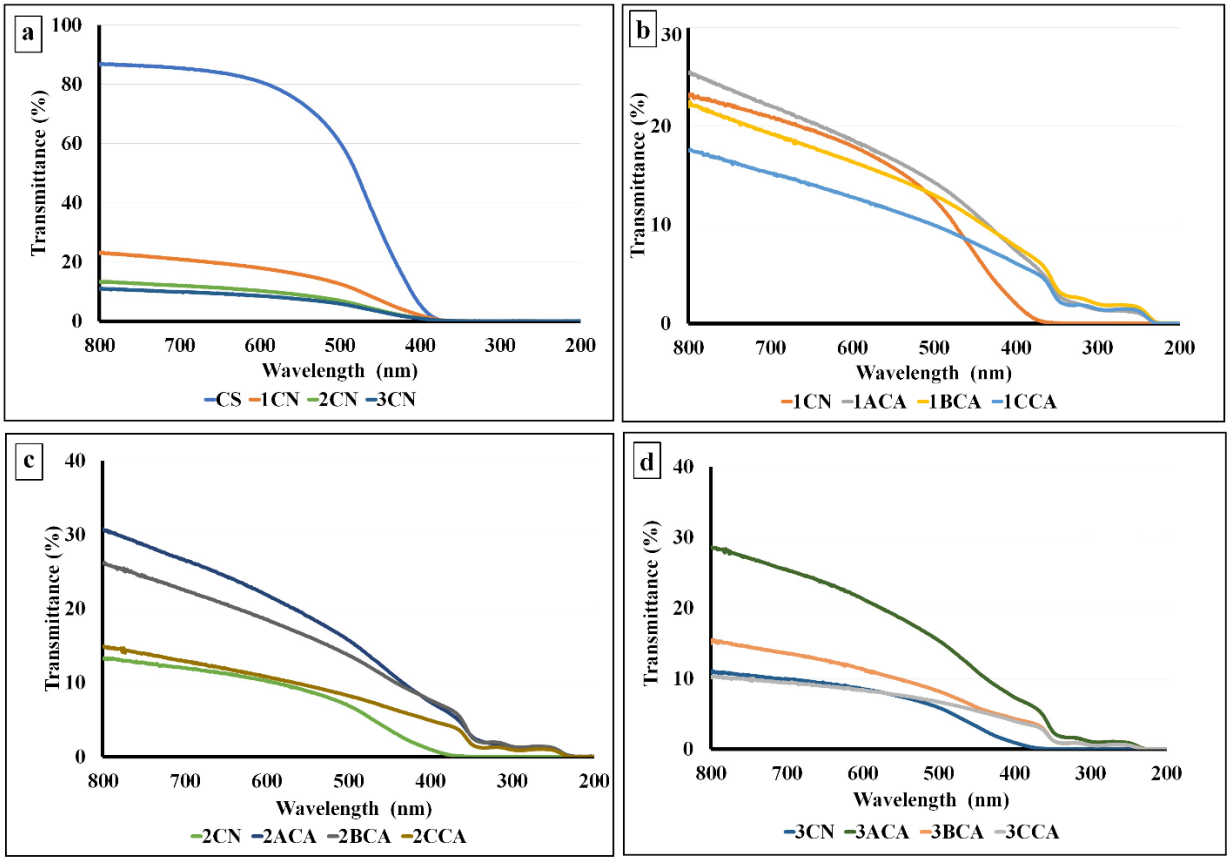

Figure 4-7. UV-Visible transmittance spectra of chitosan films and chitosan-CNF composite films with and without crosslinking a) comparison of chitosan and non-crosslinked composite films shows the decreased transmittance. b) comparison of non-crosslinked and crosslinked composite films with 10 % CNF and 20, 25 and 30 % CA c) comparison of non-crosslinked and crosslinked composite films with 15 % CNF and 20, 25 and 30 % CA d) comparison of non-crosslinked and crosslinked composite films with 20 % CNF and 20, 25 and 30 % CA

The Figure 4-7a shows the comparisons of UV-Vis light spectra of non-crosslinked composite films with chitosan films and the Figure 4-7b, 4-7c and 4-7d shows the comparison of 10, 15, 20 % CNF reinforced non-crosslinked composite films with crosslinked films. The light transmittance of pure chitosan film was between 80 to 86 % for 590 to 800 nm wavelength and 50 % at 480 nm wavelength. It was reduced drastically for the 10, 15 and 20 % CNF reinforcement in composite. For 590 to 800 nm wave length, the transmittance of 10, 15 and 20 % CNF reinforced

non-crosslinked composite films were 18~23, 10~13, 8~14 % respectively. In non-crosslinked and chitosan films, the transmittance was less than 1 % for the wavelength of 380 nm and below. The CNF fibril network in the chitosan matrix scattered the light and greatly reduced the transmittance [65]. The light transmittance of chitosan and composite films were slightly lower than values reported by Wu, Farnood et al. 2014 [17]. This may be due to the chitosan and fibril dimensions of CNF used in this study.

The transmittance of crosslinked films was affected by the amount of CNF and CA in the composites. The transmittance was crosslinked films of 10, 15 and 20 % CNF reinforcement with 20% CA was higher than the non-crosslinked films (Figure 4-7b, 4-7c and 4-7d). There was a marginal increase of transmittance in 10 % CNF reinforced composite and more than 100 % increase in 15 and 20% CNF reinforced composites. The transmittance of 25 and 30 % CA crosslinked films were less than the 20 % CA crosslinked films in all CNF reinforcement. It was less than the non-crosslinked films for 10 % CNF reinforcement and higher than the non-crosslinked composites for 15 and 20 % CNF reinforcement. The increase in transmittance by 20 % CA crosslinking was due to the increased pore volume of CNF fibril network in the composites. The citric acid cross linking formed the nanofiber bundles and increased the pore volume of CNF in the composites to increase the transmittance [66]. The closely packed molecular structure of chitosan and CNF fibril network by 25 and 30 % CA crosslinking reduced the transmittance [41, 67].

Tensile strength (TS)

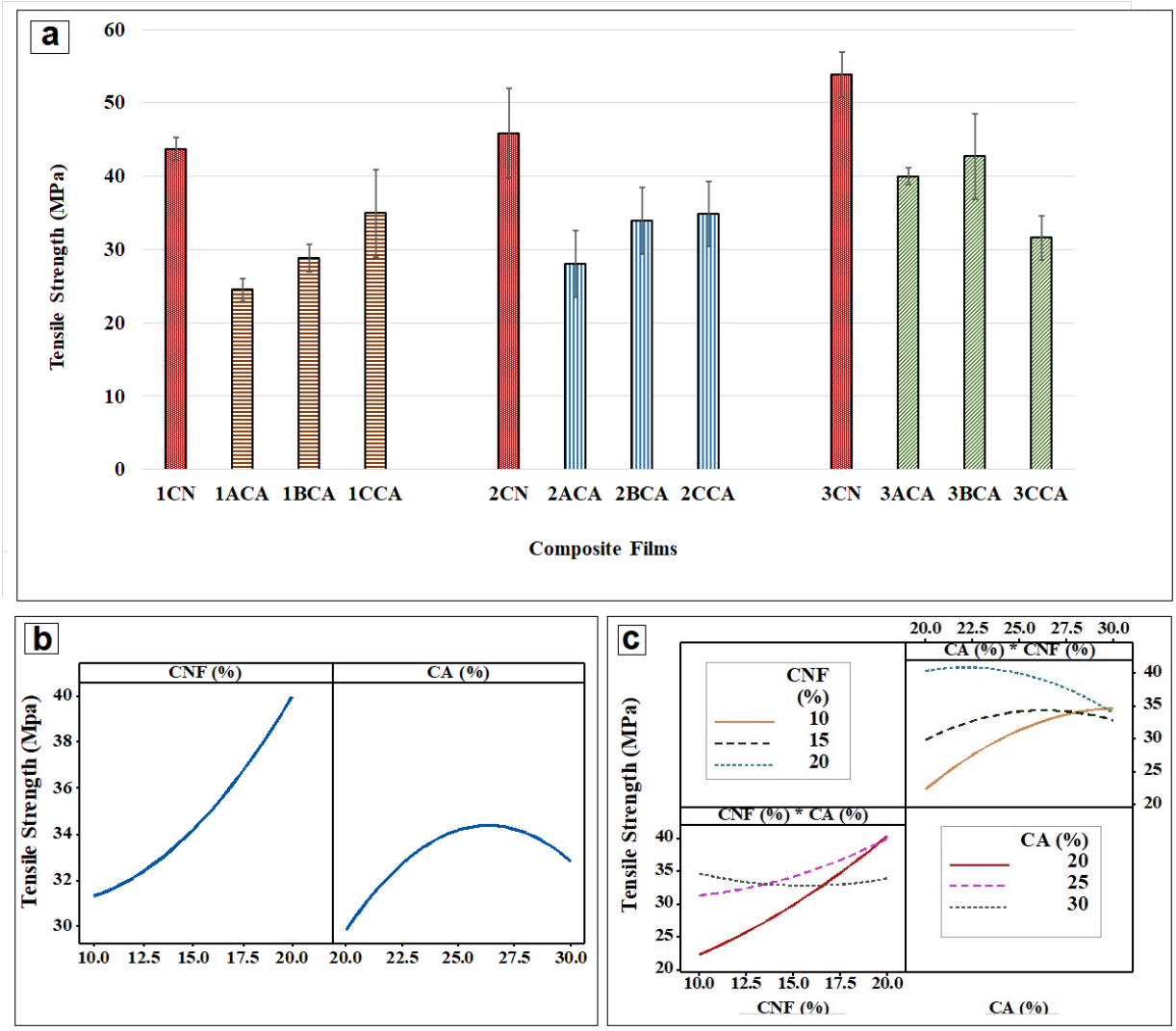

Figure 4-8. Tensile strength of composite films a) comparison of crosslinked and non-crosslinked composite films shows the reduced tensile strength in crosslinked film b) main effect plots which shows the effect of changing CNF reinforcement from 10 to 20 % and CA crosslinking from 20 to 30 %. c) interaction plots which shows the interaction of reinforcement and crosslinking for 10, 15 and 20 % CNF and 20, 25 and 30 % CA

As shown in Figure 4-8a, the CNF and CA had a considerable influence on the tensile strength of the composite films. The tensile strength of non-crosslinked composite films was increased from 44 ± 1 MPa to 54 ± 3 MPa while increasing CNF loading from 10 to 20 %. It was about 200 to 300 % higher than the chitosan films which tensile strength was 13 ± 1MPa with 20 % glycerol as plasticizer. The higher loading of CNF and the strong interlinking between the

hydroxyl groups of CNF and chitosan increased the tensile strength of non-crosslinked composite films [68-70]. However, the CA crosslinking decreased the tensile strength of composite films even with the increased loading of CNF. The crosslinking of chitosan and CNF with CA decreased the polymer chain displacement and reduced the tensile strength of composites [39, 64]. Although the use of CA decreased the tensile strength of composite films, it was comparable with the fossil-based LDPE (8~30 MPa), PP (31~43MPa) polymers and bio-based Polylactic acid (PLA) (31 MPa) polymer films [71, 72]. However, the increased loading of CNF up to 20 % moderately increased the tensile strength of crosslinked composite films.

The CNF reinforcement and crosslinking in composite affected the percentage elongation at break (EB). The EB of chitosan films was 17.64 ± 6.90 % with 20% glycerol. The glycerol interacted with polymer chain, reduced its stiffness and provided flexibility to the film. It was decreased to ~11% for the non-crosslinked composite films with 10, 15 and 20 % CNF reinforcement. As studied by Azeredo et al. 2010, the increase in CNF reduced the EB. The strong interfacial adhesion of CNF with chitosan reduced the EB in non-crosslinked films as reported in the other literatures [73-75]. The EB of the crosslinked films were between 2 to 6 % for the CNF reinforcement of 10, 15 and 20 % and CA with 20, 25 and 30%. The closely packed chitosan and CNF molecules in crosslinked films restricted the molecular mobility and reduced the EB [76-78]. However, the glycerol in the composites provided sufficient flexibility to composite films which was affected by the CNF reinforcement and CA crosslinking. The EB of the crosslinked composite films are comparable with starch-CNF (5.7 %), chitosan-CNF (5~6 %), chitosan-CNC (6 %) and PLA films [15, 18, 41, 79].

The effects of CNF and CA amounts on the tensile strength of crosslinked composite films are presented in Figure 4-8b and 4-8c. The increase in CNF loading increased the tensile strength

of cross-linked composite films, while the increase in CA loading slightly increased and flattened. Furthermore, the interaction plot indicated that the tensile strength could be increased up to the group mean value of 40 MPa at a higher CNF loading of 10 % and the lower CA loading of 20 %. Therefore, the amount of CNF and the CA requirement for the improved tensile strength of composite films could be optimized.

Optimization of composite composition

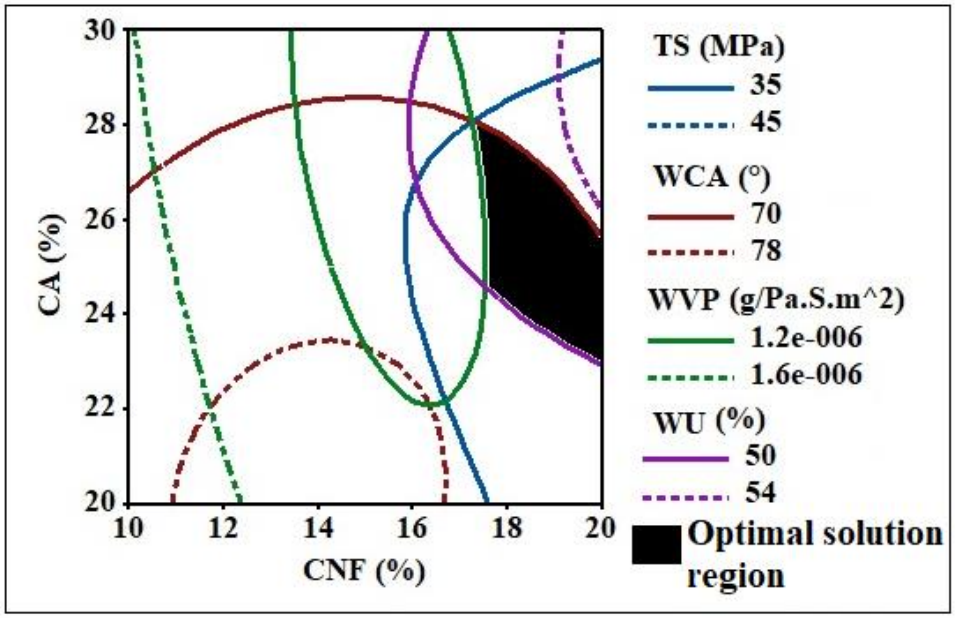

Figure 4-9. Overlaid contour plot of the tensile strength (TS), water contact angle (WCA), water vapor permeability (WVP), and water uptake (WU). The shaded region is the optimal solution region which gives the amount of CNF and CA for the best performance. The composite film studied with 20 % CNF and 25 % CA was in the optimal solution region.

The percent loading of CNF and CA were highly influenced by the water update (WU), water contact angle (WCA), water vapor permeability (WVP), and the tensile strength (TS) of composite films. The optimum value of CNF and CA were determined from the overlaid plot region by maximizing the TS and WCA while minimizing WU and WVP of crosslinked composite films as shown in Figure 4-9. The highlighted area in the plot represented the feasible optimal

solution region for all responses. It was formed by lower and upper contour lines of response surfaces corresponding to TS, WCA, WVP, and WU under optimal conditions. The limits of responses that bounded the overlaid region were between 35 to 45 MPa for TS, 70 to 78 ° for WCA, 1.2 x 10^{-6} to 1.6 x 10^{-6} g/Pa.s.m^2 for WVP and 50 to 54 % for WU. The optimal change in TS, WCA, WVP, and WU responses were obtained with 18 to 20 % of CNF and 24 to 26 % of CA for the chitosan composites.

The composite film was manufactured with 20 wt. % CNF, 25 wt. % CA and 20 wt. % GLY and remaining chitosan favored the defined optimum characteristics for packaging applications. The WU and WVP of crosslinked films with optimal composition were 70 and 50 % respectively lower than that of non-crosslinked composite films. The optimal composition of crosslinked films did not cause any significant change to the TS and WCA of composite films. Furthermore, TS and WVP of the crosslinked composite film with optimal compositions were comparable with some synthetic and biopolymers for packaging applications (Table 4-2).

As natural polymers such as chitosan and CNF are highly hydrophilic, the WCA and WU were rarely discussed in the literature. The tensile strength of the crosslinked composite film was about 40 % higher than that of different synthetic polymers and PLA-CNF composites. Young's modulus (YM) was also higher than that of synthetic and biopolymer films. The WVP of the crosslinked composite was significantly lower than that of non-crosslinked chitosan-CNF composites and was higher than that of PLA-CNF composites and synthetic polymers. But, the PLA-CNF composite manufacturing process uses harmful chemicals in the CNF acetylation or surface modification process. Hence, the CA crosslinked chitosan-CNF could be the best alternative for designing and developing sustainable packaging applications.

Table 4-2. Comparison of tensile and water vapor barrier properties of crosslinked composite films with synthetic and biopolymer films

Polymer matrix	**TS[@] (MPa)**	**YM[#] (MPa)**	**WVP[$] (g /Pa.s.m^2)**	**Remarks/ Reference**
Chitosan-CNF crosslinked composite	43	2579	1.40×10^{-6}	20 % CNF, 20 %CA, and 20 % GLY. (Current study)
Chitosan-CNF non-crosslinked composite	30	1100	1.74×10^{-6}	20 % CNF and 20 % Gly. (Azeredo et al. 2010)
PLA-CNF composite	31	2120	2.38×10^{-11}	5 % CNF. (Abdulkhani et al. 2014)
LDPE	8~30	200~500	7.64×10^{-9} ~1.15×10^{-8}	(Azeredo et al. 2010)
PP	31~43	1140~1550	6.64×10^{-9}	(Azeredo et al. 2010)

[@]Tensile Strength; [#]YM – Young's Modulus; [$]WVP – Water Vapor Permeability

Conclusions

The increasing plastic waste on land and ocean surfaces motivated the use of biopolymers for the packaging products which is about 40 % of total plastic production (350 million tons) in the world. Almost 10% of plastic land litters are discharged into ocean through storm water, rivers and wind blow. Some of the living species in marine and land habitats are ingesting the leaked plastic debris and are loading harmful pollutants to their ecosystems. It is expected that biodegradable biopolymers from renewable resources could greatly bring down the environmental impacts caused by plastic waste disposal. Hence, the most abundant biopolymers such as chitosan and cellulose were extensively explored for the development of packaging material production.

The high brittle and moisture absorbance properties of chitosan and the emergence of nanocellulose as a potential reinforcement material motivated the development of chitosan-CNF composites for packaging application. The reactive hydroxyl groups in chitosan and CNF increased the hydrophilicity and imposed poor water resistance and water vapor barrier properties. The loss of material strength by moisture absorbance and poor water vapor barrier properties of CNF reinforced chitosan was highlighted as major challenges in developing chitosan-CNF composites as potential packaging materials.

In this study, the reactive hydroxyl groups of chitosan and CNF were modified by the in-situ crosslinking with CA and the hydrophobicity and water vapor permeability of the composites were improved to suggest them as potential packaging material. The chitosan-CNF composite films were successfully synthesized by an in situ crosslinking approach with CA as a crosslinker and glycerol as the plasticizer. The hydrophobicity, water vapor permeability, and tensile strengths of the crosslinked and non-crosslinked composite films were compared. The hydrophobicity of crosslinked films was improved with reduced water uptake (up to 86 %) and increased water contact angle (up to 15 %). Similarly, the water vapor permeability of crosslinked composite films was reduced by up to 50 % with different combinations of CNF and CA mass fractions. The tensile strength and elongation at break of the crosslinked composite film was decreased due to excess crosslinking of CA. However, the composite film with optimal CNF and CA displayed comparable tensile strength and water vapor permeability with synthetic and other biopolymer composites. The addition of glycerol as plasticizer prevented the films becoming brittle due to the CNF reinforcement and CA crosslinking. The in situ crosslinking of chitosan-CNF composite films with CA exhibited the enhanced hydrophobicity and water vapor barrier properties to manufacture sustainable packaging materials. While compared to the reinforcement of CNC or surface modified

CNF/CNC, the in situ crosslinking with CA would be a prospective approach in manufacturing chitosan-CNF composites for packaging applications. Further research is required to investigate the economic and environmental impact assessments of chitosan-CNF composite films for rapid commercialization.

Acknowledgments

This project was partly financially supported by National Science Foundation's (NSF) Center for Bioplastics and Biocomposites (CB2) – A Industry-University Cooperative Research Centers (IUCRC) program. The authors acknowledge the New Materials Institute (NMI), Nano-Structured Materials Lab, Georgia Electron Microscopy of the University of Georgia (UGA) for extending the technical assistance, FTIR analysis, SEM imaging, and WCA measurement of this study.

References

1. Fernandes, S.C., et al., Novel materials based on chitosan and cellulose. 2011. 60(6): p. 875-882.
2. Szymańska, E. and K. Winnicka, Stability of chitosan-a challenge for pharmaceutical and biomedical applications. Marine drugs, 2015. 13(4): p. 1819-1846.
3. Muxika, A., et al., Chitosan as a bioactive polymer: Processing, properties and applications. International Journal of Biological Macromolecules, 2017. 105: p. 1358-1368.
4. Pastor, C., et al., Physical and antioxidant properties of chitosan and methylcellulose based films containing resveratrol. Food Hydrocolloids, 2013. 30(1): p. 272-280.
5. Nunthanid, J., et al., Physical Properties and Molecular Behavior of Chitosan Films. Drug Development and Industrial Pharmacy, 2001. 27(2): p. 143-157.
6. Wiles, J.L., et al., Water Vapor Transmission Rates and Sorption Behavior of Chitosan Films. Journal of Food Science, 2000. 65(7): p. 1175-1179.
7. H.P.S, A.K., et al., A review on chitosan-cellulose blends and nanocellulose reinforced chitosan biocomposites: Properties and their applications. Carbohydrate Polymers, 2016. 150: p. 216-226.
8. Sangroniz, A., et al., Packaging materials with desired mechanical and barrier properties and full chemical recyclability. Nature Communications, 2019. 10(1).
9. Kargarzadeh, H., et al., Advances in cellulose nanomaterials. Cellulose, 2018. 25(4): p. 2151-2189.
10. TAPPI, TAPPI in WI 3021. 2017, Standard terms and their definition for cellulose nanomaterial. WI 3021: WI 3021.

11. Moon, R.J., et al., Cellulose nanomaterials review: structure, properties and nanocomposites. Chemical Society Reviews, 2011. 40(7): p. 3941-3994.
12. Dehnad, D., et al., Thermal and antimicrobial properties of chitosan–nanocellulose films for extending shelf life of ground meat. Carbohydrate Polymers, 2014. 109: p. 148-154.
13. Marín-Silva, D.A., S. Rivero, and A. Pinotti, Chitosan-based nanocomposite matrices: Development and characterization. International Journal of Biological Macromolecules, 2019. 123: p. 189-200.
14. Hassan, M.L., et al., Chitosan/rice straw nanofibers nanocomposites: Preparation, mechanical, and dynamic thermomechanical properties. Journal of Applied Polymer Science, 2012. 125(S2): p. E216-E222.
15. Hassan, M.L., E.A. Hassan, and K.N. Oksman, Effect of pretreatment of bagasse fibers on the properties of chitosan/microfibrillated cellulose nanocomposites. Journal of Materials Science, 2011. 46(6): p. 1732-1740.
16. Fernandes, S.C.M., et al., Transparent chitosan films reinforced with a high content of nanofibrillated cellulose. Carbohydrate Polymers, 2010. 81(2): p. 394-401.
17. Wu, T., et al., Mechanical behavior of transparent nanofibrillar cellulose–chitosan nanocomposite films in dry and wet conditions. Journal of the Mechanical Behavior of Biomedical Materials, 2014. 32: p. 279-286.
18. Li, Q., J. Zhou, and L. Zhang, Structure and properties of the nanocomposite films of chitosan reinforced with cellulose whiskers. 2009. 47(11): p. 1069-1077.
19. de Mesquita, J.P., et al., Bio-based nanocomposites obtained through covalent linkage between chitosan and cellulose nanocrystals. Carbohydrate Polymers, 2012. 90(1): p. 210-217.

20. Gu, H., et al. LCA study for pilot scale production of cellulose nano crystals (CNC) from wood pulp. in Proceedings from the LCA XV Conference. 2015.

21. Peng, B.L., et al., Chemistry and applications of nanocrystalline cellulose and its derivatives: A nanotechnology perspective. The Canadian Journal of Chemical Engineering, 2011. 89(5): p. 1191-1206.

22. Alila, S., et al., Adsorption of a Cationic Surfactant onto Cellulosic Fibers I. Surface Charge Effects. 2005. 21(18): p. 8106-8113.

23. Eyley, S. and W. Thielemans, Surface modification of cellulose nanocrystals. Nanoscale, 2014. 6(14): p. 7764-7779.

24. Božič, M., et al., New findings about the lipase acetylation of nanofibrillated cellulose using acetic anhydride as acyl donor. Carbohydrate Polymers, 2015. 125: p. 340-351.

25. Huang, F., et al., Acylation of cellulose nanocrystals with acids/trifluoroacetic anhydride and properties of films from esters of CNCs. Carbohydrate Polymers, 2017. 155: p. 525-534.

26. Peng, S.X., et al., A comparative guide to controlled hydrophobization of cellulose nanocrystals via surface esterification. Cellulose, 2016. 23(3): p. 1825-1846.

27. Willberg-Keyriläinen, P., et al., Hydrophobization and smoothing of cellulose nanofibril films by cellulose ester coatings. Carbohydrate Polymers, 2017. 170: p. 160-165.

28. Tangpasuthadol, V., N. Pongchaisirikul, and V.P. Hoven, Surface modification of chitosan films. 2003. 338(9): p. 937-942.

29. Trinh, B.M. and T. Mekonnen, Hydrophobic esterification of cellulose nanocrystals for epoxy reinforcement. Polymer, 2018. 155: p. 64-74.

30. Shrestha, S., et al., Surface hydrophobization of TEMPO-oxidized cellulose nanofibrils (CNFs) using a facile, aqueous modification process and its effect on properties of epoxy nanocomposites. Cellulose, 2019. 26(18): p. 9631-9643.

31. Prat, D., et al., CHEM21 selection guide of classical- and less classical-solvents. Green Chemistry, 2016. 18(1): p. 288-296.

32. Falamarzpour, P., T. Behzad, and A. Zamani, Preparation of Nanocellulose Reinforced Chitosan Films, Cross-Linked by Adipic Acid. International Journal of Molecular Sciences, 2017. 18(2): p. 396.

33. Udoetok, I.A., L.D. Wilson, and J.V. Headley, Self-Assembled and Cross-Linked Animal and Plant-Based Polysaccharides: Chitosan–Cellulose Composites and Their Anion Uptake Properties. ACS Applied Materials & Interfaces, 2016. 8(48): p. 33197-33209.

34. Yang, C.Q., X. Wang, and I.-S. Kang, Ester Crosslinking of Cotton Fabric by Polymeric Carboxylic Acids and Citric Acid. Textile Research Journal, 1997. 67(5): p. 334-342.

35. Reddy, N., R. Reddy, and Q. Jiang, Crosslinking biopolymers for biomedical applications. Trends in Biotechnology, 2015. 33(6): p. 362-369.

36. Seligra, P.G., et al., Biodegradable and non-retrogradable eco-films based on starch–glycerol with citric acid as crosslinking agent. Carbohydrate Polymers, 2016. 138: p. 66-74.

37. Awadhiya, A., D. Kumar, and V. Verma, Crosslinking of agarose bioplastic using citric acid. Carbohydrate Polymers, 2016. 151: p. 60-67.

38. Reddy, N., Q. Jiang, and Y. Yang, Preparation and properties of peanut protein films crosslinked with citric acid. Industrial Crops and Products, 2012. 39: p. 26-30.

39. Reddy, N. and Y. Yang, Citric acid cross-linking of starch films. Food Chemistry, 2010. 118(3): p. 702-711.

40. Owi, W.T., et al., Unveiling the physicochemical properties of natural Citrus aurantifolia crosslinked tapioca starch/nanocellulose bionanocomposites. Industrial Crops and Products, 2019. 139: p. 111548.

41. Wu, H., et al., Effect of citric acid induced crosslinking on the structure and properties of potato starch/chitosan composite films. Food Hydrocolloids, 2019. 97: p. 105208.

42. Nataraj, D., et al., Crosslinked chitosan films with controllable properties for commercial applications. International Journal of Biological Macromolecules, 2018. 120: p. 1256-1264.

43. Melro, E., et al., Chitosan Films in Food Applications. Tuning Film Properties by Changing Acidic Dissolution Conditions. Polymers, 2021. 13(1): p. 1.

44. ASTM, D570 - 2005. Standard test method for water absorption of plastics. 2005, American Society for Testing and Materials.

45. Suyatma, N.E., et al., Effects of Hydrophilic Plasticizers on Mechanical, Thermal, and Surface Properties of Chitosan Films. Journal of Agricultural and Food Chemistry, 2005. 53(10): p. 3950-3957.

46. ASTM, E96 - 95. Standard test method for water vapor transmission of materials, in Annual book of ASTM standards. 1995, American Society for Testing and Materials.

47. ASTM, D882 - 18. Standard test method for tensile properties of thin plastic sheeting. 1995, American Society for Testing and Materials.

48. ASTM, D4635 - 16. Standard specification for plastic films made from low-density polyethylene for general use and packaging applications. 2016, American Society for Testing and Materials.

49. Li, H., et al., Comparison of chitosan/starch composite film properties before and after cross-linking. International Journal of Biological Macromolecules, 2013. 52: p. 275-279.

50. Foster, E.J., et al., Current characterization methods for cellulose nanomaterials. Chemical Society Reviews, 2018. 47(8): p. 2609-2679.

51. Grząbka-Zasadzińska, A., T. Amietszajew, and S. Borysiak, Thermal and mechanical properties of chitosan nanocomposites with cellulose modified in ionic liquids. Journal of Thermal Analysis and Calorimetry, 2017. 130(1): p. 143-154.

52. Khan, A., et al., Mechanical and barrier properties of nanocrystalline cellulose reinforced chitosan based nanocomposite films. Carbohydrate Polymers, 2012. 90(4): p. 1601-1608.

53. Spinella, S., et al., Concurrent Cellulose Hydrolysis and Esterification to Prepare a Surface-Modified Cellulose Nanocrystal Decorated with Carboxylic Acid Moieties. ACS Sustainable Chemistry & Engineering, 2016. 4(3): p. 1538-1550.

54. Gutiérrez, T.J. and V.A. Alvarez, Bionanocomposite films developed from corn starch and natural and modified nano-clays with or without added blueberry extract. Food Hydrocolloids, 2018. 77: p. 407-420.

55. Zarrinbakhsh, N., A.K. Mohanty, and M. Misra, Improving the interfacial adhesion in a new renewable resource-based biocomposites from biofuel coproduct and biodegradable plastic. Journal of Materials Science, 2013. 48(17): p. 6025-6038.

56. Lassila, L.V.J., et al., Evaluation of some properties of two fiber-reinforced composite materials. Acta Odontologica Scandinavica, 2005. 63(4): p. 196-204.

57. Gohil, J.M., A. Bhattacharya, and P. Ray, Studies On The Crosslinking Of Poly (Vinyl Alcohol). Journal of Polymer Research, 2006. 13(2): p. 161-169.

58. Yang, H.-S., et al., Water absorption behavior and mechanical properties of lignocellulosic filler–polyolefin bio-composites. Composite Structures, 2006. 72(4): p. 429-437.

59. Zhou, Y.J., P. Luner, and P. Caluwe, Mechanism of crosslinking of papers with polyfunctional carboxylic acids. Journal of Applied Polymer Science, 1995. 58(9): p. 1523-1534.

60. Celebi, H. and A. Kurt, Effects of processing on the properties of chitosan/cellulose nanocrystal films. Carbohydrate Polymers, 2015. 133: p. 284-293.

61. Feng, M., et al., Development and preparation of active starch films carrying tea polyphenol. Carbohydrate Polymers, 2018. 196: p. 162-167.

62. Lei, Y., et al., Investigation of the structural and physical properties, antioxidant and antimicrobial activity of pectin-konjac glucomannan composite edible films incorporated with tea polyphenol. Food Hydrocolloids, 2019. 94: p. 128-135.

63. Liu, Y., et al., Chemical modification of chitosan film via surface grafting of citric acid molecular to promote the biomineralization. Applied Surface Science, 2016. 370: p. 270-278.

64. Garavand, F., et al., Improving the integrity of natural biopolymer films used in food packaging by crosslinking approach: A review. International Journal of Biological Macromolecules, 2017. 104: p. 687-707.

65. Kumar, V., et al., Comparison of nano- and microfibrillated cellulose films. Cellulose, 2014. 21(5): p. 3443-3456.

66. Quellmalz, A. and A. Mihranyan, Citric Acid Cross-Linked Nanocellulose-Based Paper for Size-Exclusion Nanofiltration. ACS Biomaterials Science & Engineering, 2015. 1(4): p. 271-276.

67. Li, K., et al., Preparation of chitosan-sodium alginate films through layer-by-layer assembly and ferulic acid crosslinking: Film properties, characterization, and formation mechanism. International Journal of Biological Macromolecules, 2019. 122: p. 485-492.

68. Liu, D., et al., Effects of cellulose nanofibrils on the structure and properties on PVA nanocomposites. Cellulose, 2013. 20(6): p. 2981-2989.

69. Lu, Y., et al., Improved mechanical properties of polylactide nanocomposites-reinforced with cellulose nanofibrils through interfacial engineering via amine-functionalization. Carbohydrate Polymers, 2015. 131: p. 208-217.

70. Xu, J., et al., Plasticized hemicelluloses/chitosan-based edible films reinforced by cellulose nanofiber with enhanced mechanical properties. Carbohydrate Polymers, 2019. 224: p. 115164.

71. Azeredo, H.M.C., et al., Nanocellulose Reinforced Chitosan Composite Films as Affected by Nanofiller Loading and Plasticizer Content. Journal of Food Science, 2010. 75(1): p. N1-N7.

72. Abdulkhani, A., et al., A study of morphological, thermal, mechanical and barrier properties of PLA based biocomposites prepared with micro and nano sized cellulosic fibers. Cellul. Chem. Technol, 2015. 49: p. 597-605.

73. Srivastava, K.R., et al., Effect of nanocellulose on mechanical and barrier properties of PVA–banana pseudostem fiber composite films. Environmental Technology & Innovation, 2021. 21: p. 101312.

74. Cheng, S., et al., Aloe vera rind cellulose nanofibers-reinforced films. Journal of Applied Polymer Science, 2014. 131(15).

75. Yang, J., et al., Preparation and characterization of starch-based bioplastic composites with treated oil palm empty fruit bunch fibers and citric acid. Cellulose, 2021. 28(7): p. 4191-4210.

76. Wang, S., et al., Properties of polyvinyl alcohol/xylan composite films with citric acid. Carbohydrate Polymers, 2014. 103: p. 94-99.

77. Priyadarshi, R., et al., Chitosan film incorporated with citric acid and glycerol as an active packaging material for extension of green chilli shelf life. Carbohydrate Polymers, 2018. 195: p. 329-338.

78. Khouri, J., A. Penlidis, and C. Moresoli, Heterogeneous method of chitosan film preparation: Effect of multifunctional acid on film properties. Journal of Applied Polymer Science, 2020. 137(18): p. 48648.

79. Anderson, K.S., K.M. Schreck, and M.A. Hillmyer, Toughening polylactide. Polymer Reviews, 2008. 48(1): p. 85-108.

CHAPTER 5

COTTON NOIL BASED CELLULOSE MICROFIBERS REINFORCED POLYLACTIC ACID COMPOSITES FOR THE IMPROVEMENT OF WATER VAPOR AND UV BARRIER PROPERTIES IN PACKAGING FILMS[3]

[3] Prabaharan Graceraj Ponnusamy, Suraj Sharma and Sudhagar Mani. To be submitted to Journal of Applied Polymer Science.

Abstract

The cellulose reinforced polylactic acid (PLA) composites are one of the most widely explored biopolymer composites in packaging applications. The poor interfacial adhesion and dispersion of cellulose in PLA matrix pose huge challenges in tensile, water vapor, UV light barrier properties of the composites. The hydrophobic cellulose microfibers (CMF) which are isolated from the cotton noil by ball milling process are reinforced in PLA matrix phase biopolymers with polyethylene glycol (PEG) as a plasticizer by solvent casting method. The strong interfacial adhesion and enhanced dispersion of cotton noil CMF in PLA, increased the tensile, water vapor, UV light barrier properties of the composites. The ultimate tensile stress and Young's modulus of 1% CMF reinforced composites were 46% and 30% respectively higher than that of control films. A further increase in percent CMF reinforcement up to 10% slightly reduced the tensile strength of composites, but comparable to that of low-density polyethylene (LDPE) polymer. The increased CMF reinforcement increased the stress concentration regions on the film surfaces and decreased the tensile strength. The water vapor permeability was decreased while increasing the CMF reinforcement due to the increased diffusion path length by the dispersed CMF. The 20% CMF reinforcement in composite decreased the water vapor permeability by 29%. The UV light absorbance of the composite was improved up to 90% with the increase in CMF reinforcement by up to 20% due to the increased chromophore groups of cellulose. Hence, the PLA-CMF composites could be used as potential packaging materials in storing light and moisture sensitive products.

Keywords: Polylactic acid, Cellulose microfibers, Biopolymer composites, Tensile strength, Water vapor permeability

Introduction

There is a growing interest in developing biopolymer based to packaging materials to protect our environmental pollutions from solid wastes and to meet stringent environmental regulations. The growing interest in environmental protection and stringent environmental regulations increases the attraction of biopolymers for the manufacturing of packaging products. Polylactic acid (PLA) is one of the most widely explored biopolymers because of its excellent material properties such as high strength, transparency, and biodegradability [1, 2]. It is manufactured by polycondensation of lactic acid which is synthesized from the fermentation of renewable biomass such as corn, sugarcane, and cassava [3-5]. The tensile strength, Young's modulus, and elongation at break of the PLA films were between 34~50 MPa, 1~5 GPa, and 2~4% respectively [6-8]. Due to the brittleness, higher moisture absorbance, and low thermal stability characteristics, the PLA films showed inferior tensile, barrier properties than that of fossil-based polymers and posed huge challenges to substitute as a potential polymer for packaging applications [9, 10].

The cellulose fibers are biodegradable fibril networks that are mainly extracted from renewable plant and wood-based biomass. They have a high aspect ratio and surface area to consider them as reinforcement materials in biopolymer composite manufacturing. The cellulose nanofibrils (CNF) and cellulose nanocrystals (CNC) with fibril width of less than 100 nm and cellulose microfibrils (CMF) with fibril width of few nanometers to microns were mainly studied to use as reinforcement materials in PLA biopolymer composites. The reactive hydroxyl groups of cellulose fibers caused intra and intermolecular hydrogen bonds and reduced their dispersion ability in PLA. The poor interfacial adhesion between reinforcement and matrix phase materials exhibited poor mechanical and barrier properties of the composites [11, 12].

One of the methods adopted to increase the interfacial adhesion of cellulose fibers and PLA is blending with the compatibilizers. The dispersion ability of CNC and CMF in the PLA matrix was improved by mixing with montmorillonite (MMT) [13, 14]. The hybrid cellulose composites with compatibilizer (MMT) decreased the tensile strength and Young's modulus by 20% and 17% respectively and improved the water vapor permeability by 33% [14]. The MMT in PLA composite also decreased the degradation time of composites [15]. Similarly, the epoxidized soybean oil (ESO) was blended with PLA and CNF to develop biopolymer composites. Adding 10% of CNF reinforced composites, and 5% of ESO with PLA, increased the dispersibility the composite and played the role of plasticizer to increase the tensile toughness and ductility by 5 to 10 times more. The ultimate tensile strength of the composites was not changed due to the incompatibility of CNF with ESO [16].

The recent approach in improving the compatibility of PLA and cellulose fibers was the surface modification of cellulose fibers by monomer grafting, silylation, acetylation, and esterification processes. The hydroxyl groups of cellulose fibers were modified with the hydrophobic monomers to avoid aggregation. The CNF grafted with hydrophobic monomer (butyl acrylate) improved the compatibility with PLA and produced a homogeneous structure with 5% reinforcement [17]. Similarly, the silanes and esters were also substituted with hydroxyl groups of cellulose fibers to enhance the interaction between cellulose and PLA [18, 19]. The attachment of hydrophobic groups in glucose rings by surface modification processes, generated a new amorphous region and decreased the crystallinity of cellulose (53%) [20]. The reduced crystallinity of surface-modified cellulose could not make a significant improvement in the material properties. Moreover, the tensile strength of polymer composites was decreased significantly with an increase in reinforcement [21-23].

The low production yield, high production cost, and environmental impacts of CNC and CNF disintegration processes increased the attention towards the use of CMF as a potential reinforcement material for PLA [24-26]. However, the CMFs still require a surface modification step to disperse CMF in the PLA matrix. The PLA-CMF composite films showed better water vapor barrier properties but did not show any significant improvement in tensile properties due to the poor adhesion between CMF and PLA [27]. Hence, the objective of this study was to improve tensile, water vapor, and UV light barrier properties of PLA films by reinforcing hydrophobic CMFs without any surface modification step. The CMFs, extracted from cotton noil were used as reinforcement materials in this study. The cotton noil is shorter cotton fibers (~1.32 mm length) that are removed and discarded during the combing process of spun yarn production. They contain about 0.5 to 1 wt.% of natural wax on their surfaces [28]. These waxes provided hydrophobic nature to fibers and enhanced the interfacial adhesion of PLA and CMF. The cotton noil CMF reinforced PLA composite films were manufactured by solvent casting method and their tensile, water vapor, and UV barrier properties were investigated to develop them as potential biopolymer composites for packaging applications.

Experimental

Materials

The cotton noil sample was received from a manufacturer in Georgia, U.S.A, and was used without any treatment to produce CMF. The matrix phase polymer for the composite was prepared from PLA pellets (2003D, food-grade thermoplastic resin, specific gravity 1.24), supplied by NatureWorks LLC. American chemical society (ACS) certified dichloromethane (DCM), and polyethylene glycol (PEG) 8000 (M.W. - 7000~9000, specific gravity - 1.2 ±0.1 and pH @ 5%

water - 6~7) were purchased from VWR International LLC and Fisher scientific respectively and used as solvent and plasticizer in composite manufacturing.

Manufacturing of PLA- CMF composites

The CMFs were manufactured from cotton noil by ball milling process. The cotton noil fiber was milled at 20 Hz vibration frequency using a steel ball of 25 mm diameter and a grinding jar of 50 ml volume in a mixer mill (Retsch GmbH, Germany). The CMF was obtained for the ball milling time of 150 min. The control (sample code - 0CMF) and composite films were manufactured by the solvent casting method. The CMF with 1, 3, 5, 10 and 20% masses (w/w of composite) were considered as reinforcement fractions in composite film production (sample codes- 1CMF, 3CMF, 5CMF, 10CMF and 20CMF respectively). The brittle behavior of pure PLA and CMF reinforcement in composites greatly challenged the flexibility and tensile toughness of the films. Hence, the PEG (5%, w/w of films) was added as a plasticizer in control and composite film samples.

The PLA pellets and milled cotton noil were dried in an oven @ 55 °C for 48 h to evaporate absorbed moisture. The oven-dried PLA pellets (5% w/v) was added to DCM solvent and mixed vigorously in a magnetic stirrer plate at room temperature until it dissolved. The CMF and PEG were added in a completely dissolved PLA solution and were mixed for 2h. The solutions were poured in glass Petri dishes after degassing the solution for 30 min. The Petri dishes were covered with aluminum foil and DCM was slowly evaporated at room temperature in a fume hood. The dried films were peeled off from the Petri dishes after 24 h and stored in a desiccator @ 50% RH for more than 48 h before the characterization studies. Each treatment condition was repeated five times.

Fourier-transformed infrared (FTIR) spectra

The Fourier-transformed infrared (FTIR) spectra were used to characterize the chemical structure of CMFs which were manufactured by ball milling. The CMF powder was dried in a desiccator for 24h before FTIR spectra measurements in Thermo Scientific Nicolet 6700 VariGATRTM spectrometer. The FTIR spectra were recorded for three replications in absorbance mode for wave numbers 600 to 4000 cm^{-1} with a resolution of 4 cm^{-1}.

X-ray diffraction (XRD)

The crystallinity of CMFs was evaluated from X-ray diffraction (XRD) patterns, obtained from Bruker D8 Advance model XRD system. The Co tube X-ray source with wavelength of 1.79 Å, voltage and current setting of 35kV and 40mA were used in the testing. The XRD patterns were recorded for the diffraction angle (2θ) between 10 to 40° with the rate of 6°/min. The crystallinity index (CI) was calculated from the following equation [29, 30].

$$CI = \frac{I_{0\,0\,2} - I_{am}}{I_{0\,0\,2}} \times 100\ \%$$

Where

$I_{0\,0\,2}$ = Diffraction $intensity$ peak of $lattice\ plane$ $(0\ 0\ 2)$ $for\ 2\theta\ between\ 26\ °\ to\ 27\ °$

$I_{am} = Diffraction\ intensity\ of\ amorphous\ region\ for\ 2\theta\ between\ 21\ °\ to\ 22\ °$

Scanning electron microscope (SEM) study

The dimensional characteristics of CMFs were studied from a scanning electron microscope (SEM) The 15 nm gold-palladium coating was applied on CMF powders in Leica Mikrosysteme GmbH sputtering unit. The images of sputter-coated CMF were captured for the spot size of 8 nm in a Thermo Fisher Scientific Teneo (Thermo Fisher Scientific, Hillsboro, OR, USA) field electron microscope, with 5kV accelerating voltage.

Tensile strength of composite films

The tensile tests were performed according to the ASTM D882 (Standard Test Method for Tensile Properties of Thin Plastic Sheeting) standard [31]. The film specimens were loaded at 50 mm/min crosshead speed in a Shimadzu (AGS-X) tensile tester with a 1 kN load cell. The tests were performed at ambient temperature. The ultimate tensile strength and Young's modulus were recorded for the five replications of each sample.

Water vapor permeability of composite films

The water vapor permeability of films was measured by the desiccant method based on the ASTM E96 (Standard Test Methods for Water Vapor Transmission of Materials) standard [32]. The dried (at 200 °C) desiccants were filled up to the level of 6 mm from the mouth in the open mouth test cups with a mouth area of 240 mm^2. Five films from each variant were attached to the test cups and were sealed with pressure-sensitive, vinyl chloride insulating tape. All the test cup assemblies were placed in a test chamber maintained at 50 ± 5 % RH and 23 ± 2 °C. The weights of test cup assemblies with an accuracy of 0.0001 g were recorded in a 24 h interval. The changes in the weight of a test cup assembly over time were calculated by fitting a linear regression line on the recorded data. The WVP of the films was calculated from the following equation.

$$WVP = {}^{G}/_{[t \times A \times S \times (R_1 - R_2)]} \ \mathrm{g/Pa.s.m^2}$$

Where:

$G = Weight\ change\ in\ test\ cup\ assembly\ in$ g

$T = Time\ during\ which\ G\ occurred\ in$ s

$A = Test\ cup\ mouth\ area\ in$ m^2

$S = Saturation\ vapor\ pressure\ at$ 23 °C in Pa

$R1 = Relative\ humidity\ of\ chamber\ in\ fraction$

$R2 = Relative\ humidity\ at\ the\ vapor\ sink\ in\ fraction$

Ultraviolet-visible spectrometry

The ultraviolet-visible (UV-Vis) spectra of PLA and composite films were studied to understand the effect of cotton noil CMF in light transmittance. The Varian Cary® 50 spectrometer (Agilent Technologies, U.S.A.) was operated at 600 nm/min scan rate and wavelength in the range of 200 to 800 nm. The scan software version 3.0 (Agilent Technologies, U.S.A.) was used to acquire the UV-Vis data at 1 nm data interval and 0.1 s average time. The thickness of the films studied was 0.05 ± 0.01 mm. Three replications of each film were tested at ambient conditions.

Statistical analysis

The one-way ANOVA test was conducted on the measured data to analyze the effect of CMF reinforcement on tensile and water vapor barrier properties of PLA films. The significant difference in mean tensile and water vapor barrier properties values of each film type was determined at 5 % significance levels in the MATLAB software.

Results and discussions

Chemical structure of CMF

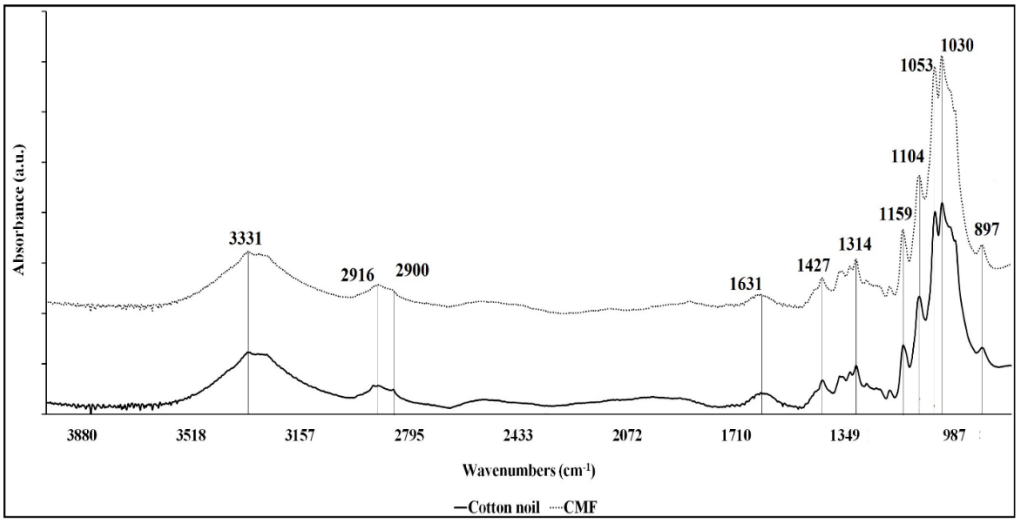

Figure 5-1. FTIR spectra of cotton noil and CMF

The FTIR spectra of cotton noil and CMF were compared as shown in Figure 5-1. The FTIR peaks confirmed that cellulose and non-cellulosic compounds such as pectin, protein, and wax were present in cotton noil and CMF [33-35]. The characteristics peaks in cotton noil and CMF have appeared at the same frequency and intensity. It revealed that the ball milling process did not affect the chemical structure of cellulose and non-cellulosic compounds presented in the cotton noil. The typical characteristic peaks corresponding to the cellulose chemical structure have appeared in both cotton noil and CMF. The broadband and strong peak at 3331 cm^{-1} were due to the stretching of cellulose -OH groups. The peaks at 2900, 1427, and 1314 cm^{-1} were attributed to the stretching and deformation frequencies of the O-C-H and H-C-H groups of cellulose. The peaks which were appeared at 1159, 1104, 1053, and 1030 cm^{-1} were assigned to the asymmetric C-O-C stretching, asymmetric in-plane stretching and C-O bond stretching respectively. The C-O-C stretching at β-(1→ 4) glycosidic bonds of the cellulose was confirmed from a small peak at 897 cm^{-1}. The characteristics peaks at 2916 and 1631 cm^{-1} in cotton noil and CMF spectra were corresponding to the asymmetrical stretching of CH_2 groups and stretching of C=O bonds of waxes and proteins or pectin [33, 34, 36, 37].

Crystallinity of CMF

The comparison of x-ray diffractograms of cotton noil and CMF are shown in Figure 5-2. The diffraction peaks have appeared for the same 2θ in cotton noil and CMF samples. The crystalline structure of cotton noil and CMF were confirmed by the appearance of diffraction peaks at 2θ = 17.48°, 19.16° and 26.52°. These peaks are corresponding to the crystallographic planes (1 0 1), (1 0 1), and (0 0 2) of cellulose as specified by the International Center for Diffraction Data (ICDD) [29]. Further, the comparison of crystallinity peaks of CMF with cotton noil showed the

changes in the intensity of peaks. The crystallinity peaks at 2θ = 17.48° and 26.52° were increased by 50 and 60% respectively after the ball milling process. It was decreased by 20% at 2θ = 19.16°.

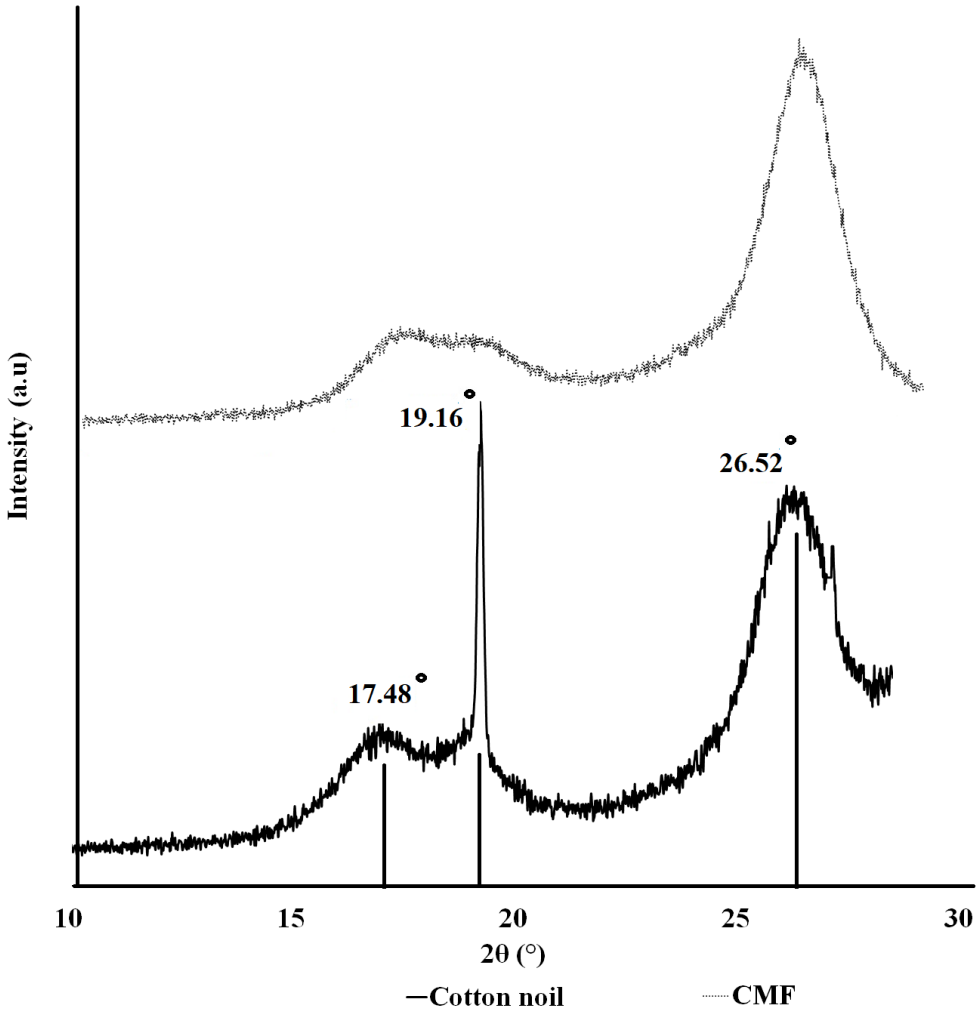

Figure 5-2. XRD diffractograms of cotton noil and CMF

The crystallinity index of cotton noil was 82.71 ± 0.47% and was marginally decreased to 79.76 ± 0.47% in CMF samples. This may be due to the ball milling process. While increasing the milling time for more than 2h, the ball milling process tends to decrease the crystallinity of cellulose due to the application of high shear and impact forces [38-40]. However, the crystallinity of manufactured CMF was higher than the surface-modified CNF (CI-53%) and CNC (CI-70%) used in the production of PLA composites [20, 41]. The ball milling process fibrillated the cotton

noil into micron-sized fibers and increased the specific surface area. The highly ordered molecular structure in the smaller crystals of cellulose surfaces was increased by the ball milling and increased crystallinity [42]. The marginal increase in the amorphous region was due to the disruption of the crystalline region in the cellulose surfaces by ball milling process [43, 44].

CMF width analysis

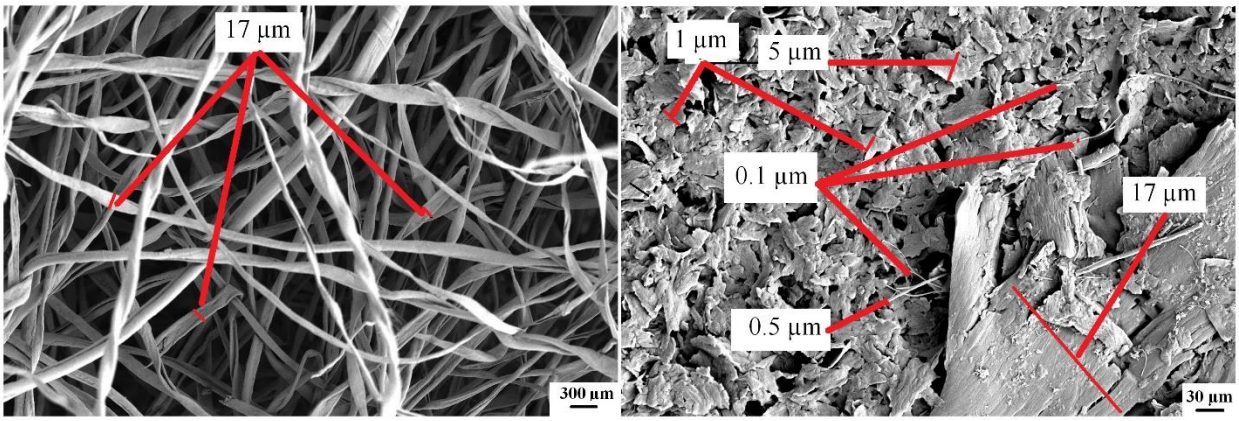

Figure 5-3. Fiber size characterization of cotton noil and CMF from SEM images

The width of CMFs and cotton noil fibers were measured from SEM images (Figure 5-3). The SEM images of cotton noil showed highly entangled fibers and posed challenges in measuring fiber length. Some of the fibers were twisted and bundled together. The width of the fibers was measured from SEM images. The mean width of fibers in cotton noil was16.90 ± 4.09 µm. The width of the fibers was substantially reduced (65%) by the ball milling process during the CMF production. The average fiber width of CMF was 5.93 ± 7.83 µm and about 90% of CMF width was distributed between 100 nm to 5.91 µm. The fiber width distribution confirmed the effective CMF fibrilization by ball milling treatment. Moreover, the SEM images evidenced the presence of CMF with fibrous surface morphology and without any agglomeration. The fibrous surface morphology of CMF was obtained by the application high of shear and impact loads in the ball milling process. The hydrophobic nature of fibers prevented the aggregation of fibers. The fibrous

surface morphology and the hydrophobic nature enabled the good dispersion ability in CMF during the composite manufacturing process.

Effect of CMF reinforcement in translucency

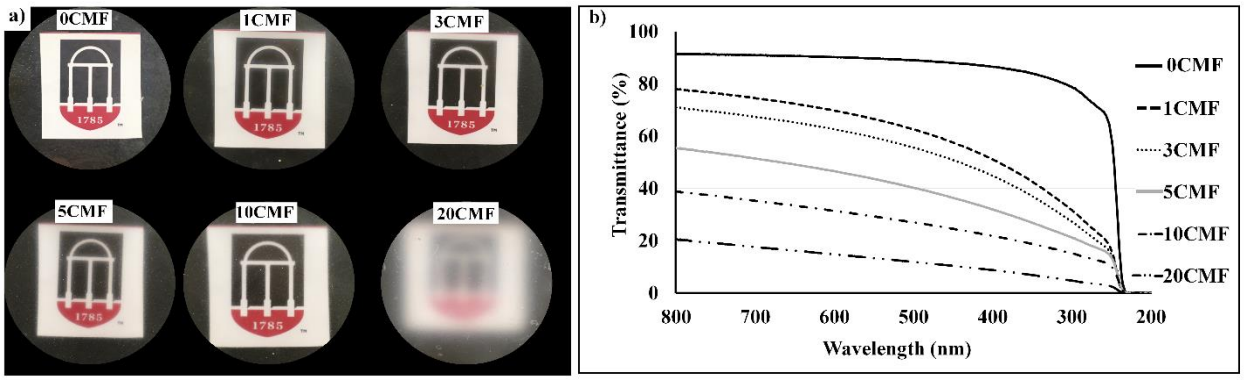

Figure 5-4. Effect of CMF reinforcement in PLA matrix composite film translucency a) qualitative assessment by visual observation b) UV-Vis spectrometry

The dispersion of CMF in the PLA matrix was analyzed from the high-quality photographs of composite films having a uniform thickness of 0.05 ± 0.01 mm as shown in Figure 5-4a.The visual evaluation of composite films showed that the control PLA film (0CMF) was completely transparent and all the details of the emblem under the film were visible. The translucency of the films was slightly reduced with the reinforcement of 1 and 3% CMF (1CMF and 3CMF) and was moderately reduced for 5 and 10% of reinforcement (5CMF and 10CMF). The aggregation of CMFs was observed only in the composite films with 20% CMF reinforcement (20CMF) with a significant increase in opacity of the film. The details of the emblem were not clear in 20% CMF reinforcement (20CMF). The uniform translucency was evidenced in the entire surface area of all the films as discussed by Tang and Liu 2008 on highly transparent polyvinyl alcohol-CNF reinforced composite films [45]. The uniform dispersion of opaque CMFs in PLA matrix polymer reduced the transparency of composite films. The CMF fibers which width was larger than 400 nm caused reflection and increased the light absorbance. The width of CMFs, the spatial distance

of fibers in the PLA matrix, and the adhesion of fibers with the PLA matrix determined the microstructure of composite and the specific translucency of the composites [46-48].

The UV-Vis spectra of PLA (0CMF) and CMF reinforced composite films (1CMF, 3CMF, 5CMF, 10CMF, and 20CMF) are shown in Figure 5-4b and the present transmittance at 600, 400, and 233 nm are given in Table 5-1. The light absorbance behavior of PLA-CMF composite was similar to the composite films reinforced with CNC, CNF and nanoclay studied in the literature [14, 19]. The CMF reinforcement in composites reduced the transmittance consistently. It was 90% at 600 nm for PLA films without CMF reinforcement and was reduced by 23 and 31% for 1 and 3% CMF reinforcement. It was further reduced by 48, 65, and 84% for the increased CMF reinforcement with 5, 10, and 20% respectively. The reduction in transmittance of composite films was dependent on the amount of CMF reinforcement in the composite. The severe light refraction, scattering, and reflection at the interfaces of 5, 10, and 20% CMF reinforcement were the reason for poor transmittance at higher CMF loading [49]. The increase in CMF reinforcement increased the light scattering area in the composite and increased the number of optical interfaces [50]. The reflection of light in the areas of reinforcement material was the major factor that reduced the transmittance [51]. The transmittance at 400 nm was 41, 48, 63, 75, and 90% less than the control film for 1, 3, 5, 10, and 20% CMF reinforcement. The improvement in UV light barrier properties of composite films with CMF reinforcement was same as the PLA-CNC composite and was better than the pure PLA films reported in the literature [52]. The self-assembled cellulose structure in the CMF improved UV absorbance in CMF reinforced composites [53]. The lowest transmittance of all films at 233 nm indicated that the films were good to absorb UVC light.

Table 5-1. Present transmittance of PLA and composite films at 600, 400 and 233 nm wavelength

Wavelength (nm)	Transmittance (%)					
	0CMF	1CMF	3CMF	5CMF	10CMF	20CMF
600	90.13	69.67	62.54	46.55	31.41	14.78
400	86.51	51.04	44.80	31.93	21.84	8.74
233	0.74	0.11	0.49	0.31	0.34	0.034

Effect of CMF reinforcement in tensile strength

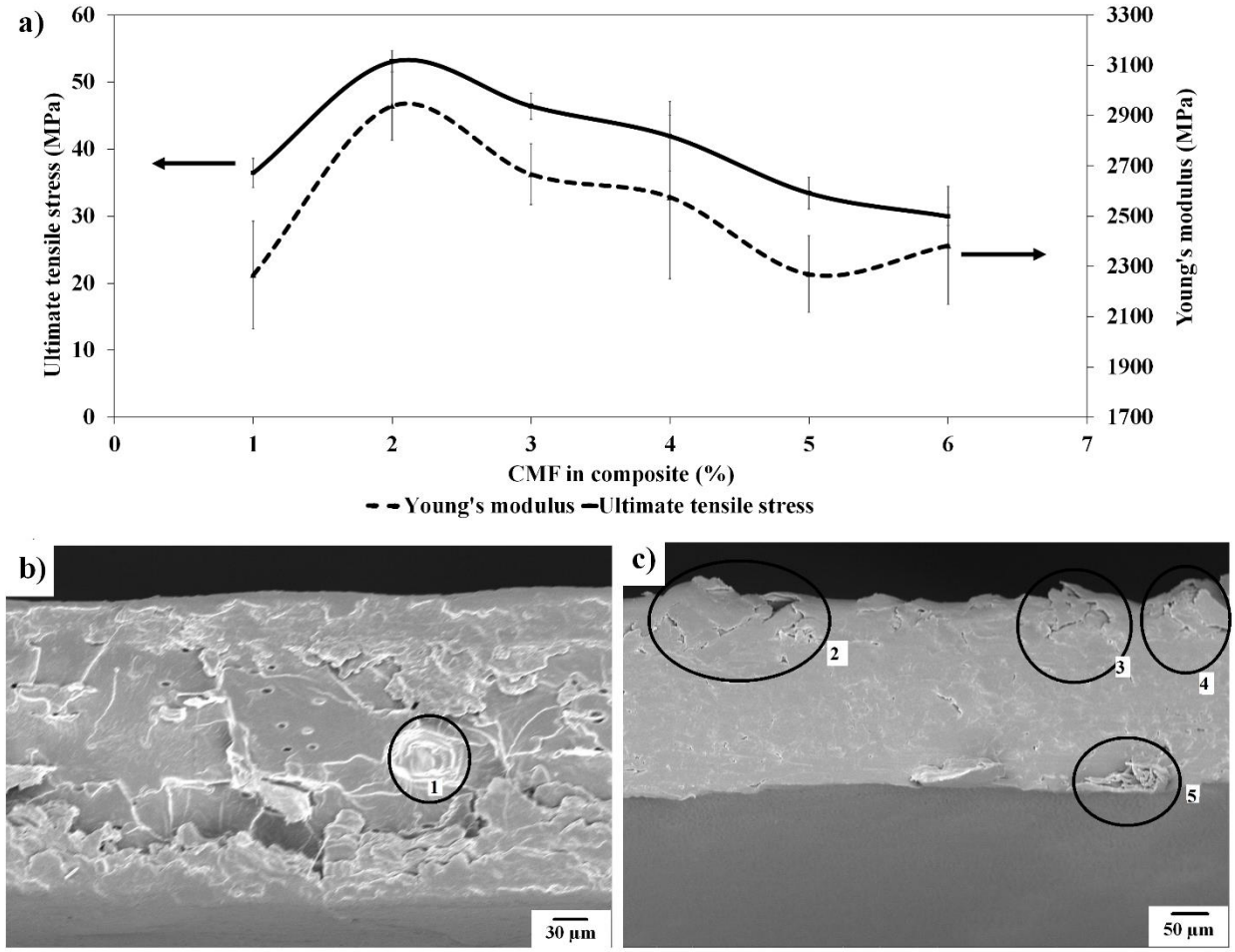

Figure 5-5. Tensile test results of PLA films with and without CMF reinforcement a) Effect of reinforcement in ultimate tensile stress and Young's modulus b) and c) Tensile fractured surface morphology of composite films with 3 and 10% CMF reinforcement

The effect of CMF reinforcement in ultimate tensile stress and Young's modulus are shown in Figure 5-5a. The ultimate tensile stress and Young's modulus of control (0CMF) film were 36.43 ± 2.19 and 2265.80 ± 214.24 MPa respectively. Similar results were reported in the literature for the cast films produced from the PLA having molecular weight 100,000 and 130,000 $gmol^{-1}$ and without plasticizer [21, 24]. The composite films exhibited a significant increase in ultimate tensile stress and Young's modulus for 1, 3, and 5% CMF reinforcement (ANOVA test results in Table 5-S1 and 5-S2). The ultimate tensile stress and Young's modulus were increased by 46 and 30% respectively for the 1% CMF reinforcement. Similarly, they were increased 27 and 18% for the reinforcement of 3% CMF and 15 and 14% for the reinforcement of 5% CMF in composites. At 10 and 20% reinforcement of CMF, the observed ultimate tensile stress and Young's modulus were less than the tensile strength of the control sample. Even though the ultimate tensile stress was reduced, they were comparable with polyethylene (22-31 MPa) and polypropylene (31-38 MPa) films [14].

Several literatures reported that the reinforcement of surface-modified CNF or CMF in PLA could increase the ultimate tensile stress and Young's modulus by 14 to 25% and 8 – 40% respectively [8, 24, 54-59]. The tensile properties of the composites were mainly affected by the CNF/CMF surface modification processes adapted in the composite manufacturing method [60, 61]. The CNF/CMF surface modifiers such as acetic anhydride, maleic anhydride, and saline reacted with the chain ends of crystallites regions and converted them into the amorphous region during chemical surface modification processes [62]. In addition to that the agglomeration of unmodified surfaces of cellulose decreased dispersion ability and reduced the tensile properties of the composite [63]. In this study, the increased tensile properties of composite films are attributed

to the hydrophobic nature of CMFs that improved the interfacial adhesion with PLA matrix and the high crystalline cellulose in the CMF.

The tensile fracture surface morphology of composite films (Figure 5-5b and 5-5c) were studied to understand the interfacial adhesion of CMFs with PLA matrix. The SEM images of the fracture surface showed the broken fibers (places marked 1 to 5 in Figure 5-5b and 5-5c) without any pulling out from the PLA matrix and confirmed the strong interfacial adhesion of CMF with PLA. The PLA-CMF interfaces enabled the strong stress transfer region to withstand increased tensile loading in composites for lower CMF concentration [64, 65]. The Figure 5-5a. shows the fractured surface of a composite with lower CMF reinforcement (3%). The surface morphology of the fractured composite was rough and irregular. At the lower percentage of CMF reinforcement, highly dispersed fibers together with PLA matrix materials were pulled out and resulted in rough and irregular surface morphology [66-69]. The strong interfacial adhesion and highly dispersed fibers exhibited increased tensile stress while compared to the control films and the 10 or higher percentage of CMF reinforcement. At the higher percentage of CMF reinforcement (10% and more), the surface morphology was smooth due to the increased brittleness of the composite by the increased CMFs (Figure 5-5b). The debonding of fibers from the PLA matrix was also evidenced on the fibers which were close to the surfaces (Figure 5-5b with marking 2 to 4). More stress concentration regions were developed in those areas to initiate the rapid crack growth. The rapid planer crack propagation due to the increased reinforcement caused the brittle failure in the composites with more than 10% CMF reinforcement [70].

Effect of CMF reinforcement in water vapor permeability

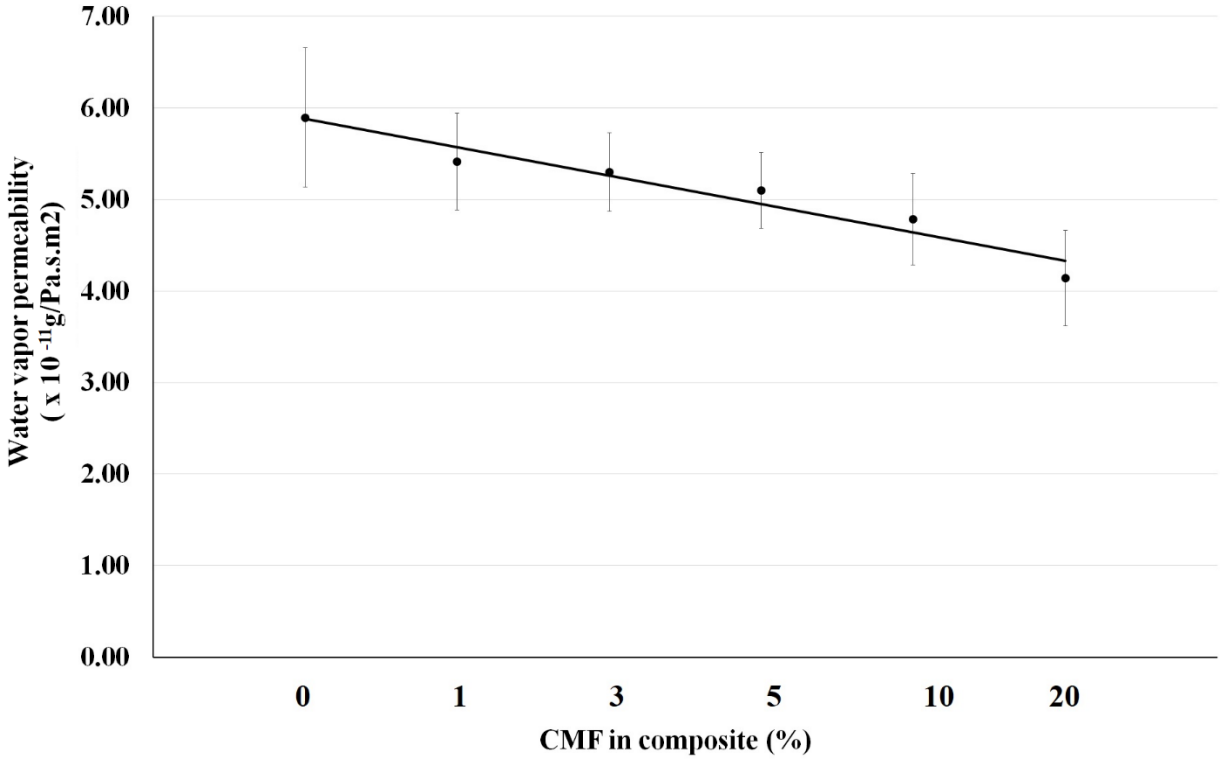

Figure 5-6. Effect of CMF reinforcement in water vapor permeability of PLA matrix composite films

The effect of CMF reinforcement in water vapor permeability (WVP) of composite films is shown in Figure 5-6. The WVP of control film was 5.90 x 10^{-11} g/Pa.s.m^2. It was ~15% higher than the 100% PLA film which was manufactured from 2002D type NatureWorks® PLA [71]. The addition of plasticizer (5% PEG) in control type PLA films increased intermolecular spacing and thereby increased the WVP in the control film. The WVP of composite films was significantly changed with the increase in CMF reinforcement percentage (See ANOVA results in Table 5-S3). While increasing the CMF in the composite by 1, 3, 5, 10, and 20%, the WVP decreased by 7, 9, 12, 18, and 29% concerning the control films (0CMF). The lowest WVP of 4.14 x 10^{-11} g/Pa.s.m^2 was obtained for CMF reinforcement of 20%. It was about 65, 208, 535, 1490, 2620% lower than the polycaprolactone, aliphatic polyester, polyester amide, cellulose acetate propionate, cellulose

acetate biopolymers respectively [72]. But, the WVP of fossil-based polymers such as low-density polyethylene and polypropylene was much lower than (up to 80%) the composite films studied. The improvement in water vapor barrier properties is in agreement with the study by Rhim et al. 2009 on PLA-nano clay composite films. The limitation of nano clay reinforcement in PLA was the decrease in tensile strength due to their poor dispersion ability in PLA [14]. Similarly, in an attempt to increase the WVP of PLA composite with surface modified CNF, the WVP was increased for the 5% or higher reinforcement. The porous structure created by the hydrophobic fibrils and unmodified hydroxyl groups increased the transport of water vapor for the higher CNF reinforcement [17]. The WVP results of our study confirmed that the hydrophobicity of PLA and CMF and the increase in diffusion path length due to the improved dispersion of CMF in PLA increased the water vapor barrier properties of composite films with the increase in CMF reinforcement [73, 74].

Conclusions

The CMFs isolated from cotton noil by a ball milling process was reinforced in PLA to produce composite films by solvent casting method. The width of the isolated CMF was distributed between 100 nm to 5.91 µm. The analysis of chemical structure confirmed the presence of cellulose and hydrophobic wax in the isolated CMFs. It was also found that the crystallinity of cellulose did not affect by the ball milling process. The crystalline, hydrophobic and opaque CMFs dispersed uniformly in the PLA matrix and reduced the translucence for CMF reinforcement. The UV light absorbance of the CMF reinforced composites was increased from 41 to 90% for the reinforcement of 1% to 20% CMF. The strong interfacial adhesion between PLA and CMF increased the tensile strength of composite films. The ultimate tensile stress and Young's modulus of 1% CMF reinforced composite film was 46 and 30% higher than the control films. The tensile strength was

decreased while increasing the CMF reinforcement from 3 to 20%. However, they were comparable with that of fossil-based polymer films such as polyethylene and polypropylene which are predominantly used in packaging applications. The good dispersion ability and strong interfacial adhesion of CMF with PLA increased the water vapor barrier properties of the composite films. The water vapor permeability was decreased with an increase in CMF reinforcement. It was reduced by 29% for the reinforcement of 20% CMF in the composite. Hence, the CMFs isolated from the cotton noil could be considered as potential reinforcement materials for the development of PLA composite and could be used as promising bio-based polymers for the packaging of UV light sensitive and moisture sensitive products.

References

1. Castro-Aguirre, E., et al., Poly(lactic acid)—Mass production, processing, industrial applications, and end of life. Advanced Drug Delivery Reviews, 2016. 107: p. 333-366.
2. Lim, L.T., R. Auras, and M. Rubino, Processing technologies for poly(lactic acid). Progress in Polymer Science, 2008. 33(8): p. 820-852.
3. John, R.P., K.M. Nampoothiri, and A. Pandey, Fermentative production of lactic acid from biomass: an overview on process developments and future perspectives. Applied Microbiology and Biotechnology, 2007. 74(3): p. 524-534.
4. Inkinen, S., et al., From Lactic Acid to Poly(lactic acid) (PLA): Characterization and Analysis of PLA and Its Precursors. Biomacromolecules, 2011. 12(3): p. 523-532.
5. Garlotta, D., A Literature Review of Poly(Lactic Acid). Journal of Polymers and the Environment, 2001. 9(2): p. 63-84.
6. Anderson, K.S., K.M. Schreck, and M.A. Hillmyer, Toughening polylactide. Polymer Reviews, 2008. 48(1): p. 85-108.
7. Raquez, J.-M., et al., Polylactide (PLA)-based nanocomposites. Progress in Polymer Science, 2013. 38(10): p. 1504-1542.
8. Li, K., et al., Surface-modified and oven-dried microfibrillated cellulose reinforced biocomposites: Cellulose network enabled high performance. Carbohydrate Polymers, 2021. 256: p. 117525.
9. Murariu, M. and P. Dubois, PLA composites: From production to properties. Advanced drug delivery reviews, 2016. 107: p. 17-46.

10. Bhasney, S.M., et al., Morphology and crystalline characteristics of polylactic acid [PLA]/linear low density polyethylene [LLDPE]/microcrystalline cellulose [MCC] fiber composite. Composites Science and Technology, 2019. 171: p. 54-61.
11. Lee, W.D., et al., Preparation and properties of layered double hydroxide/poly (ethylene terephthalate) nanocomposites by direct melt compounding. Polymer, 2006. 47(4): p. 1364-1371.
12. Mathew, A.P., K. Oksman, and M. Sain, The effect of morphology and chemical characteristics of cellulose reinforcements on the crystallinity of polylactic acid. Journal of Applied Polymer Science, 2006. 101(1): p. 300-310.
13. Arjmandi, R., et al., Partial replacement effect of montmorillonite with cellulose nanowhiskers on polylactic acid nanocomposites. 2015. 81: p. 91-99.
14. Rhim, J.-W., S.-I. Hong, and C.-S. Ha, Tensile, water vapor barrier and antimicrobial properties of PLA/nanoclay composite films. LWT-Food Science and Technology, 2009. 42(2): p. 612-617.
15. Sedničková, M., et al., Changes of physical properties of PLA-based blends during early stage of biodegradation in compost. International journal of biological macromolecules, 2018. 113: p. 434-442.
16. Meng, X., et al., Toughening of nanocelluose/PLA composites via bio-epoxy interaction: Mechanistic study. Materials & Design, 2018. 139: p. 188-197.
17. Song, Z., H. Xiao, and Y. Zhao, Hydrophobic-modified nano-cellulose fiber/PLA biodegradable composites for lowering water vapor transmission rate (WVTR) of paper. Carbohydrate polymers, 2014. 111: p. 442-448.

18. Raquez, J.M., et al., Surface-modification of cellulose nanowhiskers and their use as nanoreinforcers into polylactide: A sustainably-integrated approach. Composites Science and Technology, 2012. 72(5): p. 544-549.
19. Chi, K. and J.M. Catchmark, Enhanced dispersion and interface compatibilization of crystalline nanocellulose in polylactide by surfactant adsorption. Cellulose, 2017. 24(11): p. 4845-4860.
20. Robles, E., et al., Surface-modified nano-cellulose as reinforcement in poly(lactic acid) to conform new composites. Industrial Crops and Products, 2015. 71: p. 44-53.
21. Qu, P., et al., Nanocomposites of poly (lactic acid) reinforced with cellulose nanofibrils. BioResources, 2010. 5(3): p. 1811-1823.
22. Neves, R.M., et al., The influence of silane surface modification on microcrystalline cellulose characteristics. Carbohydrate Polymers, 2020. 230: p. 115595.
23. Wu, Q., et al., The effect of surface modification on chemical and crystalline structure of the cellulose III nanocrystals. Carbohydrate Polymers, 2020. 235: p. 115962.
24. Yetiş, F., et al., Acetylation of lignin containing microfibrillated cellulose and its reinforcing effect for polylactic acid. European Polymer Journal, 2020. 134: p. 109803.
25. Peng, S.X., et al., A comparative guide to controlled hydrophobization of cellulose nanocrystals via surface esterification. Cellulose, 2016. 23(3): p. 1825-1846.
26. Arvidsson, R., D. Nguyen, and M. Svanström, Life Cycle Assessment of Cellulose Nanofibrils Production by Mechanical Treatment and Two Different Pretreatment Processes. Environmental Science & Technology, 2015. 49(11): p. 6881-6890.

27. Abdulkhani, A., et al., A study of morphological, thermal, mechanical and barrier properties of PLA based biocomposites prepared with micro and nano sized cellulosic fibers. Cellul. Chem. Technol, 2015. 49: p. 597-605.

28. Church, J.S. and A.L. Woodhead, Cotton fiber wax and surface properties. Cotton fibers: characteristics, uses and performance. Nova Science, New York, 2017: p. 21-41.

29. Morais, J.P.S., et al., Extraction and characterization of nanocellulose structures from raw cotton linter. Carbohydrate polymers, 2013. 91(1): p. 229-235.

30. Segal, L., et al., An empirical method for estimating the degree of crystallinity of native cellulose using the X-ray diffractometer. Textile research journal, 1959. 29(10): p. 786-794.

31. ASTM, D882 - 18. Standard test method for tensile properties of thin plastic sheeting. 1995, American Society for Testing and Materials.

32. ASTM, E96 - 95. Standard test method for water vapor transmission of materials, in Annual book of ASTM standards. 1995, American Society for Testing and Materials.

33. Zhang, L., et al., Micro-FTIR combined with curve fitting method to study cellulose crystallinity of developing cotton fibers. Analytical and Bioanalytical Chemistry, 2021. 413(5): p. 1313-1320.

34. Dave, H., et al., The removal of impurities from gray cotton fabric by atmospheric pressure plasma treatment and its characterization using ATR-FTIR spectroscopy. The Journal of The Textile Institute, 2014. 105(6): p. 586-596.

35. Lin, C.-H. and Y.-L. Hsieh, Direct Scouring of Greige Cotton Fabrics with Proteases. Textile Research Journal, 2001. 71(5): p. 425-434.

36. Oun, A.A. and J.-W. Rhim, Characterization of carboxymethyl cellulose-based nanocomposite films reinforced with oxidized nanocellulose isolated using ammonium persulfate method. Carbohydrate Polymers, 2017. 174: p. 484-492.

37. Ciolacu, D., J. Kovac, and V. Kokol, The effect of the cellulose-binding domain from Clostridium cellulovorans on the supramolecular structure of cellulose fibers. Carbohydrate Research, 2010. 345(5): p. 621-630.

38. Schwanninger, M., et al., Effects of short-time vibratory ball milling on the shape of FT-IR spectra of wood and cellulose. Vibrational Spectroscopy, 2004. 36(1): p. 23-40.

39. Amiralian, N., et al., Isolation of cellulose nanofibrils from Triodia pungens via different mechanical methods. Cellulose, 2015. 22(4): p. 2483-2498.

40. Zhang, L., T. Tsuzuki, and X. Wang, Preparation of cellulose nanofiber from softwood pulp by ball milling. Cellulose, 2015. 22(3): p. 1729-1741.

41. Dhuiège, B., G. Pecastaings, and G. Sèbe, Sustainable Approach for the Direct Functionalization of Cellulose Nanocrystals Dispersed in Water by Transesterification of Vinyl Acetate. ACS Sustainable Chemistry & Engineering, 2019. 7(1): p. 187-196.

42. Ling, Z., et al., Effects of ball milling on the structure of cotton cellulose. Cellulose, 2019. 26(1): p. 305-328.

43. Fattahi Meyabadi, T., et al., Spherical cellulose nanoparticles preparation from waste cotton using a green method. Powder Technology, 2014. 261: p. 232-240.

44. Zhao, H., et al., Effects of Crystallinity on Dilute Acid Hydrolysis of Cellulose by Cellulose Ball-Milling Study. Energy & Fuels, 2006. 20(2): p. 807-811.

45. Tang, C. and H. Liu, Cellulose nanofiber reinforced poly(vinyl alcohol) composite film with high visible light transmittance. Composites Part A: Applied Science and Manufacturing, 2008. 39(10): p. 1638-1643.

46. Soykeabkaew, N., et al., Reinforcing potential of micro- and nano-sized fibers in the starch-based biocomposites. Composites Science and Technology, 2012. 72(7): p. 845-852.

47. Ng, H.K.M. and C.P. Leo, Translucent and adsorptive PVA thin film containing microfibrillated cellulose intercalated with TiO2 nanoparticles for dye removal. Colloids and Surfaces A: Physicochemical and Engineering Aspects, 2019. 578: p. 123590.

48. Wang, Z., X. Qiao, and K. Sun, Rice straw cellulose nanofibrils reinforced poly(vinyl alcohol) composite films. Carbohydrate Polymers, 2018. 197: p. 442-450.

49. Liu, R., C. Tang, and H. Liu, Cellulose Nanofiber-Protein Composite, in Handbook of Polymer Nanocomposites. Processing, Performance and Application: Volume C: Polymer Nanocomposites of Cellulose Nanoparticles, J.K. Pandey, et al., Editors. 2015, Springer Berlin Heidelberg: Berlin, Heidelberg. p. 449-464.

50. Li, B., et al., Optical and mechanical anisotropies of aligned electrospun nanofibers reinforced transparent PMMA nanocomposites. Composites Part A: Applied Science and Manufacturing, 2016. 90: p. 380-389.

51. Kurokawa, N. and A. Hotta, Thermomechanical properties of highly transparent self-reinforced polylactide composites with electrospun stereocomplex polylactide nanofibers. Polymer, 2018. 153: p. 214-222.

52. Mármol, G., C. Gauss, and R. Fangueiro, Potential of Cellulose Microfibers for PHA and PLA Biopolymers Reinforcement. Molecules, 2020. 25(20): p. 4653.

53. Abitbol, T., et al., Nanocellulose-Based Hybrid Materials for UV Blocking and Mechanically Robust Barriers. ACS Applied Bio Materials, 2020. 3(4): p. 2245-2254.

54. Iwatake, A., M. Nogi, and H. Yano, Cellulose nanofiber-reinforced polylactic acid. Composites Science and Technology, 2008. 68(9): p. 2103-2106.

55. Jonoobi, M., et al., Mechanical properties of cellulose nanofiber (CNF) reinforced polylactic acid (PLA) prepared by twin screw extrusion. Composites Science and Technology, 2010. 70(12): p. 1742-1747.

56. Suryanegara, L., A.N. Nakagaito, and H. Yano, Thermo-mechanical properties of microfibrillated cellulose-reinforced partially crystallized PLA composites. Cellulose, 2010. 17(4): p. 771-778.

57. Okubo, K., T. Fujii, and E.T. Thostenson, Multi-scale hybrid biocomposite: Processing and mechanical characterization of bamboo fiber reinforced PLA with microfibrillated cellulose. Composites Part A: Applied Science and Manufacturing, 2009. 40(4): p. 469-475.

58. Jonoobi, M., et al., A Comparison of Modified and Unmodified Cellulose Nanofiber Reinforced Polylactic Acid (PLA) Prepared by Twin Screw Extrusion. Journal of Polymers and the Environment, 2012. 20(4): p. 991-997.

59. Pandey, J.K., C.S. Lee, and S.-H. Ahn, Preparation and properties of bio-nanoreinforced composites from biodegradable polymer matrix and cellulose whiskers. Journal of Applied Polymer Science, 2010. 115(4): p. 2493-2501.

60. Klemm, D., et al., Nanocelluloses: a new family of nature-based materials. Angewandte Chemie International Edition, 2011. 50(24): p. 5438-5466.

61. Kumar, V., et al., Comparison of nano- and microfibrillated cellulose films. Cellulose, 2014. 21(5): p. 3443-3456.

62. Sawpan, M.A., K.L. Pickering, and A. Fernyhough, Effect of various chemical treatments on the fibre structure and tensile properties of industrial hemp fibres. Composites Part A: Applied Science and Manufacturing, 2011. 42(8): p. 888-895.

63. Abe, K. and H. Yano, Comparison of the characteristics of cellulose microfibril aggregates of wood, rice straw and potato tuber. Cellulose, 2009. 16(6): p. 1017-1023.

64. Jesson, D.A. and J.F. Watts, The Interface and Interphase in Polymer Matrix Composites: Effect on Mechanical Properties and Methods for Identification. Polymer Reviews, 2012. 52(3): p. 321-354.

65. Sha, J.J., et al., Measurement and analysis of fiber-matrix interface strength of carbon fiber-reinforced phenolic resin matrix composites. Journal of Composite Materials, 2013. 48(11): p. 1303-1311.

66. Miguez Suarez, J.C., F.M.B. Coutinho, and T.H. Sydenstricker, SEM studies of tensile fracture surfaces of polypropylene—sawdust composites. Polymer Testing, 2003. 22(7): p. 819-824.

67. Rojo, E., et al., Effect of fiber loading on the properties of treated cellulose fiber-reinforced phenolic composites. Composites Part B: Engineering, 2015. 68: p. 185-192.

68. Srinivasa, V., et al., Fracture morphology of carbon fiber reinforced plastic composite laminates. Materials Research, 2010. 13: p. 417-424.

69. Cheng, Q., et al., Physical and mechanical properties of polyvinyl alcohol and polypropylene composite materials reinforced with fibril aggregates isolated from regenerated cellulose fibers. Cellulose, 2007. 14(6): p. 593-602.

70. Zhao, R. and W. Luo, Fracture surface analysis on nano-SiO2/epoxy composite. Materials Science and Engineering: A, 2008. 483-484: p. 313-315.

71. Żenkiewicz, M. and J. Richert, Permeability of polylactide nanocomposite films for water vapour, oxygen and carbon dioxide. Polymer Testing, 2008. 27(7): p. 835-840.

72. Shogren, R., Water vapor permeability of biodegradable polymers. Journal of environmental polymer degradation, 1997. 5(2): p. 91-95.

73. Kristo, E., C.G. Biliaderis, and A. Zampraka, Water vapour barrier and tensile properties of composite caseinate-pullulan films: Biopolymer composition effects and impact of beeswax lamination. Food Chemistry, 2007. 101(2): p. 753-764.

74. Duan, Z., N.L. Thomas, and W. Huang, Water vapour permeability of poly(lactic acid) nanocomposites. Journal of Membrane Science, 2013. 445: p. 112-118.

CHAPTER 6

LIFE CYCLE ASSESSMENT OF MANUFACTURING CELLULOSE NANOFIBRILS REINFORCED CHITOSAN COMPOSITE FILMS FOR PACKAGING APPLICATIONS[4]

[4] Prabaharan Graceraj Ponnusamy and Sudhagar Mani. Submitted to The International Journal of Life Cycle Assessment.

Abstract

Purpose

Increased accumulation of fossil-based polymer packaging films on land and ocean surfaces posed significant environmental challenges to our ecosystem. Developing alternative packaging films with no or minimal environmental burdens is critically important to our society. Chitosan, a natural polymer reinforced with cellulose nanofibrils (CNF) can be the most promising bio-based alternatives as it possesses biodegradable, biocompatible, and antimicrobial properties for developing packaging films. This study evaluates the life cycle environmental impacts of chitosan-CNF composite films to identify the environmental hotspots that could be eliminated during large-scale production.

Methods

A cradle-to-gate life cycle assessment method was carrier out to assess the environmental impacts of manufacturing chitosan-CNF composite films for packaging applications. The main manufacturing operations include (i) production of chitosan from shrimp shell waste, (ii) CNF production from forest biomass, and (iii) production of citric acid crosslinked composite films using the solvent-casting method. Life cycle inventory data were obtained from published literature and laboratory experiments. The environmental impacts were evaluated by U.S. EPA's TRACI 2.1 impact assessment method. The effects of key process parameters on the environmental impacts of composite films were also evaluated.

Results and discussion

The global warming potential (GWP) of chitosan-CNF composite films was about 3.91 kg CO2 eq./kg of the film, which was marginally lower than that of the fossil-based low-density polyethylene (LDPE) and bio-based poly(lactic acid) (PLA) films respectively. The production of

the citric-acid crosslinked composite film contributed up to 79% of the total CO2 emissions. Among the sensitive process parameters, the use of chemicals during the deproteination of shrimp shells was the most sensitive factor. The scenario analysis showed that an increase in the CNF loading rate to improve the mechanical and barrier properties did not substantially increase the global warming potential (GWP) and other environmental impacts.

Conclusion

A cradle-to-gate life cycle assessment of the chitosan-CNF composite film has demonstrated that the overall environmental impacts were comparable or lower than that of fossil-based polymers and other biopolymers for flexible packaging applications. The development of renewable energy-based film dryers and environmentally benign methods to extract chitosan from shrimp shell waste could further reduce the GWP of composite films. When the end of life of fossil-based polymers is considered, the biodegradable nature of chitosan-CNF composite can be an environmentally attractive film for packaging applications.

Keywords: Nanocomposite, shrimp shell, wood pulp, film-casting, citric acid, global warming potential

Introduction and background

In recent years, the increasing environmental concerns related to the accumulation of non-degradable plastic waste on land and ocean surfaces strive to develop biopolymers with the most efficient ecological footprint for packaging products. The biopolymers are a class of materials derived from natural resources and possess several extraordinary properties such as non-toxicity, biodegradation, bio-compatibility, and film-forming abilities [1-3]. The biopolymers that are directly extracted from animal and plant-based biomass resources are called natural polymers [4]. Cellulose, chitin, chitosan, and starch are some of the examples of natural biopolymers [5]. Other biopolymers such as polylactic acid (PLA), polyhydroxyalkanoates (PHA), polyhydroxy butyrate (PHB), etc. are synthesized as monomers from renewable biomass resources via biochemical/biocatalytic pathways [6, 7].

Natural polymers such as starch, chitosan, and cellulose were investigated to produce biodegradable materials and packaging products [5]. Among the natural polymers, chitosan is the second most abundant polysaccharide containing β-(1→ 4) linked 2-amino-2-deoxy-D-glucan, generally derived from shrimp and crab shell wastes. It has excellent thermal stability, antifungal, and antimicrobial properties, and solvent stability properties to consider for food packaging, coating, agriculture, water engineering, cosmetics, tissue engineering, and pharmaceutical applications [8-10]. The biodegradable and biocompatible nature of chitosan prompted the exploration of its characteristics to use as a substitute for fossil-derived packaging products [10]. The brittle behavior and hydrophilic nature of chitosan reduced the barrier and mechanical properties and limited their use in packaging applications [11]. Therefore, the chitosan-based packaging films should be either cross-linked or surface modified to improve barrier properties and the mechanical properties can be improved by reinforcing it with high tensile materials such

as Cellulose Nanofibrils (CNF) in the polymer matrix to match with the properties of a synthetic polymer such as low-density polyethylene (LDPE) [12, 13].

The cellulose nanofibrils (CNFs) are nano-structured cellulose with an average diameter of less than 100 nm and a length of several micrometers. It is generally produced as hydrogels by mechanical fibrillation of bleached pulps manufactured from wood chips and plant biomass resources [14, 15]. CNFs exhibit excellent mechanical strength, a higher degree of crystallinity, and barrier properties and can be used as a reinforcing material for bio-based polymers [16, 17]. A recent study by Azeredo et al. (2010) investigated the use of CNF as a reinforcing material with chitosan to improve mechanical properties. The inherent hydrophilic nature of chitosan and CNF negatively influenced the functional characteristics of composite films while exposed under high relative humidity and moisture environment. The hydrophilic nature of chitosan-based composites was improved by the addition of inorganic nanoparticles (E.g., ZnO and Ag) or by reinforcing surface-modified nanocellulose materials [18-20]. However, the surfactants and inorganic nanofillers posed great technical challenges in achieving desired material properties and environmental performance of composite materials [21]. Hence, the nanocomposite with a crosslinker, plasticizer, and nanoscale reinforcement materials was investigated to improve mechanical and barrier properties of chitosan to develop them as potential alternate materials from renewable resources to replace LDPE polymer which is predominantly used in packaging product applications [12, 22].

From the circular materials economy perspective, it is important to select environmentally benign functional enhancers that not only offer superior functional properties but also pose no threat to the environment [23]. The life cycle assessment (LCA) is a comprehensive tool that will not only quantify the environmental impacts of a product but also highlight the concerns in energy

consumption, toxic chemicals used, and the ecological footprints [24]. It was argued that the biopolymer manufacturing processes were less environmentally friendlier than that of the conventional polymer manufacturing processes [25, 26]. However, the biodegradation nature of biopolymers after their use phase provides unique opportunities to develop sustainable packaging materials [27]. Hence, there is a growing interest in the assessment of environmental performances of manufacturing biopolymers and their composites such as chitosan-CNF composites to develop them as potential alternative packaging materials.

Earlier studies have focused on the LCA of manufacturing virgin monomers and other derivatives to compare with fossil-derived polymers. The life cycle environmental impacts of manufacturing chitosan from shrimp shells and crab shell wastes were investigated by Muñoz et al. (2018). They reported that the global warming potential (GWP) and water depletion impacts were higher from the European manufacturing plant whereas the acidification and eutrophication potentials were higher from the Indian manufacturing plant. The overall environmental impacts varied with how the shell wastes were considered to displace from their intended use such as landfilling and animal feed manufacturing. Although chitosan can be extensively studied in a wide range of fields from agriculture to biomedical applications, limited studies on the life cycle assessment of chitosan for packaging applications were investigated.

The environmental impacts of manufacturing CNF from wood pulps by four different manufacturing routes (combinations of tempo-oxidation, esterification, sonication, and homogenization) were evaluated by Li et al. (2013). Based on the laboratory scale experimental data, they reported that the combination of tempo oxidation and homogenization treatment manufacturing route had up to five times less environmental impacts in Cumulative Energy Demand (CED) and Global Warming Potential (GWP) to produce CNF. They also demonstrated

that the excessive use of chemicals and electricity during pretreatment methods substantially contributed to the overall environmental impacts of CNF production [28]. The European Commission-funded project, SUNPAP investigated various pretreatment methods to produce CNF for paper coating applications and found that the use of chemical pretreatments outweighed enzymatic pretreatments and electricity use to produce cost-competitive CNF [29]. Arvidsson et al. (2015) evaluated the CNF manufacturing by the combinations of enzymatic, chemical, and mechanical pretreatment methods by life cycle assessment and reported that the combination of enzymatic and microfluidic pretreatment methods had up to 20- and 124-times fewer impacts in CED and GWP impact respectively. In general, reducing the size of the cellulose fibers before the mechanical fibrillation process has the substantial potential to reduce the overall energy consumption of CNF production [30]. A pilot-scale experimental study by Bilodeau and Paradis (2018) has demonstrated that the overall energy consumption of CNF manufacturing can be reduced by a series of mechanical pulp fibrillation processes while improving the quality of CNFs.

Environmental performances of biopolymers have been studied to improve the manufacturing process efficiencies and to displace fossil-based polymers [31]. However, limited studies were focused on the environmental performances of biopolymer nanocomposite films which are recently explored for the manufacturing of packaging products. The LCA of the composite film manufacturing process at the product development stage can help to capture the environmental hotspots before the start of large-scale production. It can also help the decision-makers to explore the implications of environmental burden, functionalities, and uncertainties. Furthermore, the manufacturers and other stakeholders along the supply chain can understand the material characteristics and their environmental profile at early-stage production. The potential environmental benefits of using bio-based composite films over fossil-based films can also be

explored to cover a wide range of product applications. Hence, in this study, the environmental impact assessment was performed on chitosan-CNF composite films crosslinked with citric acid as a proof-of-concept for large-scale production. The LCA model was developed in SimaPro software from lifecycle inventory data of large-scale chitosan and pilot-scale CNF manufacturing processes from literature data and scaling-up of film casting processes using the laboratory data.

The main objective of this study was to conduct the life cycle assessment of manufacturing CNF reinforced chitosan composite films crosslinked with citric acid to evaluate the environmental performances. The specific objectives were to conduct the cradle to gate life cycle assessment of chitosan-CNF composite films to assess overall energy use, greenhouse gas (GHG) emissions, and other environmental impacts compared with fossil-derived polymer films, to assess the sensitivity of key parameters on the GHG and other environmental impacts of composite films and to evaluate the effects of CNF loading percent on the environmental impacts of composite packaging films.

LCA methodology

In this study, the LCA of manufacturing chitosan-CNF composite films for packaging application was performed according to the guidelines and framework model specified in ISO 14040 and ISO 14044 standards. The chitosan manufactured from the shrimp shell wastes was considered in this study. The shrimp shells are the waste product from the shrimp processing plant. The environmental impacts of shrimp food were estimated based on the inventory flow in various life cycle stages such as transportation to processing unit, food processing, distribution, consumption, and waste management. The shrimp shell are inedible wastes with no functional or economic values and are often disposed of as municipal solid wastes (MSW). Therefore, shrimp shell waste carried no environmental impacts except from the end of use phase. The emissions due to the end-of-life disposal of shrimp shells by landfills were estimated and allocated to shrimp shell

waste. In this study, the chitosan is produced from shrimp shell waste that is otherwise disposed of in landfills. The production of the chitosan process also generated protein sludge and calcium carbonate as coproducts and were considered as a substitute for nitrogen fertilizer and inert landfill product respectively and the allocations were avoided.

Goal, scope, and functional unit

The primary goal of this study was to conduct the cradle-to-gate LCA of manufacturing chitosan-CNF composite films to evaluate the environmental impacts. The scope of the study comprised of the manufacturing of acetylated chitosan from shrimp shell wastes that were otherwise landfilled, obtained from gulf coasts, the manufacturing of CNF hydrogels from softwood in the northeastern U.S., and the large-scale production of composite films by film casting method. The production of chitosan from shrimp shell waste could avoid the disposal in municipal solid waste (MSW). A major fraction of MSW is landfilled although some portions are combusted and composted. Based on the disposal percentage of MSW in the U.S., the CO2 emission from shrimp shell waste disposal was estimated using EPA emission factors corresponding to landfill, combustion, and composting of food waste and was used to define the shrimp shell waste LCI data. The fossil-based and bio-based polymer films were considered as reference systems for the comparative analysis of Global Warming Potential (GWP). The GWP of manufacturing packaging film by melt-blown film extrusion from fossil resource-based polymer materials such as polyethylene (low-density polyethylene, LDPE and high-density polyethylene, HDPE) and polypropylene (PP) and bio-based polymers such as starch and PLA were compared with the chitosan-CNF composite film manufacturing process. The tensile and barrier functions of the composites are determined by the mass fractions of CNF and citric acid in the composite films. Generally, the production unit of a typical polymer film plant is measured as the mass of the final

film rolls produced. Therefore, the functional unit of the study was chosen as one kg of chitosan-CNF composite films.

System boundary

Figure 6-1 shows the overall system boundary with key unit operations related to the manufacturing of chitosan-CNF composite film. The manufacturing process consisted of manufacturing chitosan (matrix phase polymer), CNF (reinforcing agent), citric acid (cross-linking agent), glycerol (plasticizer), and composite films by solvent casting method. For the base-case analysis, the optimal composite composition of 15% CNF and 18%glycerol (plasticizer) was considered [32]. The crosslinking reactions were performed in our research laboratory for 15, 20, and 25% citric acid concentrations as proof of study and were further confirmed by The Fourier transform infrared (FTIR) spectral data [33]. Based on our preliminary study, it was decided that about 20% of citric acid as a cross-linking agent was sufficient to improve the hydrophilic nature of the composite films. Therefore, the composition of composite film for the base case consisted of 15% CNF, 18% glycerol, 20% citric acid, and the rest from chitosan. We assumed that both citric acid and glycerol were derived from typical chemical manufacturing processes in the U.S., while the chitosan and the CNF were produced from shrimp shells and bleached wood pulp respectively.

The shrimp shell wastes discarded in municipal solid waste (MSW), which eventually reaches landfills was considered as a primary source for chitosan manufacturing. First, the shrimp shell wastes were immersed in hydrochloric acid solution (HCl) to remove inorganic minerals. Then, the demineralized shells were treated with sodium hydroxide solution to initiate deproteination to extract chitin. Then, the chitin was treated with concentrated sodium hydroxide

to produce deacetylated chitosan. The resulting chitosan from the deacetylation process was separated, dried in the air, and ground to powder to use for different applications [34].

Cellulose nanofibrils (CNFs) can be produced from the chemical pulping of wood chips followed by a mechanical fibrillation process as similar to the pilot-scale plant operation at the University of Maine (UoM), U.S.A. The softwood chips were processed by a kraft pulping process to manufacture pulp. The kraft/sulfate pulp was bleached and washed to remove excess lignin. Then, it was subjected to mechanical pretreatment by valley beating followed by series of fibrillation in the disc refiner. The fibrillated pulp in the form of hydrogels has a final solid concentration of about 3% with an average cellulose fibril diameter of 50-100 nm [35]. The CNF hydrogel was used as a reinforcing agent in the chitosan polymer matrix.

In this study, we assumed a solvent-based film-casting method to manufacture composite films. As the matrix phase and other additives are water-soluble, composite polymer mixtures in water solvent can be molded as sheets on the moving rolls and dried to produce composite films. The composite film manufacturing process consisted of polymer mixing and heating, roll casting, drying, and film winding [36]. The operating conditions for the key processes were estimated from the published literature [37-39].

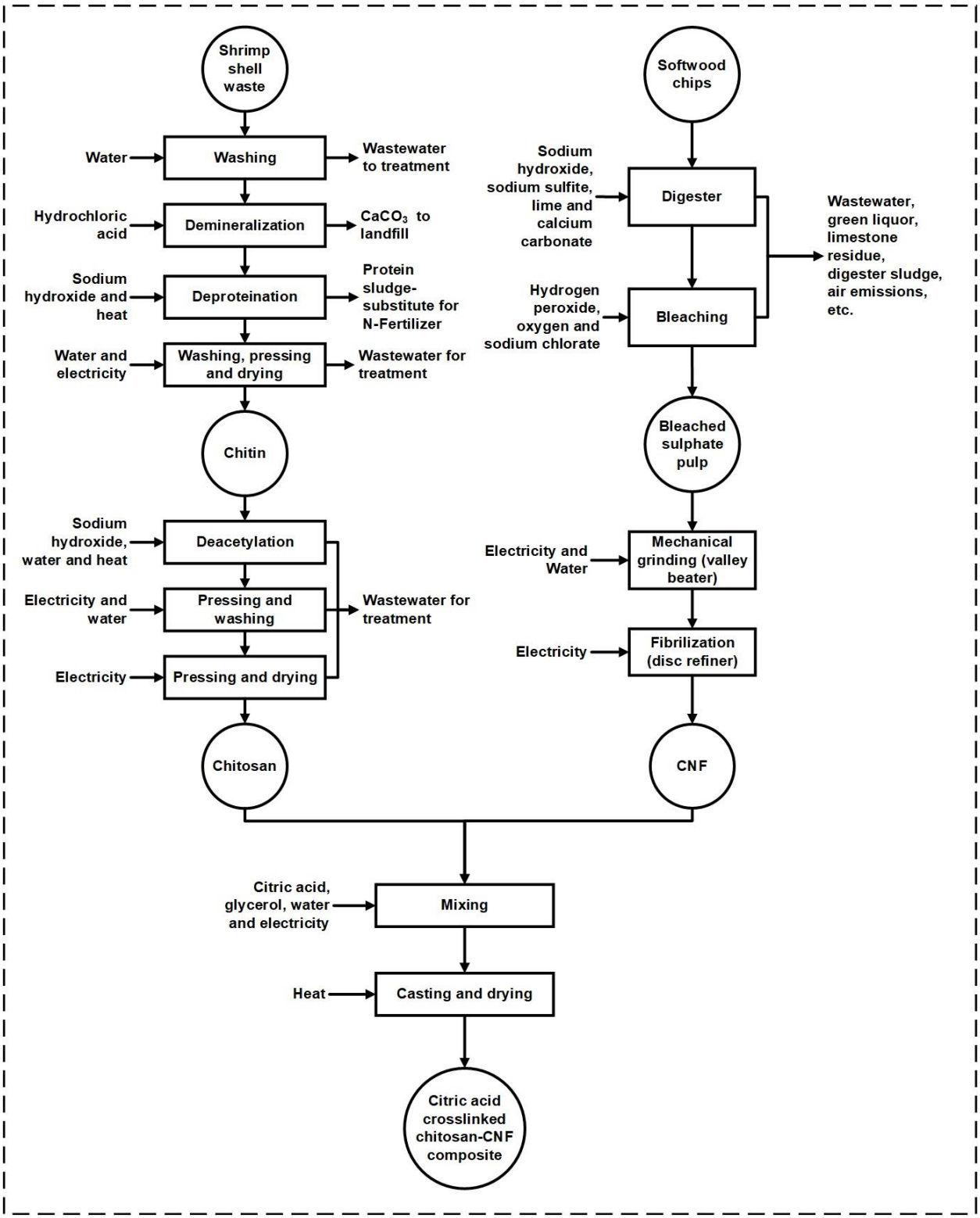

Figure 6-1. The system boundary of CNF reinforced chitosan composite film manufacturing process for environmental impact assessment

Life cycle inventory (LCI) data sources and analysis

The mass and energy input data and emission output data for each sub-process of composite film production were either obtained from US-LCI & eco-invent databases, literature sources, or estimated. The LCI data for chitosan and CNF manufacturing processes were obtained from the literature. The composite film production data were estimated from scaled-up laboratory experimental data. The datasets from US-LCI and eco-invent databases were used to model the unit processes of composite film production. The U.S geographical region-specific manufacturing activities and material resources were considered for LCI data analysis of composite film production. The heat source was either produced from biomass or natural gas sources at various stages of composite film production. The U.S. low voltage electricity mix at the grid was used to represent the electricity consumption in all stages of LCA.

The LCI data for the chitosan manufacturing process were obtained from (i) emission potential of shrimp shell disposal as food waste, (ii) materials and energy used for demineralization and deproteination treatment process for the production of chitin, and (iii) materials and energy used for the deacetylation treatment process to produce chitosan from chitin. About 217,000 MT of shrimps and lobster are harvested every year in the U.S. for domestic consumptions. They contain approximately 50% of inedible mass as shells which are disposed of as food waste in municipal solid waste (MSW) [40]. The fractions of food waste disposed of in MSW are composted, combusted, and landfilled. The greenhouse gas (GHG) emission potential from one kg shrimp shell waste was estimated from the food waste disposal fractions in MSW and the U.S. EPA's waste reduction model (WARM) food waste emission factors [41, 42]. The mass and energy balance data for converting shrimp shell waste into chitosan were obtained from Bristow (2012) and Muñoz et al. (2018). The shrimp shell waste contains approximately 16% protein, 3% chitin,

and 5% $CaCO_3$. The protein and $CaCO_3$ were recovered as protein sludge and calcium waste by-products during the chitin manufacturing process. The calcium waste was discarded as inert landfill waste and 6% of protein sludge was used to replace nitrogen fertilizer [43]. The LCI data related to air emissions, wastewater, and chitosan yield (~70%) from chitin were obtained from Bristow (2012) and Muñoz et al. (2018). It was assumed that the shrimp shell waste was directly supplied to chitosan manufacturing plants by shrimp food production industries instead of disposing at the landfill and transportation for the collection of shrimp shell waste was not accounted for. The detailed mass and energy balance data for manufacturing chitosan from shrimp waste were presented in the supplementary datasheet (Table 6-S4 to 6-S12).

Table 6-1. Summary of LCI input data used for manufacturing one kg of the chitosan-CNF composite films.

Composite film manufacturing stages	**Input-Material / Energy**	**Amount**	**Unit**	**Remarks /Reference**
CNF production	Bleached kraft pulp	1.06	kg	(Lee 2016)
	Electricity - Valley Beater	0.39	kWh	(Vaz et al. 2019)
	Electricity- Refiner	1.45	kWh	(Bilodeau and Paradis 2018)
Chitin production (Demineralization and deproteination)	Water	198.00	l	(Bristow 2012)
	Shrimp shell waste	33.00	kg	(Muñoz et al. 2018)
	HCl	4.70	kg	(Bristow 2012)
	NaOH	6.27	kg	(Bristow 2012)
	Electricity	1.30	kWh	(Muñoz et al. 2018)
Chitosan production (Deacetylation)	Demineralized and deproteinized shrimp shell waste- (Chitin)	1.41	kg	(Muñoz et al. 2018)
	Water	70.42	l	(Bristow 2012)
	NaOH	0.67	kg	(Muñoz et al. 2018)

	Heat from biomass	31.3	MJ	(Muñoz et al. 2018)
	Electricity	1.06	kWh	(Muñoz et al. 2018)
Film-casting	Water	20.67	l	Estimated
	Acetic acid	0.21	kg	
	Chitosan	0.47	kg	
	CNF	0.15	kg	
	Glycerol	0.18	kg	
	Citric Acid	0.20	kg	
	Electricity-Mixing	0.004	kW	
	Heat energy-Drying	51.00	MJ	
	Electricity - Film winding	0.00021	kW	

The LCI data for sulfate wood pulp used in CNF production were obtained based on the softwood forest management operations followed in northeastern and north-central (NE/NC) regions of the U.S.A. Natural forest regeneration without any planting model is practiced in NE/NC regions for softwood forest management operations. As for the harvesting system is considered, a mechanized timber harvesting system was used in these regions. The logs and timber are processed at the landing site with a large feller-buncher, a medium-sized grapple skidder, and in a mechanized processor to produce woodchips [44]. The softwood chips are digested in sodium sulfide and sodium hydroxide aqueous solution and kraft pulp are manufactured. Further, the residual lignin in the digested kraft pulp is removed by the bleaching process. The LCI data for the forest management operations and bleached kraft pulping process were obtained from US-LCI and eco-invent databases on the SimaPro software (see supplementary information, Table 6-S1). The LCI data of CNF isolation from softwood pulp process was estimated from the specific energy consumption of bleached softwood pulp processing in valley beater and disc refiner (see supplementary information. Table 6-S2 and 6-S3) [35, 45].

The manufacturing of flexible packaging film with a standard size of 300 x 250 x 3 mm and the production output rate of 400,000 films/day were considered for LCI data modeling of the film-casting process [37]. The hourly production rate was calculated from the packaging film size, the production output of a day, and the density of the chitosan-CNF composite film. The details on the type and the amount of materials required and the energy consumption data for water-based film-casting were estimated from the hourly production output and were summarized in the supplementary information. The specific energy consumption rate for mixing, drying, and winding operations were calculated (see supplementary information, Table 6-S13, and 6-S18) [46, 47]. The summary of input and output LCI data for one kg of the chitosan-CNF composite film are presented in Table 6-1 & 6-2 respectively.

Table 6-2. Summary of LCI output data for manufacturing one kg of the chitosan-CNF composite films.

Composite film manufacturing stages	**Output Material / Energy**	**Amount**	**Unit**	**Remarks /Reference**
Shrimp shell waste treatment	Carbon dioxide	0.42	kg	Estimated
Chitin production (Demineralization and deproteination)	Protein sludge (Substitute for nitrogen fertilizer)	0.24	kg	
	CO_2 fossil	0.7	kg	
	Ammonia	0.12	kg	(Muñoz et al. 2018)
	Dinitrogen monoxide	0.006	kg	
	Nitrogen oxides	0.06	kg	
	CO_2 biogenic	6.88	kg	
	Calcium waste	1.50	kg	
	Wastewater	198.00	l	
Chitosan production (Deacetylation)	Wastewater	70.42	l	(Bristow 2012)

The LCI data for the comparative analysis of the composite film with fossil-based and bio-based films were determined from eco-invent databases. A typical blown film process that is used in the production of synthetic resin packaging films was considered for LCI analysis. In the blown film processing method, the granular solid resins are first melted in the extruder. The molten resins are forced through an annular die unit to manufacture blown film [48]. The LCA model comprising polymer granulate material, extrusion, and blown film process was created in SimaPro software from LCI datasets of Ecoinvent databases. The Ecoinvnent database used European plastics industries data to define material, energy, and emission data of fossil-based resin granulates extruder and blown film processes. It used the production data of NatureWorks LLC and product declaration data of Materbi, Italy to model LCI data sets of PLA and starch polymer. The amount of material processed in the extruder and blown film unit was estimated using a 98% process conversion efficiency factor [49].

Lifecycle impact assessment (LCIA) and interpretation

The ISO 14042 provides guidelines that the environmental impact of a product system shall be assessed in climate change, human health, and resource depletion impact categories to describe their environmental profile. The environmental impacts of manufacturing CNF and chitosan by chemical and mechanical processes were assessed on global warming potentials, cumulative energy demand, ecosystem quality, and human health impact categories [28, 43, 50]. The obtained results on these categories exhibited a comprehensive and comparative environmental profile of material systems portrayed by various chemicals and electricity used in the process. In this study, the composite film manufacturing system consumed a considerable amount of chemicals and energy during pulp manufacturing, CNF extraction, chitosan manufacturing, and film casting processes and caused environmental impacts by the emission of pollutants and depletion of energy

resources. Fossil fuel use in electricity production and heat generation is the major contributor to climate change and resource depletion. The nitrogen and ammonia emission from the chemical recovery process of pulp production would increase acidity in air and water and could damage the respective ecosystem. The production process of hydrochloric acid and sodium hydroxide chemicals emitted substances such as chlorine, tetrachloromethane, and particulate matter, and waste heat. These emissions would cause ozone depletion, respiratory, carcinogenic, and non-carcinogenic illness. To quantify the impacts on these categories and to comply with the environmental impact assessment regulation of the U.S. Environmental Protection Agency (EPA), the TRACI 2.1 (Tool for Reduction and Assessment of Chemicals and Other Environmental Impacts) assessment method was considered for characterization of environmental impacts. The TRACI 2.1 assessment method include ozone depletion (OD), global warming potential (GWP), acidification (AD), eutrophication (EP), smog formation (SF), carcinogenic (CG), ecotoxicity (ET), non-carcinogenic (NCG), respiratory effects (RE) and fossil fuel depletion (FFD) impact categories for the assessment of environmental impact [51]. The interpretations of results were presented by contribution, comparative analysis methods to disclose the environmental impacts generated by the composite film manufacturing process. The contribution analysis was used to investigate the environmental impact contribution by the materials and energy consumed by chitosan, CNF, and film sub-manufacturing processes for the manufacture of one kg of the chitosan-CNF composite film. According to ISO 14044, the comparative analysis in LCIA is intended to disclose a competing or equivalent product system that performs the same functions. The GWP of manufacturing packaging film from polymer materials such as polyethylene (low-density polyethylene, LDPE and high-density polyethylene, HDPE) and polypropylene (PP) and

bio-based polymers such as starch and PLA were compared with the chitosan-CNF composite film manufacturing process by comparative analysis.

Sensitivity analysis

The amount of chemicals and energy used in the production of composite film were the average values obtained from the literature and or estimates to assess the environmental impacts [50]. The amount of chemicals used in pulp production process and demineralization, deproteination and deacetylation processes of chitosan manufacturing process, the electricity consumed in the CNF fibrilization process, chitin, chitosan film casting process, and heat energy used in chitosan and film casting process were critical factors that would influence the environmental impacts of the composite film production process. To investigate the uncertainties of these factors on environmental impacts, the sensitivity analysis was conducted on the variations of the amount of chemicals used during chitosan production, overall energy use, and the CNF yield from kraft pulp on the overall energy use, GHG emissions, and other environmental impacts of composite films. The amount of pulp used in CNF manufacturing was changed by ± 6% from the base-case values [50, 52]. The energy flow in all the processes was changed with ± 20% from the base-case values [53, 54]. The recommended chemical use range by Bristow et al. (2012) was considered for the sensitivity analysis study (see supplementary information, Table 6-S19).

Scenario analysis

The CNF reinforcement in the chitosan matrix was more effective in improving mechanical, barrier, and thermal properties. The chitosan and CNF have functional hydroxyl groups in their glucose units to create strong molecular network structure by hydrogen bonds [55]. The intra and inter-molecular hydrogen bonds between the reactive hydroxyl groups can be increased while reinforcing the CNF in chitosan. The dispersion ability of CNF with a specific

loading percentage in the chitosan polymer matrix could improve the mechanical properties of composite films as studied elsewhere [32, 56]. Hence, in this study, the effect of the CNF loading rate on the environmental performance of the composite film was evaluated from the baseline loading rate of 15% CNF. The three CNF loading rates considered for the scenario analysis were: i) 10%, ii) 15% and iii) 20%.

Results and discussion

Contribution analysis

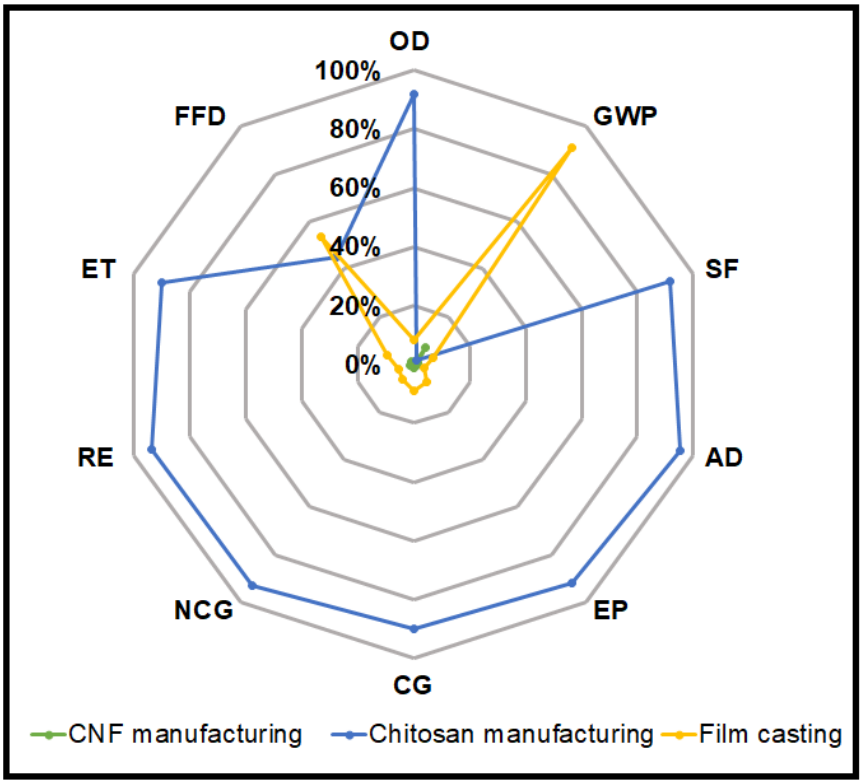

Figure 6-2. Contribution analysis of all environmental impacts of manufacturing one kg of Chitosan-CNF composite film (base case). Note: OD-Ozone Depletion in kg CFC-11 eq., GWP-Global Warming Potential in kg CO_2 eq., SF-Smog Formation in kg O_3 eq., AD-Acidification in kg SO_2 eq., EP-Eutrophication in kg N eq., CG-Carcinogenic in CTUh, NCG-Non-Carcinogenic in CTUh, RE-Respiratory Effects in kg PM2.5 eq., ET-Ecotoxicity in CTUe and FFD-Fossil Fuel Depletion in MJ surplus

Figure 6-2 shows the overall environmental impacts of chitosan-CNF composite films with relative contributions from sub-processes. Among the three sub-processes, the CNF manufacturing

process has the lowest environmental impact contributions, which is due to the limited use of CNF (15% by mass) for reinforcing purposes. Overall, the CNF manufacturing process contributed less than 7% of the total emission to produce composite films. The largest environmental impact contributions from the CNF manufacturing process were Global Warming Potential, GWP (7%), Smog Formation, SF (2%), Respiratory Effects, RE (1%), and Fossil Fuel Demand, FFD (1%). The relative percent contributions of material and energy used in manufacturing CNF on various environmental impacts are shown in Figure 6-3. The electricity use for the mechanical pretreatment and fiber defibrillation to produce CNF from the kraft pulp had a larger contribution to GWP. Overall, the GHG emission potential of the mechanical pretreatment method considered in this study (1.84 kg CO_2 eq./ kg of CNF) was much lower than that of the combination of chemical and mechanical treatment methods evaluated by Li, Q., et al. (2013) (190-1160 kg CO_2 eq./ kg of CNF) and Arvidsson, R., et al. (2015) (1.20-99 kg CO_2 eq./ kg of CNF). However, the fibrillation quality of CNF varies widely from each pretreatment method to utilize for a wide range of applications. Standardization of CNF properties and other quality parameters are important for commercial production. For flexible packaging applications, the mechanical and barrier properties are important and can be achievable through mechanical pretreatment methods.

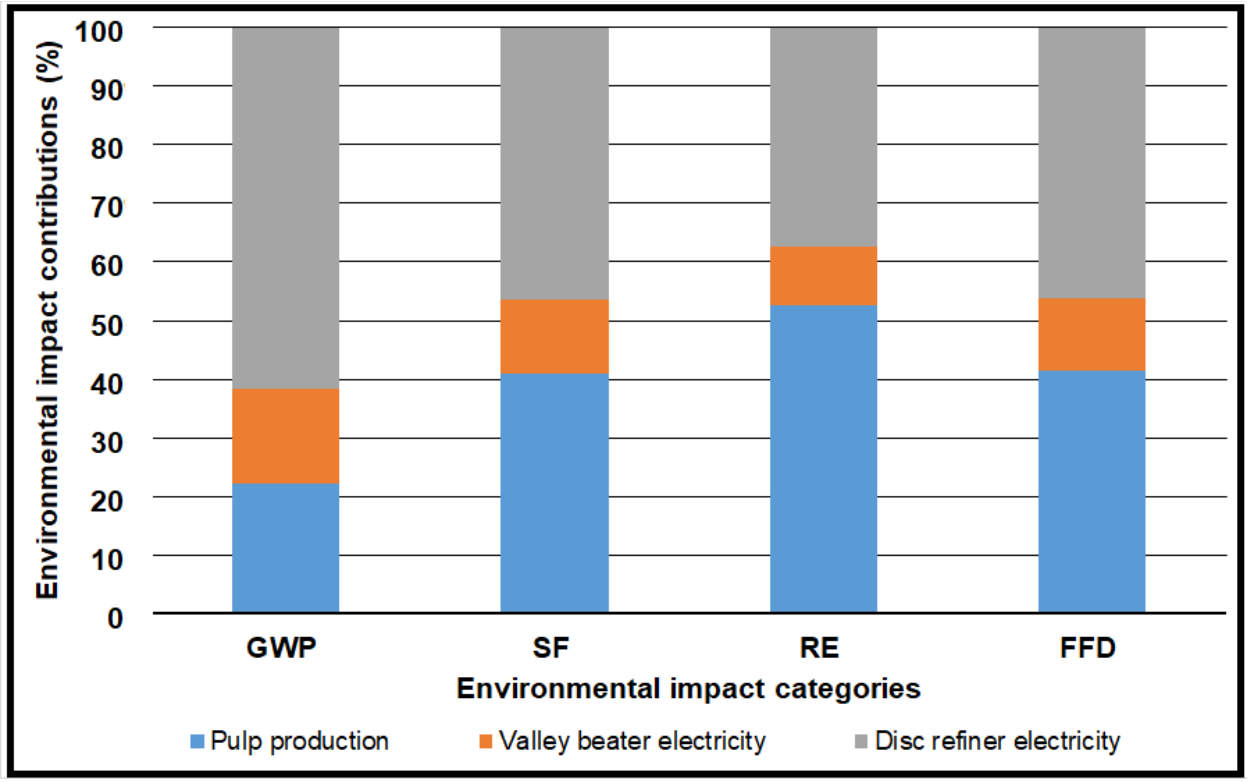

Figure 6-3. The percent contributions of environmental impacts from the CNF manufacturing process in one kg of the composite film production. Note: GWP – Global Warming Potential in kg CO_2 eq., SF-Smog Formation in kg O_3 eq., RE-Respiratory Effects in kg PM2.5 eq. and FFD-Fossil Fuel Depletion in MJ surplus

The chitosan manufacturing process had a relatively larger contribution to all environmental impacts except GWP and FFD (Figure 6-2). The larger contribution of the environmental impacts such as - OD, ET, RE, NCG, CG, AD, EP and SF was due to the use of chemicals during chitosan extraction from shrimp shell wastes (Figure 6-4). In this study, the shrimp shell waste which would otherwise be landfilled was diverted for the production of chitosan. The avoided CO2 emission by the production of chitosan from shrimp would be captured in the chitosan-CNF composite. As the chitosan and CNF are biodegradable polymers, the CO2 can be sequestrated after use and disposal as composts. Also, the chitosan manufacturing process produces a co-product, protein sludge, which was assumed to displace nitrogen fertilizer and the corresponding displacement savings or credits on different impact categories were also accounted

for. These savings or credits in different impact categories were shown as negative emissions in Figure 6-4. The other wastes generation streams, limestone residues, and wastewaters were disposed of as wastes. The chemicals such as sodium hydroxide and hydrochloric acid used in deproteination and demineralization processes were major contributors to the environmental impacts of chitosan as observed by Muñoz et al., 2018. To reduce or limit the chemicals used in the deproteination and demineralization processes, several laboratory-scale alternate treatment methods such as the use of organic acid, biological fermentation process, dehydration, and temperature-induced fermentation by hot glycerol and enzymatic treatments were explored by several researchers [57-62]. Recently, Yang, et al. (2019) proposed a novel method that uses hot water and carbonic acid for demineralization and deproteinization of shrimp shell waste [63]. Hu et al., (2020) employed an instant catapult steam explosion method along with weaker acids to effectively demineralize and deproteinize shrimp waste to produce chitin. If such environmentally friendly methods can be soon commercialized, the environmental impacts of composite film production can also be substantially reduced.

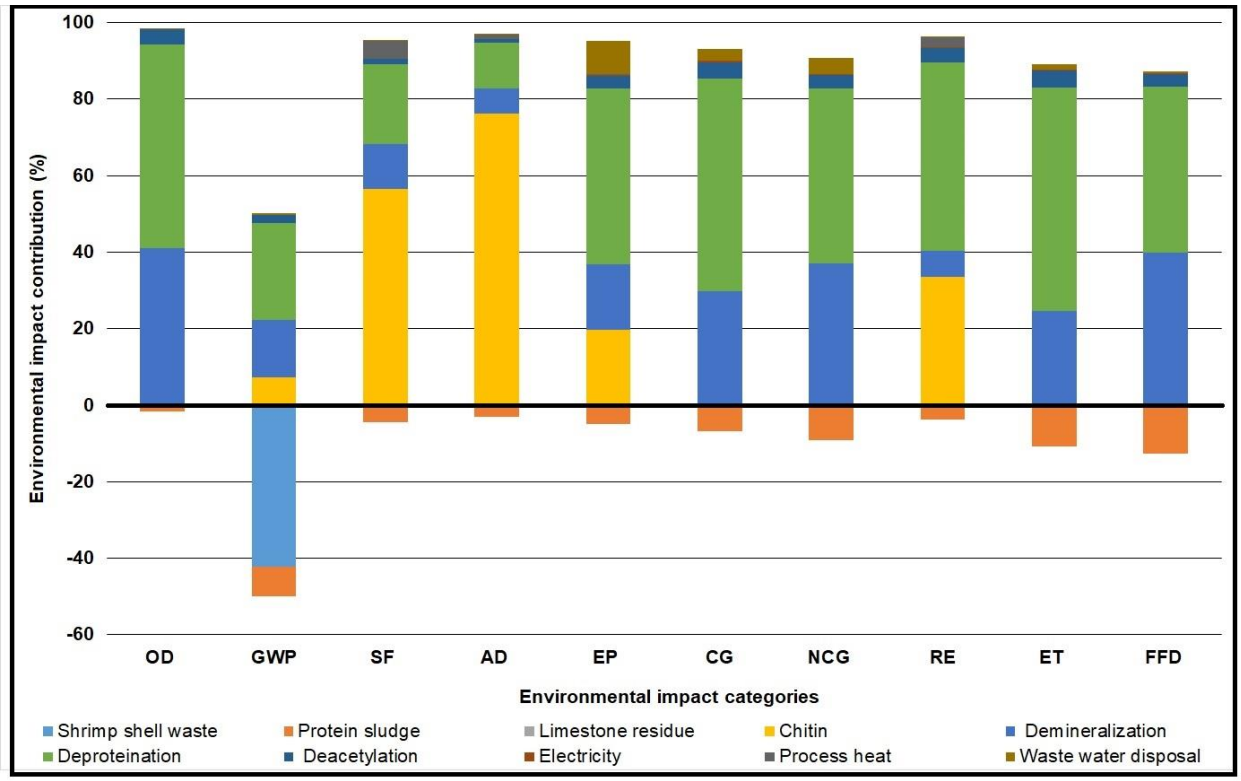

Figure 6-4. The percent contributions of environmental impacts from the chitosan manufacturing process in one kg composite film production. Note: OD-Ozone Depletion in kg CFC-11 eq., GWP-Global Warming Potential in kg CO_2 eq., SF-Smog Formation in kg O_3 eq., AD-Acidification in kg SO_2 eq., EP-Eutrophication in kg N eq., CG-Carcinogenic in CTUh, NCG-Non-Carcinogenic in CTUh, RE-Respiratory Effects in kg PM2.5 eq., ET-Ecotoxicity in CTUe and FFD-Fossil Fuel Depletion in MJ surplus

The film-casting process contributed 90% of GWP and 50% of FFD to produce composite films, while the other impact categories contributed less than 10% (Figure 6-2). Figure 6-5 shows the detailed breakdown of various processes that contributed to the overall environmental impacts of the film-casting process. The heat supplied for drying of film and the citric acid used in the crosslinking process had substantially contributed to all environmental impact categories. As the composite films are soluble in acidic water, a water-based casting method should be followed to produce flexible films and the thermal drying process can be unavoidable. To mitigate the emission contribution by the drier, the fossil-based energy resources could be displaced by renewable resources to reduce overall GHG emissions. Currently, the dryers used in fabric industries, paper

industries, and biomass production industries are shifting to renewable energy resources to mitigate the fossil energy use [64-66]. Technological advancement and environmental awareness are major motivational factors for the use of renewable energy resources for the drying process. Hence, the biopolymer dryer with a biomass heating source would be a potential emission reduction strategy for the film casting process. Similarly, the environment-friendly CNF surface modifier such as oxalic acid can be used to increase the barrier properties while reducing the environmental impact of composite films [67]. The biodegradable nature of all the constituents in the composite films.

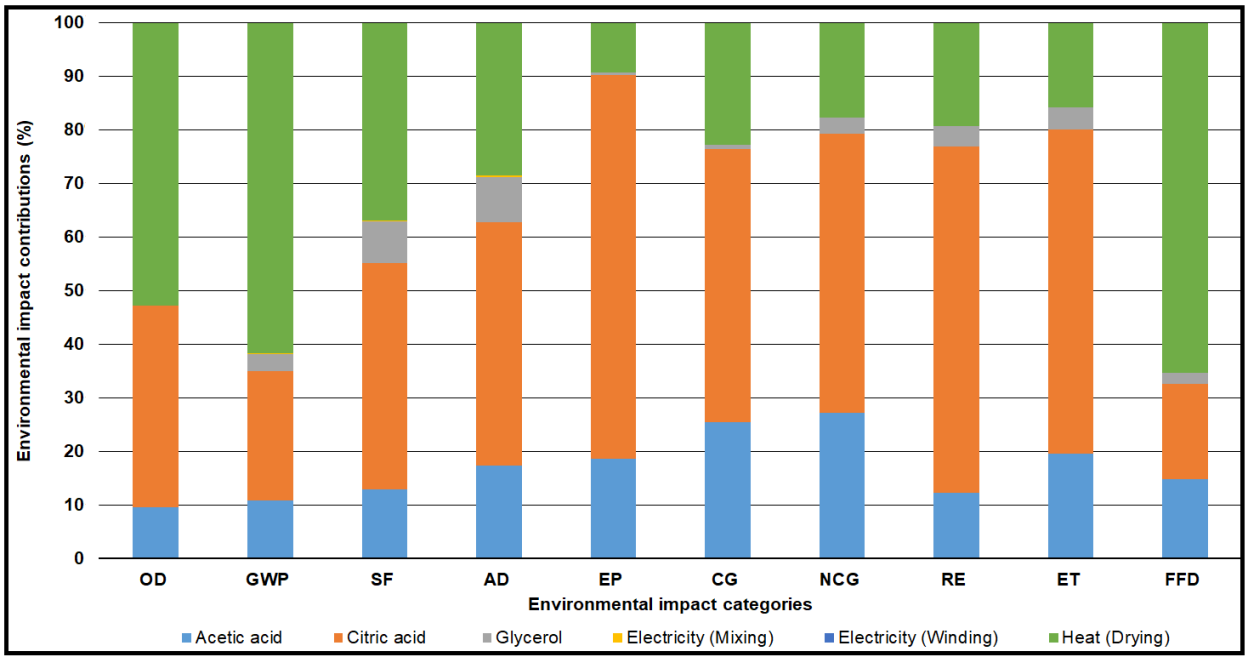

Figure 6-5. The percent contributions of environmental impacts from the film-casting process in one kg composite film production. Note: OD-Ozone Depletion in kg CFC-11 eq., GWP-Global Warming Potential in kg CO_2 eq., SF-Smog Formation in kg O_3 eq., AD-Acidification in kg SO_2 eq., EP-Eutrophication in kg N eq., CG-Carcinogenic in CTUh, NCG-Non-Carcinogenic in CTUh, RE-Respiratory Effects in kg PM2.5 eq., ET-Ecotoxicity in CTUe and FFD-Fossil Fuel Depletion in MJ surplus

Impact comparison with fossil-derived polymer films

Figure 6-6 shows the carbon footprints of chitosan-CNF composite film and compared them with fossil and other biopolymer-based films. The film-casting process contributed the

largest carbon footprint (GWP - 3.57 kg CO_2 eq./ kg of the composite film) of chitosan-CNF composite films, but the carbon footprint of chitosan-CNF composite material production was much lower (0.34 kg CO_2 eq./ kg of the film) than that of other competitive fossil and biopolymer-based resin production. A closer examination of all the input materials showed that heat energy supplied for the drying process contributed 2.20 kg CO_2 eq./ kg of the film, which is expected from the process run by fossil fuels. However, opportunities exist to replace dryer fuels with renewable sources (e.g., biomass, solar energy) to further reduce the GWP of composite films. Renewable energy resources reduce CO2 emissions to a greater extent. They are emerging as efficient and clean alternate energy resources for the fossil-based resources. About 23% of energy use from renewable resources would bring down the CO2 emission by 74%. Hence, the composite film dryer which uses renewable energy resources can cut down the CO2 emission during the drying process. In addition, the manufacturing of biopolymers such as PLA and starch polymers had a larger GWP than that of fossil-derived polymers and our composite films. Overall, if natural polymers such as chitosan, CNF can be effectively blended and functionalized to improve mechanical and barrier properties, they can be environmentally more benign than other competitive biopolymers.

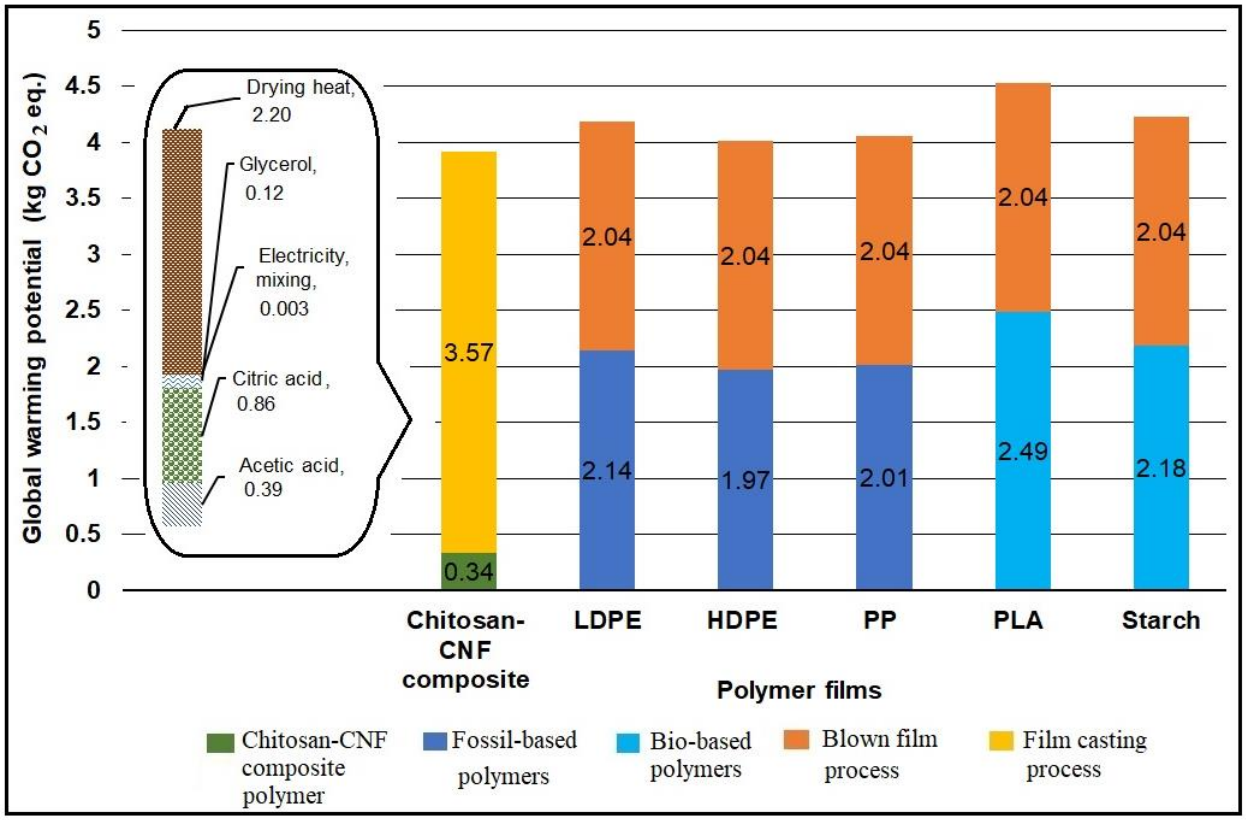

Figure 6-6. Carbon footprint of the chitosan-CNF composite film along with fossil and biopolymer-based films and the environmental impact contribution by the film casting process. Note: LDPE-Low Density Polyethylene, HDPE-High density polyethylene, PP-Polypropylene, PLA-Polylactic Acid

Sensitivity analysis

Figure 6-7 shows the sensitivity of key parameters influencing the environmental impacts of chitosan-CNF composite films. The process parameters with more than 10% change from baseline results were identified as the most sensitive process parameters that would affect the environmental impacts of composite films [68]. The deproteination process parameter was the most sensitive process parameter affecting all the environmental impacts, although it had the highest impact on the GWP with the sensitivity factors of 28%. It was also relatively sensitive to other environmental impact categories such as ET, CG, NCG, OD, RE, and EP with the sensitivity factor of 13%, 12%, 10%, 10%, 10%, and 9% respectively. Therefore, future research could be

directed to develop, optimize, and commercialize environmentally friendly deproteination methods to replace the NaOH-based method for shrimp wastes to produce chitosan. The demineralization and overall energy use parameters were the other parameters that influenced the GWP potential of composite films. Although the demineralization process parameter was the second most sensitive parameter, it did not substantially influence any of the other impact categories. The overall energy use, deacetylation, and CNF yield from wood pulp did not significantly affect any of the impact categories.

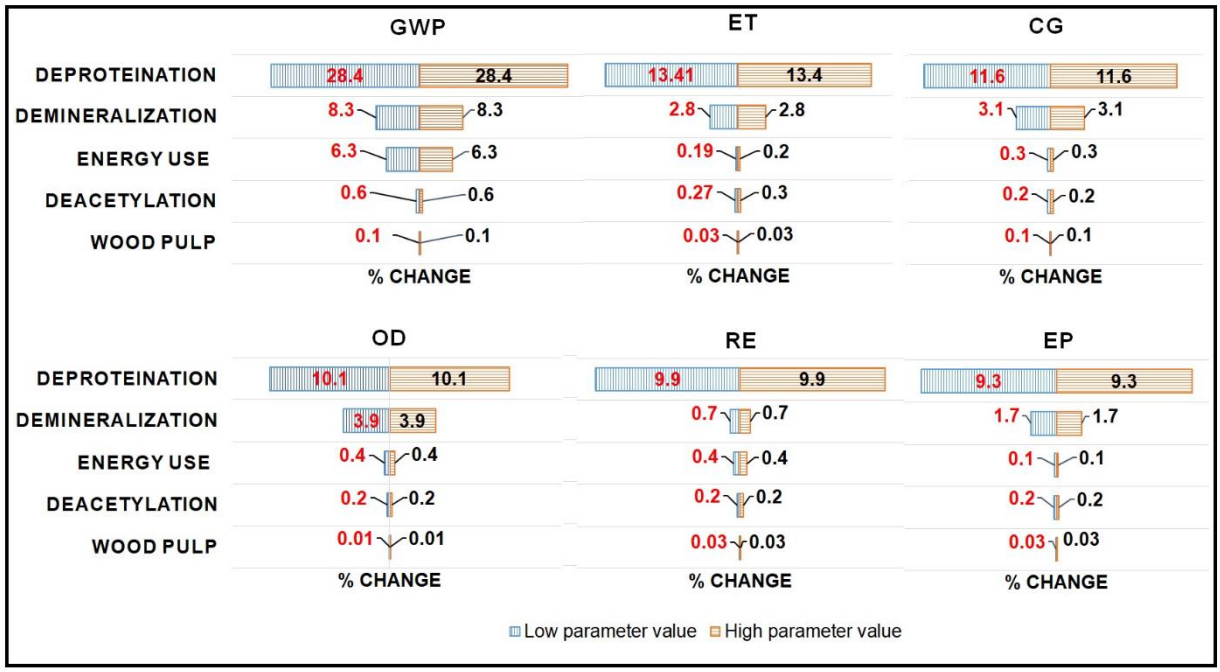

Figure 6-7. Sensitivity analysis on the major environmental impact categories of the chitosan-CNF composite film. Note: GWP-Global Warming Potential, ET-Ecotoxicity, CG-Carcinogenic, OD-Ozone Depletion, RE-Respiratory Effects, and EP-Eutrophication.

Scenario analysis

The CNF loading percent on the chitosan matrix can determine the achievable tensile and barrier properties of composite films. The maximum tensile strength of 55 MPa and water vapor barrier properties of 14 g.mm/kPa.d.m^2 were obtained for chitosan-CNF composite with 10 to 20% CNF and 20% glycerol [32]. The effect of the CNF loading percent on the impact of GWP was

evaluated at three different loading rates and compared with PLA and starch-based biopolymer films. The ± 5% change in CNF loading percent showed marginal change (± 2%) in GWP. Hence, increasing the CNF loading rate of up to 20% to improve the overall mechanical and barrier properties of composite films did not substantially increase the GWP. Furthermore, the increased GWP was lower or comparable to that of other biopolymer-based films such as PLA (4.53 kg CO_2 eq./kg) and starch (4.22 kg CO_2 eq./kg). Therefore, CNF reinforced chitosan films can be the most environmentally benign flexible composite films for packaging applications.

Conclusions

A cradle-to-gate life cycle assessment of chitosan-CNF composite films was conducted to evaluate the environmental impacts and compare them with other fossil-derived and biopolymers-based flexible films for packaging applications. The GWP of manufacturing chitosan-CNF composite film was about 3.91 kg CO2 eq./kg of composite film and was comparable or lower than that of fossil-derived and other biopolymer-based flexible films. The water-soluble nature of composite polymers required more energy to evaporate water to produce composite films. Thus, the energy required for the film drying was the major contributor of GWP followed by citric acid use for in-situ crosslinking of composite films. Therefore, developing an energy-efficient film drying technology would be critical to further reduce the GWP of composite films. The sensitivity analysis study revealed that the use of sodium hydroxide during deproteination of shrimp shell waste was the most sensitive parameter that influenced all the environmental impact categories evaluated. Therefore, the development of novel demineralization and deproteination of shrimp shell waste to produce chitosan could further reduce the overall environmental impacts of composite films. The scenario analysis demonstrated that the change in loading percent of CNF as a reinforcing agent did not substantially increase the GWP of composite films. In addition, the

biodegradability of all the constituents on the composite films could have huge potential for the commercial production of flexible packaging films. The emergence of chitosan-CNF composite films would also have the potential to replace fossil-derived packaging films accumulated on land and ocean surfaces to a greater extent. However, the current study has also identified potential environmental hotspots in the large-scale production of chitosan-CNF composite films. The use of NaOH, HCl, and fossil energy during the composite film manufacturing process were identified as the critical factors that could contribute to higher environmental impacts. Hence, it would be appropriate to explore the alternate routes to extract chitosan from shrimp shell wastes and alternative film drying processes to avoid greater environmental consequences during the manufacturing of composite films. The chitosan-CNF composite films are biodegradable and can be composted and used as fertilizer replacement. Furthermore, the end of life of chitosan-CNF composite films by composting should be further studied. In addition, the functional unit considered in this study was based on the mass fractions which would determine the composite material properties such as tensile and barrier properties. The change in the functional unit could also potentially alter the environmental performance. Future research is directed to evaluate the economic potential of composite films over commercial fossil-derived films and to promote the acceleration of scale-up and commercial production of chitosan-CNF composite films for packaging applications.

Acknowledgments

The authors acknowledge the partial financial support by the National Science Foundation's (NSF) Center for Bioplastics and Biocomposites (CB2) – A Industry-University Cooperative Research Centers (IUCRC) program, the University of Georgia (UGA).

References

1. Cha, D.S. and M.S. Chinnan, Biopolymer-Based Antimicrobial Packaging: A Review. Critical Reviews in Food Science and Nutrition, 2004. 44(4): p. 223-237.
2. Schiffman, J.D. and C.L. Schauer, A review: electrospinning of biopolymer nanofibers and their applications. Polymer reviews, 2008. 48(2): p. 317-352.
3. Van Vlierberghe, S., P. Dubruel, and E. Schacht, Biopolymer-based hydrogels as scaffolds for tissue engineering applications: a review. Biomacromolecules, 2011. 12(5): p. 1387-1408.
4. Rhim, J.-W. and P.K.W. Ng, Natural Biopolymer-Based Nanocomposite Films for Packaging Applications. Critical Reviews in Food Science and Nutrition, 2007. 47(4): p. 411-433.
5. Cazón, P., et al., Polysaccharide-based films and coatings for food packaging: A review. Food Hydrocolloids, 2017. 68: p. 136-148.
6. Fan, Y., C. Zhou, and X. Zhu, Selective Catalysis of Lactic Acid to Produce Commodity Chemicals. Catalysis Reviews, 2009. 51(3): p. 293-324.
7. Zinn, M., et al., Tailored Synthesis of Poly([R]-3-hydroxybutyrate-co-3-hydroxyvalerate) (PHB/HV) in Ralstonia eutropha DSM 428. Acta Biotechnologica, 2003. 23(2-3): p. 309-316.
8. Srinivasa, P.C. and R.N. Tharanathan, Chitin/Chitosan — Safe, Ecofriendly Packaging Materials with Multiple Potential Uses. Food Reviews International, 2007. 23(1): p. 53-72.

9. Zargar, V., M. Asghari, and A. Dashti, A Review on Chitin and Chitosan Polymers: Structure, Chemistry, Solubility, Derivatives, and Applications. ChemBioEng Reviews, 2015. 2(3): p. 204-226.
10. Wang, H., J. Qian, and F. Ding, Emerging Chitosan-Based Films for Food Packaging Applications. Journal of Agricultural and Food Chemistry, 2018. 66(2): p. 395-413.
11. Nunthanid, J., et al., Physical Properties and Molecular Behavior of Chitosan Films. Drug Development and Industrial Pharmacy, 2001. 27(2): p. 143-157.
12. Guerrero, P., et al., Crosslinking of chitosan films processed by compression molding. Carbohydrate Polymers, 2019. 206: p. 820-826.
13. Mujtaba, M., et al., Current advancements in chitosan-based film production for food technology; A review. International Journal of Biological Macromolecules, 2019. 121: p. 889-904.
14. Turbak, A., F. Snyder, and K. Sandberg, Microfibrillated Cellulose, in Washington, DC: US Patent and Trademark Office. 1983, International Telephone and Telegraph Corporation, New York, N.Y. .
15. Lee, H., J. Sundaram, and S. Mani, Production of cellulose nanofibrils and their application to food: a review. Nanotechnology, 2017: p. 1-33.
16. Abdul Khalil, H.P.S., et al., Cellulose Reinforced Biodegradable Polymer Composite Film for Packaging Applications, in Bionanocomposites for Packaging Applications, M. Jawaid and S.K. Swain, Editors. 2018, Springer International Publishing: Cham. p. 49-69.
17. Ng, H.-M., et al., Review of Nanocellulose Polymer Composite Characteristics and Challenges. Polymer-Plastics Technology and Engineering, 2017. 56(7): p. 687-731.

18. Hernández-Hernández, E., et al. Changing the surface characteristics of CNF, from hydrophobic to hydrophilic, via plasma polymerization with acrylic acid. in Journal of Nano Research. 2010. Trans Tech Publ.

19. Indumathi, M., K.S. Sarojini, and G. Rajarajeswari, Antimicrobial and biodegradable chitosan/cellulose acetate phthalate/ZnO nano composite films with optimal oxygen permeability and hydrophobicity for extending the shelf life of black grape fruits. International journal of biological macromolecules, 2019. 132: p. 1112-1120.

20. Rhim, J.-W., et al., Preparation and characterization of chitosan-based nanocomposite films with antimicrobial activity. Journal of agricultural and food chemistry, 2006. 54(16): p. 5814-5822.

21. Capadona, J.R., et al., A versatile approach for the processing of polymer nanocomposites with self-assembled nanofibre templates. Nature Nanotechnology, 2007. 2(12): p. 765-769.

22. Srinivasa, P., M. Ramesh, and R. Tharanathan, Effect of plasticizers and fatty acids on mechanical and permeability characteristics of chitosan films. Food hydrocolloids, 2007. 21(7): p. 1113-1122.

23. MacArthur, E., Towards the circular economy. Journal of Industrial Ecology, 2013. 2: p. 23-44.

24. Crippa, M., et al., A circular economy for plastics: Insights from research and innovation to inform policy and funding decisions. 2019.

25. Brusseau, M.L., Chapter 32 - Sustainable Development and Other Solutions to Pollution and Global Change, in Environmental and Pollution Science (Third Edition), M.L. Brusseau, I.L. Pepper, and C.P. Gerba, Editors. 2019, Academic Press. p. 585-603.

26. Curran, M.A., Life-Cycle Assessment, In Encyclopedia of Ecology (Second Edition), B. Fath, Editor. 2016, Elsevier: Oxford. p. 359-366.

27. Tabone, M.D., et al., Sustainability Metrics: Life Cycle Assessment and Green Design in Polymers. Environmental Science & Technology, 2010. 44(21): p. 8264-8269.

28. Li, Q., et al., Nanocellulose Life Cycle Assessment. ACS Sustainable Chemistry & Engineering, 2013. 1(8): p. 919-928.

29. Forsström, U. SUNPAP, scale-up nano particles in modern papermaking. in 2010 TAPPI International Conference on Nanotechnology for the Forest Product Industry. 2010. TAPPI Press.

30. Lee, H. and S. Mani, Mechanical pretreatment of cellulose pulp to produce cellulose nanofibrils using a dry grinding method. Industrial Crops and Products, 2017. 104: p. 179-187.

31. Yates, M.R. and C.Y. Barlow, Life cycle assessments of biodegradable, commercial biopolymers—A critical review. 2013. 78: p. 54-66.

32. Azeredo, H.M.C., et al., Nanocellulose Reinforced Chitosan Composite Films as Affected by Nanofiller Loading and Plasticizer Content. 2010. 75(1): p. N1-N7.

33. Udoetok, I.A., L.D. Wilson, and J.V. Headley, Self-Assembled and Cross-Linked Animal and Plant-Based Polysaccharides: Chitosan–Cellulose Composites and Their Anion Uptake Properties. ACS Applied Materials & Interfaces, 2016. 8(48): p. 33197-33209.

34. Bristow, J., Chitosan manufacturing process, in United States Patent 2012, Agratech International, Inc., Goose Creek, SC (US) p. 1-14.

35. Bilodeau, M.A. and M.A. Paradis, High efficiency production of nanofibrillated cellulose. 2018.

36. Siemann, U., Solvent cast technology – a versatile tool for thin film production, in Scattering Methods and the Properties of Polymer Materials, N. Stribeck and B. Smarsly, Editors. 2005, Springer Berlin Heidelberg: Berlin, Heidelberg. p. 1-14.

37. Choi, B., S. Yoo, and S.-i. Park, Carbon footprint of packaging films made from LDPE, PLA, and PLA/PBAT blends in South Korea. Sustainability, 2018. 10(7): p. 2369.

38. Moberg, T., et al., Rheological properties of nanocellulose suspensions: effects of fibril/particle dimensions and surface characteristics. Cellulose, 2017. 24(6): p. 2499-2510.

39. Srinivasa, P., et al., Properties of chitosan films prepared under different drying conditions. Journal of Food Engineering, 2004. 63(1): p. 79-85.

40. CARROAD, P.A. and R.A. TOM, Bioconversion of shellfish chitin wastes: process conception and selection of microorganisms. Journal of Food Science, 1978. 43(4): p. 1158-1161.

41. EPA. Sustainable Materials Management (SMM) - Materials and Waste Management in the United States Key Facts and Figures. Environment and Conservation 2017.

42. EPA, Documentation for Greenhouse Gas Emission and Energy Factors Used in the Waste Reduction Model (WARM). 2019.

43. Muñoz, I., et al., Life cycle assessment of chitosan production in India and Europe. The International Journal of Life Cycle Assessment, 2018. 23(5): p. 1151-1160.

44. Oneil, E.E., et al., Life-cycle impacts of inland northwest and northeast/north central forest resources. Wood and Fiber Science, 2010. 42: p. 29-51.

45. Vaz, Á., et al., Energy efficiency in low consistency refining: a study using a Valley beater. Nordic Pulp & Paper Research Journal, 2019. 34(1): p. 67-74.

46. CheCalc. Agitator Power. 2015; Available from: https://checalc.com/solved/agitator.html.

47. Kemp, I.C., Fundamentals of energy analysis of dryers. Modern drying technology, 2012. 4: p. 1-46.

48. Spalding, M.A. and A. Chatterjee, Handbook of industrial polyethylene and technology: Definitive guide to manufacturing, properties, processing, applications and markets set. 2017: John Wiley & Sons.

49. Wernet, G., et al., The ecoinvent database version 3 (part I): overview and methodology. The International Journal of Life Cycle Assessment, 2016. 21(9): p. 1218-1230.

50. Arvidsson, R., D. Nguyen, and M. Svanström, Life Cycle Assessment of Cellulose Nanofibrils Production by Mechanical Treatment and Two Different Pretreatment Processes. Environmental Science & Technology, 2015. 49(11): p. 6881-6890.

51. Bare, J., et al., Tool for the Reduction and Assessment of Chemical and other Environmental Impacts (TRACI). 2012.

52. Lee, H., Preparation and characterization of cellulose nanofibrils using various pretreatment techniques. 2016, University of Georgia.

53. Boxman, S.E., et al., Life Cycle Assessment of a Commercial-Scale Freshwater Aquaponic System. Environmental Engineering Science, 2016. 34(5): p. 299-311.

54. Ghamkhar, R., et al., Life cycle assessment of a cold weather aquaponic food production system. Journal of Cleaner Production, 2020. 244: p. 118767.

55. Phanthong, P., et al., Nanocellulose: Extraction and application. Carbon Resources Conversion, 2018. 1(1): p. 32-43.

56. Fernandes, S.C.M., et al., Transparent chitosan films reinforced with a high content of nanofibrillated cellulose. Carbohydrate Polymers, 2010. 81(2): p. 394-401.

57. Charoenvuttitham, P., J. Shi, and G.S. Mittal, Chitin Extraction from Black Tiger Shrimp (Penaeus monodon) Waste using Organic Acids. Separation Science and Technology, 2006. 41(6): p. 1135-1153.

58. Chen, X., et al., Recovery of Chitin from Antarctic Krill (Euphausia superba) Shell Waste by Microbial Deproteinization and Demineralization. Journal of Aquatic Food Product Technology, 2017. 26(10): p. 1210-1220.

59. Devi, R. and R. Dhamodharan, Pretreatment in Hot Glycerol for Facile and Green Separation of Chitin from Prawn Shell Waste. ACS Sustainable Chemistry & Engineering, 2018. 6(1): p. 846-853.

60. Ghorbel-Bellaaj, O., et al., Chitin extraction from shrimp shell waste using Bacillus bacteria. International Journal of Biological Macromolecules, 2012. 51(5): p. 1196-1201.

61. Jo, G.-H., R.-D. Park, and W.-J. Jung, Enzymatic production of chitin from crustacean shell waste. Chitin, Chitosan, Oligosaccharides and Their Derivatives, 2010: p. 37-45.

62. Mahmoud, N.S., A.E. Ghaly, and F. Arab, Unconventional approach for demineralization of deproteinized crustacean shells for chitin production. Am. J. Biochem. Biotechnol, 2007. 3(1): p. 1-9.

63. Yang, H., et al., Toward the shell biorefinery: processing crustacean shell waste using hot water and carbonic acid. ACS Sustainable Chemistry & Engineering, 2019. 7(5): p. 5532-5542.

64. Bhattacharya, S.C., T. Ruangrungchaikul, and H.L. Pham, Chapter 240 - Design and Performance of a Hybrid Solar/Biomass Energy Powered Dryer for Fruits and

Vegetables, in World Renewable Energy Congress VI, A.A.M. Sayigh, Editor. 2000, Pergamon: Oxford. p. 1161-1164.

65. Ndukwu, M.C., et al., Exergetic sustainability and economic analysis of hybrid solar-biomass dryer integrated with copper tubing as heat exchanger. Heliyon, 2020. 6(2): p. e03401.

66. Yahya, M., et al., Performance and economic analyses on solar-assisted heat pump fluidised bed dryer integrated with biomass furnace for rice drying. Solar Energy, 2018. 174: p. 1058-1067.

67. Li, D., J. Henschen, and M. Ek, Esterification and hydrolysis of cellulose using oxalic acid dihydrate in a solvent-free reaction suitable for preparation of surface-functionalised cellulose nanocrystals with high yield. Green Chemistry, 2017. 19(23): p. 5564-5567.

68. ISO, E., 14044: 2006. Environmental management-Life cycle assessment-Requirements and guidelines. European Committee for Standardization, 2006.

CHAPTER 7

CONCLUSION AND RECOMMENDATIONS

Conclusion

The accumulation of plastic packaging waste in the ocean and on the land have raised serious environmental concerns and necessitated the development of environmentally friendly packaging materials from renewable resource. The cellulose Nanofibrils (CNF), a nanostructured cellulose and its composites were extensively studied to use them as potential packaging materials due to their biodegradability, biocompatibility, excellent physical and mechanical properties. This dissertation was aimed to address the research gap in the production of nanocellulose and their composites for packaging applications. The specific objectives of this dissertation were to develop novel methods to produce high-solid content CNF hydrogels, to develop chitosan-CNF composites with improved water vapor barrier and hydrophobic properties, to develop PLA-cellulose microfibril (CMF) composite with enhanced tensile, and water vapor barrier properties and to assess the life cycle environmental impact of manufacturing chitosan-CNF composite film to present as proof – of – concept for large scale production. The key findings from this research work are as follows.

To produce high solid content CNF, the cellulose fibers were pretreated by two chemical pretreatments (with 2% CMC and 1% NaOH) with various mall milling time before high-pressure homogenization. The ball milling after the knife mill pretreatment processes significantly reduced the fiber dimensions, enhanced the dispersion ability and prevented clogging of cellulose fibers during the homogenization process. The processing ability of homogenizer was also improved

three times while compared to the control sample without ball milling treatment. The CNF hydrogel with the maximum of 6% solid content was able to achieve by this CNF manufacturing method. The manufacturing method did not affect the chemical structure and other properties of CNF hydrogel, but marginally increased the thermal stability. The crystallinity of CNF was increased by up to 10% at 45 min ball milling treatment time. The CNF fibrillation increased more fiber surface area for hydrogen bonding, entanglement in fiber network structure and the tensile strength of CNF films. Moreover, the CNF fibril width distribution from 20 to 40 nm proved that the fibrillization process could able to produce consistent quality fibrils from knife milled cellulose powder.

The CNF emerged as potential reinforcement materials due to their high aspect ratio, stiffness and specific area. The CNF were reinforced in natural biopolymers such as chitosan and starch and synthetic biopolymers such as PHA, PHB, PLA, etc. to develop biopolymer composites for packaging applications. In this work, the chitosan-CNF composite was manufactured using citric acid as a crosslinker by in-situ approach to study the mechanical and barrier properties of natural biopolymers for packaging applications. The citric acid crosslinking was confirmed from the FTIR peak at 1710 cm^{-1} wavenumber corresponding to the ester bonds. The water uptake and water vapor permeability of composite films were reduced by up to 86 and 50% respectively due to the effective crosslinking of chitosan-chitosan and chitosan-CNF molecules. The 20% of CNF and 25% of citric acid in chitosan composite was determined as an optimal amount of reinforcement and crosslinker that maximized the tensile strength, hydrophobicity and minimized water vapor barrier properties of composite film. The improvement of chitosan properties with CNF as reinforcement and citric acid as crosslinker demonstrated that chitosan-CNF composite can be potential alternative to displace fossil-based polymers for packaging applications.

To develop synthetic biopolymer-cellulose composites for packaging application, cellulose microfibrils (CMF) produced from cotton noil was reinforced with PLA biopolymer to produce composite films. The hydrophobic nature of noil fibers played a key role in improving the dispersion stability and the interfacial adhesion of composite films. Further, the crystallinity of CMFs did not affect the interfacial adhesion with PLA biopolymer matrix. The tensile and water vapor and UV light barrier properties were improved by the CMF reinforcement in PLA biopolymer. The ultimate tensile stress and Young's modulus of 1% CMF reinforced composites were 46% and 30% higher than that of the control films. The tensile strength of 1, 3, 5 and 10% CMF reinforced composites was decreased with further increase in CMF percent, but was comparable with that of low-density polyethylene (LDPE) polymer which is predominantly used in packaging applications. The water vapor barrier properties were improved while increasing the CMF reinforcement on the composites.

A cradle-to-gate life cycle assessment of chitosan-CNF composite films were conducted to assess the environmental impacts of composite films for packaging applications. The proof-of-concept approach was adapted to estimate the environmental impacts of large-scale production from laboratory film casting process. The LCA study revealed that about 79% of environmental impacts were caused by the citric acid and heat energy used during the film casting step. The carbon footprint of composite film was 7 and 16% less than that of the fossil-based low-density polyethylene (LDPE) and poly (lactic acid) (PLA) biopolymer films respectively. The sensitivity analysis identified that the use of sodium hydroxide used in the deproteination was the most sensitive process parameter influenced that global warming potentials (GWP) of composite films. An increase in CNF loading rate by up to 20% did not affect the GWP of composite films.

Recommendations

The future research can be focused on scaling up and commercial production of CNF from NaOH pretreated short cellulose fibers for producing highly dispersible and consistent quality CNFs for various applications. In addition, the scaling up of water based solvent casting method should be further investigated to optimize the casting temperature, film quality and energy consumption of large-scale production plant.

The environmental impacts of biopolymer composites are scare in the literature. Therefore, a comprehensive life cycle assessment tools should be developed to screen biopolymers that are not only environmentally benign, but also economically competitive to commercial fossil-based polymers for packaging applications. Therefore, the life cycle assessment should be combined with techno-economic assessment of biopolymer composites to promote the market penetration of both natural and synthetic biopolymers on the sustainable packaging industry.

APPENDIX A

SUPPLEMENTARY INFORMATION- PRODUCTION AND CHARACTERIZATION OF HIGH SOLID CONTENT CELLULOSE NANOFIBRILS FROM PRETREATED FLUFF PULP

Statistical analysis

The one-way ANOVA test was performed to study effect of pretreatment process on feedstock cellulose fiber dimension (width and length) reduction, CNF solid content percentage, zeta potential, crystallinity, and fibril width. The data for statistical tests were obtained from optical microscope images, moisture test, zeta potential measurements, XRD test and SEM images. The hypotheses of the statistical tests were defined and tests were performed in MATLAB software. The anova1() function was used to return 'p' value and ANOVA table. The variation between samples and within samples (Error) were listed in ANOVA table. The significant difference across the mean value of samples were determined from returned 'p' value and conclusion about null hypothesis was reported. The multcompare () function was used make pairwise comparison of sample means and to study pretreatment effects on CNF samples manufactured. The Tukey's honestly significant difference procedure was used to test hypothesis.

Effect of pretreatment process on feedstock cellulose fiber width

The following hypothesizes were tested to investigate effect of pretreatment process on width of feedstock cellulose fibers.

Null hypothesis: The mean width of cellulose fibers produced by different pretreatment methods are same.

Alternate hypothesis: The mean width of cellulose fibers produced by different pretreatment methods are not same.

Inference: The 'p' value is less than 0.05. Hence, null hypothesis was rejected. The multiple comparison test indicated that pretreated sample means were different from control sample

Table 3-S1. One-way ANOVA significance test results of fiber width

Source	Sum of squares	Degrees of freedom	Mean square	F value	Prob > F
Variation between CNF samples	32880.6	6	5480	301.53	8.7787×10^{-115}
Error	4779.8	263	18.17		
Total	37660	269			

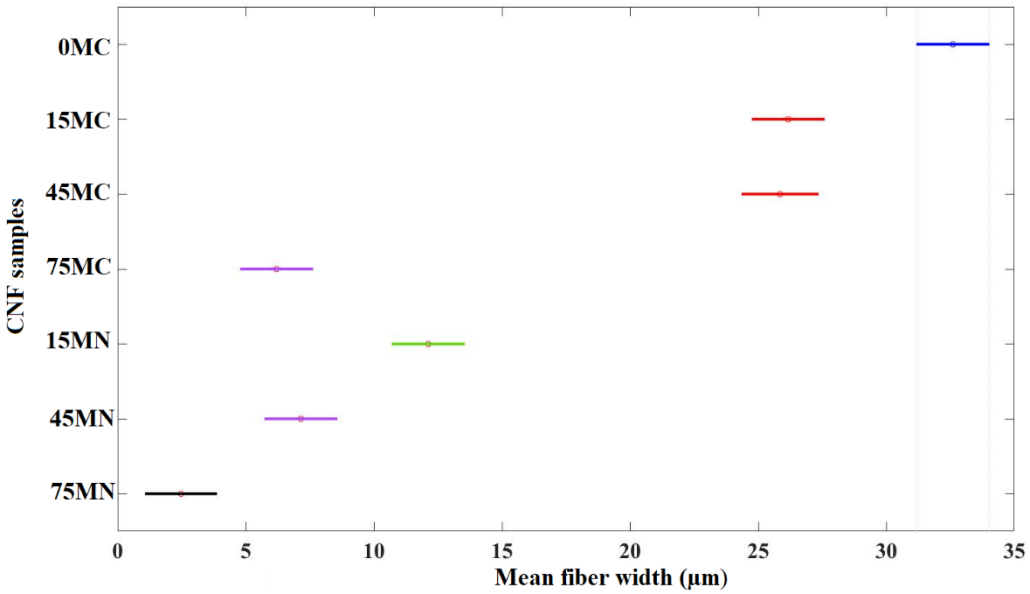

Figure 3-S1. One-way ANOVA multiple comparison test of pretreated cellulose fiber width

Effect of pretreatment process on feedstock cellulose fiber length

The following hypothesizes were defined to investigate effect of pretreatment on length of feedstock cellulose fiber.

Null hypothesis: The mean length of cellulose fibers produced by different pretreatment methods are same.

Alternate hypothesis: The mean length of cellulose fibers produced by different treatment methods are not same.

Inference: The 'p' value in ANOVA table is less than 0.05. Hence, the null hypothesis was rejected. The pairwise multiple comparison test results are presented in Figure 3-S2. The effect of all pretreatments on fiber length reduction were significantly different from control sample.

Table 3-S2. One-way ANOVA significance test results of fiber length

Source	Sum of squares	Degrees of freedom	Mean square	F value	Prob > F
Variation between CNF samples	4.54028×10^{6}	6	756713.5	68.73	5.3745×10^{-51}
Error	2.88452×10^{6}	262	11009.6		
Total	7.4248×10^{6}	268			

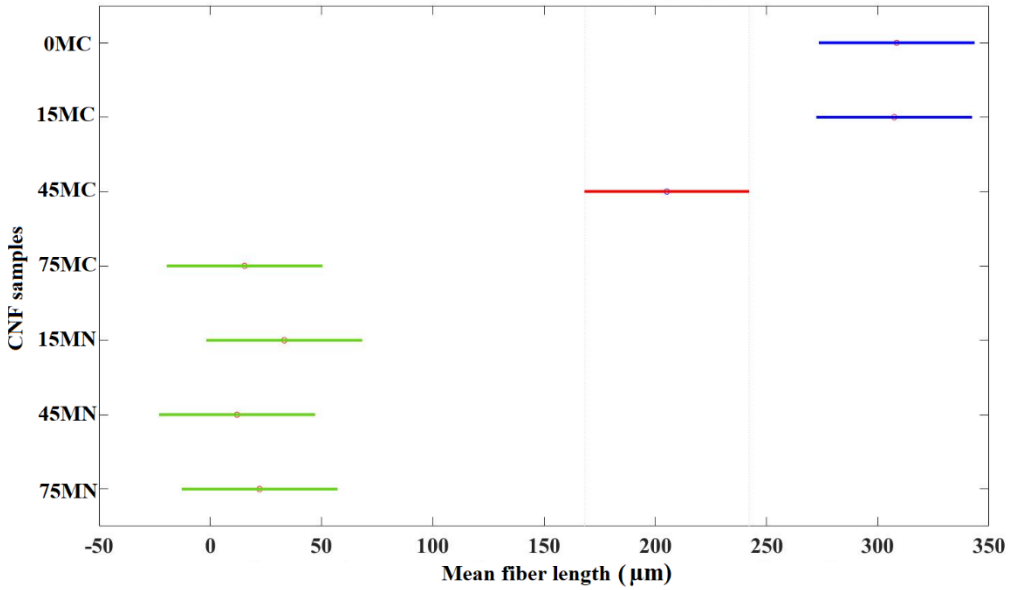

Figure 3-S2. One-way ANOVA multiple comparison test of pretreated cellulose fiber length

Effect of pretreatment process on CNF hydrogel solid content

The following hypothesizes were tested to investigate effect of pretreatment on solid content percentage in CNF hydrogel.

Null hypothesis: The mean solid content of CNF hydrogel produced by different pretreatment methods are same.

Alternate hypothesis: The mean solid content of CNF hydrogel produced by different treatment methods are not same.

Inference: The 'p' value in ANOVA table is less than 0.05. Hence, null hypothesis was rejected. The means values of CNF samples such as 0MC, 15MC and 45MC are different from other samples.

Table 3-S3. One-way ANOVA significance test results of solid content percentage in CNF hydrogel

Source	**Sum of squares**	**Degrees of freedom**	**Mean square**	**F value**	**Prob > F**
Variation between CNF samples	0.0032	6	0.00053	21.59	5.89984×10^{-35}
Error	0.00138	56	0.00002		
Total	0.00459	62			

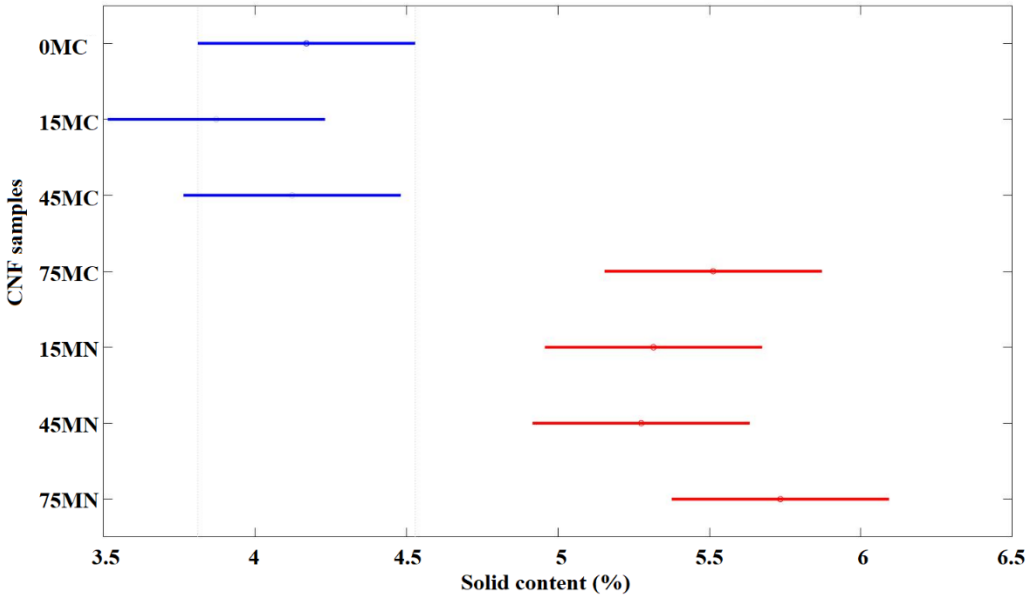

Figure 3-S3. One-way ANOVA multiple comparison test of CNF hydrogel solid content percentage

Effect of pretreatment process on zeta potential

The null and alternate hypothesis of zeta potential parameter were defined for one-way ANOVA test.

Null hypothesis: The mean zeta potential of CNF hydrogel produced by different pretreatment methods are same.

Alternate hypothesis: The mean zeta potential of CNF hydrogel produced by different treatment methods are not same.

Inference: The 'p' value in ANOVA table is less than 0.05. Hence, the null hypothesis was rejected. The mean values of Ref. CNF samples are different from other samples.

Table 3-S4. One-way ANOVA significance test results of zeta potential

Source	Sum of squares	Degrees of freedom	Mean square	F value	Prob > F

Variation between CNF samples	2774.31	7	396.33	9.48	$6.86928x10-^{10}$
Error	6980.25	167	41.798		
Total	9764.55	174			

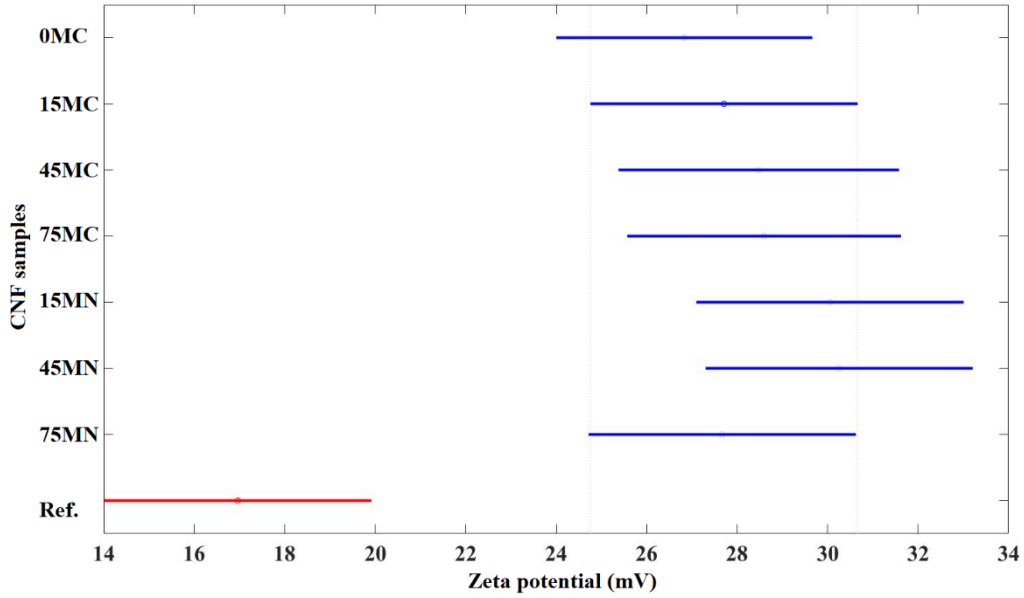

Figure 3-S4. One-way ANOVA multiple comparison test of zeta potential

Effect of pretreatment process on crystallinity

The null and alternate hypothesis of crystallinity index parameter were defined for one-way ANOVA test.

Null hypothesis: The mean crystallinity index of CNF hydrogel produced by different pretreatment methods are same.

Alternate hypothesis: The mean crystallinity index of CNF hydrogel produced by different treatment methods are not same.

Inference: The 'p' value in ANOVA table was greater than 0.05. Hence, null hypothesis was accepted. The mean values of crystallinity index were same for all samples.

Table 3-S5. One-way ANOVA significance test results of crystallinity index

Source	Sum of squares	Degrees of freedom	Mean square	F value	Prob > F
Variation between CNF samples	195.429	7	27.9186	1.16	0.376
Error	384.361	16	24.0226		
Total	579.79	23			

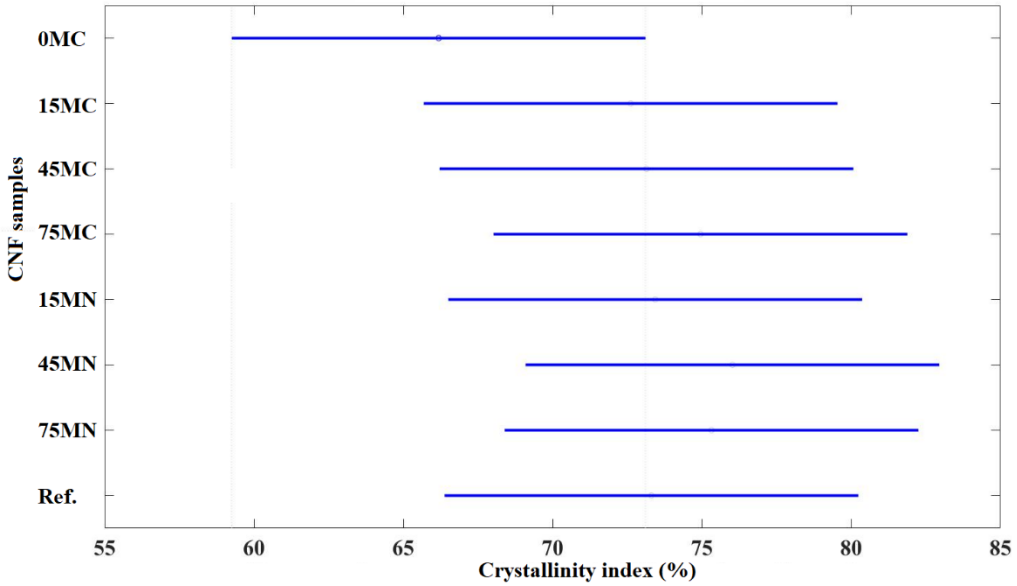

Figure 3-S5. One-way ANOVA multiple comparison test of crystallinity index

Effect of pretreatment process on CNF width

The following hypothesizes tested to investigate effect of pretreatment on CNF hydrogel fibril width.

Null hypothesis: The mean fibril width of CNF hydrogel produced by different pretreatment methods are same.

Alternate hypothesis: The mean fibril width of CNF hydrogel produced by different treatment methods are not same.

Inference: As the $p<0.05$, null hypothesis was rejected. The mean width of control and Ref. samples were different from pretreated samples.

Table 3-S6. One-way ANOVA significance test results of CNF width

Source	Sum of squares	Degrees of freedom	Mean square	F value	Prob > F
Variation between CNF samples	71503.6	7	10214.8	99.04	1.53109×10^{-103}
Error	81168.8	787	103.1		
Total	152672.4	794			

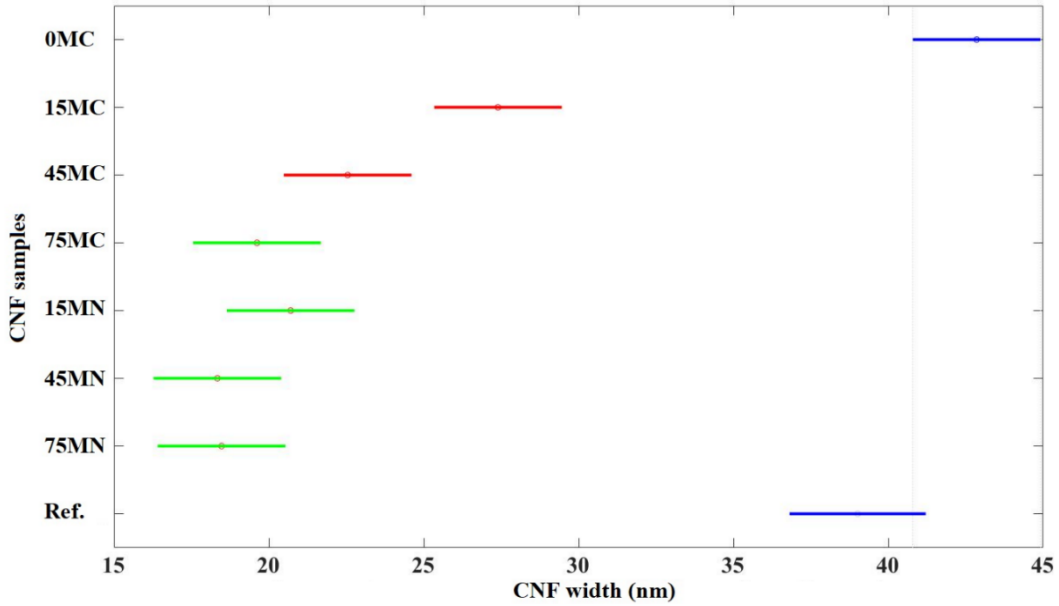

Figure 3-S6. One-way ANOVA multiple comparison test of CNF width

APPENDIX B

SUPPLEMENTARY INFORMATION - COTTON NOIL BASED CELLULOSE MICROFIBERS REINFORCED POLYLACTIC ACID COMPOSITES FOR THE IMPROVEMENT OF WATER VAPOR AND UV BARRIER PROPERTIES IN PACKAGING FILMS

Statistical analysis

Table 5-S1. One-way ANOVA table of ultimate tensile stress

Source	Sum of squares	Degrees of freedom	Mean square	F value	Prob > F
Variation between samples	1862.56	5	372.512	39.3	$8.56x10^{-11}$
Error	227.51	24	9.48		
Total	2090.07	29			

Table 5-S2. One-way ANOVA table of Young's modulus

Source	Sum of squares	Degrees of freedom	Mean square	F value	Prob > F
Variation between samples	$1.73x10^{6}$	5	346207	6.32	0.0007
Error	$1.31x10^{6}$	24	54776.30		
Total	$3.05x10^{6}$	29			

Table 5-S3. One-way ANOVA table of water vapor permeability

Source	Sum of squares	Degrees of freedom	Mean square	F value	Prob > F
Variation between samples	$8.97x10^{-22}$	5	$1.79x10^{-22}$	4.95	0.003
Error	$8.70x10^{-22}$	24	$3.62x10^{-23}$		
Total	$1.77x10^{-21}$	29			

APPENDIX C

SUPPLEMENTARY INFORMATION - LIFE CYCLE ASSESSMENT OF MANUFACTURING CELLULOSE NANOFIBRILS REINFORCED CHITOSAN COMPOSITE FILMS FOR PACKAGING APPLICATIONS

LCI data

CNF production

Table 6-S1. LCI data of pulp production

Process stages		Input/output	Inventory details	Amount	Unit
Softwood chips production for pulp manufacturing	Forest Operation	Process output	Softwood, Low intensity management	119.61	m3
		Input from Nature and Technosphere	Carbon dioxide	83272.00	kg
			Felling	4.67	h
			Chain sawing	10.61	h
			Loading	8.28	h
			Skidding	11.22	h
	Wood Chips	Process Output	Softwood Chips	1	m^3
		Input from Nature and Technosphere	Wood Chopping	169.00	kg
			Pulpwood, softwood, average, low intensity management, NE-NC NREL/RNA U-Modified	0.36	kg
Pulp Production	Pulp	Process Output	Bleached sulfate pulp	1.00	kg
	Biomass Resource for Pulp	Input from Nature and Technosphere	Softwood Chips	0.004	m3
	Water		Water	0.06	m3

	Digester	Sodium hydroxide, without water, in 50% solution	0.02	kg
		Sodium sulfite	0.00003	kg
		Magnesium sulfate	0.003	kg
		Sulfur dioxide, liquid	0.0004	kg
	Recovery	Sodium sulfate, anhydrite	0.0003	kg
		Quicklime, milled	0.008	kg
		Calcium carbonate	0.002	kg
		Sulfur	0.00007	kg
		Digester sludge	-0.00023	kg
	Bleaching	Hydrogen peroxide, without water, in 50% solution state	0.01	kg
		Oxygen, liquid	0.02	kg
		Sodium chlorate, powder	0.01	kg
		Ozone, liquid	0.00003	kg
		Sodium formate	0.0008	kg
		Sodium hypochlorite, without water, in 15% solution state	0.0002	kg
		Sulfuric acid	0.027	kg
	Other Chemicals	Chemical, inorganic	0.0001	kg
		Chemical, organic	0.002	kg
		EDTA, ethylenediaminetetraacetic acid	0.0005	kg
		Malusil	0.0004	kg
	Electricity and Heat	Electricity, high voltage	0.037	kWh
		Heavy fuel oil	0.006	kg
		Light fuel oil	0.004	kg
		Natural gas, high pressure	0.0001	m3

			Natural gas, high pressure	0.008	m3
			Methanol	0.0001	kg
			Methanol, from biomass	0.002	kg
			Waste packaging paper	-0.0005	kg
			Waste paper, unsorted	-0.00003	kg
			Wood chips, dry, measured as dry mass	0.49	kg
			Wood pellet, measured as dry mass	0.008	kg
	Transport		Transport, freight train	0.33	tkm
			Transport, freight, lorry >32 metric ton, euro5	0.26	tkm
	Infrastructure		Pulp factory	4.07E-11	p

Table 6-S2. LCI dataset of CNF isolation process

Data Type	Value	Units	Reference
Specific energy consumption of valley beater	0.386	kWh/kg	(Vaz et al. 2019)
Specific energy consumption of refiner	1.45	kWh/kg	(Bilodeau and Paradis 2018)

Table 6-S3. LCI data used in SimaPro to represent the CNF production from softwood bleached sulphate pulp by Valley Beater and Disc Refiner

Process Input				
Material / Energy	**Amount**	**Unit**	**SimaPro Dataset Used**	**Reference**
Inputs from Technosphere (materials/fuels)				
Bleached Sulphate Pulp	1.06	kg	Sulfate pulp, bleached | sulfate pulp production, from softwood,	Table 6-S1

			bleached | Cut-off, U-Modified	
Inputs from Technosphere (electricity/heat)				
Electricity - Valley Beater	0.386	kWh	Electricity, at grid, US/US	Table 6-S2
Electricity-Refiner	1.45	kWh	Electricity, at grid, US/US	Table 6-S2
Process Output				
Material / Energy	Amount	Unit	SimaPro Dataset Used	Reference
Outputs to Technosphere (Products and co-products)				
CNF	1	kg	CNF-Valley Beater - Modelled	

Chitosan production

Table 6-S4. Emission factors for food waste end of life management options from EPA WARM model

Food waste end of life options	Emission factors ($kgCO_2$ eq./ kg)	Reference
Composting	-0.198415979	(EPA 2019)
Combustion	-0.143300429	
Landfilling	0.595247937	

Table 6-S5. CO_2 Emission from shrimp shell waste disposed as MSW and managed by different end of life options

Shrimp shell waste end of life options	Disposal fraction	Emission ($kgCO_2$ eq. / kg)	Remarks
Composting	0.047385	-0.009402	Disposal fraction was estimated from 10 years data of food waste disposal for different end of life options (EPA 2017)
Combustion	0.184614	-0.026455	
Landfilling	0.768000	0.457151	
Total	1.000000	0.421293	Emission = Disposal fraction x Emission factors

Table 6-S6. Composition of Shrimp Shell (Muñoz et al. 2018)

Dry matter	**Protein**	**Chitin**	**$CaCO_3$**
(kg/kg shrimp waste)	(kg/kg dm)	(kg/kg dm)	(kg/kg dm)
0.25	0.65	0.15	0.2

Table 6-S7. Data resource for LCI data of chitosan manufacturing process (Ref. 1) (Bristow 2012)

Process	**Material Input**	**Amount**	**Liquid to Solid Ratio**
Chitin Manufacturing			
Wash	Water		6L/kg of shrimp shell
Demineralization	HCl	0.9 to 1.1 M (HCl: 0.0365 kg/mole)	4L/kg of shrimp shell
Deproteination	NaOH	4 to 6 % w/v	4L/kg of demineralized shell
Chitosan Manufacturing			
Deacetylation	NaOH	45 to 50 % w/w	50L/kg of chitin

Table 6-S8. Resource for LCI data of chitosan manufacturing process (Ref. 2) (Muñoz et al. 2018)

A. Manufacturing of 1 kg chitin			
Input / Output Material & Energy	**Amount**	**Unit**	**SimaPro Dataset**
Avoided Product			
Protein sludge	4	kg	Protein sludge
Calcium waste	1.5	kg	Calcium carbonate, precipitated {RER}| calcium carbonate production, precipitated | Cut-off, U
Infrastructure			
Technosphere (Materials and Energy)			
Shrimp shell	33	kg	Shrimp shell - Modelled
Electricity	1.3	kWh	Electricity, medium voltage, certified electricity, at grid/US* US-EI U
Emissions			
CO_2 fossil	0.7	kg	Carbon dioxide, fossil
B. Manufacturing of 1 kg chitosan			

Technosphere (Materials and Energy)			
Chitin	1.41	kg	
Heat from biomass	31.3	MJ	Combustion, dry wood residue, AP-42/MJ/RNA
Electricity	1.06	kWh	Electricity, medium voltage, certified electricity, at grid/US* US-EI U

Table 6-S9. LCI data resource for 1 kg of protein sludge production (Muñoz et al. 2018)

Input / Output category	Amount	Unit	SimaPro Dataset
Avoided products/services:			
Protein sludge	1	kg	Protein sludge - Modelled
Technosphere (Materials and Energy)			
N fertilizer	-0.06	kg	Nitrogen fertilizer, as N {GLO}| market for | Cut-off, U
Emissions to air:			
Ammonia	0.03059	kg	Ammonia
Dinitrogen monoxide	0.00144	kg	Dinitrogen monoxide
Nitrogen oxides	0.01461	kg	Nitrogen oxides
CO_2 biogenic	1.72	kg	Carbon dioxide, biogenic

Table 6-S10. LCI Data - Shrimp shell waste

Process Input				
Material / Energy	**Amount**	**Unit**	**SimaPro Dataset Used**	**Reference**
Inputs from nature (resources)				
Process Output				
Material / Energy	Amount	Unit	SimaPro Dataset Used	Reference
Outputs to Technosphere (Products and co-products)				
Shrimp shell as MSW waste	1.00	kg		
Outputs to Technosphere (Emissions to Air)				
Carbon dioxide	0.42	kg		Table 6-S5

Table 6-S11. LCI Data - Chitin manufacturing -base case

Process Input				
Material / Energy	**Amount**	**Unit**	**SimaPro Dataset Used**	**Reference**
Inputs from nature (resources)				
Water	198.00	l	Water, unspecified natural origin, US	Table 6-S7
Inputs from Technosphere (materials/fuels)				
Shrimp Shell	33.00	kg	Shrimp shell - Modelled	Table 6-S8 A
HCl for demineralization	4.70	kg	Hydrochloric acid, 30% in H2O, at plant/US- US-EI U	Table 6-S7
NaOH for deproteination	6.27	kg	Sodium hydroxide, without water, in 50% solution state {GLO}| market for | Cut-off, U	Table 6-S7
Inputs from Technosphere (electricity/heat)				
Electricity	1.30	kwh	Electricity, medium voltage, certified electricity, at grid/US* US-EI U	Table 6-S8 A
Process Output				
Material / Energy	Amount	Unit	SimaPro Dataset Used	Reference
Outputs to Technosphere (Products and co-products)				
Chitin	1.00	kg	Chitin - Modelled	
Outputs to Technosphere (Avoided Products)				
Nitrogen fertilizer	0.24	kg	Nitrogen fertilizer, as N {GLO}| market for | Cut-off, U	Table 6-S8 A& Table 6-S9
Emission to Air				
CO_2 fossil	0.7	kg	Carbon dioxide, fossil	Table 6-S8 A
Ammonia	0.12236	kg	Ammonia	Table 6-S8 A & Table 6-S9
Dinitrogen monoxide	0.00576	kg	Dinitrogen monoxide	
Nitrogen oxides	0.05844	kg	Nitrogen oxides	
CO_2 biogenic	6.88	kg	Carbon dioxide, biogenic	
Outputs to Technosphere (Waste and Emissions to Treatment)				
Calcium waste	1.50	kg	Disposal, limestone residue, 5% water, to inert material landfill/US* US-EI U	Table 6-S8 A

Waste water	198.00	l	Treatment, sewage, to wastewater treatment, class 1/US* US-EI U	

Table 6-S12. LCI Data - Chitosan manufacturing - base case

Process Input				
Material / Energy	**Amount**	**Unit**	**SimaPro Dataset Used**	**Reference**
Inputs from nature (resources)				
Chitin	1.41	kg	Chitin - Modelled	Table 6-S8 B
Water	70.42	l	Water, unspecified natural origin, US	Table 6-S7
Inputs from Technosphere (materials/fuels)				
NaOH-deacetylation	0.67	kg	Sodium hydroxide, without water, in 50% solution state {GLO}| market for | Cut-off, U	Table 6-S7
Inputs from Technosphere (electricity/heat)				
Heat from biomass	31.3	MJ	Combustion, dry wood residue, AP-42/MJ/RNA	Table 6-S8 B
Electricity	1.06	kWh	Electricity, medium voltage, certified electricity, at grid/US* US-EI U	Table 6-S8B
Process Output				
Material / Energy	**Amount**	**Unit**	**SimaPro Dataset Used**	**Reference**
Outputs to Technosphere (Products and co-products)				
Chitosan	1.00	kg	Chitosan - Modelled	
Waste water	70.42	l	Treatment, sewage, to wastewater treatment, class 1/US* US-EI U	

Film casting process

Table 6-S13. Packaging film size, production output-base case

Parameter	**Value**	**Unit**	**Reference**
Packaging film size	300x250x.3	mm x mm x mm	(Choi et al. 2018)
Production rate	400000	Pieces/day	

Chitosan -CNF density	1.1	g/cm3	Measured from the citric acid cross linked CNF reinforced chitosan film manufactured in lab
Packaging film mass output/day (Dry film)	9900	kg/day	Packaging film mass output/day = Volume of film produced in day x density of the film
Packaging film mass output/ hour (Dry Film)	412.5	kg/h	Packaging film mass output/ hour = (Packaging film mass output/day) / 24
Surface Area of packaging film production / hour	1250	m2/h	Total area of film produced in one hour
Cast film roll dimension (WxL)	1.98 x 631.31	m x m	Width of the roll assumed is 78 inches

Table 6-S13A. Packaging film size, production output- scenario-1

Parameter	Value	Unit	Reference
Packaging film size	300x250x.3	mm x mm x mm	(Choi et al. 2018)
Production rate	400000	Pieces/day	
Chitosan -CNF density	1.1	g/cm3	Measured from the citric acid cross linked CNF reinforced chitosan film manufactured in lab
Packaging film mass output/day (Dry film)	9900	kg/day	Packaging film mass output/day = Volume of film produced in day x density of the film
Packaging film mass output/ hour (Dry Film)	412.5	kg/h	Packaging film mass output/ hour = (Packaging film mass output/day) / 24
Surface Area of packaging film production / hour	1250	m2/h	Total area of film produced in one hour
Cast film roll dimension (WxL)	1.98 x 631.31	m x m	Width of the roll assumed is 78 inches

Table 6-S13B. Packaging film size, production output- scenario-2

Parameter	**Value**	**Unit**	**Reference**
Packaging film size	300x250x.3	mm x mm x mm	(Choi et al. 2018)
Production rate	400000	Pieces/day	

Chitosan -CNF density	1.1	g/cm3	Measured from the citric acid cross linked CNF reinforced chitosan film manufactured in lab
Packaging film mass output/day (Dry film)	9900	kg/day	Packaging film mass output/day = Volume of film produced in day x density of the film
Packaging film mass output/ hour (Dry Film)	412.5	kg/h	Packaging film mass output/ hour = (Packaging film mass output/day) / 24
Surface Area of packaging film production / hour	1250	m2/h	Total area of film produced in one hour
Cast film roll dimension (WxL)	1.98 x 631.31	m x m	Width of the roll assumed is 78 inches

Table 6-S14. Hourly production of chitosan- 15% CNF composite film manufacturing by solvent casting - Mass flow calculations-base case

Materials	Amount	Unit	Remarks
Chitosan	193.875	kg	47% in composite composition
CNF dry mass	61.875	kg	15% CNF loading in composite film
CNF hydrogel with 3% dry mass	2062.5	kg	CNF with 3% concentration- Determined based on present commercial / pilot scale CNF production from University of Maine
Citric Acid	82.5	kg	20% in composite film- Determined based on experiment
Glycerol	74.25	kg	18% w/w of composite film (Azeredo et al. 2010)
Water	6462.5	l	3% w/v chitosan solution - Determined based on composite films manufactured in lab by solvent casting
Acetic acid	64.6	l	1% w/v aqueous solution is used to dissolve chitosan

Table 6-S14A. Hourly production of chitosan- 20% CNF composite film manufacturing by solvent casting - Mass flow calculations- scenario-1

Materials	Amount	Unit	Remarks
Chitosan	173.25	kg	42 % in composite composition

CNF dry mass	82.5	kg	20% CNF loading in composite film
CNF hydrogel with 3% dry mass	2750.0	kg	CNF with 3% concentration- Determined based on present commercial / pilot scale CNF production from University of Maine
Citric Acid	82.5	kg	20% in composite film- Determined based on experiment
Glycerol	74.25	kg	18% w/w of composite film (Azeredo et al. 2010)
Water	5775.0	l	3% w/v chitosan solution - Determined based on composite films manufactured in lab by solvent casting
Acetic acid	57.8	l	1% w/v aqueous solution is used to dissolve chitosan

Table 6-S14B. Hourly production of chitosan- 20% CNF composite film manufacturing by solvent casting - Mass flow calculations- scenario-2

Materials	Amount	Unit	Remarks
Chitosan	214.5	kg	52 % in composite composition
CNF dry mass	41.25	kg	10% CNF loading in composite film
CNF hydrogel with 3% dry mass	1375.0	kg	CNF with 3% concentration- Determined based on present commercial / pilot scale CNF production from University of Maine
Citric Acid	82.5	kg	20% in composite film- Determined based on experiment
Glycerol	74.25	kg	18% w/w of composite film (Azeredo et al. 2010)
Water	7150.0	l	3% w/v chitosan solution - Determined based on composite films manufactured in lab by solvent casting
Acetic acid	71.5	l	1% w/v aqueous solution is used to dissolve chitosan

Table 6-S15. Mixing power / kg polymer calculation-base case

Parameter	Value	Unit	Remarks	Reference
Volume of mixture used in reactor (Batch Volume) (V)	8525	l	Calculated from the volume of water and CNF hydrogel used in the reactor	
Reactor nominal volume	12500	l	Reactors overall volume with 50% more free volume is assumed	Pfaudler DIN BE Reactors catalogue
Agitator diameter /Reactor diameter	0.4			
CNF density	1000.0	kg/m 3		The University of Maine product specification datasheet
CNF viscosity	100.0	cP		(Moberg et al. 2017)
Scale of agitation	5.0		Followed in most chemical industry	https://checalc.com/solved/agitator.html?
Mixing motor power	1.8	kW		
Mixing power / kg polymer composite film	0.004	kWh		

Table 6-S15A. Mixing power / kg polymer calculation- scenario 1

Parameter	Value	Unit	Remarks	Reference
Volume of mixture used in reactor (Batch Volume) (V)	8525	l	Calculated from the volume of water and CNF hydrogel used in the reactor	
Reactor nominal volume	12500	l	Reactors overall volume with 50% more free	Pfaudler DIN BE Reactors catalogue

Agitator diameter /Reactor diameter	0.4		volume is assumed	
CNF density	1000.0	kg/m3		The University of Maine product specification datasheet
CNF viscosity	100.0	cP		(Moberg et al. 2017)
Scale of agitation	5.0		Followed in most chemical industry	https://checalc.com/solved/agitator.html?
Mixing motor power	1.8	kW		
Mixing power / kg polymer composite film	0.004	kWh		

Table 6-S15B. Mixing power / kg polymer calculation- scenario 2

Parameter	Value	Unit	Remarks	Reference
Volume of mixture used in reactor (Batch Volume) (V)	8525	l	Calculated from the volume of water and CNF hydrogel used in the reactor	
Reactor nominal volume	12500	l	Reactors overall volume with 50% more free volume is assumed	Pfaudler DIN BE Reactors catalogue
Agitator diameter /Reactor diameter	0.4			
CNF density	1000.0	kg/m3		The University of Maine product specification datasheet
CNF viscosity	100.0	cP		(Moberg et al. 2017)
Scale of agitation	5.0		Followed in most chemical industry	https://checalc.com/solved/agitator.html?

Mixing motor power	1.8	kW	
Mixing power / kg polymer composite film	0.004	kWh	

Table 6-S16. Heat energy required for the evaporation of solvent (q) (kJ/s) from 1 kg of dry composite film-base case

Parameter	**Value**	**Unit**	**Remarks**
Latent heat of water (h_w)	2282.5	(kJ/kg)	@ 90° C
Mass water to be evaporated (W)	20.67	kg	3% w/v concentration of CNF and Chitosan was estimated for 1 kg of film
Heat energy needed for drying (Q)	47171.67	kJ	$Q=W \times h_w$
Dryer efficiency	80.00	%	
Heat energy needed for drying	58965	kJ	
Heat energy required for heating 1 kg film	51.00	MJ	

Table 6-S16A. Heat energy required for the evaporation of solvent (q) (kJ/s) from 1 kg of dry composite film- scenario 1

Parameter	**Value**	**Unit**	**Remarks**
Latent heat of water (h_w)	2282.5	(kJ/kg)	@ 90° C
Mass water to be evaporated (W)	20.67	kg	3% w/v concentration of CNF and Chitosan was estimated for 1 kg of film
Heat energy needed from steam for drying (Q)	47171.67	kJ	$Q=W \times h_w$
Dryer efficiency	80.00	%	
Heat energy needed for drying	58965	kJ	
Heat energy required for heating 1 kg film	51.00	MJ	

Table 6-S16B. Heat energy required for the evaporation of solvent (q) (kJ/s) from 1 kg of dry composite film- scenario 2

Parameter	Value	Unit	Remarks
Latent heat of water (h_w)	2282.5	(kJ/kg)	@ 90° C
Mass water to be evaporated (W)	20.67	kg	3% w/v concentration of CNF and Chitosan was estimated for 1 kg of film
Heat energy needed from steam for drying (Q)	47171.67	kJ	$Q=W \times h_w$
Dryer efficiency	80.00	%	
Heat energy needed for drying	58965	kJ	
Heat energy required for heating 1 kg film	51.00	MJ	

Table 6-S17. Power required for winding 1 kg of composite film in a roll-base case

Parameter	Value	Unit	Remarks
Composite film winding amount	1	kg	1 kg of composite film was considered for winding 1 turn in roll
Length of composite film which weigh 1 kg	0.653	m	
Diameter (D) of the roll which make 1 turn roll with 1kg composite film	0.208	m	$\pi \times D$= Length of 1 kg composite film
Torque required to wind 1kg of composite film	2.041	NM	
Power required for winding 1 kg of composite film with 1 rpm speed	0.214	W	

Table 6-S17A. Power required for winding 1 kg of composite film in a roll- scenario 1

Parameter	Value	Unit	Remarks
Composite film winding amount	1	kg	1 kg of composite film was considered for winding 1 turn in roll
Length of composite film which weigh 1 kg	0.653	m	

Diameter (D) of the roll which make 1 turn roll with 1kg composite film	0.208	m	π x D= Length of 1 kg composite film
Torque required to wind 1kg of composite film	2.041	NM	
Power required for winding 1 kg of composite film with 1 rpm speed	0.214	W	

Table 6-S17B. Power required for winding 1 kg of composite film in a roll- scenario 2

Parameter	**Value**	**Unit**	**Remarks**
Composite film winding amount	1	kg	1 kg of composite film was considered for winding 1 turn in roll
Length of composite film which weigh 1 kg	0.653	m	
Diameter (D) of the roll which make 1 turn roll with 1kg composite film	0.208	m	π x D= Length of 1 kg composite film
Torque required to wind 1kg of composite film	2.041	NM	
Power required for winding 1 kg of composite film with 1 rpm speed	0.214	W	

Table 6-S18. LCI data of chitosan-CNF composite film casting-base case

Process Input				
Material / Energy	**Amount**	**Unit**	**SimaPro Dataset Used**	**Reference**
Inputs from nature (resources)				
Water	20.67	l	Water, unspecified natural origin, US	3% w / v concentration solution
Inputs from Technosphere (materials/fuels)				
Acetic acid	0.21	kg	Acetic acid, 98% in H2O, at plant/US- US-EI U	1% w/v Acetic acid to dissolve chitosan
Chitosan	0.47	kg	Chitosan - Modelled	Table 6-S14
CNF	0.15	kg	CNF - Modelled	Table 6-S14
Glycerol	0.18	kg	Glycerin, at biodiesel plant/kg/RNA	

Citric Acid	0.20	kg	Citric acid {RNA}| production | Cut-off, U	
Inputs from Technosphere (electricity/heat)				
Heat energy-Drying	51.00	MJ	Heat, district or industrial, natural gas {GLO}| market group for | Cut-off, U	Table 6-S16
Electricity-Mixing	0.004	kW	Electricity, at grid, US/US	Table 6-S15
Electricity - Film winding	0.00021	kW	Electricity, at grid, US/US	Table 6-S17
Process Output				
Material / Energy	**Amount**	**Unit**	**SimaPro Dataset Used**	**Reference**
Outputs to Technosphere (Products and co-products)				
Chitosan - CNF composite film	1.00	kg		

Table 6-S18A. LCI data of chitosan-CNF composite film casting-scenario 1

Process Input				
Material / Energy	**Amount**	**Unit**	**SimaPro Dataset Used**	**Reference**
Inputs from nature (resources)				
Water	20.67	l	Water, unspecified natural origin, US	3% w / v concentration solution
Inputs from Technosphere (materials/fuels)				
Acetic acid	0.21	kg	Acetic acid, 98% in H2O, at plant/US- US-EI U	1% w/v Acetic acid to dissolve chitosan
Chitosan	0.42	kg	Chitosan - Modelled	Table 6-S14A
CNF	0.20	kg	CNF - Modelled	Table 6-S14A
Glycerol	0.18	kg	Glycerin, at biodiesel plant/kg/RNA	
Citric Acid	0.20	kg	Citric acid {RNA}| production | Cut-off, U	
Inputs from Technosphere (electricity/heat)				
Heat energy-Drying	51.00	MJ	Heat, district or industrial, natural gas {GLO}| market group for | Cut-off, U	Table 6-S16A

Electricity-Mixing	0.004	kW	Electricity, at grid, US/US	Table 6-S15A
Electricity - Film winding	0.00021	kW	Electricity, at grid, US/US	Table 6-S17A

Process Output				
Material / Energy	**Amount**	**Unit**	**SimaPro Dataset Used**	**Reference**
Outputs to Technosphere (Products and co-products)				
Chitosan - CNF composite film	1.00	kg		

Table 6-S18B. LCI data model of chitosan-CNF composite film casting- scenario 2

Process Input				
Material / Energy	**Amount**	**Unit**	**SimaPro Dataset Used**	**Reference**
Inputs from nature (resources)				
Water	20.67	l	Water, unspecified natural origin, US	3% w / v concentration solution
Inputs from Technosphere (materials/fuels)				
Acetic acid	0.21	kg	Acetic acid, 98% in H2O, at plant/US- US-EI U	1% w/v Acetic acid to dissolve chitosan
Chitosan	0.52	kg	Chitosan - Modelled	Table 6-S14B
CNF	0.10	kg	CNF - Modelled	Table 6-S14B
Glycerol	0.18	kg	Glycerin, at biodiesel plant/kg/RNA	
Citric Acid	0.20	kg	Citric acid {RNA}| production | Cut-off, U	
Inputs from Technosphere (electricity/heat)				
Heat energy-Drying	51.00	MJ	Heat, district or industrial, natural gas {GLO}| market group for | Cut-off, U	Table 6-S16B
Electricity-Mixing	0.004	kW	Electricity, at grid, US/US	Table 6-S15B
Electricity - Film winding	0.00021	kW	Electricity, at grid, US/US	Table 6-S17B
Process Output				
Material / Energy	Amount	Unit	SimaPro Dataset Used	Reference
Outputs to Technosphere (Products and co-products)				

Chitosan - CNF composite film	1.00	kg

Table 6-S19 Sensitivity analysis - Process parameters and parameter values

Process Parameters	Low	High	Unit	Remarks
Mass flow parameters				
Bleached sulphate pulp	1	1.12	kg	± 6% from baseline values
HCl for demineralization	4.23	5.17	kg	0.9 to 1.1 M (Bristow 2012)
NaOH for deproteination	5.02	7.52	kg	4 to 6 % w/v (Bristow 2012)
NaOH for deacetylation	0.64	0.71	kg	45 to 50 % w/w (Bristow 2012)
Energy flow parameters (electricity/heat)				
Electricity-Valley beater pretreatment	0.31	0.46	kWh	± 20% from baseline values
Electricity-Refiner	1.16	1.74	kWh	
Electricity- Chitin manufacturing	1.04	1.56	kwh	
Heat from biomass -Chitosan manufacturing	25.04	37.56	MJ	
Electricity - Chitosan	0.85	1.27	kWh	
Heat energy- Film drying	40.8	61.2	MJ	
Electricity-Mixing	0.004	0.005	kW	
Electricity- Film winding	0.0002	0.0003	kW	